Developing High Performance Linear Carangiform Swimming

By

Richard James Clapham

A thesis submitted for the degree of Doctor of Philosophy

School of Computer Science and Electronic Engineering

University of Essex, Colchester, Essex, United Kingdom

July 2015

Abstract

This thesis examines the linear swimming motion of Carangiform fish, and investigates how to improve the swimming performance of robotic fish within the fields of kinematic modeling and mechanical engineering, in a successful attempt to replicate the high performance of real fish. Intensive research was conducted in order to study the Carangiform swimming motion, where observational studies of the common carp were undertaken.

Firstly, a full-body length Carangiform swimming motion is proposed to coordinate the anterior, mid-body and posterior displacements in an attempt to reduce the large kinematic errors in the existing free swimming robotic fish. It optimizes the forces around the centre of mass and initiates the starting moment of added mass upstream therefore increasing performance, in terms of swimming speed. The introduced pattern is experimentally tested against the traditional approach (of posterior confined body motion). A first generation robotic fish is devised with a novel mechanical drive system operating in the two swimming patterns. It is shown conclusively that by coordinating the full-body length of the Carangiform swimming motion a significant increase in linear swimming speed is gained over the traditional posterior confined wave form and reduces the large kinematic errors seen in existing free swimming robotic fish (Achieving the cruising speeds of real fish).

Based on the experimental results of the first generation, a further three robotic fish are developed: (A) *iSplash*-OPTIMIZE: it becomes clear that further tuning of the kinematic parameters may provide a greater performance increase in the distance travelled per tail beat. (B) *iSplash*-II: it shows that combining the critical aspects of the mechanical drive system of *iSplash*-I with higher frequencies and higher productive forces can significantly increase maximum velocity. This prototype is able to outperform real Carangiform fish in terms of average maximum velocity (measured in body lengths/ second) and endurance, the duration that top speed is maintained. (C) *iSplash*-MICRO: it verifies that the mechanical drive system could be reduced in scale to improve navigational exploration, whilst retaining high-speed swimming performance. A small robotic fish is detailed with an equivalent maximum velocity (BL/s) to real fish.

Acknowledgements

I wish to express my deep appreciation to the many people that helped to support this project. I would first like to thank Professor Huosheng Hu for his help and guidance in the work performed on this project, the time spent answering my many questions and especially for the opportunity to return to postgraduate study, where I was able to continue working on a subject I have the greatest passion for. The funding support from Essex University Scholarships and Research Grants are gratefully appreciated. I would like to thank as well my board members Professor Klaus McDonald-Maier and Professor Paul Scott, who gave me essential guidance and great encouragement. I would like to thank all the members of the Robotics Group past and present, in particular Mr. Robin Dowling for the enjoyable working environment they have created, although I wasn't able to be present in the office as often as I would have liked.

Last of all I want to thank my family, especially my farther Richard Clapham Senior for the uncountable hours of engineering guidance, discussions and financial support. Without his patience this project would have been made vastly more difficult. I would also like to thank my uncle, William Clapham for sharing his physics knowledge and feedback. I would thank my mother, sister and my cherished partner Miss Agi Borbely for their love and support.

Acronyms

BCF	Body and Caudal Fin
MPF	Median and Paired Fin
UV	Underwater Vehicle
AUV	Autonomous Underwater Vehicle
Re	Reynolds Number
Sw	Swimming Number
AR	Aspect Ratio
$b2$	Fin Span
Sc	Projected Fin Area
F_R	Reaction Force
SMA	Shape Memory Alloy
ICPF	Ionic Conducting Polymer Film
CNT	Carbon Nano tube
G9	Generation Nine
F_L	Lateral Force
F_T	Thrust Force
c_1	Linear Wave Amplitude Envelope
c_2	Quadratic Wave
λ	Body Wave Length
y_{body}	Transverse Displacement of the Body
x	Displacement Along the Main Axis
k	Wave Number
ω	body wave frequency
P	Adjustable Parameters of Swimming Pattern
DOF	Degree of Freedom
N	Number of Links in Series
L_2	Posterior link of the discrete structure
P_2	Amplitude offset
P_1	Predetermined maximum crank offset
P_{1x}, P_{1y}	The coordinates of P_1

P_{2x}, P_{2y}	The coordinates of P_2
ω_1	Angular Velocity
V_{P2}	Velocity Vector
V_{p2x}, V_{p2y}	Decomposed vectors of the velocity vector V_{P2}
CFD	Computation Fluid Dynamics
DPIV	Digital Particle Image Velocity
CPP	Central Pivot Point
COG	Center of Gravity
DC	Direct Current
Dv	Viscous Drag
Cf	Drag Coefficient
S	wetted surface area
p	Water Density
St	Strouhal number
f	oscillation frequency
A	Dispersed wake width
U	average forward velocity of fish
T	Time-averaged thrust production
P	Time-averaged power required
N	Froude efficiency
CST	C Sharp Turn
$C\text{-}_{start}$	Curvature that resembles a letter C
$S\text{-}_{start}$	Curvature that resembles a letter S
V	Velocity
L	Length of Body
IMU	Inertia Management Unit
IR	Infrared
NACA	National Advisory Committee for Aeronautics
GUI	Graphic User Interface
PLA	Polylactic acid
ABS	Acrylonitrile Butadiene Styrene
MPa	Megapascal

Contents

List of Figures

List of Tables

Chapter 1

Introduction

This thesis describes the development of four generations of robotic fish, which lead to a greater understanding of the factors essential for high performance propulsion. It details the observational studies, swimming mechanics theory, mechanical design, construction methods and experimental testing which was undertaken to lead to a high performance of robotic fish. This chapter presents the motivation, objectives, challenges, methodology, scientific contributions and the outline of the thesis.

1.1. Motivation

To navigate through a marine environment, a robotic vehicle requires mobility to effectively contend with the physical forces exerted by the surrounding fluid [165; 166]. These physical forces applied to the underwater vehicle (UV) can lead to inaccurate navigation and even failure of the operation as traditional propeller driven systems are unable to adapt to the dynamic environment due to their low locomotive efficiencies of energy transfer and manoeuvrability. Current rotary propeller driven vehicles operating during low speed locomotion have particularly high cost of transport requiring a large power supply increasing body size. In addition the drive method of rigid hull UVs create large propulsive wakes causing increased environmental noise [1; 11; 13; 66; 68; 112].

In contrast, live fish can coordinate their body motions in harmony with the surrounding fluid generating large transient forces efficiently and have demonstrated the ability to extract

energy from upstream vortices [1; 11; 112]. Hence, the underwater vehicles with bio-robotic propulsion can provide greater mobility, unobtrusive navigation, reduced noise to the environment and a lower cost of transport. Some operational examples are military surveillance, mine countermeasure, inspection, pollution mapping, sea bed exploration and locomotion through areas of thick debris.

Up to now, most work in robotic fish has focused on the hydrodynamic drive mechanism but robotic fish were unable to gain the locomotive efficiencies of live fish. Some examples of novel design approaches are Barrett's hyper-redundant Robotuna, achieving a maximum velocity of 0.65 body lengths/ second (BL/s) (0.7m/s) [113], Anderson's VCUUV with 0.5BL/s (1.2m/s) [121], Yu's discrete structure with 0.8BL/s (0.32m/s) [116], Wen's Carangiform with 0.98BL/s (0.58m/s) [75], Liu and Hu's G9 with 1.02BL/s (0.5m/s) [8] and Valdivia y Alvarado's compliant method with 1.1BL/s (0.32m/s) [117]. The straight-line speed of current robotic fish, peaking at approximately 1.1BL/s is unpractical for real world marine based environments.

In comparison, Bainbridge's intensive observational studies measured live fish to attain an average maximum velocity of 10 body lengths/ second [51; 112]. A single high performance of a Cyprinus carpio was noted, achieving the swimming speed of 12.6BL/s (1.7m/s) with a stride rate of 0.7. However, it is noted that the endurance of real fish at the highest velocities is limited and burst speeds can only be maintained for short durations of approximately one second. Velocities were measured to decrease to 7BL/s in 2.5s of swimming, to 5BL/s in 10s and to 4BL/s in 20s [51]. Hence the efficient performance of fish is limited and to achieve a robotic underwater vehicle with high speeds practical for real world applications we should aim to outperform real fish in terms of the duration at top speed.

There are numerous challenges to address within the field of robotic fish, including locomotion, high-speed swimming gaits, acceleration, horizontal and vertical plane mobility, efficient behaviours, high force transfer, station holding, precision trajectories, efficient energy transfer, reduced internal mechanical lose, accurate geometries, high performance propulsion, accurate body wave parameters, high stride rate, on-board powers supply, obstacle avoidance and robustness, etc.

In terms of the locomotion challenge, it has become clear that a robotic underwater vehicle cannot navigate through the most physically demanding environments, linear propulsion is key factor and was chosen as the research aim in this thesis. Reproducing the propulsive force

of fish is a complex challenge as the development of a novel mechanism must take a number of factors into consideration. The problems can be classified under two main categories:

1) ***Kinematics*:** Current robotic fish cannot achieve accurate replication of the linear swimming motion as free swimming platforms generate kinematic parameter errors and therefore reduced propulsion. Accurately matching the kinematic data of real fish is complex and free swimming robotic fish applying posterior confined displacements have shown kinematic parameter errors [20; 116; 117; 157; 171] (Section 3.3). In particular, the lateral (F_L) and thrust (F_T) forces are not optimized. As a result, large anterior destabilization in the yaw plane is generated due to the concentration of posterior thrust, recoiling around the centre of mass. Consequently the inaccurate anterior kinematics creates significant posterior midline displacement errors. Hence, the linear locomotive swimming motion over the full length of body has large matching errors in comparison to real fish (Section 3.4) leading to reduced propulsive force and a higher cost of transport.
2) ***Mechanical Drive System*:** Current robotic fish have low force transfer due to the complexity of developing the powertrain, limited by mass and volume distribution accuracy, low force and frequencies and internal mechanical losses (Section 3.5). The mechanical drive systems are unable to replicate the high performance swimming of real fish, as developing a powertrain requires the ability to generate accurate kinematics in combination with efficient high energy transfer, so that high speeds and endurance are attainable. The prominent methods of discrete link (multiple servo motor) assemblies [8; 20; 57; 60; 76; 77; 79; 116], compliant (single servo motor) structures [69; 117; 135; 157] and hyper-redundant (single actuator) mechanisms [113; 121; 156] have many factors which greatly limit the drive system. Therefore they are unable to generate high propulsive locomotion by transferring the deployed actuators output with high energy efficiency.

1.2 Research Questions

To develop advanced robotic fish with high performance linear swimming, we have to address some key challenges on their kinematics, mechanical engineering, morphology and fluid mechanics. The research conducted in this thesis investigation aims to address the following questions:

(1) How can the kinematic parameter errors within the linear swimming motion of free swimming robotic fish be reduced?

The observed swimming motion of existing robotic fish has large kinematic errors in comparison to real fish over the full body length. In particular the head swing amplitude is far greater than real fish as a consequence of the large posterior forces creating destabilizing around the centre of mass. This anterior recoil in turn creates posterior errors. Therefore posterior kinematic errors in comparison to the applied traditional kinematic pattern are generated, as the observed anterior and posterior amplitudes of robotic fish are approximately equal (Section 3.3). This configuration of parameters also generates an inaccurate central pivot point location, a critical characteristic of the Carangiform swimming motion. It is therefore necessary to understand real fish in terms of fluid flow theory and their swimming mechanics (Section 3.4). The thesis investigation begins by analysing published studies of real fish and undertaking intensive observational studies to build a precise kinematic model of the parameters over the full-body length. Hence we include all variables of the midline kinematics and the morphological structure throughout the body wave cycle of every segment of the body so that a greater precision coordinated propulsive mechanism is developed.

(2) How should the kinematic model be validated?

The kinematic accuracy and parameters can be validated through experimental testing by obtaining the midline parameters which may be plotted against the desired amplitude envelopes of the anterior and the posterior for comparison (Section 4.5.2). A further series of experiments can be conducted in order to verify the swimming motions by evaluating the locomotive performance in terms of speed, force, energy consumption and the distance travelled per tail beat. By tuning the kinematics, it provides a direct effect on the swimming speed of the vehicle, therefore providing an accurate measure of swimming performance if the swimming motions are deployed upon the same platform. Efficiency of the kinematics directly affects the distance travelled per tail beat (Section 4.5.3-4.5.6). The stride rate of the swimming motion provides us with the efficiency of the kinematic parameters. We can further analyse the variables within the body wave by isolating individual segments of the build during operation, therefore providing a measure of each segments (anterior, mid-body, posterior) contribution to the propulsive wave. Tuned kinematics should provide a greater maximum velocity based on the theory of added

mass, this is the propulsive method applied by Carangiform fish, in which inertia force propulsion is generated by creating a reaction force against the mass of the water.

(3) How to develop a mechanical drive system capable of two interchangeable swimming patterns?

For the highest precision during experimental testing of the two swimming motions, a platform should be easily modified so that its individual segments can be active or inactive during actuation (Sections 4.2, 4.5.3 and 5.2). The factors of morphology and energy transfer are crucial to the performance output of a swimming robotic vehicle. Hence slight changes will directly affect produced velocities therefore a single prototype will need to be devised with easy to configure structural arrangements (Chapters 4-7). To solve the problems outlined above, the research must begin by analysing the drive system of existing builds, addressing the limitations of the devised systems and discussing solutions due to the current low performance in comparison to the efficiency and speed of real fish (Chapter 3). As a high frequency and force production actuator must be deployed for high performance, we should consider how the rotary motion may be transferred to oscillatory motion and distributed to the discrete links without high internal mechanical losses.

(4) How to greatly increase the performance of the mechanical drive system?

If the key kinematic parameters of real fish are generated there is potential to greatly increase the maximum velocity of robotic fish. We can take the finding of [51; 112; 118] in which real Carangiform fish were measured to only increase their tail beat frequency to raise their swimming speed when swimming at a frequencies of 5hz or above. Hence we look to precisely replicate the kinematic pattern of fish swimming at the speed > 5Hz. This theory is reaffirmed by Lighthill, who noted that fish only increase their amplitude whilst below 5Hz (Section 3.4). To achieve this, the devised robotic fish must be robust, compact, naturally buoyant, carrying its own power supply, with a high power density and able to effectively transmit large forces at intensively high tail oscillations, whilst maintaining accurate kinematics. If these challenges are achieved, a high-speed propulsive vehicle may be realized and capable of generating the maximum velocity and stride rates of real fish (Chapter 6).

(5) How to achieve a compact build?

To increase navigational exploration and reduce the forward resistance, a mechanical drive system with the smallest geometric profile (wetted area) is desirable. The miniaturization of an underwater vehicle can provide greater mobility, unobtrusive navigation, reduced noise to the environment and a lower cost of transport. Therefore, it is desirable to optimally design a high speed swimming fish with the smallest morphological structure, hence achieving a high power density ratio. The big challenge is to transfer the energy from the actuator into the required fish body wave motion under the structural and materials limitation. As the body profile magnitude decreases, the challenge of devising a high power density prototype increases.

1.3. Research Objectives

This research project considered the factors contributing to the low hydrodynamic performance of current robotic fish within linear locomotion and aimed to achieve the high swimming performance of real fish with eight main objectives:

(1) To introduce a new swimming pattern to reduce the kinematic parameter errors by coordinating transverse displacements along the body length (Section 3.4).

(2) To devise a prototype that operates in two swimming patterns, for a thorough investigation of the Carangiform swimming motion to be conducted (Chapters 4-7).

(3) To significantly increase force transfer by achieving a high power density ratio in combination with an efficient mechanical energy transfer (Chapters 4,6 and 7).

(4) To achieve unrestricted high force swimming by realizing a prototype capable of carrying a high powered energy supply (Chapter 6).

(5) To develop a structurally robust mechanical drive system capable of high frequencies (Chapters 4,6 and 7).

(6) To greatly reduce forward resistance by engineering a streamlined body considering individual parts' geometries and alignment throughout the kinematic cycle (Chapters 4,6 and 7).

(7) To develop a prototype to improve stability in the vertical and specifically the horizontal plane, by optimizing the lateral and thrust forces around the centre of mass, so that the free swimming prototype's unsteady oscillatory motion during intensively high frequencies is stabilized to achieve a more efficient force transfer (Chapters 4,6 and 7).

(8) To conduct a series of experiment tests measuring the prototype's achievements in terms of kinematic data, speed, thrust, stride rate and energy consumption in relation to driven frequency (Chapters 4-7).

1.4 Thesis Contributions

The purpose of this thesis is to thoroughly investigate the kinematic pattern of Carangiform fish, and engineer a mechanical drive system capable of high performance swimming. On this account, the thesis is focused on the improvement of linear locomotive performance of robotic fish in order to provide knowledge and guidance to designers, researchers and students working in the following areas: (a) Biological inspired robotics, (b) Marine robotics, (c) Kinematics, (d) Biological fish studies (e) Mechanical engineering. The main contributions of this thesis can be summarised as follows:

1) A novel kinematic swimming pattern for the Carangiform linear swimming motion is introduced based on intensive observational studies (Chapters 3 and 4). It greatly reduced the large kinematic errors seen in the existing free swimming robotic fish with the traditional posterior confined approach. The proposed pattern coordinated the anterior, mid-body and posterior displacements of body wave and optimized the reaction forces around the center of mass. The coordinated body motion achieved precise kinematic parameters in relation to real fish and reduced kinematic matching errors over the full body length. In particular the introduced body motion was able to reduce the anterior recoil, and generate an effective propulsive mechanism. In addition, it was found that applying a small change to the full-body length swimming pattern at the mid-body stage, a significantly reduction in performance of 28.6% is seen, hence indicating the importance of anterior, mid-body and posterior coordination.

2) A novel robotic fish (First generation, *iSplash*-I) was created, which has a mechanical drive system with two operational swimming patterns. Its full-body Carangiform swimming motion significantly outperformed the traditional posterior confined undulatory swimming pattern approach in terms of the speed measured in body lengths/ second by 27%, achieving a consistent maximum velocity of 2.8BL/s at 6.6Hz with a *Sw* of 0.42. The prototype was able to greatly improve the swimming speed of existing robotic fish, and achieved low energy consumption by developing a free running and morphologically accurate mechanical drive system able to swim at a maximum velocity

of 2.8BL/s whilst consuming only 7.68W. Throughout the test runs, the applied frequencies increased velocity in both operational modes without early peak, decline or failure. This matches Bainbridge's study of real swimming fish, measuring no noticeable change in kinematics after tail oscillations are over 5Hz.

3) A novel robotic fish (Third generation, *iSplash*-II) was developed Chapter 6, which has a mechanical drive system able to outperform real fish, in terms of the recorded average maximum velocity of real fish measured in BL/s. It is robust, compact, naturally buoyant with a high power density (with the primary actuator 75% of the total mass) able to effectively transmit large forces at intensively high tail oscillation frequencies for untethered high-speed propulsion. It achieved a maximum velocity of 11.6BL/s (i.e. 3.7m/s) at 20Hz with a high stride rate of 0.58 and a force production of 9N. In addition, it was able to accelerate to steady state swimming in an approximate time of 0.6s, and showed no signs of early peak or decline in velocity as frequencies were raised.

4) The *iSplash*-II, a 3rd generation of robotic fish, was presented in Chapter 6, which has a mechanical drive system able to outperform the endurance of real fish in terms of the duration that top speed is maintained. It was able to maintain endurance at 11.6BL/s for duration of approximately ten minutes, far greater than the recorded measurement of endurance in real fish of approximately one second during burst swimming at their maximum velocity.

5) A novel robotic fish (Fourth generation, *iSplash*-Micro) was created with a reduced scale mechanical drive system able to generate an equivalent average maximum velocity to real Carangiform fish (Chapter 7). It has greatly simplified structural built at the millimetre scale and is able to accurately replicate the kinematic parameters of the posterior confined undulatory swimming pattern of real fish at high frequencies. By developing large scale dorsal and pelvic fins relative to body size, the reaction forces were optimized around the centre of mass, generating an accurate anterior amplitude effectively stabilizing the platform in the horizontal and vertical planes. This enabled a predictable adjustment of the anterior and posterior kinematic amplitude parameters so that large posterior propulsive forces and amplitudes could be generated and accurate straight-line trajectories attained. It is 50mm in body length achieved a consistent free swimming speed of 10.4BL/s (i.e. 0.52m/s) at a frequency of 19Hz with a stride rate (*Sw*) of 0.54 and a low energy consumption of 0.8W.

1.5 Thesis Outline

Overall the thesis addresses many challenges that are examined in depth throughout the eight Chapters. A flow chart of the thesis structure is given by Figure 1.1, which illustrates the links among the chapters that are related.

Chapter 2 (Background) presents an extensive survey consisting of two main sections. The first section provides an overview of the most prospective aspects of underwater mobility found in nature, thoroughly identifying the various adaptations in morphology and swimming mechanics. Many various calculations to measure efficiency of the diverse swimming motions are identified. Secondly, the chapter surveys the current state of the art robotic vehicles, detailing the capabilities of conventional and biological inspired vehicles. The survey identifies the kinematic accuracy of their swimming motion and their swimming performance, and identifies various opportunities to achieve scientific contributions.

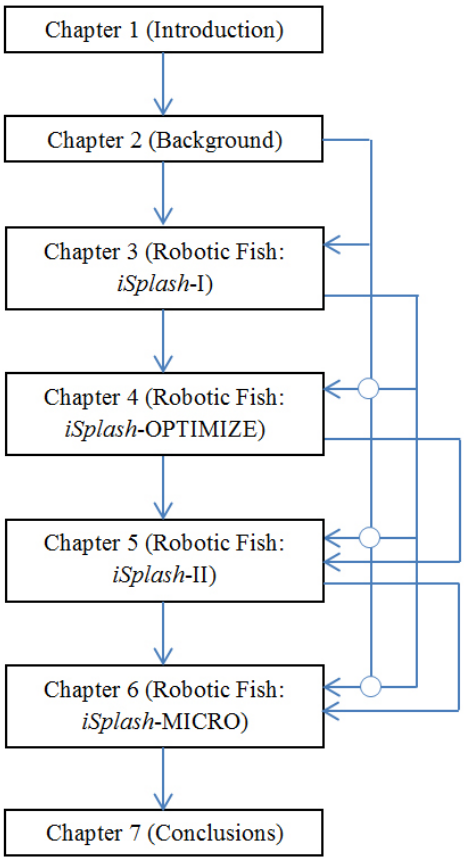

Figure 1.1: Flow chart of chapters

Chapter 3 (Linear Locomotion) identifies the research path, describing linear swimming performance of underwater robotics as a great challenge within the research field to address. The chapter initially investigates the kinematics, morphology and swimming mechanics of existing robotic fish detailing their current swimming ability. The traditional approaches to the problem are detailed and prospective future approaches discussed. The chapter presents the observational studies undertaken on real fish and details the proposed swimming pattern to overcome previous kinematic errors within the wave form. The state of the art mechanical engineering developments are detailed and the problems addressed along with possible solutions for increasing the performance of the mechanical drive system, which paves the way for the four novel robotic fish developed in Chapters 4-7.

Chapter 4 (Robotic Fish: *iSplash*-I) presents the first generation of robotic fish with the linear Carangiform swimming motion. It has two operational swimming patterns, i.e. the traditional posterior confined swimming motion and the full-body coordinated swimming pattern proposed in Chapter 3. The experiments are conducted to measure the speed, energy consumption, force production and kinematic accuracy of each of the two swimming patterns. The results show that the proposed Carangiform swimming motion approach significantly outperforms the traditional posterior confined swimming pattern in terms of kinematic accuracy and the average maximum velocity, achieving greater speeds than previously robotic fish, approximately equivalent to the cruising speeds of real fish. The chapter includes re-evaluation of the 1st generation fish with three further experimental tests: (i) The full-body swimming motion was analysed by modifying the mechanical structure so that the individual segments are restricted from motion, therefore providing a measure of their contribution to the performance. (ii) The developed skin was experimentally tested to measure the improvement in swimming speed and reduced energy consumption due to its deployment. (iii) The caudal fin was optimized according to morphological shapes of real fish. The increase in swimming speed is measured for each of the individual tails, showing a significant performance gain over the initially deployed tail that is morphological accurate to a Carangiform fish.

Chapter 5 (Robotic Fish: *iSplash*-OPTIMIZE) presents the 2nd generation robotic fish which has the coordinated full-body length swimming motion for accurate kinematics and the increased swimming performance. It is based on the 1st generation of robotic fish with further tuning of the kinematics parameters. The chapter details the mechanical design and construction methods of deploying a single actuator to drive adjustable discrete links across

the full-body length and presents the linear Carangiform swimming patterns to be investigated. The main focus is on optimizing the kinematics parameters of its linear Carangiform swimming motion in order to improve the distance travelled per beat. The experimental procedure and results are given detailing the discoveries and identifying future directions.

Chapter 6 (Robotic Fish: *iSplash*-II) introduces a new robotic fish, *iSplash*-II, capable of outperforming real Carangiform fish in terms of average maximum velocity (measured in body lengths/second) and endurance, the duration that top speed is maintained. The prototype significantly increases the linear swimming speed of robotic fish, achieving consistent untethered stabilized swimming speeds. The chapter details the investigation of swimming patterns, new fabrication technique and developed mechanical drive system. The experimental results show that the prototype effectively transmits large forces at high frequencies to obtain high-speed propulsion. The novel mechanical drive system is able to optimize the lateral and thrust around the centre of mass, generating accurate kinematic displacements and greatly increasing the magnitude of added mass. In addition, the field trials show that the third generation is able to replicate the key swimming properties of real fish. As frequencies increase, the prototype increases its velocity without early peak, decline or failure, indicating that only an altered frequency is required to increase swimming speed.

C**hapter 7** (Robotic Fish: *iSplash*-MICRO) presents the fourth generation, a millimetre scale robotic fish, able to accurately generate the posterior undulatory pattern of the Carangiform swimming mode, at intensively high frequencies. It is 50mm in length and able to generate an equivalent average maximum velocity to real fish, measured in body lengths/ second (BL/s). During marine exploration, a miniaturized underwater vehicle (UV) can benefit operations by allowing greater mobility as the turning diameter and body geometry is small. The new construction method for micro builds is described, detailing the applied kinematic swimming pattern and introduces a novel destabilization solution to reduce anterior recoil, whereby an investigation into anterior stabilization is made in an attempt to reduce the large kinematic errors and optimize the reaction forces around the centre of mass. Lastly the field trials undertaken and the experimental results are presented, detailing the results of a small fish achieving a high performance consistent free swimming speed with low energy consumption.

Chapter 8 (Conclusions) summarises the whole thesis, identifying the scientific contributions and discussing the discoveries made during the development and experimental work of the four generations of robotic fish. Lastly, some future directions are given to briefly outline the opportunities for further performance increase.

Chapter 2

Literature Review

The literature review begins with the field of biological studies in Section 2.1, where the thorough research carried out on fish and underwater mammals is comprehensively presented, systematically identifying the various adaptations in morphology and swimming mechanics. The methods for analysing the propulsive mechanisms are given. This section provides an outline of the most prospective aspects of underwater mobility found in nature, from which a suitable propulsion method can be chosen. Section 2.2 reviews the current state of the art underwater robotic vehicles, detailing the abilities of conventional and biological inspired vehicles such as their categories and swimming performance. Lastly a summary is given in Section 2.3, detailing the critical aspects of background research from which the direction of the thesis is determined (Chapter 3).

2.1. Swimming Patterns and Physiology

The investigation of how fish swim has been studied for thousands of years from the first notes of Aristotle to the recent computational analysis techniques of Computational Fluid Dynamics (CFD) and Digital Particle Image Velocity (DPIV) (Sections 2.1.8). The previous literature, which has provided the basis for the robotic fish builds developed by many teams over the last two decades, will be discussed in detail in this following section.

2.1.1. Morphology Classification Scheme

A mechanical propulsor is identified by the prominent swimming mode employed for thrust generation and its mechanical configuration [1] (Figure 2.1). The classification scheme originally proposed by Breder is based on two main aspects (i) the extent to which propulsion lies along the gradient of oscillatory and undulatory motion and (ii) the body structure that is most significant in generating thrust [2]. The prominent categories are defined as:

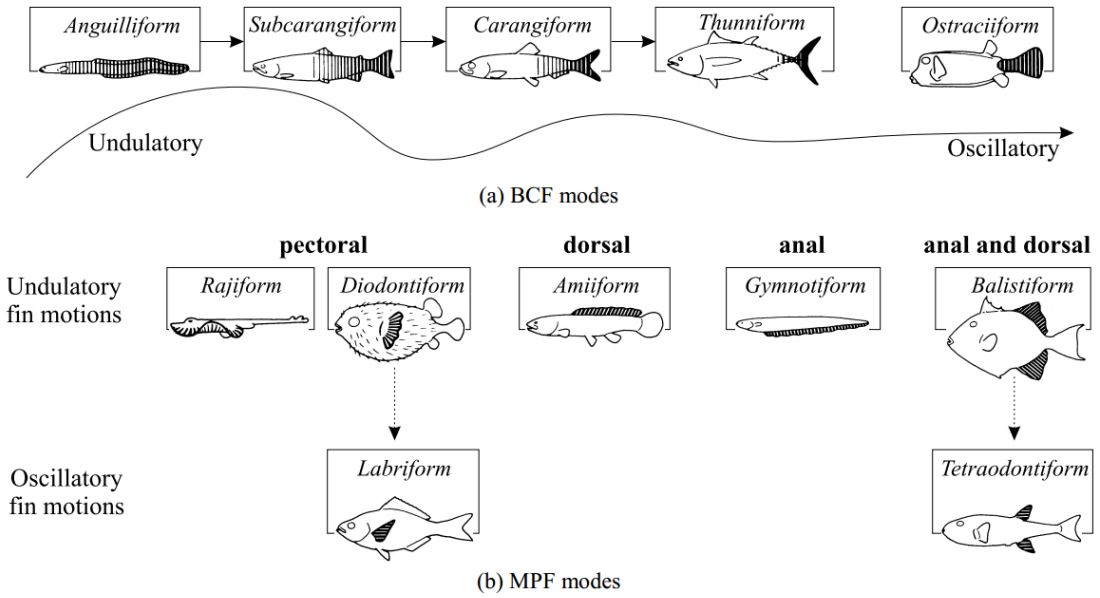

Figure 2.1: The morphological swimming modes from Undulatory to Oscillation [7].

- ***Median and/or Paired Fin*** **(MPF) –** Propulsion is generated by coordinated movements of multiple multifaceted low aspect ratio control fins where the body is held rigid and applies either undulatory, oscillatory or rowing techniques of the pectoral, pelvic, anal and dorsal fins. MPF swimming modes have high propulsive efficiencies whilst operating at low speeds and the ability of precise adjustments of the control surface to generate small corrective forces and counteract destabilization [3].
- ***Body and/or Caudal Fin*** **(BCF) –** The morphological structure of BCF swimming modes can be identified by the fraction of their body which is displaced laterally along the wavelength and the scale of the amplitude envelope of the propulsive wave. Propulsion is generated by large body displacement of propagating undulatory waves or oscillatory caudal fin motions that produce greater thrust, higher velocity and locomotive cruising efficiencies than MPF propulsion [4; 112].

The following prominent swimming modes are defined:

- *Anguilliform Swimmers:* BCF i.e. Anguilla (Eel) – Characterized by elongated slender bodies which create large amplitude displacements to the expense of increasing frictional drag. Thrust is produced by propagation of the entire body, sending a transverse wave from the anterior to posterior, providing the advantage of dexterous manoeuvrability [7; 16; 112; 119].
- *Carangiform Swimmers*: BCF i.e. Cyprinus carpio (Common Carp) – With limited anterior motion BCF mechanics utilize a posterior propagating wave a third of the body length growing in amplitude towards the tail. Defined as fast, manoeuvrable and generalist locomotion, Carangiform swimmers have higher velocities than Anguilliform configurations, but turning and burst acceleration is compromised by the rigidity of their anterior [6; 15; 118; 122; 160].
- *Subcarangiform Swimmers*: BCF i.e. Oncorhynchus mykiss (Rainbow Trout) – The Subcarangiform and Carangiform can apply almost identical body wave motions for linear swimming with a posterior propagating wave third to half the body length. Subcarangiform swimmers have greater dexterity along the body length utilized for greater locomotive mobility [6; 15; 59; 122].
- *Thunniform Swimmers*: BCF i.e. Thunnis Alalunga (Albacore Tuna) – Efficient lift based propulsion produced by an oscillatory caudal fin that provides > 90% of the thrust allowing high cruising speeds to be maintained. The Thunniform hydro-dynamic profile is optimized for high-speed swimming at high Reynolds numbers at the expense of inefficient low speed locomotion, manoeuvring and acceleration. This reduced pressure drag body shape combined with a high aspect ratio stiff caudal fin provides the greatest swimming efficiency during linear locomotion [5; 16; 119; 169].
- *Ostraciiform Swimmers*: BCF i.e. Ostracion Cubicous (Yellow Boxfish) – Propulsion is generated from varying fin-beat combinations of oscillatory caudal and pectoral fins which generate thrust for both forward locomotion and stabilizing. They are characterized by a rigid carapace and keels which form sharp corners which the boxfish utilizes to induce circulation of upstream vortices and trimming forces to help stabilize and reduce drag in dynamic environments [7; 8].
- *Labriform Swimmers*: MPF i.e. Lepomis Macrochirus (Bluegill Sunfish) – Coordinated movement of multiple multifaceted control fin surfaces achieve efficient propulsion at

slow speeds. Highly manoeuvrable as they are characterized by instability, requiring constant expenditure to generate balancing forces. The large wetted surface area of the body dampens inertia recoil forces arising from posterior thrust, creating almost no body motion and reducing pressure drag [9; 42; 110; 145; 147].

- *Gymnotiform Swimmers*: MPF i.e. Apteronotus Albifrons (Black Ghost Knifefish) – Undulatory ventral ribbon fin that runs the lateral length of their body that generates a sinusoidal travelling wave capable of varying individual force components and complex interactions of thrust vectors. Omnidirectional locomotion, despite their stretched straight profile being capable of producing only slight curvature [7; 10].
- *Balistiform swimming*: MPF Rhinecanthus Aculeatus (Picasso Triggerfish) – Aquatic propulsion by means of undulatory movements of the median (dorsal and anal) fins utilized as the primary mode of transport. This form of propulsion is an adaptation for highly efficient movement within complex environments such as coral reefs. [108; 109].

2.1.2. Non-dimensional Parameters and Key Metrics

To analyse propulsive efficiency and its components the following prominent non-dimensional parameters and metrics are considered:

Reynolds number (*Re*) is defined as:

$$Re = LU/v \tag{2.1}$$

where L is the length of the main thrust propulsor, U is the swimming velocity and v is the kinematic viscosity of water (1.044×10^{-6} m^2/s for sea water at $20^{o}C$). High Reynolds regimes are adopted by most fish and marine mammals which operate in the range of $Re > 10^5$, where transition from laminar to turbulent flow can occur and inertial forces are dominant and viscous forces are negligible. If $Re < 1$ viscous forces are dominant [11; 170].

Viscous drag (*Dv*) is defined as:

$$Dv = 1/2 C_f S U^2 p \tag{2.2}$$

This is a standard Newtonian equation where Cf is a drag coefficient which is related to the Reynolds number, S is the wetted surface area, U is the forward velocity of the fish and p is water density (1000 kg/m^3). The laminar and turbulent drag coefficients are 1.328 $Re^{-0.5}$ and 0.074 $Re^{-0.2}$ respectively [12].

Strouhal number (*St*) is defined as:

$$St = fA/U \tag{2.3}$$

where f is the oscillation frequency, A is the dispersed wake width (approximately the tail peak-to-peak amplitude) and U is the average forward velocity.

The St Number is a prominent parameter for analysing BCF propagating motion and the thrust generated is considered optimal if the Strouhal number is in the range of $0.25 < St < 40$. Triantafyllou *et al* considers the Strouhal number as a thrust coefficient estimated by the wake shed from the trailing edge [5; 11].

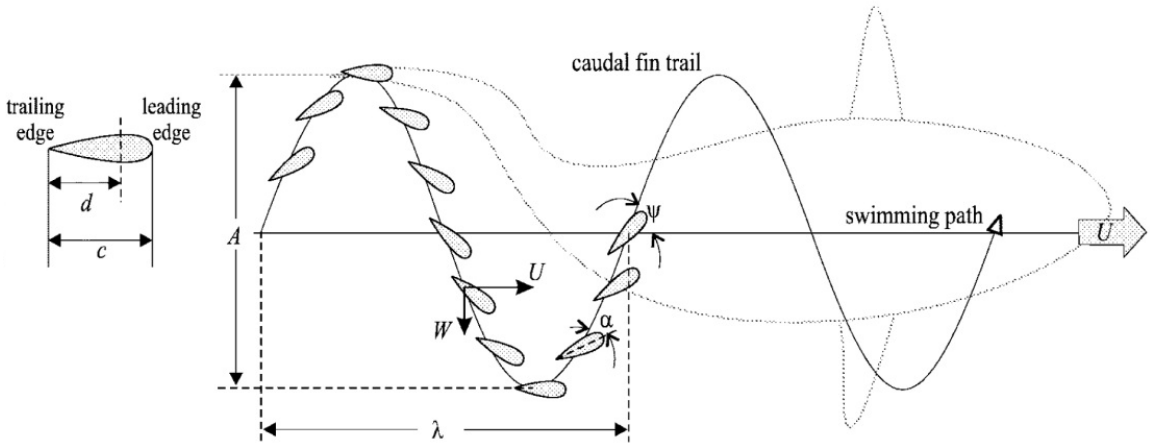

Figure 2.2: Showing the trail of an oscillating fin illustrating the amplitude A, wavelength λ, feather angle ψ, and attack angle α of the caudal fin [170].

The Strouhal number is used within this research as a frequency parameter during analysis. An effecting attribute to the St is the maximum angle of attack of the oscillatory caudal fin which should be between $15 < \alpha < 25$ degrees with the pitching movement leading the heaving motion by around 75º (Figure 2.2). Velocities are measured in body lengths per second (BL/s), which is a recognized measurement for comparing linear efficiencies of fish and biological inspired robotics (Section 3.1).

Froude efficiency (n) is defined as:

$$n = (T)U/(P) \tag{2.4}$$

A common measure of swimming efficiency where U is the average positive velocity of the fish, T is the time-averaged thrust produced, and P is the time-averaged power required. A relationship between Froude number and manoeuvrability has been identified [13]. Calculated efficiencies are recorded in the range of 90% for Carangiform swimmers [6].

Swimming Number (Sw) is defined as:

$$Sw = U/fl \tag{2.5}$$

where U denotes swimming velocity, f denotes the tail beat frequency and l denotes the body length [118]. A prominent parameter for analysing body and caudal fin locomotive performance is the distance travelled per body length during one caudal fin oscillation (Figures 2.3 and Table 2.1).

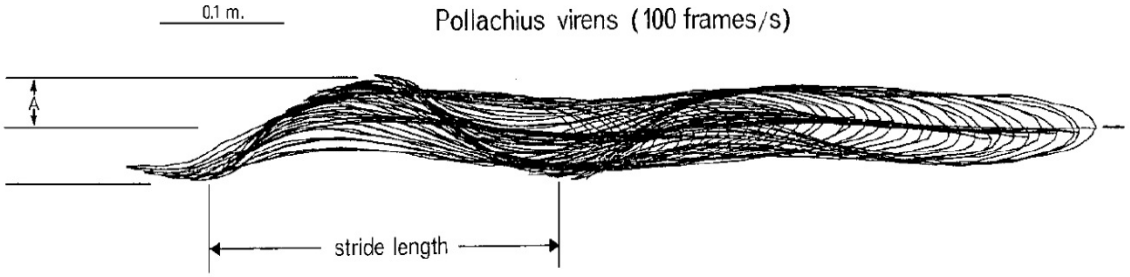

Figure 2.3: Measuring the distance travelled per tail beat, a calculation of stride efficiency introduced by Nagai [118].

Table 2.1: Swimming Number of the most highly efficient fish and marine mammals (Adapted from M. Nagai, 2002 [118]).

Species	Swimming Numer (Observer)
Dolphin	0.82 (Nagai)
Carp	0.70 (Nagai)
Dace	0.63 (Bainbridge)
Trout	0.62 (Bainbridge)
Goldfish	0.61 (Bainbridge)
Tilapia	0.58 (Nagai)

Aspect Ratio (*AR*) is defined as:

$$\mathrm{AR} = b^2/Sc \tag{2.5}$$

where b squared is the fin span and Sc is the projected fin area (Figure 2.4).

High aspect ratio caudal fins developed on Thunniform propulsion lead to improved efficiency as resistance is reduced in relation to the thrust or lift produced (AR values range 4.5 - 7.2). High aspect ratio fins' thrust efficiencies are enhanced by leading edge suction bought on by the oscillatory motions of the stiff fin and a sharp sweepback angle where the curvature of its leading edge avoids boundary layer separation [7].

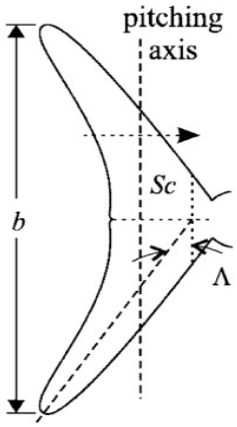

Figure 2.4: Side view of a caudal fin, indicating the elements required to calculate its aspect ratio [7].

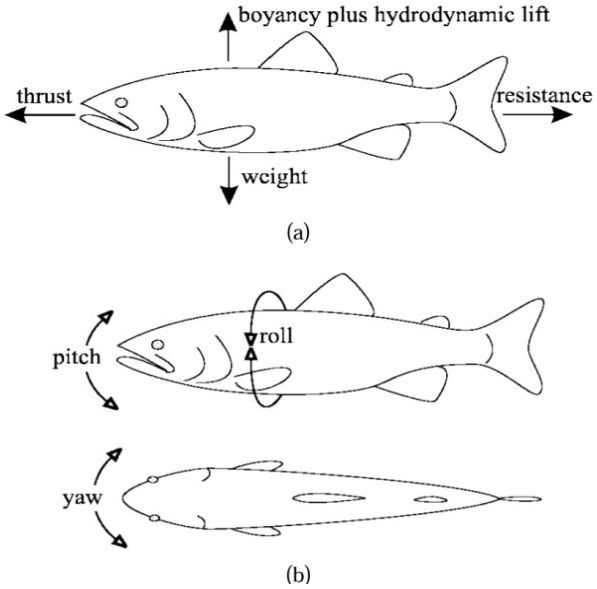

Figure 2.5: Forces and moments on a swimming fish: buoyancy, thrust drag and gross weight contributions to the force balance, rolling, pitching and yawing moments respectively. Angular velocity components in roll, pitch and yaw [170].

2.1.3. Mechanics of Swimming

The transfer of momentum into the surrounding fluid from active fish muscle generates propulsion. As a fish activates its body or fin mechanism displacement due to the incompressibility of fluid creates reactive forces [1; 2; 15; 38; 40]. The momentum conservation principle requires that the mechanical thrust of tail beat cycle during fluid body interaction must be greater than the combination of total resistance and energy dissipation to

provide positive activity in the horizontal plane. In the vertical plane hydro-static forces buoyancy, weight and hydrodynamic lift are constantly acting (Figure 2.5).

2.1.4. MPF Locomotion

Undulatory and oscillatory appendages of the MPF swimming mode provide hydrodynamic efficiency by manipulating the fluid body interactions during manoeuvring, stabilizing and locomotion [3; 4; 9; 10; 31; 80; 81]. A significant advantage of median fins structure is the elaborate control of individual force components, length, curvature, angle of attack, stiffness, damping, flexibility and inter-distancing of span. The propulsive force of the median fin can be simplified and calculated by the pressure rise in the fluid passing across the fin known as *actuator-disc theory* which consists of the force exerted by oscillatory motion and the area of the expressed wave along the fin [32]. Blake identified two main oscillatory motions for fin based propulsion:

- *Rowing* – Consisting of a power and recovery stroke, this two-phase action moves perpendicular to the body at high angles of attack and higher velocities then the overall body. The basic positive thrust motion for this locomotion can be described as a figure of eight pattern which has control over amplitude, undulation and phase of the whole fin. During the recovery stokes the control surface reduces resistant forces by contracting the span width of the fin membrane and fin rays. Rowing or drag-based force mechanisms are measured to be more efficient at lower speeds [33; 5].
- *Lift Based* – Characterized by heave and pitch motions of large aspect ratio pectoral fins, generating forces in the plane perpendicular to the fin motion during up/ down strokes. The oscillating Thunniform caudal fin is a lift based propulsor with a high aspect ratio profile, which minimizes cross flow disturbances and delays stall during large angles of attack [34; 13].

MPF swimming modes have high propulsive efficiencies and the ability of precise adaptions of the control surface to generate small corrective forces and counteract destabilization. The dexterity of the fin can increase propulsion and manoeuvring efficiencies by applying techniques such as increasing displacement of fluid between body and fin during the contraction stage [31] (Figure 2.6).

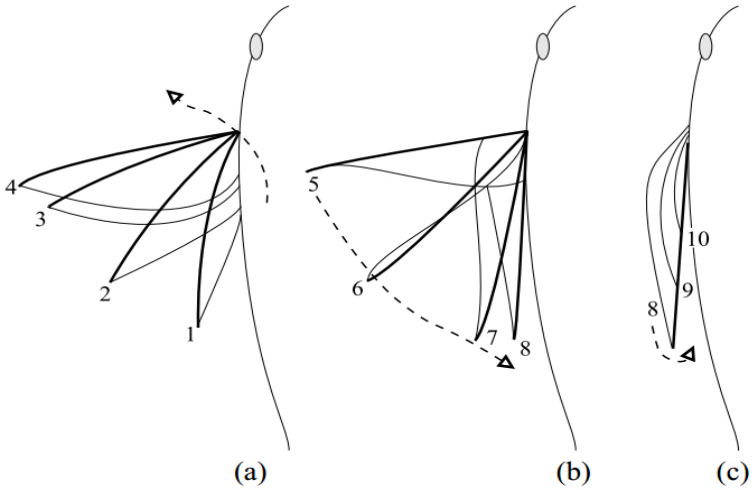

Figure 2.6: Illustrating the motion of median and/or paired fin propulsion [170]. a-c represent the stages of the contraction, which provides propulsion.

2.1.5. Fast Starts and Rapid Manoeuvring

Fast starts are identified as transient bursts of acceleration mainly adopted by fish for predator- prey encounters [35; 36; 38; 40; 41]. Beamish in 1978 defined the three major categories of swimming locomotion: sustained (> 200 min), prolonged (20 s to 200 min) and burst (<20 s) [37]. Under these definitions a fast-start is classified as burst swimming activity where duration lasts for less than approximately 1s. This instantaneous acceleration in a pike has been measured as high as 245 ms^{-2} [38]. Fast-start activity is differentiated by a C-start or S-start pose at the beginning of the contraction stage [39] (Figure 2.7).

This action of acceleration is broken into three stages 1. *Preparatory* (< 30ms), 2. *Propulsive*, 3. *Variable*. The preparatory stage is size and velocity dependent as large fish and faster contractions have greater turning arches. High level accelerations are achieved due to the combination of body motion and high power production effectively being transferred into momentum [40, 41]. An applied technique of manoeuvring at high speed also combines the ability to suddenly stop [42]. This behaviour utilizes the extensions of the appendages to create maximum drag resistance without loss of control and error in orientation.

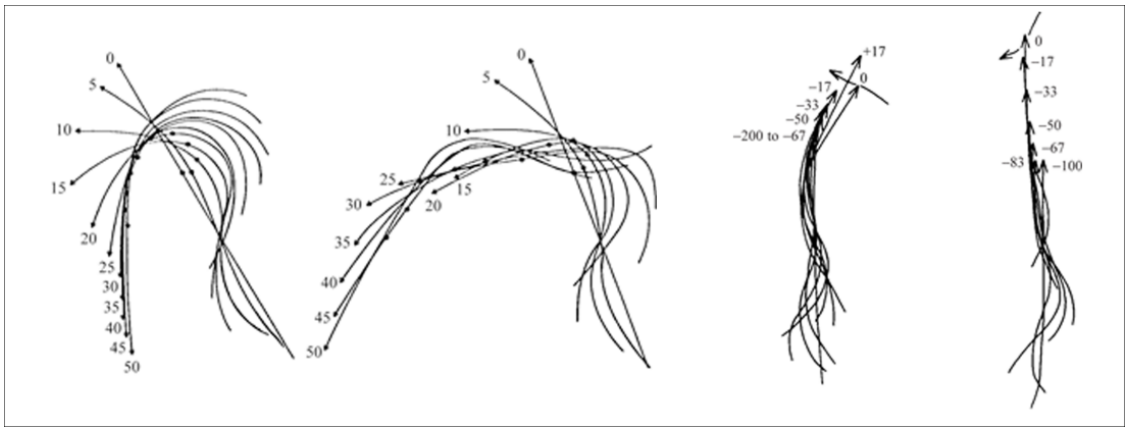

Figure 2.7: The body motions adopted by C-start and S-start acceleration [41].

2.1.6. Drag Reduction Techniques

Displacement of the body during body deformation is estimated to increase viscous drag compared to an equivalent sized rigid body [43]. A boundary layer effect occurs when the velocity of the fluid-body interactions increases and the boundary layer thins increasing shear stress. The surrounding near-body fluid conditions affect the drag resistance. To counteract this fish have evolved optimized drag reduction mechanisms [44]:

- *Friction drag techniques* [111]: mucous layers, riblets (Figures 2.8(a) and (b)) [150; 151], canals, bumps, scales and pores and effluent from the gills, modify the boundary layer by the extension, reduction, suction and the acceleration of flow. Reducing turbulent skin friction, surface shear stress and negative momentum are dynamic mechanisms used to stabilize the boundary layer, prevent separation and provide redistribute of fluid from high to low pressure regions. An injection of high momentum fluid into the boundary layer has the capacity to delay both transition and separation by introducing kinetic energy and extending the laminar region of flow [21]. A significant body of research has been conducted related to viscous dampening and the theory of *Gray's Paradox* which measured a dolphin's thrust at seven times its calculated muscle power. The solution to Gray's Paradox was the exaggerated calculation of drag with turbulent boundary conditions and the dolphin swimming during a burst of acceleration [45].

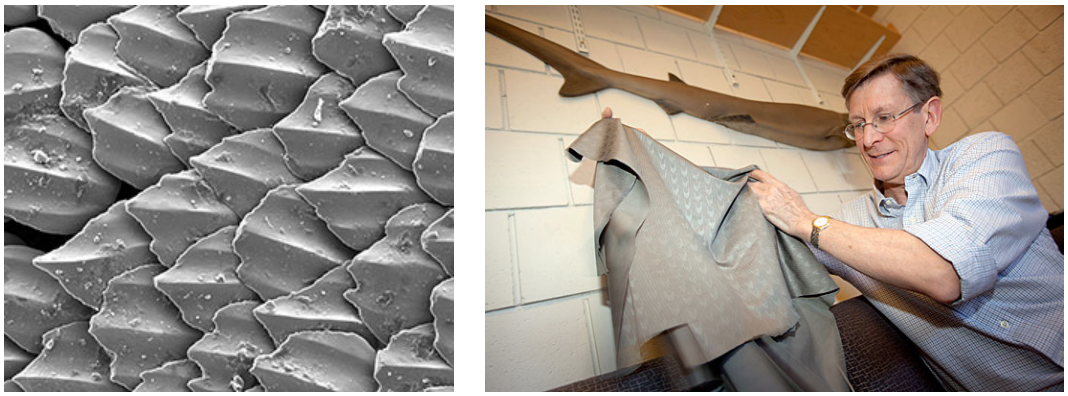

(a) (b)

Figure 2.8: Shark skin scale friction drag reduction techniques, used to develop swimming clothing for athletes and found to greatly improve swimming speed times [150; 151].

- *Pressure drag techniques*: pressure drag is dependent on the interaction of the boundary layer pressure gradient where efficiency can be enhanced by the optimization of a hydro-static streamlined profile. The increase of adhesion of the boundary layer transition from laminar to turbulent along the gradient of the body can reduce boundary layer resistance by favourably positioning the maximum thickness of the cross section, reducing the adverse pressure and adding momentum to boundary layer, preventing separation occurring [43]. Pressure drag techniques include: high aspect ratio caudal fins found on the Thunniform swimming mode [14], control surfaces retraction from drag resistant positions [42] and leading edge manipulation of fluid flows [31]. Leading edge suction adaptions such as the tubercles placed across a whale's flipper can smooth cross flow and delay stall until around 31^{o}, three times the pitch angle of conventional aerofoils, increasing efficiencies to around 20% [46] (Figures 2.9(a) and (b)).

(a)

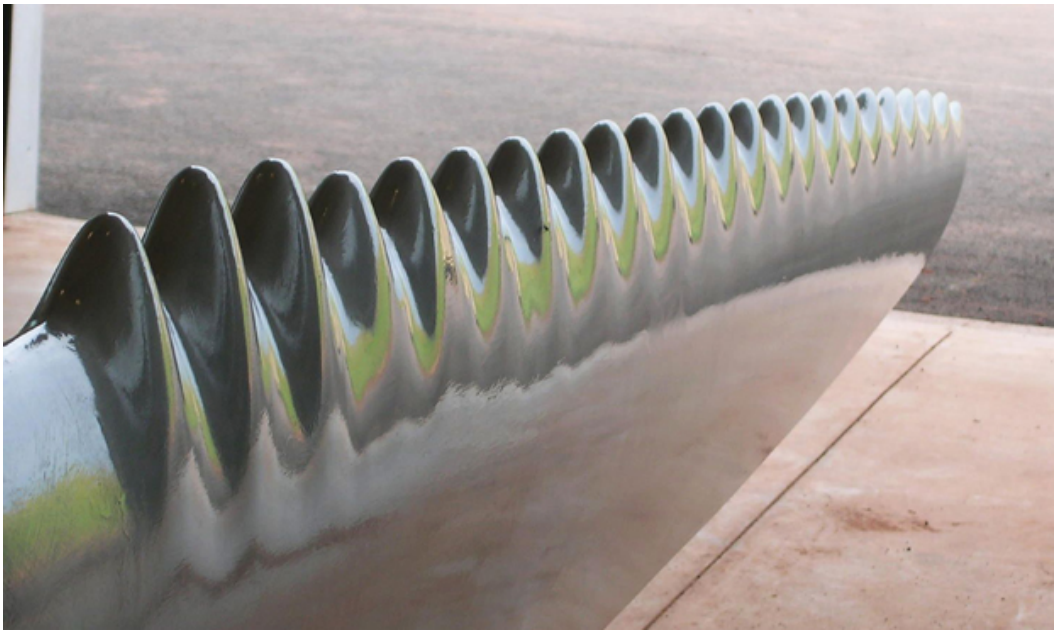

(b)

Figure 2.9(a): Showing the tubercles of a whale's flipper which can smooth cross directional flow and delay stall. Figure 2.9(b): A developed fan blade inspired by the tubercles of a whale and measured to increase energy efficiency. [151; 152].

Drag is directly proportional to the velocity of the moving body squared. As such the high levels of performance are assumed to be dependent on the adaptions which reduce drag and

efficient techniques are applied when possible (such as hitching [47], burst and coast [48,49] and swimming in formation [50]). One of the highest measured swimming speeds is a a Bonito fish (Thunniform) with a length of 0.9m which was measured at a speed of 16.7m/s (60km/h) relating to BL/s = 18.6. The kinematic relationships of the following variables effect velocities and efficiency:

a) Distance travelled per beat (Hz) is governed by amplitude [1; 2; 51; 118].
b) Amplitude increases with frequency up to 5Hz and is typically one-fifth of the body length measured from tail tip to tail tip throughout the cycle [112; 118; 51].
c) Frequency attainability decreases with size of the fish [51].
d) Body flexibility and stiffness controls propulsive wave length [52; 134].
e) Frequency is directly related to velocity, at the highest efficiencies this becomes a ratio close to 1:1 and is suggested to be a benchmark and barrier of producing technically efficient locomotion [17; 118; 51].

These variables, which are used to calculate the Strouhal number can estimate the mechanical power of the propulsive surge, gain the highest propulsive productivity meaning that a fish could use minimal energy to propel themselves over a larger distance [53].

2.1.7. Stability vs. Manoeuvrability

A neutrally buoyant fish moving in a constant straight line motion by Newton's law has instantaneous perfect balance between all the hydro-static and hydro-dynamic forces acting on it. The body of a fish in resting position is defined as stable if the relative position of buoyancy is higher than the centre of mass, due to gravitational forces. This morphological trait is an open loop stability where feedback is unrequired and additional forces must be applied to produce locomotion at the expense of energy. Most fish are classed under the term *Inverted Pendulums* which are closed loop unstable platforms governed by feedback sensors to stabilize [3; 54].

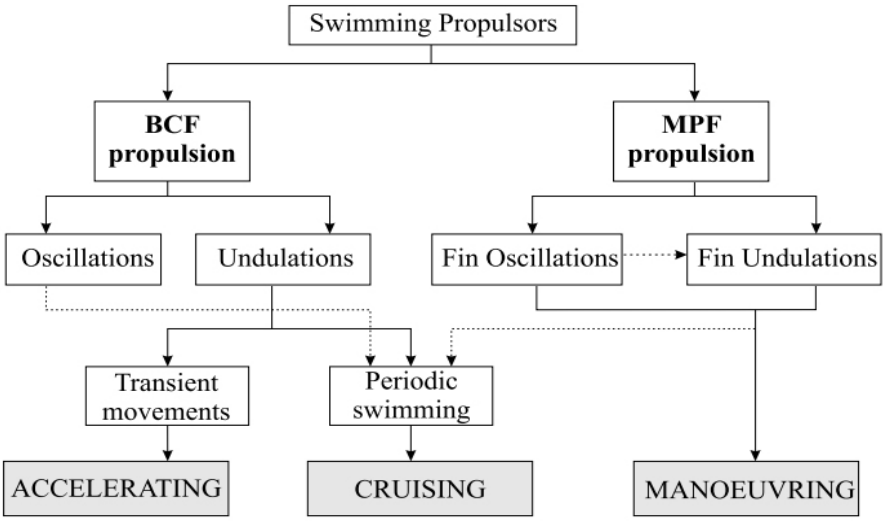

Figure 2.10: The categories of acceleration to manoeuvring [3].

Webb has identified three morphological adaptions: *accelerating, cruising* and *manoeuvring* (Figure 2.10) [119]. Clarifying there is a trade-off between stability and manoeuvrability and an energy trade-off between the requirement to expend energy stabilizing or the need to cause a stable platform configuration to be put in motion [3]. The un-stabilizing lateral forces of BCF propulsion create displacement anteriorly in yaw as the compressed posterior elliptical cross section will pivot the body around the centre of mass. Lighthill suggested that the evolution of vertical compression, reduced depth at the peduncle, increased depth of body towards the anterior along with reactionary forces from the fins minimize recoil forces [55; 112]. Various self-correcting control systems have evolved and been studied which include: the effects of body elasticity [56], recoil movements [57], the interaction of the caudal fin with the vortex sheets shed from dorsal fins [4] and body depth relative to thrust and drag [58].

2.1.8. Computational Investigations

Computational Fluid Dynamics (CFD) and Digital Particle Image Velocity (DPIV) utilize computational techniques to advance the level of data acquisition when modeling three dimension flow patterns of the propagating wave. CFD and DVIP modeling is used to examine the three-dimensional unsteady flow field and patterns, produced thrust, thrust efficiency, lift and drag forces, wake dynamics and pressure fields. These variables and computational techniques can calculate the distribution of pressure, viscous, thrust and

hydrodynamic forces of individual joints and moments along the length of the kinematic model.

Vortex shedding is a non-linear complex effect that can be computationally modelled that analytical modeling simplifies, CFD can improve upon analytical theories by solving the Navier-Stokes equations [59]. DVIP specifically has been used to examine the function of individual fins and their hydrodynamic interaction and flow forces. Through high speed video recording detailed kinematic analysis can be obtained of the acceleration, its flow behaviour and calculated thrust. This can be recorded in three dimensions as the experiment can be conducted twice from the horizontal and vertical planes.

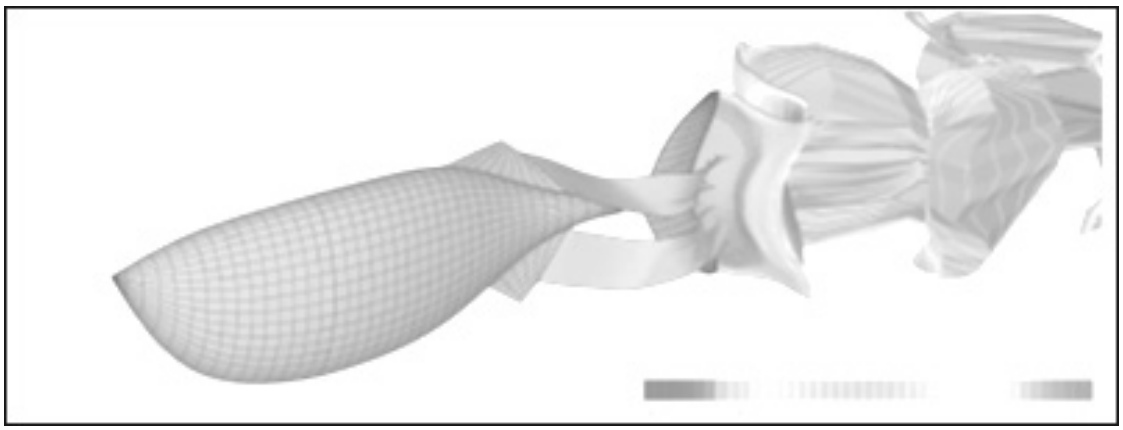

Figure 2.11: 3D visualization of the 3D wake dynamics produced in CFD [6].

Wolfgang *et al* has made a thorough analysis of the propulsive wave of BCF propulsion from the quantitative use of DVIP and CFD modelling processes that enhance the accuracy in calculating flow fields [6]. Flow visualization techniques revealed near-body interaction prior to the peduncle and caudal fin start the manipulation of the bound vortices (Figure 2.11). Due to the displacement of the contracted mid-body a negative bound vortice develops. This is coordinated downward and dispersed into the wake of the peduncle with a positive vorticity. This study of unsteady three dimensional velocity fields has superseded the use of analytical theories that cannot take into account complex modelling techniques of flow fields and wake dynamics. Wolfgang *et al's* numerical and experimental research has shown the formed vortices propagated within the mid-section, detached before the peduncle and are manipulated by the caudal fin to form the increased scale vortical patterns characterized by the reverse von Karman Street. This research has shown that the coordination of vortices is fundamental to propulsion mechanics and is enhanced by the optimizing of the frequency, constructive interaction and spacing of bound vortices [6].

Anderson *et al* made use of DVIP over several experimentations. Particle pairs and edge detection algorithms were used to measure the boundary layer flow vectors and thrust by calculating the displacement over time. The research observed the boundary layer during the displacement of the travelling wave and of a rigid body moving at the same velocity. The results clarified that a swimming fish contends with greater frictional drag than a rigid body fish. The zero velocity of the fluid on the surface of the fish was observed to show no separation during swimming deformation or a stretched straight profile [43].

2.2. Biomimetic Design and Control Methods

The careful examination of the structure of biological systems during analytical, experimental and computational modelling has shown that many drag-reduction and hydro-dynamic techniques are utilized during efficient propulsion. Attempts to emulate these aspects for real world applications have been seen: manipulation of shoals [60], pollution mapping [61], mine detection [13], noiseless electromagnetic field reduction tasks [62] and rigorous littoral conditions where propeller blades become entangled by debris [63]. There are several main aims that are called of a biological inspired machine, a few are identified: prolonged periods of time whilst submerged, station holding in strong flows, precise low speed manoeuvring, sharp turn fast-starts, trajectory planning and power efficient swimming [64].

2.2.1. Conventional Underwater Vehicles

The current requirements of underwater propeller driven vehicles exceeds their agility [13; 65; 66; 67; 68], as the inefficiency of propulsion at low speeds limits navigation during tasks situated in confined, dynamic and unstructured environments [12; 165; 166]. The manoeuvrability of fish in comparison to steady-state hydrodynamic underwater vehicles (Figure 2.12) is contrasted in Table 1 (All data is given where possible).

The comparisons in Table 2.2 indicate that the replication of fishes turning rates, turning radius and sudden acceleration will dramatically improve underwater vehicle locomotive performance [68]. Webb notes there has become a shift in the desired ability of an Autonomous Underwater Vehicle (AUV) from high speed linear velocity to low speed manoeuvring [58]. Navy underwater propulsors and platforms have been engineered over many years and have reached a high level of propulsive efficiency, operating consistently at high velocities but show low efficiencies in turning manoeuvres where a reduction in speed >

50% is required [12, 67]. When operating at low speeds a propeller thrusts perpendicular to the desired direction, the majority of power expelled to rotate is unused and energy conversion is < 40% [34].

Table 2.2: Comparison of propeller driven vehicles.

Mode	Size m	Turning radius BL	Turning Rates °/s	Acceleration g
Fish	0.04 – 0.39	0.00.0.47	425.6-7300.6	8.2-11.2
Marine mammals	0.09-0.24		575-690	5.13
AUV	0.5-3	2-3		
REMUS AUV	1.3	2.9		
USS Albacore	40		3.2	

Rigid bodied hulls have been improved by biological research. A concept design has been proposed that places control surface fins around the centre of mass of an AUV to aid manoeuvring at low speeds [65]. In instances where organisms exhibit superior performance to engineering systems, features of the organism can be extracted for replication as emulating the performance of animals could effectively reduce the time of developing novel engineering solutions [167].

Figure 2.12: Remus-6000 [12; 153].

2.2.2. BCF Bio-Inspired Robotics

The First Robotic Fish -

A significant study by Barrett *et al* at MIT in 1994 effectively applied biomimetic energy efficient behaviours to a robotic system to mimic the oscillating flapping foil motions of

Thunniform propulsion [14; 113] (Figure 2.13). It was built to test behavioural drag-reduction mechanics and demonstrated high levels of mobility during manoeuvring by dramatically improving the rate of acceleration and turning radii in comparison to propeller driven submarines. Robotuna achieved 0.6 BL/s and was constructed with over 3000 parts. Barrett found that swimming drag is lower for an undulating body than that of a rigid body, recording efficiencies as high as 91%; re-examination of the existing data is required. Measuring the utility of these fluid-body interactions has generated focus of improving underwater vehicle propulsion by using biological studies.

Figure 2.13: Robotuna [14].

Generating Acceleration -

The environmental parameters and physical forces vary in every application. Researchers look to the vast morphological traits of nature to provide the most feasible attributes for their system and as such numerous bio-inspired methods have been applied. For example, Triantafyllou *et al* [38] attempted to imitate the impressive starting performance of a pike and calculate the potential stored energy needed to generate acceleration faster than any man-made vehicle, for applications such as station holding in large perturbations. A spring steel beam was covered in urethane rubber and then was held in a 23cm curvature which had 3.8J of potential energy (Figure 2.14). The potential energy in the beam was then transferred into the fluid, thereby accelerating the fish. The acceleration was measured to be $40ms^{-2}$ and maximum final velocity around $1.2ms^{-1}$ compared to real fish with acceleration of 120ms (Table 2.3). The hydrodynamic efficiency of the model was found to be 10% compared to the acceleration of real fish at 16-39%.

Table 2.3: Summary of *Esox* species fast-start performance (Adapted from [38]).

Authors	Common name	Fast-start type	Method (Hz)	Maximum acceleration (m s^{-2})	Maximum velocity (L s^{-1}, m s^{-1})	Duration (ms)	Body length (m)
Weihs [5]	Pike	ER	40	50	–	–	–
Webb [13]	Tiger musky	ER	250	39.5	7.2, 1.6	115	0.217
Rand and Lauder [14]	Chain pickerel	FS	200	21.1 (mean)	9.0, 2.5	92	0.273
Webb [15]	Tiger musky	ER	60	15 (mean)	21, 1.4	–	0.065
Harper and Blake [1]	Northern pike	ER	Acc	120.2 (mean)	10.5, 3.97	108	0.378
Harper and Blake [1]	Northern pike	FS	Acc	95.9 (mean)	8.2, 3.1	133	0.378
Frith and Blake [16]	Northern pike	ER	250	151.3 (mean)	8.7, 3.5	129	0.400

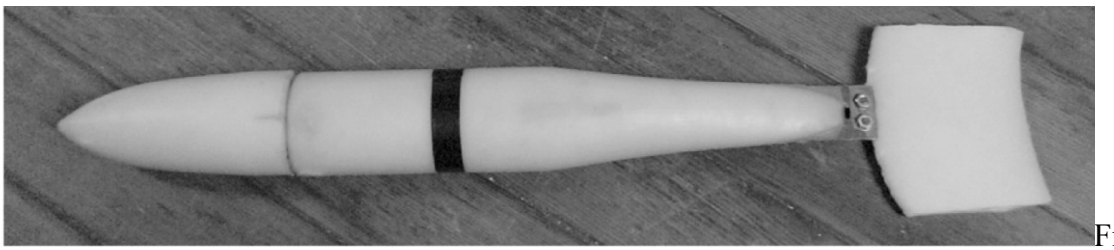

Figure 2.14: A spring steel beam was covered in urethane rubber devised in [38].

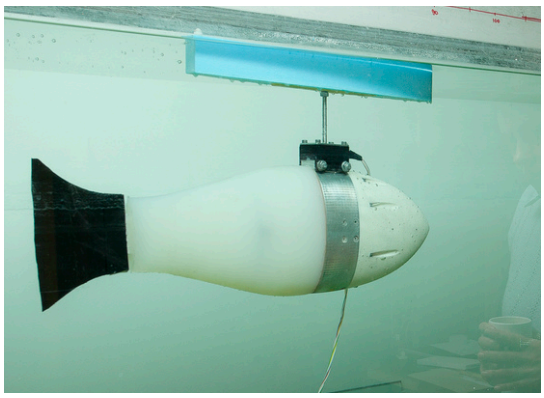

Figure 2.15: The compliant tail structure developed by FILOSE [70].

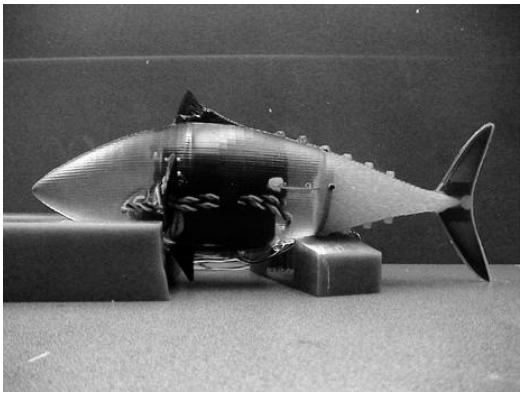

Figure 2.16: MIT's compliant tail structure [69].

Compliant Material Construction -

Valdivia's [69; 117] (Figure 2.16) and Kruusmaa *et al's* [70, 71] (Figure 2.15) approach used a compliant material construction method. They were able to mimic the undulatory swimming motion with a single actuator and have validated their use by producing the highest efficiencies. By varying the stiffness of materials the compliant tail can mimic the body displacements due to the pressure of water. Valdivia has validated its use by finding the highest efficiencies in linear locomotion so far. Reaching 1.1BL/s at 3.5HZ, a quality of this simplification is the opportunity of cheap manufacture, allowing for production of multiple robots that could swarm, map and reduce the time needed to gather data.

Autonomous Robotic Fish -

The first attempt of an autonomous bio-robotic fish was the VCUUV designed by Anderson at MIT [72] (Figure 2.19). This was successfully built upon Barrett's research but an effective autonomous vehicle was not realized until Liu and Hu in 2005, who achieved multiple swimming gaits such as C-sharp turn and cruise straight by applying a digital approximation method [20] (Figures 2.17 and 2.18). By using a discrete assembly structure and optimizing the head swing amplitude significantly improved linear locomotion efficiency.

This discrete assembly method has been found to produce the most advanced biomimetic robotic fish to date and achieved fully autonomous navigation. Current research has extended the multilink joint alignment modelling [73; 74; 75; 76; 77; 78], with improvements in the angular rates of C-sharp turn from 120º to 200º [13; 79], by increasing the lateral wetted area which was found directly proportional to angular force. An efficient C-sharp turn manoeuvre is required for autonomous navigation but the mimicry is still a distinctive margin away as the kinematic replication has proven to be complex fluid- body motion.

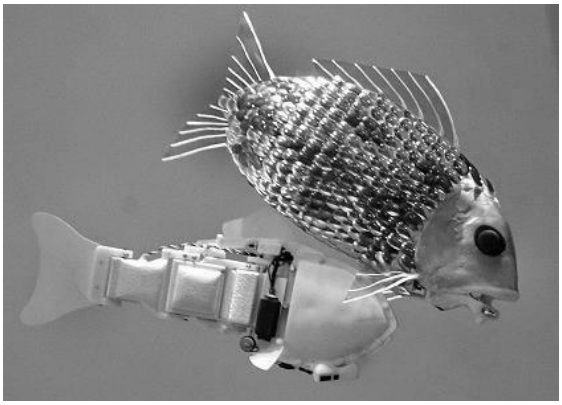

Figure 2.17: The Autonomous G14 [20].

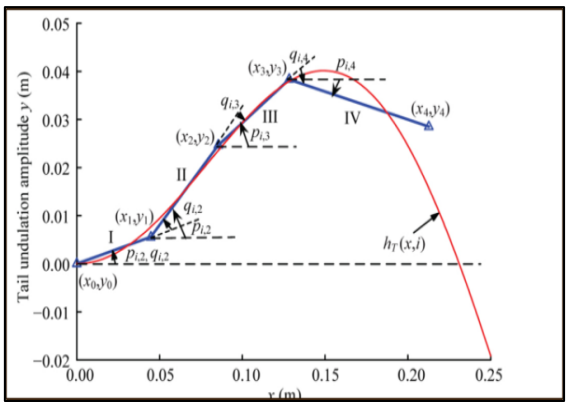

Figure 2.18: Joint alignment overlay of travelling wave [20].

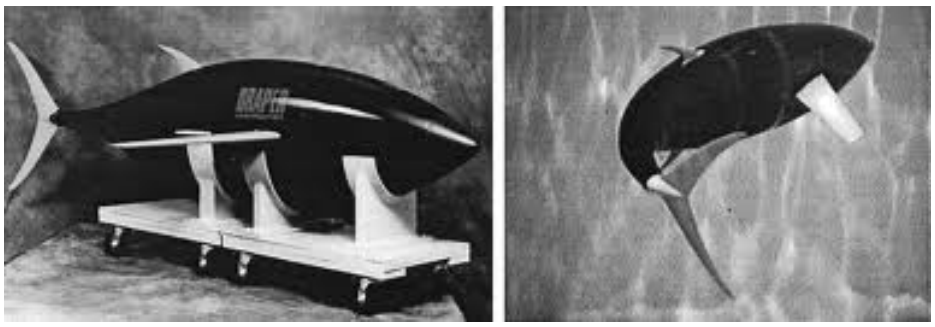

Figure 2.19: VCUUV [72].

Table 2.4: Current robotic fish builds.

Mode	Research Group	Name, Year	C-Turn	Control Surfaces	Autonomous	Actuator	Speed m/s	Length m	Bl/s
Body And Caudal Fin (BCF)	MIT, USA	Robotuna, 1994	N/A	N/A	N/A	Dc Servo motor	1.2	1.2	1.0
	Draper Laboratory, USA	VCCUV Vehicle, 1998	N/A	N/A	N/A	hydraulic cylinder	1.2	2.4	0.6
	MIT,USA	RoboPike	N/A	N/A	N/A	DC motor	0.09	1.0	0.1
	MIT,USA	Compliant, 2004	N/A	N/A	N/A	2 DC motor	0.32	0.3	1.1
	ESSEX, UK	Robotic Fish, 2006	Yes	N/A	Yes	Air cylon. & spring	0.3	0.35	1.0
	Institute of automation, China	Dolphin, 2007	N/A	N/A	N/A	DC Motor	0.8	1.3	0.6
	Nanyang Singapore	Carangiform	N/A	N/A	N/A	Dc Servo motor	0.35	0.65	0.5
	Maritime Research Institute, Japan	UPF2001, 2001	N/A	N/A	N/A	DC Servo motor	0.95 at 9.5 Hz	0.97	0.97
	Beijing University of Aeronautics & Astronautics, China	SPC-III, 2007	N/A	N/A	N/A	10 DC servo motors	1.03	1.6	0.6
	Tokyo Institute of Tech., Japan	Dolphin, 1999	N/A	N/A	N/A	DC servo motors	1.2	1.75	0.6
Undulation (MPF)	Nanyang Singapore	Robot fish, 2005	Yes	N/A	N/A	17 DC servo motors	0.4	1.0	0.4
	National Univ. of Defence Tech., China	Undulating Fin, 2004	Yes	N/A	N/A	DC servo motors	0.7	0.5	1.4
	Osaka Univ., Japan	Rajiform, 2006	Yes	N/A	N/A	DC servo motors	0.4 m/s at 2 Hz	1.0	0.4

2.2.3. MPF Bio-Inspired Robotics

Pectoral Fins -

The theoretical and experimental investigations of flow patterns and wake dynamics by Lauder *et al* [80; 9; 4; 81; 3] (Figure 2.21) Bandyopadhyay [82; 83; 31] and Triantafyllou *et al* [5] have shown the infinity complex nature of three dimensional body displacements

during manoeuvring and linear locomotion. Lauder's extensive body of research at Harvard has shown that Median/Paired Fin swimmers such as the Bluegill Sunfish, continuously counteracts its instability by adapting multiple control surfaces distributed around its centre of mass, simultaneously interacting with each other by creating reactive forces and manipulating the surrounding fluid. Examination of individual components of the control surface has extended this research by controlling curvature [81; 84], the interaction of vortices [33], the configuration of multiple control surfaces distributed around a centre of mass [57; 8; 76] and modular setups to calculate the optimal angle of attack of a lift based propulsion [85].

Gymnotiform Robotic Fish -

MacIver [10] constructed the complex sinusoidal travelling wave of the Knifefish, for its low speed effective control properties and vertical propulsion technique (Figure 2.20).

Figure 2.20: Knifefish Prototype [10].

Figure 2.21: Pectoral fin Mechanism [80].

The propulsive undulatory fin design which runs along the length of the body could enable implementation within a rigid hull. The findings of this study have shown that implementing the capabilities of a Gymnotiform could allow previous underwater vehicles to move omnidirectional over shorter period of time as they record high efficiencies at low speeds. The integration of dexterous fins increases energy expenditure as the production of dynamic control surfaces creates inconsistency and increased propulsive cost. The replication of a multifaceted undulatory fin motion has been tested on Manta ray fin [86] and undulatory pectoral fins [87; 88].

2.2.4. Novel Engineered Structures

The observed similarities in morphological and mechanical adaptions used by marine organisms have evolved along lines of common descent. As such significant irregularities in configuration and mechanical propulsions are not realized. Adherence to natural design may produce impractical results, which will obstruct the development of engineered systems. There are several approaches that show progress in mechanical propulsors based upon biological inspiration: zero-mass pulsatile jets [89], pneumatic rubber actuators [90] (Figures 2.22), simplification [91], conventional AUV's with flapping foils [63], controlling the stiffness of spine [52], electromagnets contained with a soft-body [92], mechanical accumulators [93], Piezoelectric actuators [94], ultrasonic thrusters [95] and wire driven [168].

Soft Body Robotic Fish -

The most recent development in robotic fish is from MIT in 2014 [135] (Figures 2.23), utilizing a small gas pump to drive the tail and provide a posterior confined body motion. The developed prototype also employs a compliant structure, the development aimed to improve the internal mechanical efficiency losses by removing slices from inside the solid silicone tail seen in the previous MIT robotic fish [17]. This development may also provide increased amplitudes for compliant structure robotic fish. Currently the prototype is unable to generate a linear swimming motion.

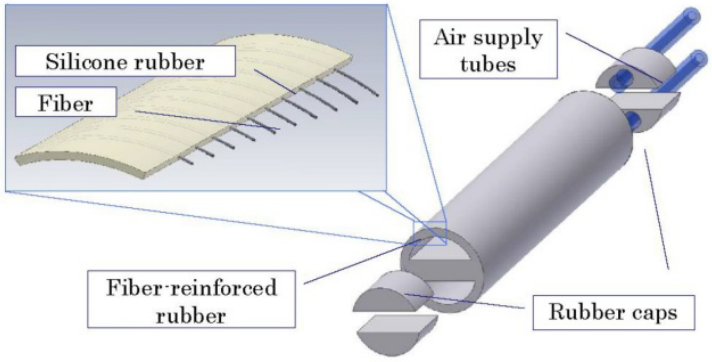

Figure 2.22: Basic structure of the bending pneumatic rubber actuator [90].

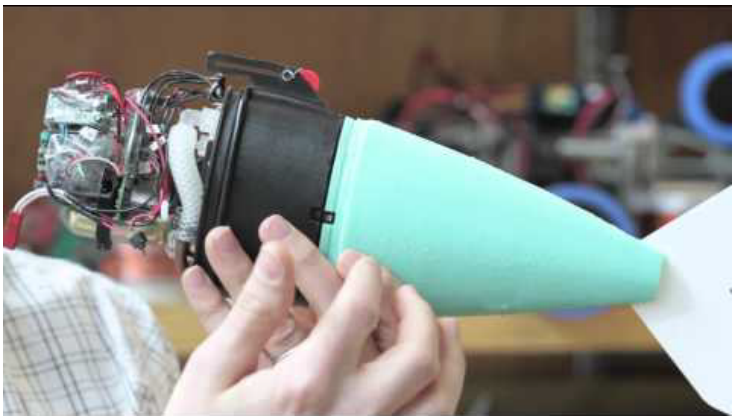

Figure 2.23: Self-contained soft bodied robotic developed in 2014 [135].

Artificial Muscle -

A natural muscle resembles a contracting linear motor which can shorten actively but requires an external force to stretch [96; 64]. The active and mechanical properties of animal muscles serve as a benchmark for artificial muscles. Current artificial muscle work is aimed at the miniaturized vehicles as this technology and has proven potential in centimetre scale robotics as the swimming motion requires less force [97; 83]. A compact biomimetic design structure made of continuous elements that can produce significant bending deformations under low voltages has the potential to be a light, silent and powerful resource for biological inspired robotics. The efficiency of current artificial muscle is low compared to the optimized Dc motor with efficiencies > 95% but the potential has been shown and engineers are progressing away from large, cumbersome materials to small complaint heterogeneous parts [13]. The prominent compositions for artificial muscle are identified as:

- *Ionic Conducting Polymer Film (ICPF) (Electroactive polymers and Conducting Polymers)* – This material's contraction can be created by < 5V ~1Amp and has an efficiency of < 1%. Significant volume change in response to electrical stimulation is provided and the measured electromagnetic field of the ICPF actuator is negligible. Respond time is in the range of (ms – s) and shows high strength (with a low weight) in comparison to the voltage applied (lithium coin [81]). Currently the propulsion is weak and shows lack of long-term stability [81; 96; 98; 99].
- *Shape Memory Alloys (SMA)* – SMA material is capable of changing its crystallographic structure from the change in temperature. Has the advantage of a small size to high force capability, simplicity of actuation mechanism, low driving voltages and silent actuation. Currently the nonlinear characteristics of the phase transformation make SMA actuators

difficult to control accurately. They also show fatigue over repetitive cyclic loading, low energy efficiency requiring comparatively large current requirements and slow response times in the range of (s – min) [62; 83]. Nitinol is one of the most commercially available SMAs, showing a high recovery stress > 500MPa, a reasonable operational strain ~4% and a long life up to 10^6 cycles [83].

- *Carbon Nano tube (CNT)* – This material performs in saltwater and at low frequencies, showing the potential to convert mechanical energy from currents pressures in the ocean into electrical energy. CNT made of durable carbon molecules of the nanometre scale with comparatively high strength. Their small size makes them a good candidate for generating control surfaces [13].

2.2.5. Perceptual Mechanisms

Transient alterations from un-expedited objects and the surrounding physical forces may require a multifaceted platform with the ability of keeping an unstable structure on its desired trajectory without fluctuation. To accomplishing real-time autonomous navigation within the confines of an unstructured and dynamic environment, bio-inspired behaviours and sensory feedback systems must be integrated into a system to achieve precision stabilization and trajectories.

The lateral line consisting of an array of olfactory, acoustical and tactile sensors distributed along the length of the body of the fish utilizes the water flow across the fish's body to detect pressure discontinuities such as disruptions and acceleration in the fluid. (Sutherlin & Waddy 1975; Braun & Coombs 2000) [30]. The aforementioned research by Triantafyllou *et al* has shown that by sensing and selecting favourable conditions in the external flow such as the patterns of the Karman vortex street, there is great potential to improve energy economy. A challenge of achieving real-time autonomy is to constantly and independently recognise and extract the necessary environmental information from the uncertainty of the observation [100]. To complete autonomous navigation, feedback hardware must be implemented within a closed loop system. The task is to apply limited sensors due the constraints of the profile. The necessary sensors are identified:

- *Tactile Sensors* – Navigation can be affected by adverse flow. To counteract this integration of tactile sensors create a closed loop feedback system detecting flow variation where previously external cameras were called upon [101]. Within this research

domain the prominent bodies of work are: A stress-driven flow sensor [102], side-mounted pressure transducers [103], Low *et al*'s fabrication of a lateral line, measuring low level changes in flow pressure and direction [58] and the research team FILOSE, who fabricated and embedded perceptual sensors to detect flow pressure variations and orientate a platform to its desired position [104].

- *Vision based Sensors: 1) Infrared, Camera and Ultrasonic Sensors* – Observational information of the surrounding geometry is gathered by individual or arrays of signal data. These sensors allow for detection of visible changes in the environment. Due to the surrounding fluid noise is created which decreases range resolution (< 80cm for infra-red sensor), localization precision and identification of extracted features. Limitations such as undetectable objects can be resolved partly by applying a threshold to the received data from the accelerometer so that sharp increases in velocity are associated with collisions [100]. *2) Pollution Sensors* – task related sensors can be chosen to detect unwanted pollutants and measure the behaviour of underwater ecosystems, as consistent data acquisition will provide a complete representation of the environment [63].
- *Energy Economy Sensors: 1) Pressure Sensors* – The acting water pressure provides information which can be used to measure the depth, the environment and counteract the added resistance by applying an increased frequencies or force during locomotion at greater depths to obtain a constant linear velocity. As a safety precaution the pressure sensor can provide accurate information to gauge when the underwater vehicle is lifted from its environment [63; 100]. 2) *Rotary Encoder, Voltage and Current Sensors* – Positional feedback and power consumption information of the individual joints can be acquired to calculate a precise measurement of the overall energy economy. The system may include placement of a threshold as an indication of low level battery power [67].
- *Orientation Sensors* - The state of orientation plays a vital part in navigation as unstable structures must constantly re-correct destabilization due to disturbances in the environment and inefficiencies in the propulsion mechanism. The platform must be aware of its state within three dimensions: The *longitudinal-vertical plane* motions are defined as the surge (horizontal displacement), heave (vertical displacement) and pitching (lateral axis) and the *lateral-horizontal plane* which are defined as yaw (about vertical axis), roll (about longitudinal axis) and slip (lateral displacement). A nine degree of freedom (DOF) rotation, acceleration, and magnetic Inertia Management Unit (IMU) are utilized for

stabilizing systems and realising the state of absolute orientation from a calculated angular velocity. An IMU consists of the following sensors: 1) *Accelerometer* 2) *Gyroscope* 3) *Compass.* Miniaturization of IMU's with full measurable angular velocity of *360*º±, allows for precise data acquisition module to be embedded within a small platform [67; 106]. Deploying a solitary IMU will generate inaccurate data as the positional errors will acclimate over time. Hence an IMU should be used in combination with vision based sensors, distance sensors, global positioning systems or other positioning sensors where possible so that a more accurate reference point can be calculated [106].

2.2.6. Behavioural Control Architecture

For the locomotion of an autonomous fish it is necessary to apply a set of rules that governs behaviour. When planning for unknown and unstructured environments the following biological inspired behaviours are identified:

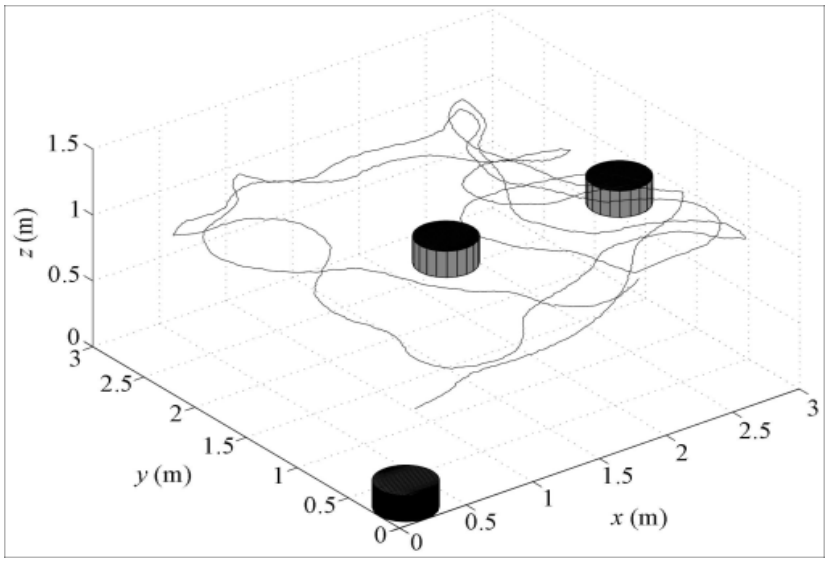

Figure 2.24: 3D platform simulator. Behaviour testing of the G9 robotic fish [107].

- *Mapping Behaviours 1) Object Follow 2) Object Avoidance* (Figure 2.24) [78] *3) Station Holding 4) Straight Swim 5) Straight Swim in Turn 6) Sharp Turn 7) Fixed Plane Locomotion 8) Ascent and Descent 9) Escape* – A real-time motion planning method was employed for the developed G9 build by Lui and Hu as a suitable method to process and respond to the observational information gathered from the vision based sensors [100].

The Behaviour testing of the G9 robotic fish within a three dimensional platform simulator is shown in Figure 2.25.

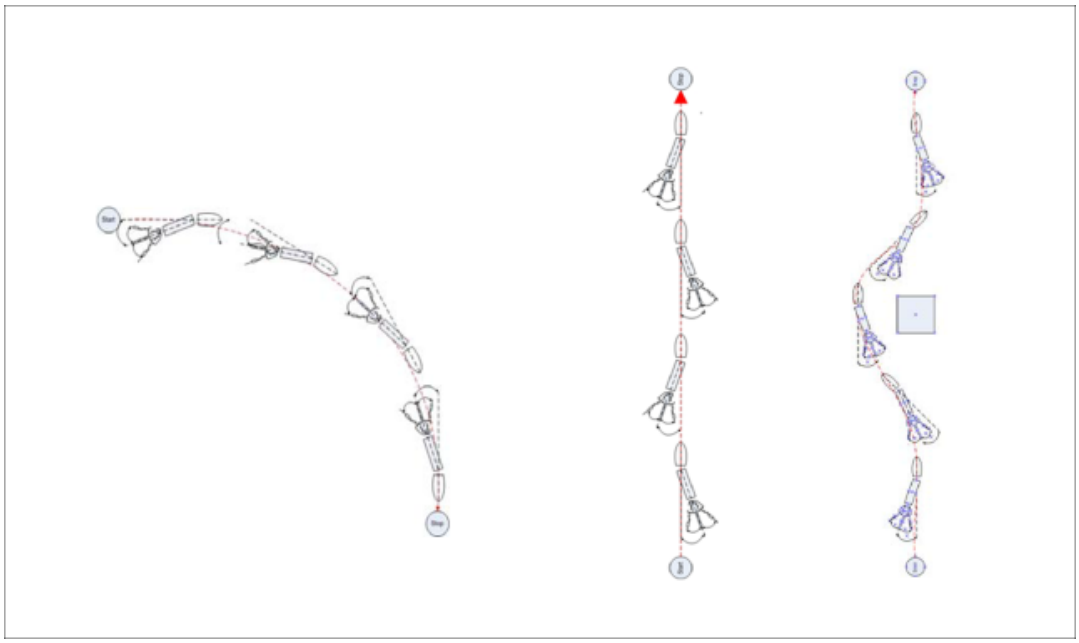

Figure 2.25: Trajectory tracking and object avoidance, aided by an overhead position data system [78].

- *Efficient Swimming behaviours – 1) Periodic Swimming Mode* – Navigation may call various swimming gaits to be applied based upon the available appendages, such as; BCF Forward Swimming, BCF Turning in Advancing, MPF Forward and Backward Swimming, MPF Turning and braking [57]. *2) Efficiency Swimming Gaits* – various swimming behaviours found in nature may be intelligently applied if possible to reduce energy expenditure such as burst and coast, schooling, drafting, hitching and passive resonances with externally created vortices.
- *Safety Behaviours – 1) Recharge and Surface* – An indication from the system voltage sensors will adjust the current behaviour to swim the platform towards the charging station or empty its water chambers to surface and signal for retrieval. AUV's currently make use of a fault tolerant system, if a fault is indicated below a chosen threshold the system can be adjusted and the current task may still be completed [67].

2.3. Summary

This chapter presented an extensive survey consisting of two main sections. Firstly, the intensive research undertaken on fish and underwater mammals was given, thoroughly

identifying the various adaptations in physiology. In particular the swimming mechanics of propulsion were detailed. The individual swimming modes were given (Section 2.1) discussing the fraction of wave length displaced and its effect of swimming performance, indicating the advanced mobility of BCF propulsion. We can see the graduation from Anguilliform to Thunniform within the BCF propulsive mode and its relationship to performance in terms of manoeuvring and the linear swimming efficiency. The swimming efficiency of the diverse swimming motions can be measured by the key metrics given in Section 2.1.2. In particular the swimming speed is measured in BL/s and the swimming efficiency measured in distance travelled per tail beat using the Swimming number. To achieve greater swimming ability we must understand the mechanics of swimming. An outline was given in Section 2.1.3 and thoroughly discussed in the following chapter. Lastly in Section 2.1.6 the various adapted drag reduction techniques used to increase swimming performance were given, identifying that their implementation onto a robotic vehicle may be required for high performance locomotion.

Section 2.1 provided an overview of the most prospective aspects of underwater mobility found in nature. Secondly, the chapter surveyed the developments in the state of the art robotic vehicles (Section 2.2), detailing the capabilities of conventional and biological inspired vehicles. The survey categorised the developed builds and identified their swimming performance. Detailing the gap in performance between conventional propeller driven vehicles (Section 2.2.1) and real fish, furthermore the attempts of replicating the swimming performance were given (Section 2.2.2-2.2.7), where the complex challenge of replicating the manoeuvrability and swimming speeds of real fish is indicated. The second section provided an overview of current engineering within the field of marine robotics from which the research direction was selected.

The following chapter focuses on the investigation of the linear swimming motion of Carangiform fish, initially analysing the kinematics, morphology and swimming mechanics of existing robotic fish detailing their current swimming ability (Section 3.1). The traditional approaches to the problem are detailed (Section 3.3) and prospective future approaches discussed (Section 3.4). The chapter presents the observational studies undertaken on real fish and details the proposed swimming pattern to overcome previous kinematic errors within the wave form. Furthermore the recent mechanical engineering developments are detailed (Section 3.5) and the problems addressed along with possible solutions for increasing the performance of the mechanical drive system.

Chapter 3

Linear Locomotive Swimming and Novel Swimming Pattern

3.1. Introduction

To improve underwater vehicles there are many aspects of locomotion and navigation to address. Linear propulsion could be considered a great challenge to achieve and systemically the first, due to the large gap in speed between current robotic fish and real fish. For example, if we took horizontal plain mobility as the first challenge to overcome and developed a mechanism upon the current low speeds of robotic fish, the fluid body interaction may be vastly different from a platform that has a high maximum velocity equal to real fish, as the reaction time to turn is reduced and the required forces are greatly increased. This problem also relates to many other aspects in mobility, behavioral techniques and communication.

Detailed in the previous chapter current UV's have particularly high cost of transport during low speed mobility [66]. This is where fish excel, generating large transient forces efficiently by coordinating their body motion [112; 1]. In addition, adversely the dynamic environment can be advantageous to fish locomotion, as they demonstrate the ability to extract energy from the upstream vortices [11]. There is great potential to improve UV's by imitating the propulsive motion with the highest locomotive performance, operating within the desired environment and Reynolds numbers. Although most work within the field of biomimetic underwater propulsion has focused on the hydrodynamic mechanism, there are

still many aspects of locomotion to address. The current design approaches of robotic Carangiform swimmers have achieved low speeds which are unpractical for real world applications, peaking at 1.1BL/s. In comparison, live fish are able to attain an average maximum velocity of 10 body lengths/ second [51; 118]. A single high performance of a Cyprinus carpio was noted, achieving the swimming speed of 12.6BL/s (1.7m/s) with a Swimming number (*Sw)* of 0.66. (Some studies found the a average maximum velocity of 6BL/s [112])

BCF swimmers have the fastest recorded swimming speeds in nature. Therefore the investigation of the BCF swimming mode during linear locomotive swimming was selected for replication. Modeling from body and/or caudal fin (BCF) swimmers, the chosen Carangiform swimming mode can be identified by the wave length and amplitude envelope. The Cyprinus carpio (common carp) has been chosen specifically for its high locomotive performance [118]. In particular, the distance travelled per tail beat of the common carp is highly efficient measuring a *Sw* of 0.66. The distance traveled per body length during one caudal fin oscillation is a prominent parameter for analyzing body and caudal fin locomotive performance. The common carp's swimming effeciency is only second to the swimming motion of the Tursiops (Bottlenose dolphin) with a *Sw* of 0.82.

The research project investigated the contributing factors to the low hydrodynamic performance of current robotic fish within linear locomotion and proposed two main objectives for the background analysis:

(1) Undertake intensive observational studies of real Carangiform fish, identifying the kinematic parameter's errors in comparison with robotic fish and recorded data from biological studies.

(2) Identify the factors within the mechanical drive systems of current robotic fish that influence the current low linear locomotive swimming speeds.

3.2. The Traditional Approach

Accurately replicating the kinematic parameters of the linear swimming motion has proven to be difficult and free swimming robotic fish have significant kinematic parameter errors. The lateral and thrust forces are not optimized and as a consequence excessive anterior destabilization in the yaw plane due to the concentration of posterior thrust creates reaction forces (F_R) around the centre of mass. In turn the anterior creates posterior displacement errors. As a result the body wave motion along the full length of body has large matching

errors in comparison to the swimming patterns of live fish, leading to reduced performance and high cost of transport.

The required propulsion method of straight line swimming can be calculated using the Reynolds number (*Re*), defined as $Re=UL/v$, where U denotes the speed, L denotes the body length and v is the viscosity of water. Re relates to the ratio of inertia to viscous forces. If the *R*e is large, the viscous forces are negligible (*Re* 10^3-10^7) [122]. Viscous force is dominant when the body length is approximately <1mm. The two methods of propulsion are categorized as: (i) Inertia Force Propulsion, generating locomotion by creating a F_R against the mass of the water. (ii) Resistance Force Propulsion, adopting a kinematic motion to generate locomotion from the viscosity of the water.

The kinematic swimming motion during linear locomotion of the common carp is studied due to its high locomotive efficiency [51; 118]. The selected Carangiform is categorised under the body and/or caudal fin swimming mode and applies the swimming method of inertia force propulsion, identified by the portion of the body length actively displaced i.e. wave form and amplitude envelope. The form of this propulsive segment, within the horizontal plane is traditionally represented by a travelling wave. This body motion, adopted in previous robotic fish builds (Thunniform, Sub-Carangiform and Carangiform) applies a rigid mid-body and anterior, concentrating the undulatory motion to the posterior end of the lateral length. Typically limited to <1/2 of the body length, the posterior propagating wave smoothly increases in amplitude towards the tail, consisting of one positive phase and one negative phase [112]. The commonly adopted model proposed in [113], is in the form of:

$$y_{\text{body}}(x,t) = \left(c_1 x + c_2 x^2\right)\sin\left(\text{k}x + \omega t\right) \qquad (3\text{-}1)$$

where y_{body} is the transverse displacement of the body; x is the displacement along the main axis starting from the nose of the robotic fish; $k = 2\pi/\lambda$ is the wave number; λ is the body wave length; $\omega = 2\pi f$ is the body wave frequency; c_1 is the linear wave amplitude envelope and c_2 is the quadratic wave.

The parameters P = $\{c_1, c_2, \text{k}, \omega\}$ can be adjusted to achieve the desired posterior swimming pattern for an engineering reference, shown in Figure 3.1.

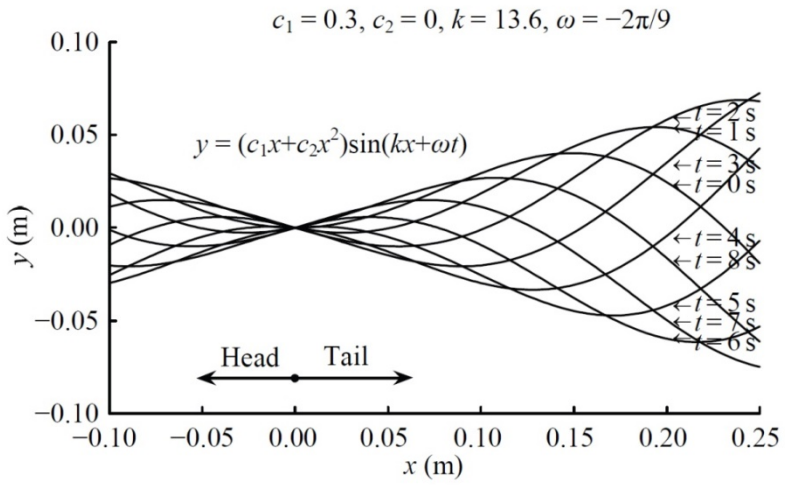

Figure 3.1: An example of the traditional approach to modelling the body wave displacements [20].

3.2.1. Robotic Fish Kinematics

Although most work has focused on hydrodynamic mechanisms, current robotic fish are unable to gain the locomotive efficiencies of live fish, proving a complex challenge. There are two limitations in particular:

(i) They cannot achieve accurate replication of the linear swimming motion as free swimming robotic fish generate kinematic parameter errors and therefore reduced propulsion (Section 3.3.1).

(ii) They have low force transfer due to the complexity of developing the powertrain, limited by inaccurate mass and volume distribution, low force and frequencies and internal mechanical losses, detailed thoroughly in Section 3.5.

Below the two most developed free swimming robotic fish are detailed identifying their generated kinematic patterns and swimming performance in terms of distance travelled per beat and body lengths per second:

G9 from Essex -

The developed build from Lui and Hu [20] is an autonomous free swimming robotic fish able to swim at 1.02 BL/s. Their approach to implementing the kinematics of the swimming motion was to apply the traditional posterior confined body wave motion to generate propulsion. It can be seen in Figure 3.2 that the anterior amplitude was larger than the posterior amplitude. This is a critical problem of free swimming robotic fish. In consideration of this, the following equation was developed to take into account the large head swing

amplitude which is the result of unstable reaction forces along the body length [20] (Figure 3.3). This equation is defined as:

$$y_{\text{body}}(x,t) = \left(c_1 x + c_2 x^2\right)\sin\left(\mathrm{k}x + \omega t\right) - c_1 x \sin\left(\omega t\right) \qquad (3\text{-}2)$$

The amplitude measurements given in Table 3.1 are in degree, measured from the maximum head swing amplitude within the cycle. Without the measurement of the central pivot point the amplitude measurements cannot be used as an accurate measure of amplitude. However, we can see that reducing the amplitude of the anterior was successful in increasing swimming speed and improved the accuracy of the posterior kinematics by reducing the recoil and therefore the generated forward resistance.

We can use the data given in [20] to calculate the swimming efficiency of the reduced head amplitude of G9 by applying the equation (3-2), which was employed to improve swimming performance, by using the Swimming Number [118]. This measure provides us with a gauge of the distance travelled per tail beat (This measurement does not take into consideration the energy consumption, which must be recorded experimentally). We can see the traditional approach (Method A) measured a *Sw* of 0.47 and a swimming speed of 0.6BL/s and the applied swimming motion to compensate the recoil (Method C) measured a *Sw* of 0.78 and a swimming speed of 1.02BL/s (Within the measurement of *Sw* we must also take into account the drifting caused by the generated speeds of G9). Although the swimming speeds are low in comparison to real fish the method of reducing the anterior amplitude to generate accuracy of the posterior kinematics greatly increased the swimming performance of G9. It is noted that the recorded reduced head amplitude is still far greater than observed in real fish, which is described in Section 3.4.

Table 3.1: The amplitude angles of the head and tail for comparison between methods. We can see the improvement by applying Method C [20].

	Ideal swimming	Method A	Method B	Method C
Head Swing amplitude A_h	33.4	43.9	36.5	34.8
Tail flapping amplitude A_t	31.3	24.5	32.8	32.1
Swimming speed S_b	2.00	0.62	0.83	1.02

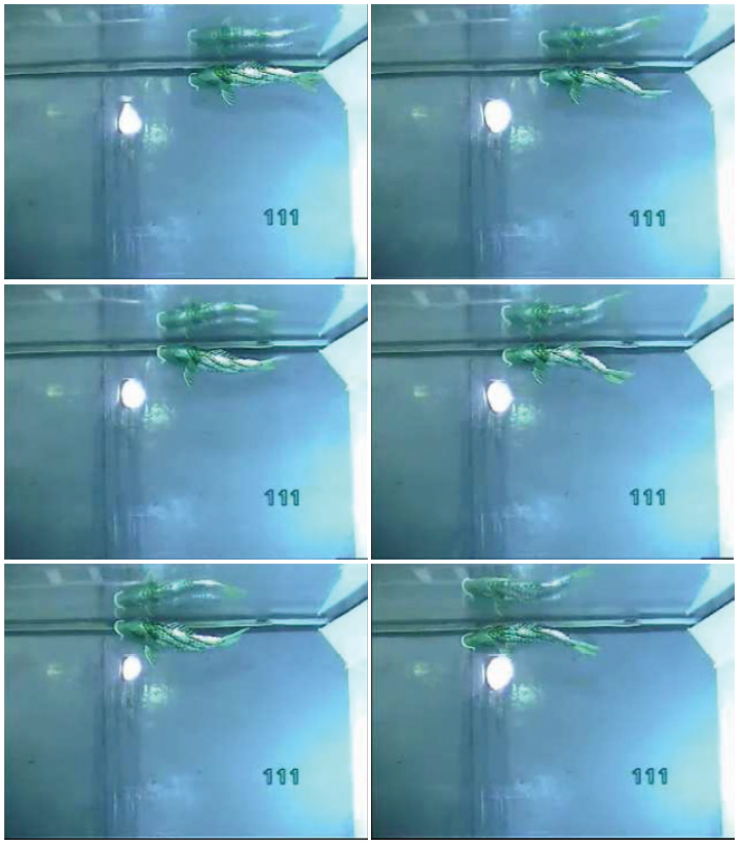

Figure 3.2: Video sequence of G9 during straight-line swimming, achieving 0.2m/s at 0.5Hz. (time step of 1s between clips). We can see the large anterior recoil parameters as given in Table 3.1) [20].

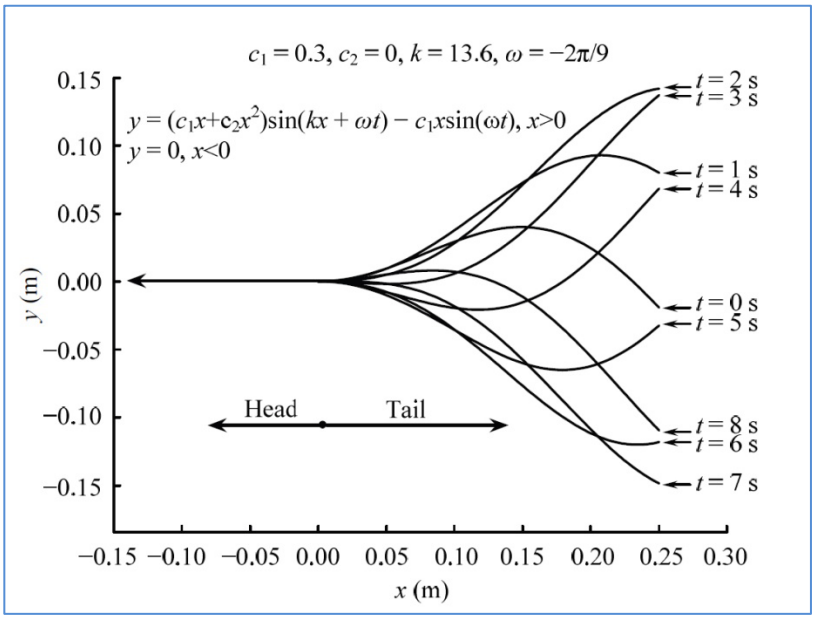

Figure 3.3: The generated body displacement taking into account the head swing amplitude [20].

Compliant Structure from MIT –

The devised compliant structure with a body length of 0.3m by Valdivia y Alvarado [69; 117] achieved 1.1BL/s at 3.5Hz with a force production of 0.2N. The kinematic data of the swimming motion over the full body length was not given in published papers, however we can use the video data given to assess the swimming motion by making snap shots of the prototype during swimming at its maximum velocity. Shown in Figure 3.4 we can see that the anterior amplitude is approximately equal to the posterior amplitude, therefore generating significant kinematic parameter errors within the body wave (Figure 3.5).

Figure 3.4: Video sequence of the compliant structure during linear locomotion. The anterior amplitude is approximately equal or greater than the posterior amplitude [154].

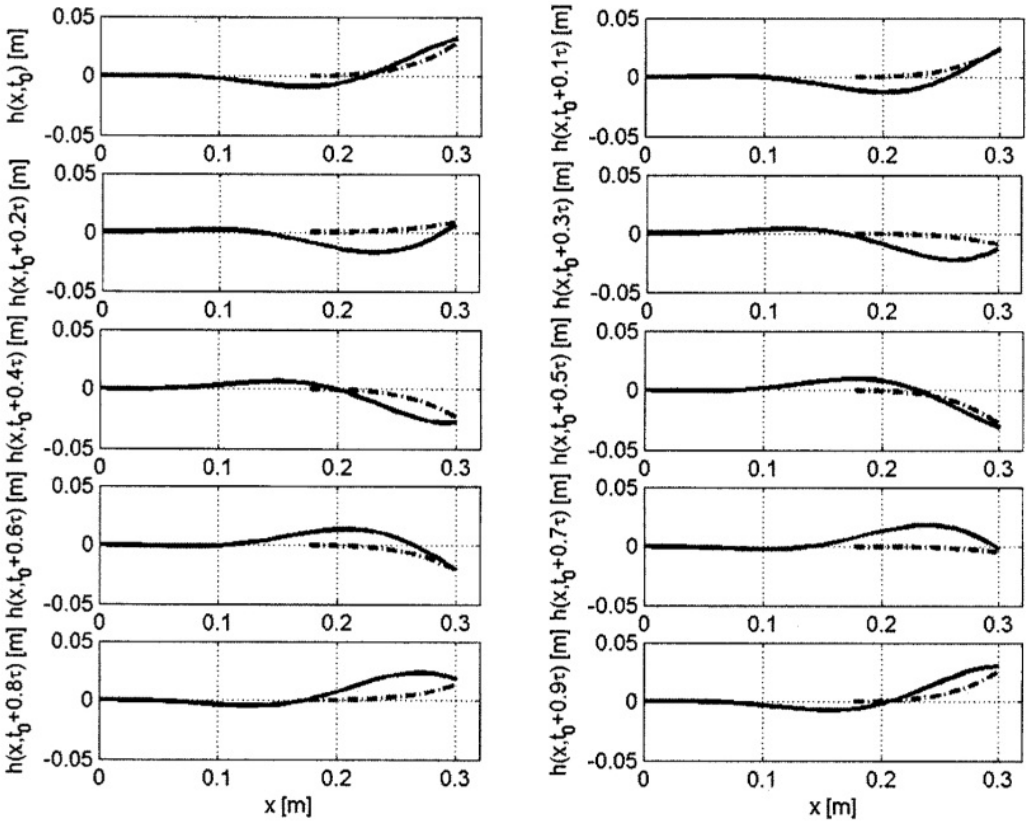

Figure 3.5: Comparison of desired and modelled kinematic behaviour for Tail 1. (-) Desired, (- -) Model [69; 117].

The posterior kinematics were closely analysed whilst the anterior to mid-body portion of the body is held rigid by a support beam. In Figure 3.5 we can see the errors. In particular the posterior amplitude is smaller than required and without the flexibility essential to generate the undulatory motion with precision, due to the construction of the build which is discussed in Section 3.5.2. We can calculate the swimming number using the data given which provides a measure to identify the efficiency of the swimming pattern. We can see the prototype measured a *Sw* of 0.30 at the swimming speed of 1.1BL/s. The achieved *Sw* of the compliant structure is lower than G9 [4] therefore if the G9 drive system was able to raise its frequency to equal 3.5Hz its maximum velocity would be far higher. The limitations of the discrete link structure of G9 are discussed in Section 3.5.2.

3.3. The Proposed Full-body Swimming Pattern

Observational studies were undertaken to investigate the kinematic pattern and morphological structure of the Carangiform swimming motion during straight line swimming. This study was conducted as current robotic fish have significant kinematic errors compared to the conventional travelling wave model (shown in Figure 3.1) and real fish as detailed in the following section (shown in Figure 3.6).

3.3.1. Observational Studies & Proposed Kinematic Pattern

By comparing Figures 3.1, 3.2, 3.4 and 3.6 we can see the simplified travelling wave is not a precise replication of the Carangiform wave form during linear locomotion. Shown in Figure 3.6 is the tracked midline of a common carp, measured by Nagai [118], the parameters are identical to the studies of Videler in [160]. The generated image provides measurements of the posterior amplitude, wave length, curvature, anterior amplitude, central pivot point and the body length of a comparable sized fish (36cm).

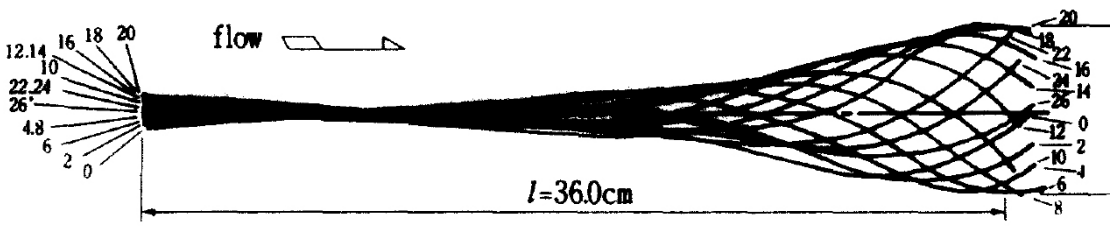

Figure 3.6: The midline parameters of a common carp during locomotion. We can see the small anterior amplitude produce by real fish [118].

Figure 3.7 shows a Sub-Carangiform rainbow trout fish during cruise swimming. The original video capture was recorded at Bath University [158]. The figure shows the provided video cut into snap shots so that we can analyse the morphological and kinematic parameters closely. Although the fish is only swimming at cruising speeds, we can see that the outer profile when viewed on maximum curvature (Images 3 and 6) throughout the body wave cycle has one lateral length is almost completely flat approximately from the head to the peduncle. This profile is comparable to an aerofoil in which one side is longer in length generating a pressure and velocity variation in the surrounding flow [161].

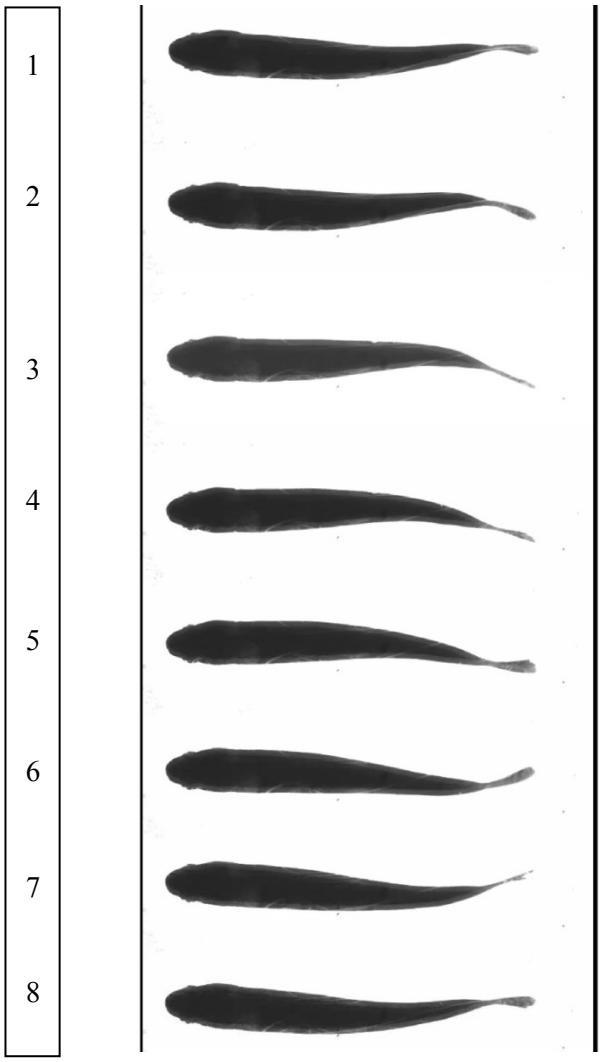

Figure 3.7: Rainbow trout swimming in a laminar flow in the test tank of Bath University [158].

We can therefore assume the swimming fish shown in Figure 3.7 may be applying this method of propulsion to increase propulsive efficiencies. We can also see that the midline has

a slow curvature from the anterior tip to tail tip. Although the curve has a shallow camber, the anterior and mid-body motion might be crucial in improving the swimming propulsion. By comparing the swimming motion to the swimming motion traditional employed for propulsion (Figure 3.1) we can identify large differences within the kinematic wave along the length of the body.

The efficiency of fish and their dexterity is highlighted during the analysis of the interaction with the *Karman Street Vortex*. This is an array of detached vortices with alternating directional velocity, as illustrated in Figure 3.8 (It is noted that the wake of an undulating fin is the reverse of the well documented *Karman Vortex Street*). When a flexible passive body resonates within the flow patterns dispersed from an upstream bluff body (*Karman Vortex Street)* forward locomotion can be created from negative power [30]. These tests were carried out using a dead trout and a passive flapping foil and found that both foils could extract sufficient energy to overcome drag. In Figure 3.9, we can see the flexibility of a rainbow trout which can curve the anterior, mid-body and posterior body sections. These experiments were undertaken to understand the morphological structure within the horizontal plane. Snap shots of the experimental testing undertaken by MIT of a deceased trout during fluid-body interaction with the fluid flow of the *Karman Street Vortex* are shown in Figure 3.10. The rainbow trout at certain stages of the body cycle adopts a greater camber than during low speed swimming seen in Figure 3.7. Hence the displacements within the midline curve are greater in the anterior and mid-body.

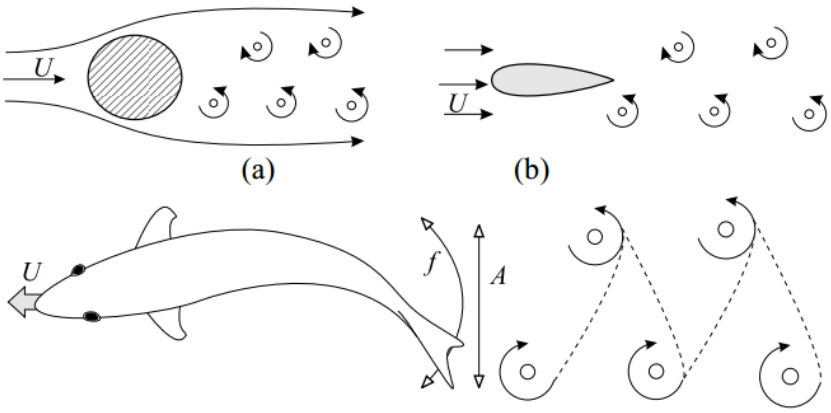

Figure 3.8: Illustrations of the Reverse Karman Vortex Street and Reverse von Karman Vortex Street [7].

Figure 3.9: A deceased trout during experimental testing of its curvature.

Figure 3.10: A deceased trout during fluid-body interaction with the fluid flow of the *Karman Street Vortex*. We can see the large camber generated and smooth curve from head to tail [156].

Figures 3.11-3.12 show snap shots of a Carangiform common carp during high speed swimming approximately above 3BL/s. The footage was taken from a video of koi carp within a large garden pond. The figure shows that the adopted swimming motion applies a smooth curvature from head to tail with greater camber than the measured camber of a slow cruising fish (Figure 3.7). Notably the camber is approximately accurate to a fish during interaction with the *Karman Street Vortex* (Figure 3.10) and Figure 3.6 and 3.7. The observed midline parameters are attuned with the measurements of Lighthill [112] whose finding measured fish to have increased amplitudes up to tail beat frequencies 5Hz.

Through the investigation into the Carangiform swimming motion we have found that the traditional approach of posterior confined kinematics has significant errors. The observations of real fish and the published studies have provided the key parameters of the full body motion swimming pattern that must be implemented to replicate an accurate body precise to Carangiform fish. By applying this method robotic fish may use less energy to propel themselves over larger distances as the same fluid body interaction applied by real fish may occur. The observed posterior amplitude of live fish is 0.1 of the body length, measured from

the midline to the furthest lateral tail excursion. The location of the pivot point is optimum at 0.15-0.25 [118]. The anterior amplitude measured at the furthest tip on the head is optimal in the range of 0.04. Large or small amplitudes generate a body motion pattern with inaccurate parameters which directly relates to a reduction in efficiency [21].

Figure 3.11: A Koi Carp during cruise swimming. The outer geometries within the horizontal plane are comparable in profile to a lifting foil.

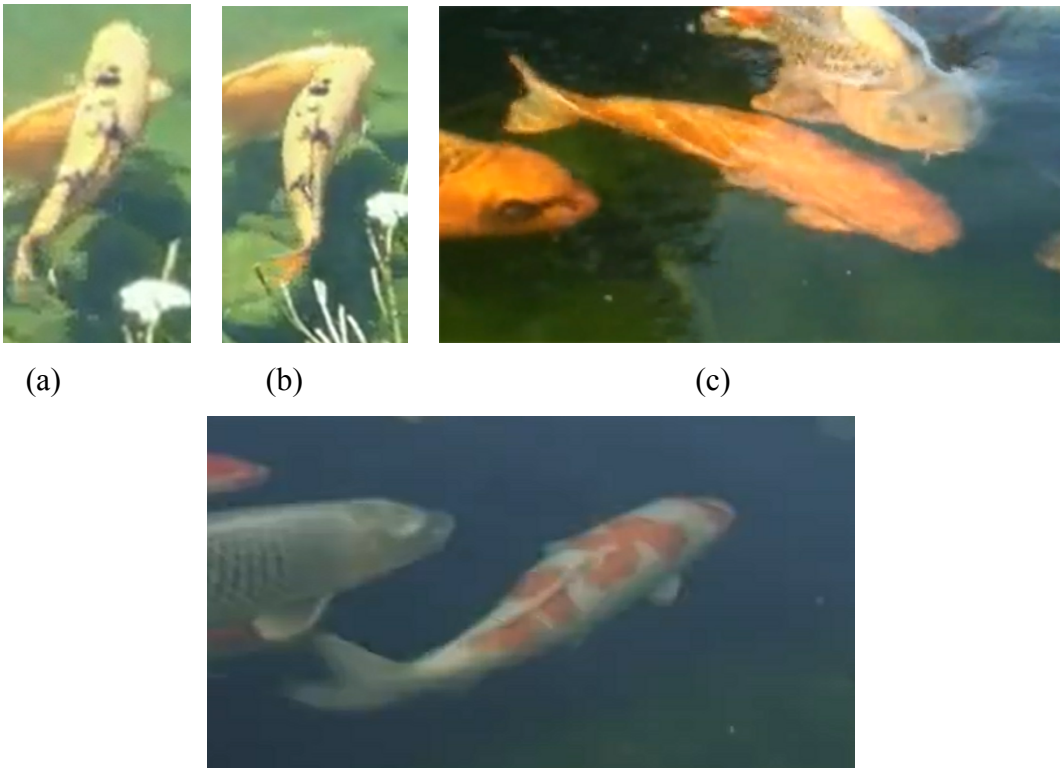

(a) (b) (c)

(d)

Figure 3.12: Carp during linear swimming. We can see the smooth curvature from head to tail and the outer profile resembling a lifting foil.

As detailed in Section 3.3.4 fish generate forward thrust by transferring momentum from their body muscles or fins to the water effectively. There are two prominent methods:

(i) Lift-Based (or vorticity) method

(ii) Drag-based (or added mass) method

Most fish have evolved employing the method of added mass, where by the passage of transverse body waves along the body towards the tail (as adopted by the selected common carp). Lift based propulsion is traditionally only considered for lunate tail propulsion methods. Here we propose that the outer profile is accurate with the profile of an aerofoil and therefore Carangiform fish may also produce propulsion thrust by combining lift based propulsion with added mass.

It has been observed that the aerofoil section NACA (12)520 based on camber, chord and thickness can be utilized to illustrate the outer structure profile of Carangiform fish on its maximum midline curvature [162]. As seen in experimental testing of aerofoil once the anterior tip is offset over a certain degree from center, the fluid flow is stalled, therefore increasing resistance during forward motion [34; 163; 164]. We can apply this fluid-body interaction to the problem of large anterior amplitudes during free swimming of robotic fish.

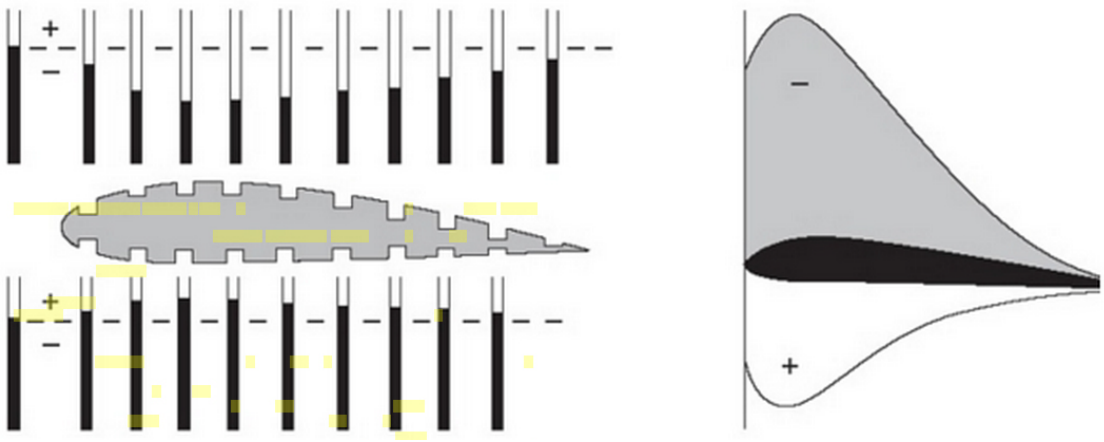

Figure 3.13: Pressure distribution around a lifting foil. (+) Indicates an increase in pressure. (-) Indicates a decreased pressure in the surrounding air flow. The individual bars illustrate the pressure variation at each point of the aerofoil [161].

The following describes the method of lift based propulsion, from which we can relate to the observational studies and the mechanics of swimming: as a lifting foil passes through fluid the displacement of the fluid around it generates forces which act upon the foil (Figure 3.13). Considering the differences in the pressure above and below an aerofoil or hydro foil in a fluid as the fluid density remains the same at the swimming speeds of real fish we can gauge, that there are differences within the velocity of the flow [161]. Figure 3.13 shows Lanchesters circulation theory, the typical pressure distribution around a lifting foil, illustrating how the velocity differences arise. We can see in Figure 3.13 the aerofoils profile

is identical to the observational studies of fish during low swimming speeds shown in Figures 3.7 and 3.11-3.12. Hence lift forces may be generated from a net difference in the pressure of the fluid on either side of a fish.

3.3.2. Proposed Kinematic Parameters

As previously mentioned, accurately matching the kinematic data of real fish is complex and free swimming robotic fish applying posterior confined displacements have shown kinematic parameter errors [20; 117]. In particular, the lateral (F_L) and thrust (F_T) forces are not optimized. As a result, large anterior destabilization in the yaw plane is generated due to the concentration of posterior thrust, recoiling around the center of mass. Consequently the inaccurate anterior kinematics create significant posterior midline displacement errors. Hence, the linear locomotive swimming motion over the full length of body has large matching errors in comparison to real fish leading to reduced propulsive force and a higher cost of transport.

Added Mass **-** Propulsion of Carangiform swimming is associated with the method of added-mass [119]. As each propulsive segment of the travelling wave passes backwards along a fish, the momentum of the water passing downstream is altered. This causes a reaction force F_R from water onto the propulsive segment. F_R normal to the propulsive segment is decomposed into the lateral F_L component which can lead to energy loss and anterior destabilization and the thrust F_T component providing propulsion increasing in magnitude towards the tail. The overall magnitude of added-mass passing downstream can be approximated as the water mass accelerated and its acceleration.

The precise motions of the structures of real fish have been observed during locomotion. It was proposed to improve the large kinematic errors seen in robotic fish, that the first stage is to precisely replicate the observed swimming kinematics within the horizontal plane. The challenge is to significantly reduce the anterior amplitude of free swimming robotic fish and achieve a midline curve alignment with the observed parameters of a common carp along the full body length. This is estimated to generate higher performance based on the propulsive method of added mass. Hence the following body motion parameters of a full-body coordinated swimming motion was proposed, established based on the undertaken observational studies (Figures 3.7 and 3.11-3.12) and published data (Figure 3.6) from literature, which have provided an initial engineering reference. The wave form motion first

developed for a discrete rigid anterior prototype in [20] can be extended to represent the proposed full body motions in the form of:

$$y_{\text{body}}(x,t) = \left(c_1 x + c_2 x^2\right)\sin\left(\mathrm{k}x + \omega t\right) - c_1 x \sin\left(\omega t\right) \qquad (2)$$

The relationships between the defined parameters P = $\{c_1, c_2, k, \omega\}$ can first be found by evaluating the x location pivot at 0. The results of applying the equation (2) to the G9 platform's posterior swimming motion reduced the head swing of the G9 build by 42%, so that the head amplitude was approximately equivalent to the posterior amplitude. Although the generated maximum swimming speed was low the equation was the first development in reducing the recoiling motion in free swimming robotic fish and showed the potential to generate further improvement in swimming speeds by tuning the kinematic parameters and therefore the reaction forces. Therefore it was proposed that initiating the starting moment of added mass upstream and optimizing the F_L and F_T forces around the center of mass will increase the overall magnitude of thrust contributing to increased forward velocity.

Fraction of body displaced –

In the kinematic pattern of the proposed full-body length swimming motion the fraction of body length displaced is equal to the Anguilliform swimming mode (Figure 3.14(a)) but reflects changes in the wave form. In Figure 3.15(a) we can see the Anguilliform swimming pattern is defined by large amplitude undulations propagating from nose to tail. The newly introduced full-body coordinated motion applies an oscillatory motion to head and mid-body and pivots the entire body around a single point associated with the Carangiform fish swimming motion [2].

Although this is the first account to propose a full-body length body motion, mechanisms such as "vortex peg" or "undulating pump" (Figure 3.16) and flow visualization techniques have been proposed [23][6] from published biological studies, indicating a possible fluid body interaction that contributes to propulsive thrust is generated upstream to the posterior section. The muscle activity in the anterior has been measured to be low, suggesting that accurate modeling of the kinematics could be more significant than anterior force in improving energy transfer.

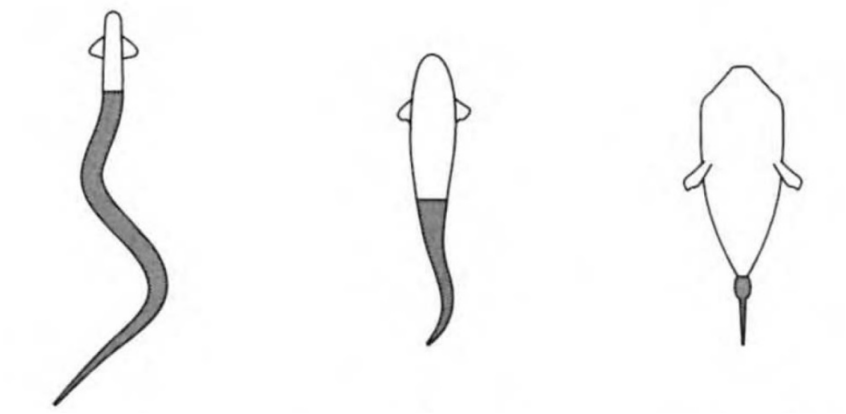

(a) (b) (c)

Figure 3.14: (a) Anguilliform; (b) Carangiform; (c) Ostraciiform. Classification of the Swimming Style of Fish [2]

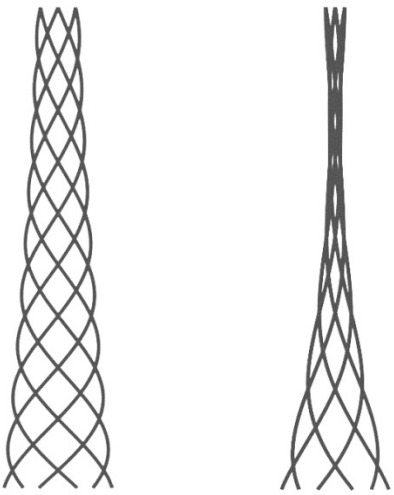

(a) (b)

Figure 3.15: The wave forms of an (a) Anguilliform; (b) Carangiform [19].

The BCF fluid-body mechanics is complex and many constituting theories have been proposed to analyse this motion but these theories still remain unclear: *undulating pump mechanism* [22], *large-amplitude elongated-body theory* [17], *vortex peg mechanism* [23], *2-D lunate tail wing theory* [19], *resistive hydrodynamic model* [24], *2D waving plate theory* [25], *vorticy control mechanism* [26] and *3D waving plate theory* [27].

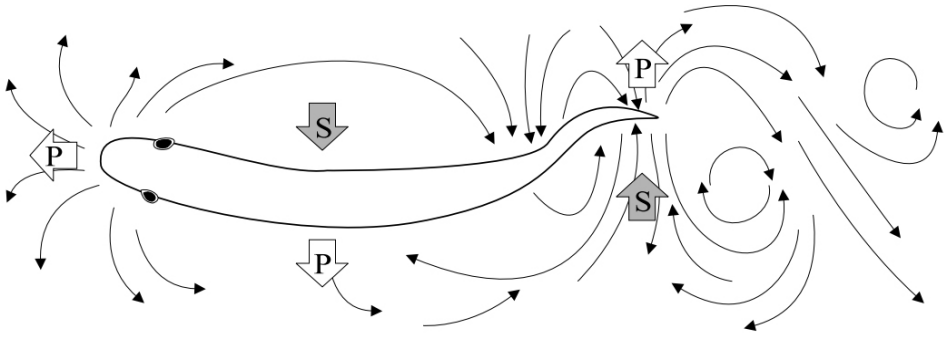

Figure 3.16: The flow field surrounding a Carangiform fish, as obtained from PIV data. The symbols P and S correspond to pressure and suction zones that form the basis of the "undulating pump" mechanism [7].

As previously mentioned, anterior destabilization has been difficult to control [20; 116; 117; 157] as passive rigid anterior mechanisms recoil around the center of mass. Free swimming robotic fish have excessive head swing, similar in magnitude to the posterior, which increases drag. The proposed linear swimming pattern will drive the anterior into the unwanted yaw direction, in an attempt to reduce amplitude errors by optimizing the F_R around the center of mass. It has also been noted in [112], that the morphological adaptations of reduced depth at the peduncle, increased depth of body towards the anterior and vertical compression minimize recoil forces. Hence these stabilizing factors will be applied as accurately as possible to the developed robotic fish generations presented in Chapters 4-7.

3.4. Mechanical Drive Systems

In Section 3.1, an overview of the kinematic parameters generated by biological underwater robotics was investigated. This section now focuses on linear locomotive mechanical drive systems. The following presents the highest performing vehicles to date. Mechanical structure constraints set a great challenge when modeling the displacements within the travelling wave and generating efficient energy transfer. The highest performing robotic fish typically adopt either a discrete assembly, compliant structure or hyper-redundant method but are all seen to have limitations, as reproducing the propulsive force of fish is a complex challenge. The development of a novel mechanical drive system capable of high performance linear locomotion must take a number of factors into consideration, some are listed below:

- Morphological properties
- Weight distribution

- Efficient transmission principles
- Power density constraints
- Kinematic parameters
- Friction Reduction
- Rotary to linear oscillation drive systems
- Control surfaces
- Tail beat frequency
- Force transfer
- Volume distribution
- Power transfer
- Caudal fin optimization
- Wetted area (Friction drag)
- Actuator selection
- Power supply
- Power density ratio
- Acceleration mechanism
- Natural buoyancy
- Structural robustness
- Optimal cross section to reduce forward resistance
- Increasing endurance
- Horizontal and vertical plane stability
- Transition phase between body and tail

The next stage of analysis is to assess the limitations and problems with the mechanical drive systems of the state of the art robotic fish. The platforms are categorised by their applied actuation method below.

3.4.1. Hyper-redundant Drive System

The developed robotic fish Robotuna (Figures 3.17 and 3.18) [113] achieved a swimming speed of 0.65 body lengths per second and comprises of a mechanism with approximately three thousand parts. This resulted a large scale build approximately one meter in length with internal mechanical loses of 10% whilst actuating a low frequency of 1Hz. The number of parts also reduces the robustness of the system. The VCUUV developed at MIT [72]

achieved 0.61BL/s and had a limited maximum frequency of 1Hz due to its complex mechanism. Hyper-redundant mechanisms (Figures 3.17-3.20) are employed to generate smoother, more precise curves in an attempt to create kinematic accuracy. The number of links in a build is typically <6 due to structural limitations, more links reduce curve alignment errors. The aim of the design is to improve complexity of motion without an increase of structural parts. An advantage of the build is the deployment of a single actuator to generate the body wave motion as a single actuator build could achieve high tail beat frequencies and force.

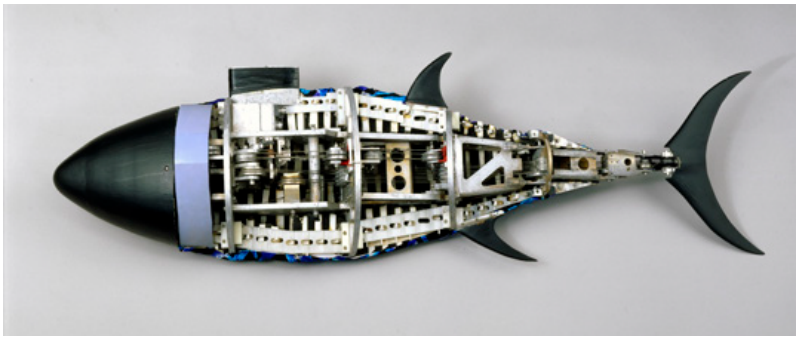

Figure 3.17: The developed hyper-redundant drive system – Robotuna. Comprising a mechanism with an approximate three thousand individual parts [113].

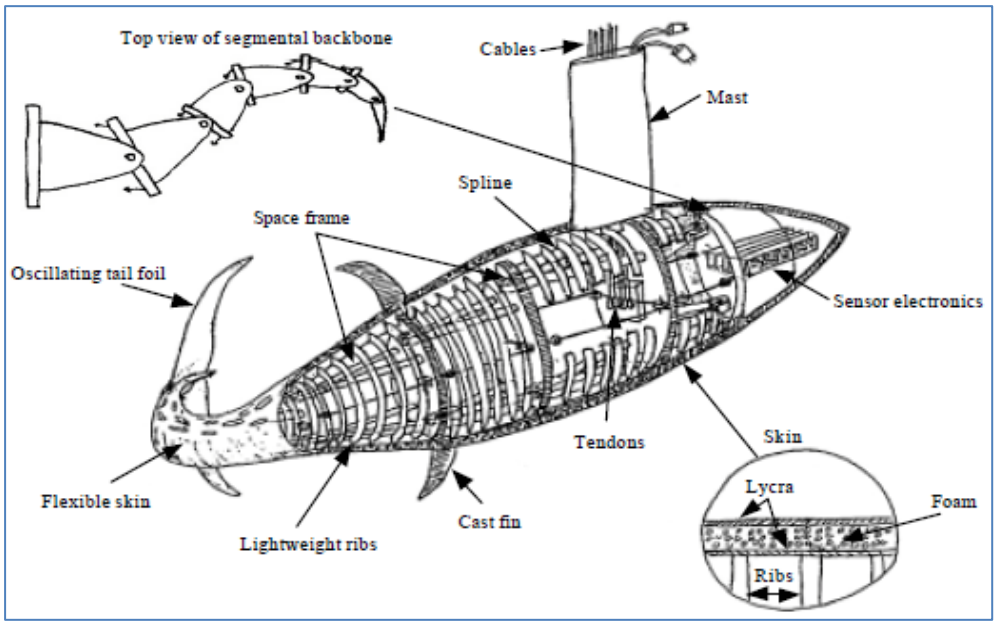

Figure 3.18: The developed hyper-redundant drive system – Robotuna. The outer skin is removed in the illustration, detailing several of the individual parts [113].

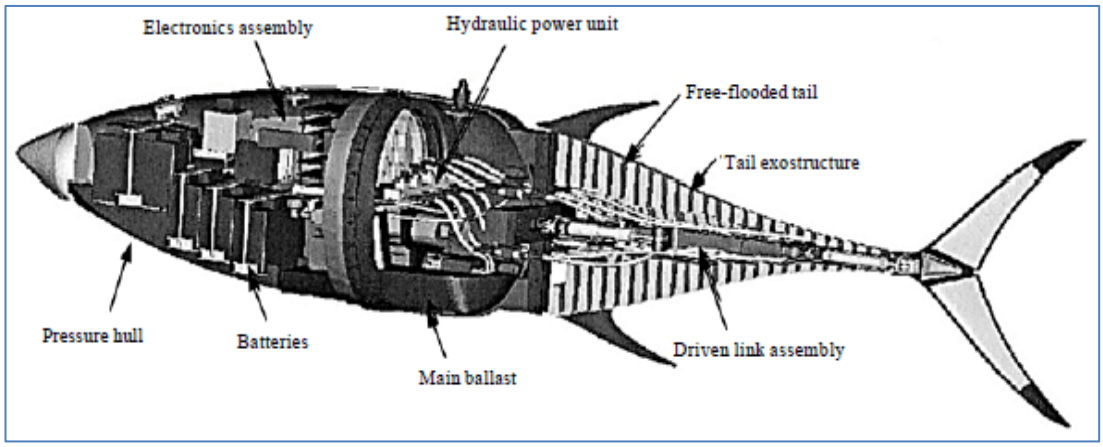

Figure 3.19: The developed hyper-redundant drive system VCCUV [72]. 2.4 meters in length and weighs 173kg with a maximum velocity of 0.61 body lengths per second.

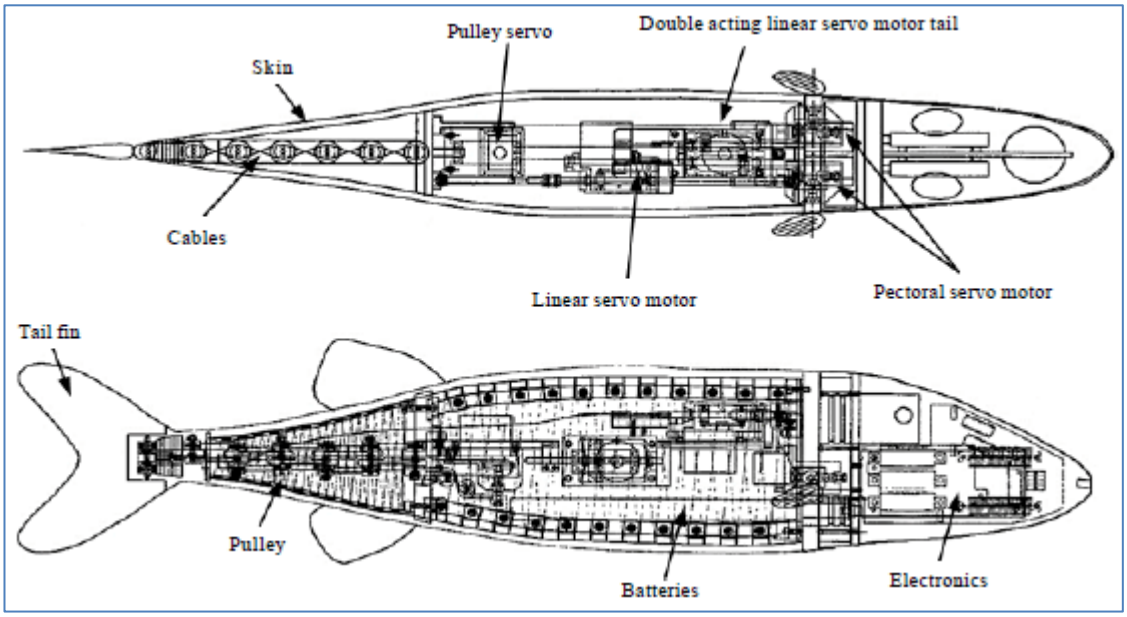

Figure 3.20: The developed hyper-redundant drive system – RoboPike [158].

3.4.2. Compliant Structure

The most developed build within the field of compliant structures is the prototype devised by Valdivia y Alvarado [69; 117], which achieved 1.1Bl/s at 3.5Hz (Figure 3.23(a)). The devised structure by MIT deploys a single actuator to generate the swimming motion of a travelling wave. Increasing endurance is a desirable feature of a UV. Current robotic fish are still limited to short operational times as energy losses can be produced in many stages of the mechanical transfer. Recent designs have found it advantageous to utilize a single electrical

motor for actuation, as the classical actuator is still the most effective way of providing power and reduces energy consumption over multilink discrete assemblies.

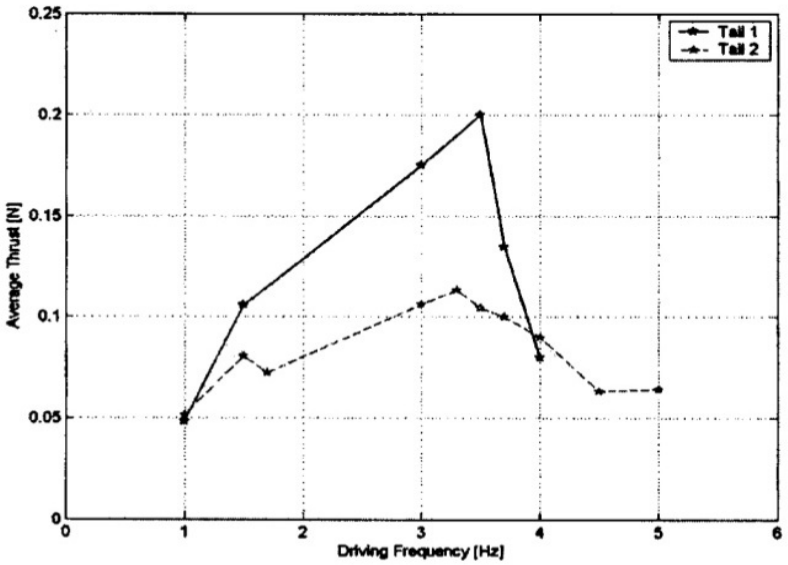

(a) The average thrust

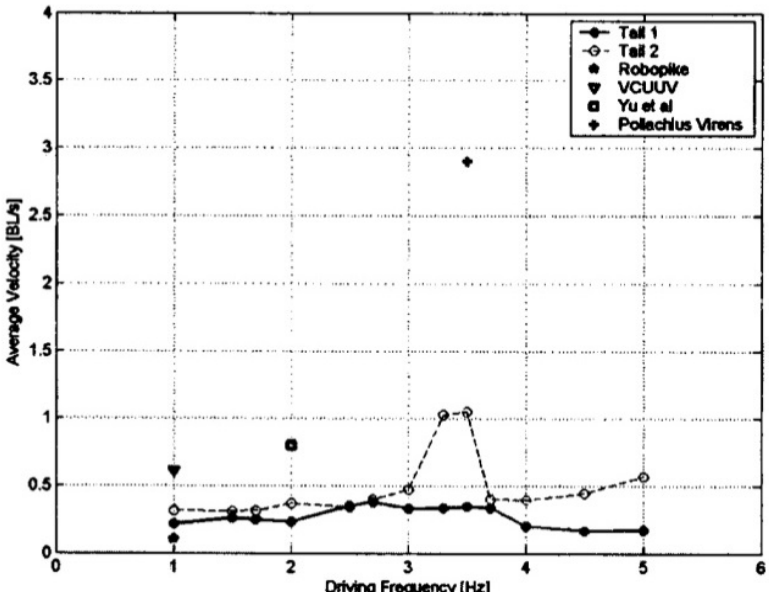

(b) The average velocity

Figure 3.21: (a) The compliant structure from MIT. We can see that the prototype generated 1.1Bl/s at 3.5Hz with a thrust production of 0.2N. (b) As the Hz's are raised the prototype peaks and then reduces in swimming speed [69; 117].

Mass and volume distribution are key principles of stability in the horizontal and vertical planes [3]. A single actuator power transmission system can be positioned in the optimum

location. In contrast multilink motor assemblies are limited as mass and volume are confined to the posterior, as seen in Section 3.5.3.

It was detailed in Section 3.2.3 that the posterior kinematics have significant errors. A compliant body structure generates its swimming motion by the use of a silicone moulded tail that is oscillated by a single servo motor, the required undulatory motion is achieved by the pressure of the surrounding fluid deforming the tail at different rates due to the thickness of the structure having a varied rigidity.

The inability to generate accurate kinematics is due to the ability of varying the stiffness in tune with different tail beat frequencies. Therefore as the frequency of the tail beat is raised the prototype's kinematics generates greater errors reducing the swimming speed. As shown in Figure 3.21 the prototype's swimming speed peaks early at 3.5Hz whilst the drive system is capable of greater Hz the swimming speed and thrust continues to decrease. In addition we can see that the drive system has a significant fault in mechanical efficiency. To generate the tail motion the silicon must be pinched between the actuator and the drive plate. This can be seen in Figure 3.23(a) [117] and also Figure 3.23(b) on the compliant structure developed by FILOSE (Figures 3.22) [157]. It is estimated that the force required to crush the silicone significantly increases energy consumption. In addition this structural constraint will limits the amplitude generated by the tail.

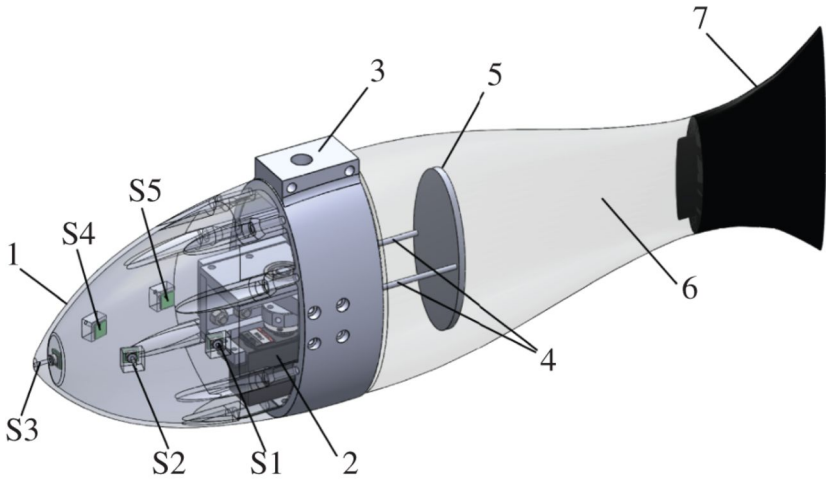

Figure 3.22: The developed fish by FILOSE. A compliant structure devised with a similar construction method as the build by MIT, whereby a silicone tail is utilized to provide the swimming motion [157].

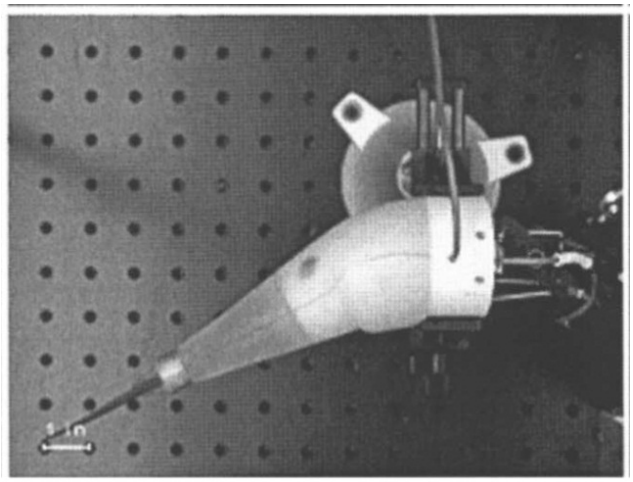

(a)

(b)

Figure 3.23: (a) The developed fish by MIT [117]. (b) The developed fish by FILOSE. In both builds we can see that when the tail is positioned towards its maximum amplitude the silicone structure creates mechanical efficiencies [157].

3.4.3. Discrete Link Structures

The developed fish G9 by Liu and Hu [20; 100; 107] is a discrete link structure utilizing a series of servo motors located along the midline of the fish. This method, although typically adopted by robotic fish is significantly limited by force and frequency due to the oscillatory motion of the DC servo motors, as even the fastest servo motors are limited to a few Hz a second due to the oscillatory motion of stopping and starting [155].

The morphology of the structure is also subject to errors in weight and volume distribution, as the servo motors must be positioned at the posterior of the fish constraining the geometry of the tail and increasing weight at the posterior (Figure 3.24), therefore increasing the anterior recoil around the centre of mass [112], as we can see in Figure 3.2.

Figure 3.24 is the discrete link structure, a series of servo motors connected in line which has become the most popular method to building robotic fish due to its advantages in

simplifying the construction and ability to generate the posterior undulatory motion [8; 20; 57; 60; 76; 77; 79]. We can see in Figure 3.25 that the discrete link structure of five links and four joints distributed along the lateral length can approximately generate the required kinematics of the posterior parameters without large errors in the curve alignment.

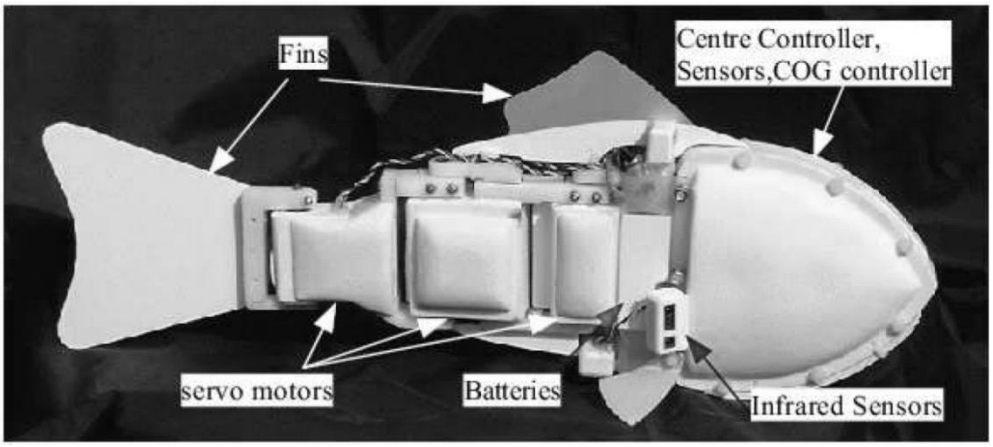

Figure 3.24: The developed fish G9 by Lui and Hu. A discrete link structure utilizing a series of servo motors located along the midline of the fish [20].

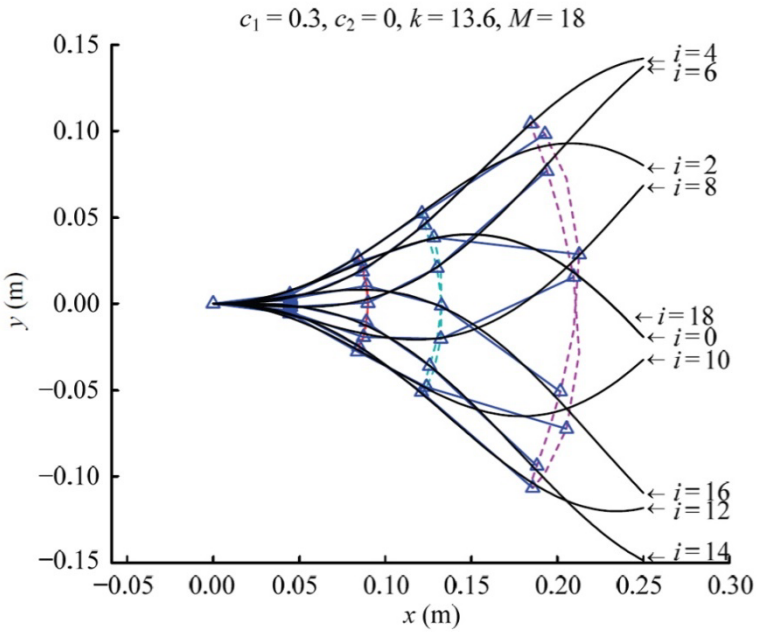

Figure 3.25: The developed fish G9 by Lui and Hu. The discrete link structure provides an accurate curve alignment with the deployed wave pattern [20].

3.5. Summary

This chapter presented an investigation of the linear locomotive swimming pattern of Carangiform fish. The traditional approach to implementing the Carangiform swimming

motion was discussed in (Section 3.3), identifying the errors within the kinematic parameters in comparison to real fish during swimming (At very low and cruising speeds of approximately 3BL/s). The observational studies undertaken on real fish were detailed, the analysis identified that a tuned full-body length swimming motion is required for accurate replication of the linear Carangiform body wave (Section 3.4). As current robotic fish have low swimming speeds and inaccurate swimming kinematics, developing a build with the greatest accuracy in body wave parameters is the highlighted as the first stage in development (Section 3.3.1).

Although only slight, displacement in the anterior and mid-body portion of the body length was observed (Section 3.4.1). This motion provides a smooth curve from head to tail, which may lead to greater efficiency in swimming performance. Therefore the proposed Carangiform swimming motion is a body wave with a coordinated anterior, mid-body and posterior whereby the anterior drives the head into the direction of unwanted recoil in an attempt to reduce the anterior destabilization and generate precise parameters over the full length of motion (Section 3.4.2).

The challenges of developing a high performance mechanical drive system were discussed identifying the advantages of applying a single rotary actuator in combination with as few mechanical links as possible whilst retaining accurate curve alignment (Section 3.5). By deploying a single actuator the opportunity for high forces and high frequencies is possible. To generate propulsion the drive system must be able to effectively transmit the rotatory motion of the actuation into the oscillatory and undulatory motion of a swimming fish. This will require a high-performance prototype, robust, compact, naturally buoyant, carrying its own power supply, with a high power density and able to effectively transmit large forces at intensively high tail oscillation frequencies for untethered high-speed propulsion.

The next stage of the research is to implement the information learnt from the background investigation. The development and experiments of four generations of robotic fish are presented in the following chapters.

Chapter 4

iSplash-I: Implementing Coordinated Full-body Swimming Pattern

This chapter presents the first generation, *iSplash*-I (Figures 4.1 and 4.2) [114; 132], a Carangiform robotic fish with a high performance full body coordinated swimming motion, able to generate a maximum velocity over current published robotic fish, equivalent to the cruising speeds of real fish. The remainder of the chapter is organized as follows: After Section 4.1 Introduction and Section 4.2 Research Objectives, Section 4.2 presents the traditional model and introduces a new approach. Section 4.3 describes the new construction method. Section 4.4 describes the field trials undertaken and the experimental results obtained. Section 4.5 presents the further experimental analysis. Concluding remarks and future work are given in Section 4.6

4.1 Introduction

An experimental investigation of the linear Carangiform swimming motion was conducted. A novel mechanical drive system was devised operating in two swimming patterns. A thorough comparison between a traditional posterior confined undulatory swimming pattern and the introduced full-body length swimming pattern was made. As estimated in Chapter 3 the newly introduced swimming motion, based on intensive observational studies (Section 3.4.1), was measured to coordinate the body displacements reducing the large kinematic errors seen

in free swimming robotic fish, by optimizing the F_T and F_L forces around the center of mass and initiating the starting moment of added mass upstream. From the comparison the proposed Carangiform swimming motion significantly outperformed the traditional approach in terms of speed measured in body lengths/ second, achieving a maximum velocity of 3.4BL/s and consistently achieved a velocity of 2.8BL/s at 6.6Hz.

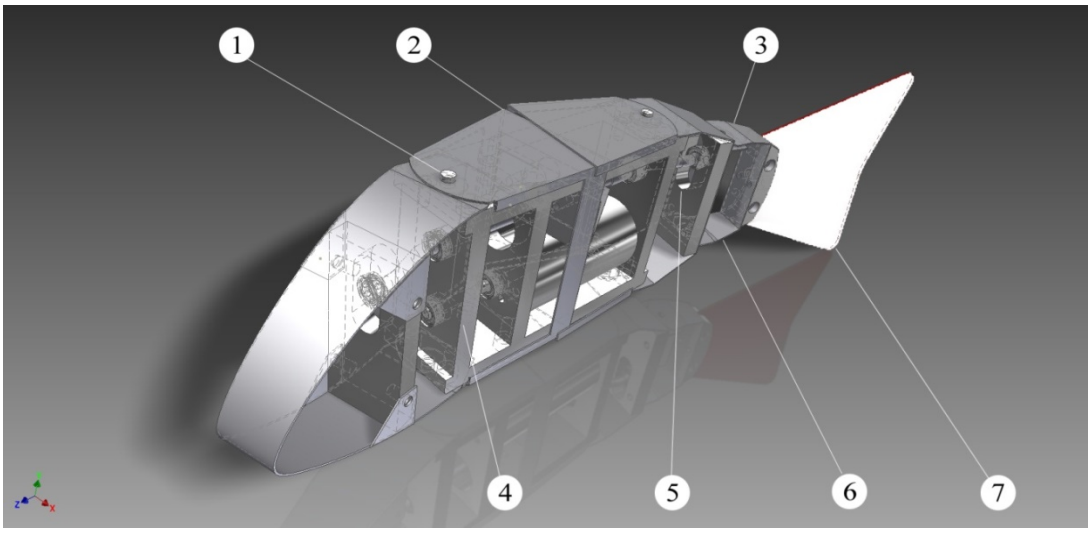

Figure 4.1: *iSplash*-I: 1-Anterior motion link; 2-Mid-body passive links; 3-Think peduncle; 4-Transmission system spur gears; 5-Driven tail plate link IV; 6-Expandable tendons passively actuating link V; 7-Interchangable compliant low aspect ratio caudal fin.

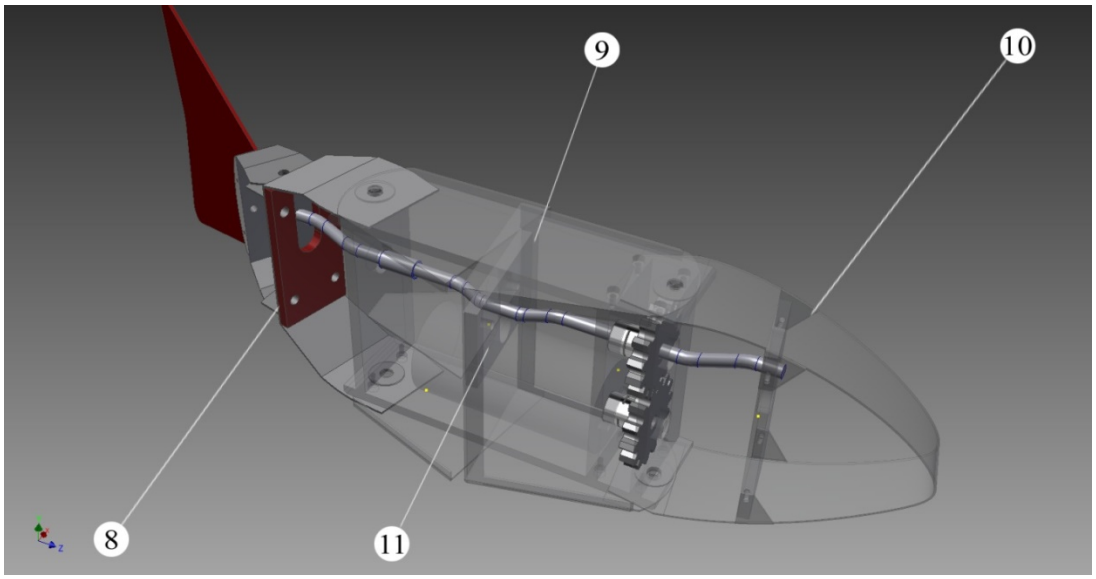

Figure 4.2: 8-Final link V; 9-Outer space frames; 10-Link I drive plate; 11-Mid-body drive plate.

Underwater exploration is a physically demanding task. A robotic vehicle must navigate in an unpredictable surrounding environment, which includes many disturbances and non-uniformities due to the transient changes exerted from the liquid. These physical forces applied to the underwater vehicle (UV) can lead to inaccurate navigation and even failure of the operation if a robotic vehicle is unable to adapt to the dynamic environment. This is where fish excel, generating large transient forces efficiently by coordinating their body motion [1; 112]. In addition, adversely the dynamic environment can be advantageous to fish locomotion, as they demonstrate the ability to extract energy from the upstream vortices [11]. There is great potential to improve underwater robotic locomotion by imitating the swimming fish with the highest locomotive performance operating within the desired environment and Reynolds numbers. Hence, it is necessary to develop a robotic fish able to generate the highest swimming speeds of real Carangiform fish, i.e. an average maximum velocity of 10BL/s [51; 118; 159].

Most work in biomimetic underwater propulsion has focused on hydrodynamic mechanisms. The current low speeds of robotic swimmers are unpractical for real world applications, peaking at speeds of 1.1BL/s. The highest recorded speeds, in terms of BL/s are:

(1) Valdivia y Alvarado's compliant structure assembly achieving a velocity of 1.1BL/s (0.32m/s) [117; 69].

(2) Liu's G9 Carangiform swimmer achieving a velocity of 1.02BL/s (0.5m/s) [20].

(3) Yu's optimized discrete assembly prototype achieving a velocity of 0.8BL/s (0.32m/s) [116].

Chapter 3 detailed the complex challenge of reproducing the propulsive force of a fish, as the development of a novel mechanism must take into consideration a combination of morphological properties, weight distribution, efficient transmission principles, power density constraints and kinematic parameters. In particular accurately replicating the linear swimming motion has proven to be difficult and free swimming robotic fish have significant kinematic parameter errors. The forces are not optimized and as a consequence excessive destabilization in the yaw plane due to the concentration of posterior thrust creates reaction forces around the centre of mass. In turn the anterior creates posterior displacement errors. As a result the body wave motion along the full length of body has large matching errors in comparison to the swimming patterns of live fish leading to reduced performance and high cost of transport.

4.2. Research Objectives

This research considered the factors contributing to the low hydrodynamic performance of current robotic fish within linear locomotion and proposed four main objectives:

(i) Implement the new swimming pattern to reduce the kinematic parameter errors by coordinating transverse displacements along the body length.

(ii) Allow for efficient energy transfer by engineering a mechanism that takes into account hardware and material constraints so that propulsion is reduced.

(iii) The developed prototype improves stability in the vertical and the horizontal plane, by optimizing the lateral and thrust forces around the center of mass.

(iv) Validate the proposed swimming motion by realizing a mechanism capable of consistent free swimming operation, measuring its achievement in terms of speed, thrust and energy consumption over a range of frequencies.

4.3. Applying the Full-Body Swimming Motion

Added Mass **-** Propulsion of Carangiform swimming is associated with the method of added-mass [119]. As each propulsive segment of the travelling wave passes backwards along a fish, the momentum of the water passing downstream is altered. This causes a reaction force F_R from water onto the propulsive segment. F_R normal to the propulsive segment is decomposed into the lateral F_L component which can lead to energy loss and anterior destabilization and the thrust F_T component providing propulsion increasing in magnitude towards the tail. The overall magnitude of added-mass passing downstream can be approximated as the water mass accelerated and its acceleration.

Therefore it was proposed that initiating the starting moment of added mass upstream and optimizing the F_L and F_T forces around the center of mass would increase the overall magnitude of thrust contributing to increased forward velocity. In consideration of this, we designed a novel robotic fish which can operate in two swimming patterns:

Mode 1: The Traditional Approach –

This method adopted by existing robotic fish applies a rigid mid-body and anterior. Concentrating the undulations to the posterior end of the body length, varying in amplitude along the lateral length smoothly increases towards the tail. This approach will be described

as Mode 1 and illustrated in Figure 4.3. The posterior confined kinematics of the Carangiform is of the form [20] (Detailed thoroughly in Section 3.3):

$$y_{\text{body}}(x,t) = \left(c_1 x + c_2 x^2\right)\sin\left(\text{k}x + \omega t\right) \tag{4.1}$$

where y_{body} is the transverse displacement of the body; x is the displacement along the main axis beginning at the nose; k =2π/λ is the wave number; λ is the body wave length; $\omega = 2\pi f$ is the body wave frequency; c_1 is the linear wave amplitude envelope and c_2 is the quadratic wave. The parameters P = {c1,c2,k,ω} can be adjusted to achieve the desired posterior swimming pattern for an engineering reference.

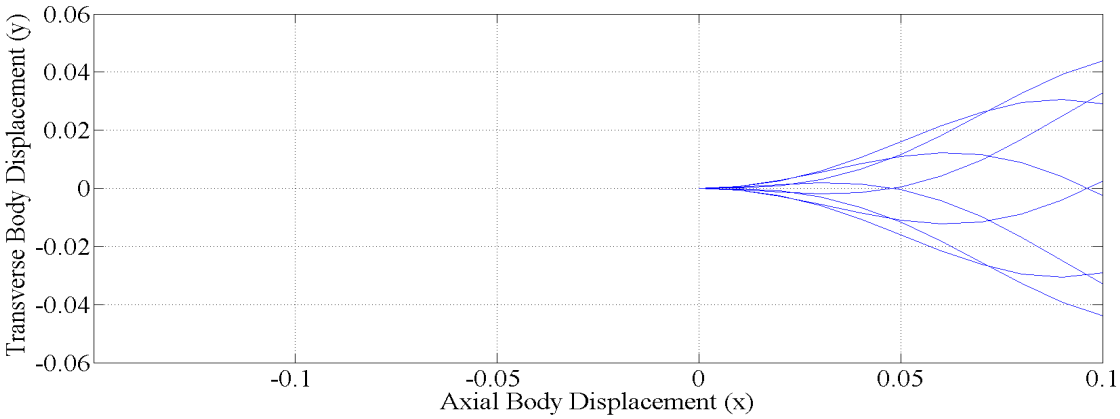

Figure 4.3: Mode 1: Wave form is confined to the posterior 2/5. Parameters have been determined from experimental tests.

Mode 2: Proposed Full-Body Swimming Motion –

This method is based on the intensive observation and fluid flow assumptions proposed in Chapter 3. A new full-body Carangiform swimming pattern is introduced, to coordinate the anterior, mid-body and posterior body motions in an attempt to reduce kinematic parameter errors, this will be described as Mode 2, illustrated in Figure 4.4. The models midline and body motion parameters were first established based on observation and published data from literature providing an initial engineering reference. The wave form [20], an adaption of (4.1) can be extended to generate the midline parameters of the full body motions of Mode 2 in the form of:

$$y_{\text{body}}(x,t) = \left(c_1 x + c_2 x^2\right)\sin\left(\text{k}x + \omega t\right) - c_1 x \sin\left(\omega t\right) \tag{4.2}$$

The newly introduced Mode 2 applies an oscillatory motion to head and mid-body which pivots around a single point associated with the Carangiform fish swimming motion

[112].The relationships between the defined parameters P = {0.44,0,21.6,8} shown in Figure 4.4 can first be found by evaluating the x location pivot at 0.

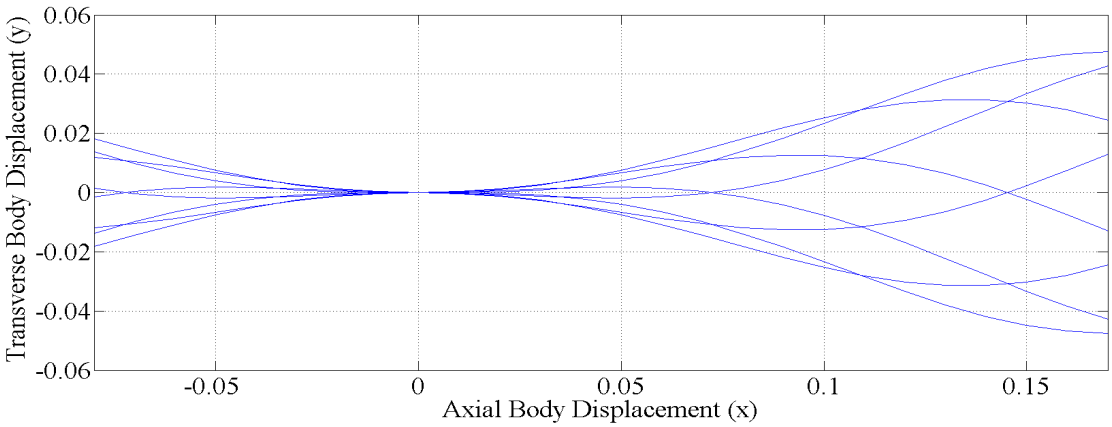

Figure 4.4: Mode 2: Full-body coordination. The kinematic parameters have been determined from experimental tests.

This is the first account of applying full-body actuation to a research prototype fish. We aim to mimic the observed kinematic pattern as precisely as possible, since the muscle activity in the anterior has been measured to be low, suggesting that accurate modeling of the kinematics could be more significant than anterior force in improving energy transfer.

As previously mentioned, anterior destabilization has been difficult to control [116; 20; 117] as passive rigid anterior mechanisms recoil around the center of mass. Hence, free swimming robotic fish have excessive head swing, similar in magnitude to the posterior which increases drag. The proposed Mode 2 drives the anterior into the unwanted yaw direction, in an attempt to reduce amplitude errors by optimizing the F_R around the center of mass. It has also been noted in [112], that the morphological adaptions of reduced depth at the peduncle, increased depth of body towards the anterior and vertical compression minimize recoil forces and were considered during the development of the mechanical drive system.

4.4. Construction Method

4.4.1. Mechanical Design

Mechanical structure limitations set a great challenge when modeling the displacements within the travelling wave. Current methods typically adopt either a discrete assembly [116; 20] or compliant structure [117; 69], but both are seen to have limitations. A construction method using structural compliance combined with a rigid discrete assembly is proposed. The

arrangement distributes four links and 1 passive link along the axial length shown in Figure 4.5 - 4.8. Mode 1 disregards transverse displacements of links I, II, III whereas Mode 2 actuates all links along the axial length to provide anterior and mid-body transversal displacements. The development allowed for both Modes of operation to be applied to the same prototype by adjusting the configuration. Uniform material properties were chosen for links I-III and stiffness distribution begins at link III and continues to the tail tip. To provide the undulatory motion a compliant caudal fin is attached to the link V and is actuated by tendons anchored to the main housing rear bulkhead. The developed mechanism allows for the expansion of the tendons and material stiffness of the caudal fin to be adjusted experimentally to provide the targeted curves during free swimming at various frequencies.

The approximation of a traveling wave using joints I-V and turning angles of Links I-IV are shown in Figure 4.5. Details of the fully discretized body wave fitting method are given in [20; 116]. The location of joints in the series can be determined by parameterized fitment to a spatial and time dependent body wave. The discrete construction method can be defined as a series of links or N links. N being the number of links after joint 1 typically <6 due to structural limitations, more links reduces curve alignment errors. The aim of the design is to improved complexity of motion without an increase of structural parts. In Figure 4.5 of the link end points it can be seen that the arrangement of link's distributed along the length of the body provides an accurate curve alignment reducing large errors and excrescences in the outer profile.

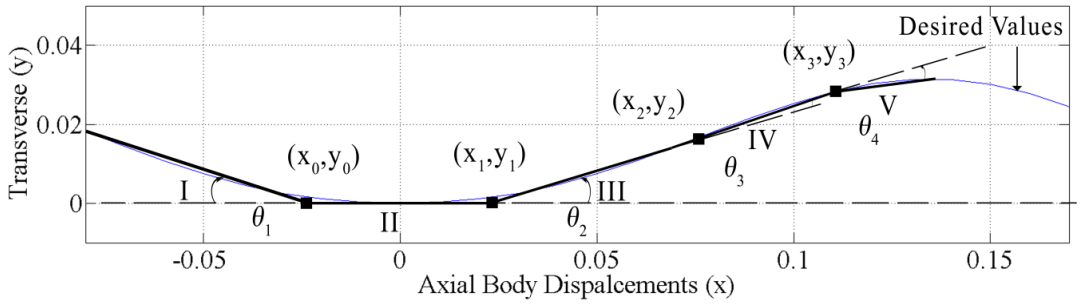

Figure 4.5: Link approximation.

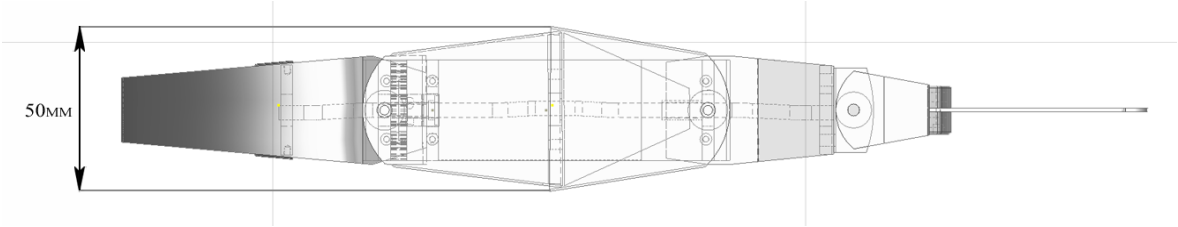

Figure 4.6: Plan view (taken from above).

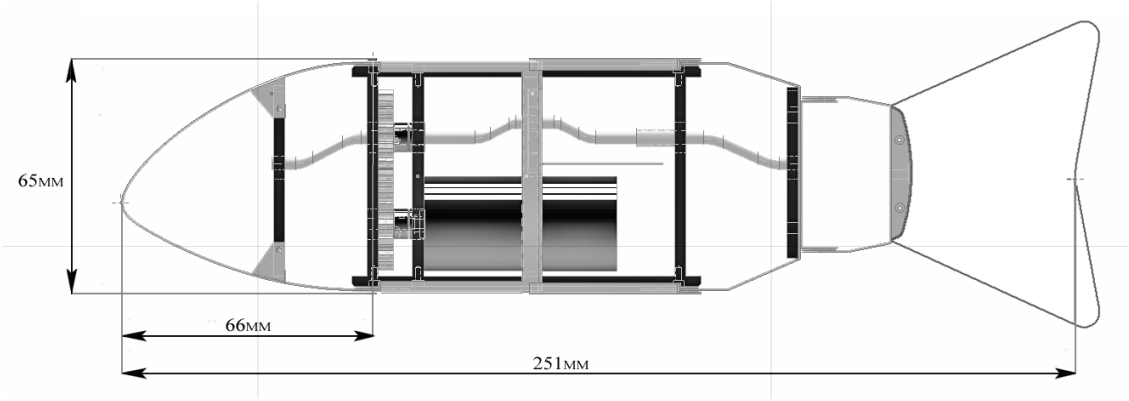

Figure 4.7: Profile view (taken from the side).

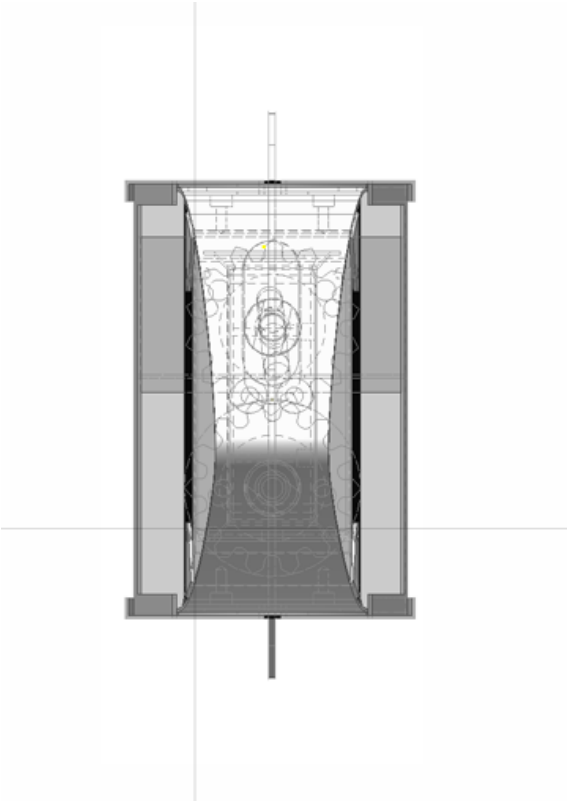

Figure 4.8: Front view.

4.4.2. Aerofoil Profile

In addition it has been observed that the aerofoil section NACA (12)520 based on camber, chord and thickness can be utilized to illustrate the outer structure profile of Mode 2 which is proposed contributes to the fluid flow interaction (Section 3.4.1) (Figures 3.8 and 3.13-3.17).

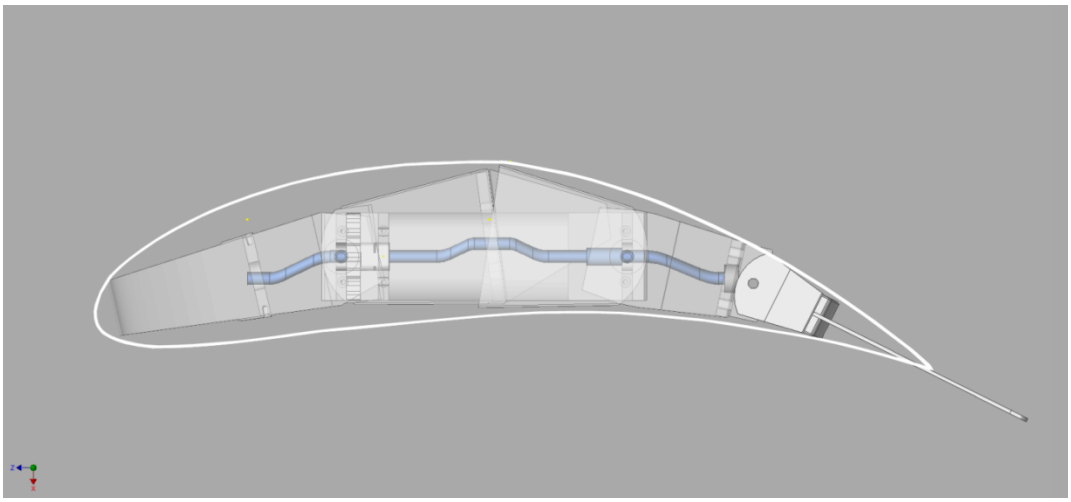

Figure 4.9: Outline line illustrating the NACA(12)520 aerofoil, Prototype is shown on its maximum moment of curvature during the body wave cycle.

4.4.3. Power Transmission System

The developed transmission system providing rotary power to linear oscillations is illustrated in Figures 4.10 and 4.11. All actuated links are directly driven by the five bearing crank shaft providing an equal power distribution. The developed mechanical design required high-precision engineering of the chassis and crankshaft to avoid deadlock and reduce friction. The driven link amplitudes are determined by the offset cranks, L_3 represents one of the discrete links of the structure.

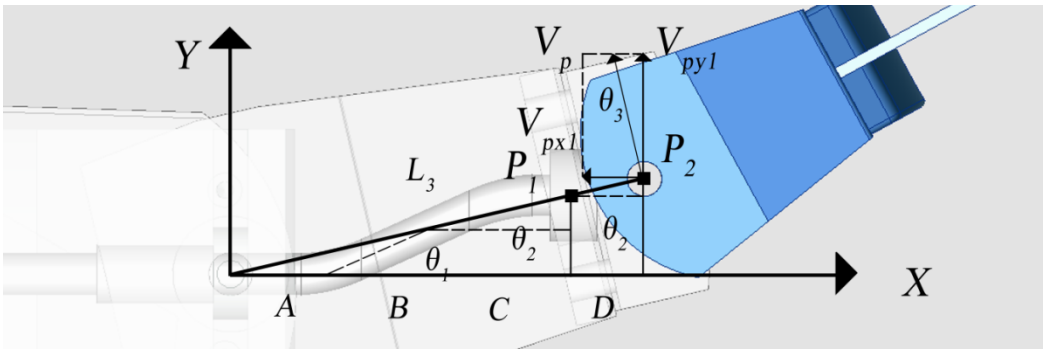

Figure 4.10: Schematic drawing of the tail offset drive crank and linkage.

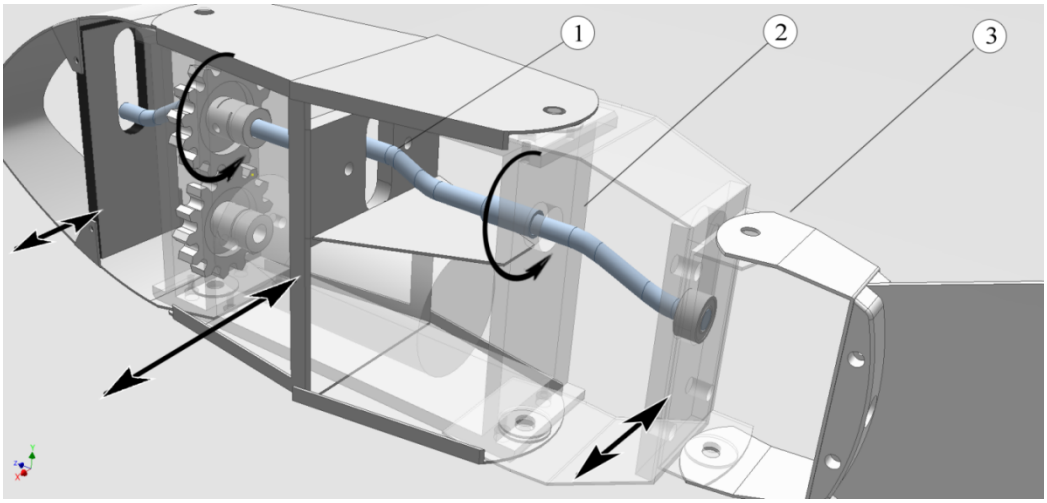

Figure 4.11: Power transmission system: 1-Transision plate; 2-Crankshaft; 3-Free end of link and connecting pivot.

The maximum amplitude of the link length L_3 at point P_2 is determined by P_1 the predetermined maximum crank offset. P_1 and P_2 can be derived by:

$$\begin{cases} P_{x1} = A + B\cos\theta_1 + C\cos\theta_2 \\ P_{y1} = B\sin\theta_1 + C\sin\theta_2 \end{cases} \begin{cases} P_{x2} = P_{x1} + D\sin\theta_2 \\ P_{y2} = P_{y1} + D\sin\theta_2 \end{cases} \quad (4\text{-}3)$$

The length of L_3 is derived by $L_3^2 = Px_2^{2+} Py_2^2$. The coordinates of the free end or connecting pivot P_2 are obtained by:

$$\begin{cases} X_{p2} = L_3\cos\theta_3 \\ Y_{p2} = L_3\sin\theta_3 \end{cases} \begin{cases} V_{px2} = -\omega\sin\theta_3 \\ V_{py2} = \omega\cos\theta_3 \end{cases} \quad (4\text{-}4)$$

where Xp_2 and Yp_2 are the X and Y coordinates of point P_2, respectively. The velocity vector V_{P2} perpendicular to L_3 is obtained by differentiating Xp_2 and Yp_2 with respect to time. Where V_{P2} is decomposed into V_{px2} and V_{py2} and ω1 is the angular velocity of link L_3.

4.4.4. Fabrication

The *iSplash*-I shown in Figures 4.13 and 4.14 was engineered as a morphological approximation of the common carp. The physical specifications are given in Table I. A structurally robust prototype was devised, allowing for consistency of operation at high frequencies, as force has to be applied to the water and reactively, the opposing force applied to the vehicle. All structural parts were precision engineered, hand fitted and assembled. A consideration of the development took into account hardware and material constraints so that geometric and kinematic parameters are not affected. The hydro-static streamlined profile

was optimized by favorably positioning the maximum thickness of the cross section, reducing pressure drag. In [118], the cross section has been measured to be optimal at 0.2 of the body length. These aspects relate to the amount of resistance during forward motion and were taken into consideration within the design.

The side view of the mechanical drive system is shown in Figures 4.12 super imposed onto the side profile of a common carp. We can see that the mechanical structure was devised to be an accurate replica of the body structure of the common carp with an approximately even offset from the outer profile to allow for an outer skin.

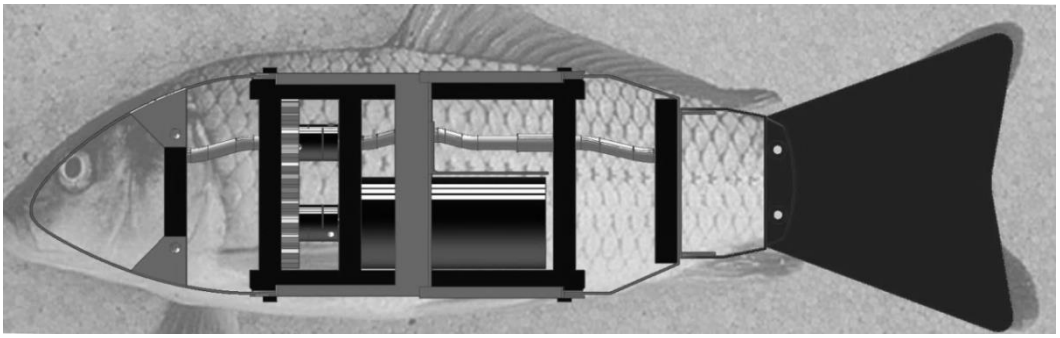

Figure 4.12: Showing the mechanical drive system superimposed onto the side profile of a common carp. The arrangements of the links are distributed over the full body length to provide the potential of coordinated body wave.

Increasing endurance is a desirable feature of an UV. Current robotic fish are still limited to short operational times as energy losses can be produced in many stages of the mechanical transfer. Recent designs have found it is advantageous to utilize a single electrical motor for actuation [117]. The classical actuator is still the most effective way of providing power at high frequencies and reduces energy consumption over multilink discrete assemblies. Weight distribution and mass are key principles of stability in the horizontal and vertical planes. A single actuator power transmission system can be positioned in the optimum location. In contrast multilink servo assemblies are limited as weight and mass are confined to the posterior.

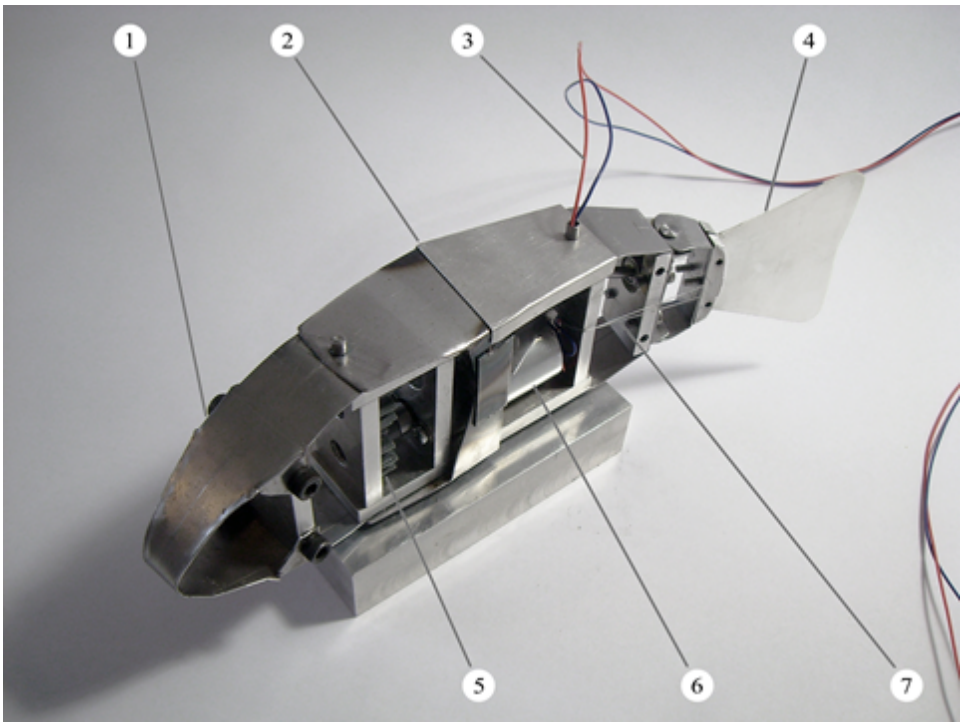

Figure 4.13: Inner Structure of *iSplash*: 1-Mild steel space frame; 2-Mid-body driven plate; 3-External source cables; 4-Polypropylene caudal fin; 5-Aluminium main bulkhead; 6-electric motor; 7-Offset crank shaft.

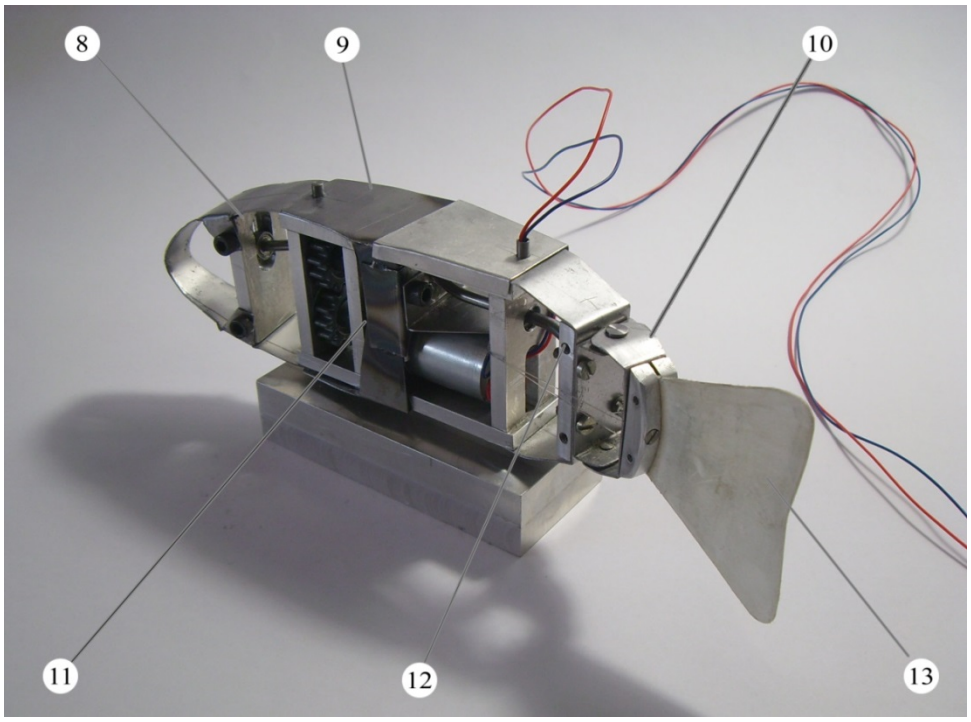

Figure 4.14: 8-Anterior driven plate; 9-Mid-body space frame; 10-Stainless steel peduncle; 11-Transmission system; 12-External power source wire exit; 13-Most compliant point of build.

The body has open loop stability if the relative position of buoyancy is higher than the center of mass as the surrounding fluid counterbalances the gravitational weight [3]. Therefore the hydrostatic buoyancy level and stability were solved by adjusting material properties and configuration. During free swimming stability was found to be particularly difficult to maintain during high frequencies. Lastly, the inner structure of the prototype is negatively buoyant. A significant development of the prototype was a watertight skin that allowed unrestricted flexing of the external surface and provided the volume needed to maintain neutral buoyancy.

Table 4.1: The physical parameters of *iSplash*-I.

Parameter	Specific Value
Body Size: m	0.25 x 0.05x 0.0 62
Body Mass : Kg	0.367
Maxium Velocity: BL/s (m/s)	3.4 (0.88)
Noload Maximum Frequency: Hz	8
Actuator	Single Electric motor
Power Supply	12V Pb External Battery Supply
Fabrication	Low Tolerance Engineering
Materials	Aluminum, Mild Steel, Stainless
Swimming Mode	Linear Locomotion
Outter Structure & Skin Material	Polypropylene Polystyrene
Thickness of Caudal Fin : mm	1
Caudal Fin Material	Polypropylene
Caudal Fin Aspect Ratio: AR	1.73

4.5. Experimental Procedure and Results

4.5.1. Field Trials and Experimental Setup

A series of experiments were undertaken in order to verify the proposed swimming pattern by assessing the locomotive performance of Modes 1 and 2 in terms of speed, thrust and energy consumption at frequencies in the range of 2-8Hz. Experiments were conducted within a 1 x 0.5 x 0.25 m test tank. Due to the short distances available, steady state free swimming over a distance of 0.5m was used to measure speed with a 0.5m acceleration distance. The prototype had sufficient space to move without disturbances from side boundaries and the free surface.

Measurements were averaged over many cycles once consistency of operation was achieved and steady state swimming was obtained.

Although measured during experimental testing of the velocity to be more mechanically efficient with an oil filled structure, the developed skin proved inconsistent for testing. All runs were completed actuating the prototype with a water filled structure. This method allowed consistency of operation as buoyancy within the testing tank dimensions was difficult to maintain and provided stabilized swimming whilst skimming the bottom of the tank. It was found during runs when the skin came loose, the build became negatively buoyant, destabilized or the cross-sectional area was increased, dramatically reducing velocity.

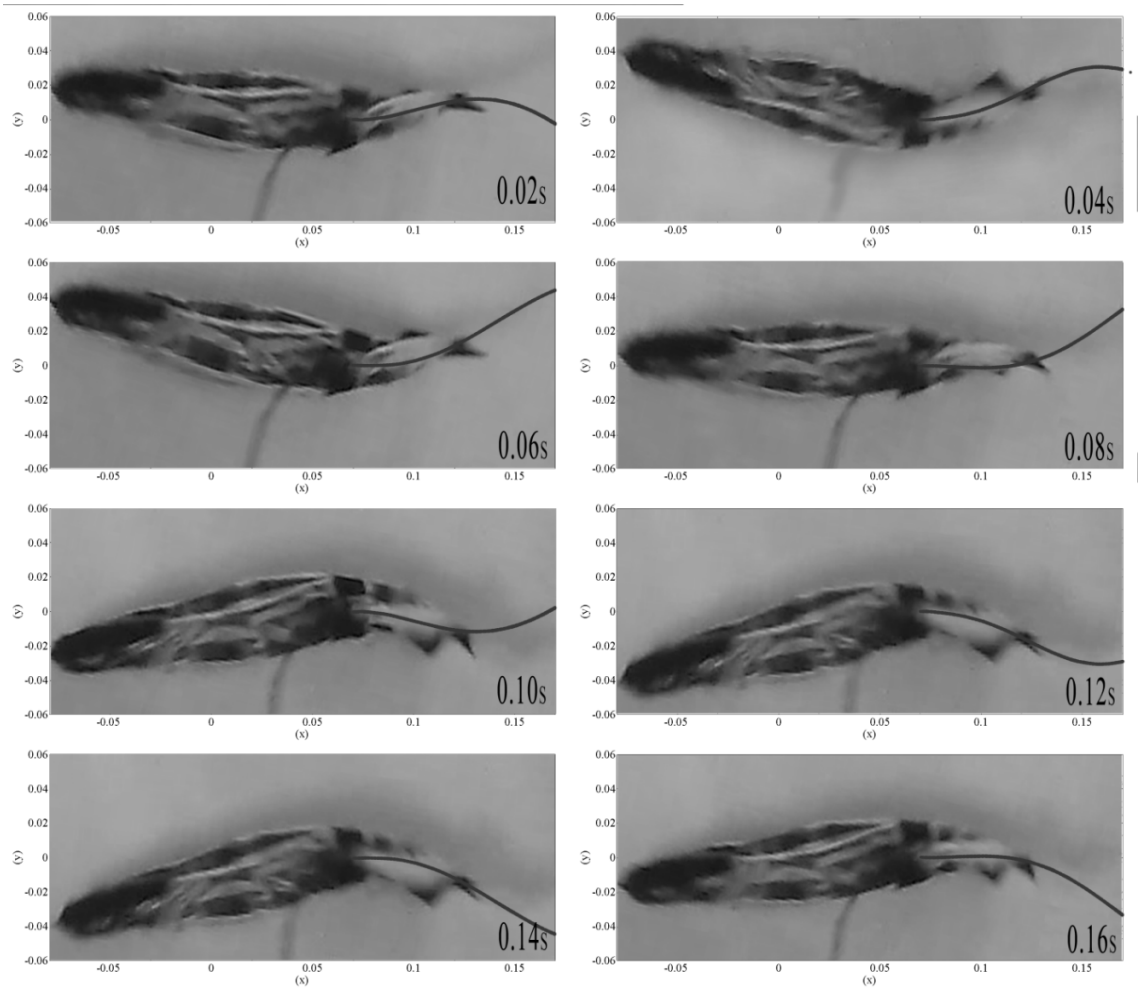

Figure 4.15: Mode 1 during one body cycle, eight instances every 0.02s.

4.5.2. Swimming Pattern Observation

Figures 4.15 and 4.16 show snapshots of Mode 1 and Mode 2 in eight instances with time intervals of 0.02s throughout one body cycle. The midline was tracked at 50 frames per second to provide the amplitude envelopes of the anterior and posterior for comparison. Good agreement with fish kinematic data is a difficult task and current free swimming robotic fish have shown excessive head and tail amplitude errors.

When comparing Modes 1 and 2, Mode 2 was found to reduce the head amplitude by over half from 0.17 (0.044m) of the body length in Mode 1 to 0.07 (0.018m). The tail amplitude should be in the range of 0.18-0.22 [51; 118], both Modes 1 and 2 are 0.17 (0.044m). The location of the midline pivot point should be in the range of 0.15-0.25 of the body length [118]. Mode 2 has a reduced error location of 0.33 in comparison to Mode 1 of 0.5. Indicating Mode 2 significantly reduces matching errors.

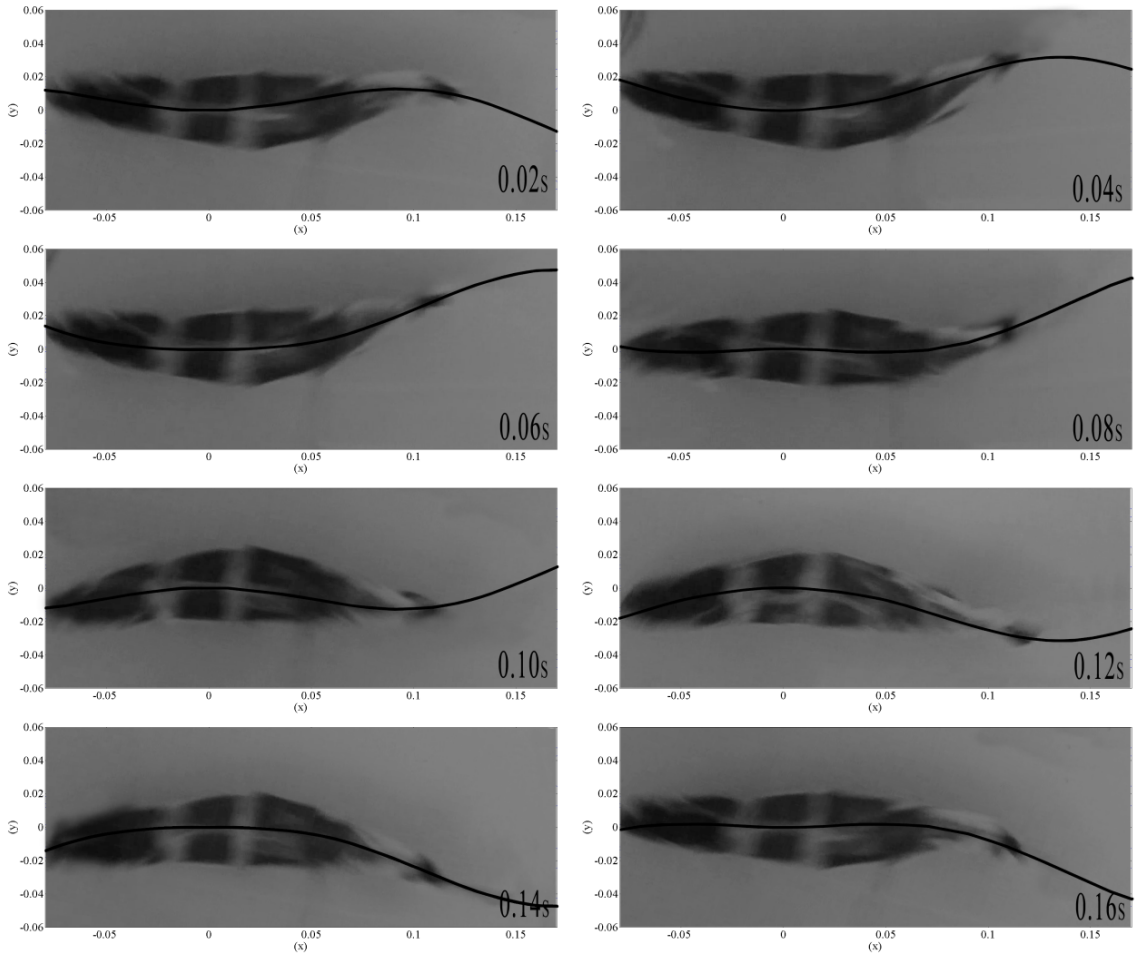

Figure 4.16: Mode 2 during one body cycle, eight instances every 0.02s. Mode 2 (Figure 4.4) significantly reduces the anterior amplitude. The location of the midline pivot point

should be in the range of 0.15-0.25 of the body length. Mode 2 has a reduced error location of 0.33 in comparison to Mode 1 of 0.5.

In addition it was observed due to the heterogeneous build the posterior 2/5 of the body length deforms due to stiffness distribution providing a smooth transition phase between body and tail. Although high aspect ratio (AR) caudal fins have been found to produce greater efficiency [11], in initial testing a low aspect ratio tail provided higher speeds. AR is calculated using: AR=b^2/Sc where b squared is the fin span and Sc is the projected fin area. AR in this case was 1.73.

Table 4.2: Comparison of Test Results between Modes 1 & 2.

Parameters	Mode 1	Mode 2
Reynolds Number: *Re* (10^5)	1.3	1.6
Shrouhal Number: *St*	0.48	0.41
Maxium Thrust: N	0.63	1.17
Consistant Maxium Velocity: BL/s (m/s)	2.2 (0.55)	2.8 (0.70)
Frequency: Hz	6.1	6.6
Max Power Comsumption Air: W	3.48	3.76
Max Power Comsumption Water: W	5.76	7.68
Swimming Number: *Sw*	0.36	0.42
Head Swing Amplitude: m	0.044	0.018
Tail Swing Amplitude: m	0.044	0.044
Test Run Distance: m	0.5	0.5

4.5.3. Average Energy Economy (W)

In Figure 4.17 the average energy economy in relationship to driven frequency is shown, comparing both Modes in air and water. This comparison was used to measure the value of the increased resistance during locomotion due to the surrounding liquid. The measuring of

the energy economy and thrust took many cycles to average, as the swimming motion produces fluctuating readings within a single body motion cycle. Both Modes actuating in water resulted in an increase in energy consumption. Mode 2 increasing from 3.76W to 7.68W and Mode 1 increased from 3.48W to 5.76W.

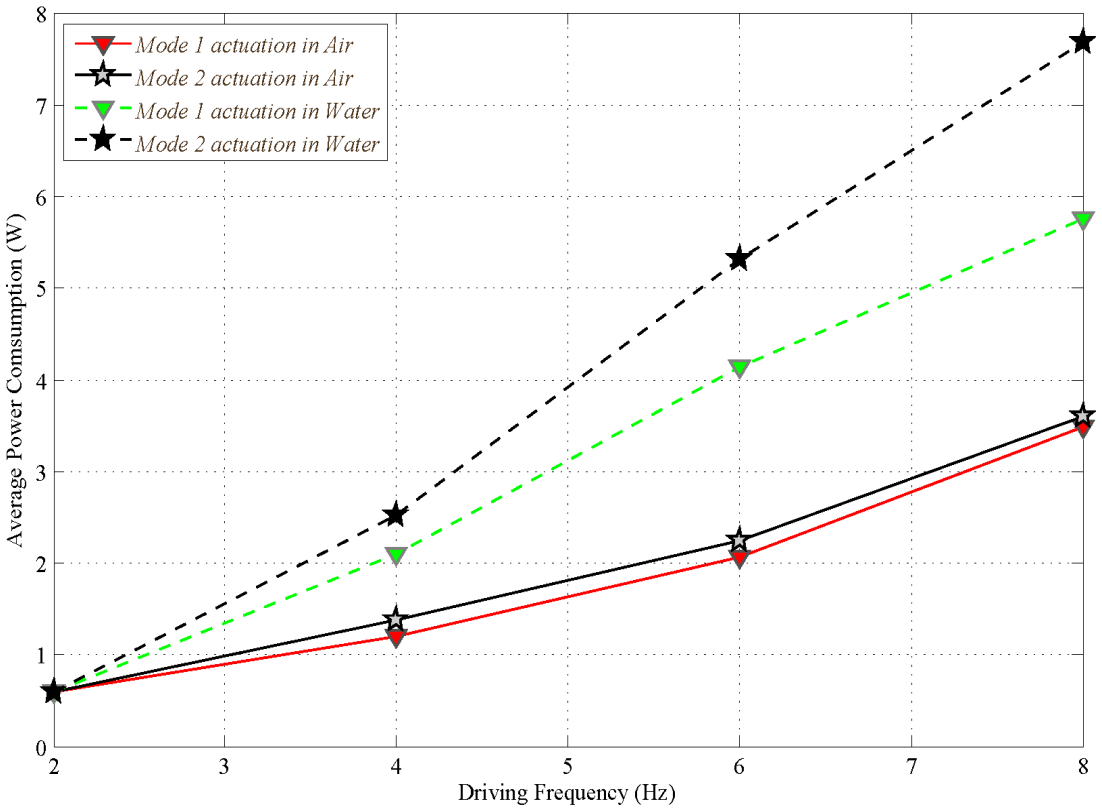

Figure 4.17: Comparison of average electrical power consumption over driven frequency of both Modes, actuating in air and water.

4.5.4. Average Velocity (BL/s)

As the configurations of robotic fish show various hardware and morphological properties, the main value of comparison has become speed divided by body length (BL/s). In this case the body length is measured from nose tip to the most posterior extremity of the tail.

The relationship between velocity and driven frequency is shown in Figure 4.18. The corresponding values of Modes 1 and 2 during consistent swimming were measured and compared to current robotic fish. Mode 1 achieved maximum velocity of 2.2Bl/s (0.55m/s), at 6.1Hz. Mode 2 increased maximum velocity to 2.8BL/s (0.70m/s) at 6.6Hz. Mode 2 has significantly increased performance in comparison with current robotic fish which typically

peak around 1BL/s. An initial value of 3.4BL/s (0.87m/s) at 6.8Hz was recorded by Mode 2 with an oil filled structure. Sealing the developed skin when in contact with oil was difficult and leaks consistently affected stability and buoyancy dramatically affecting performance.

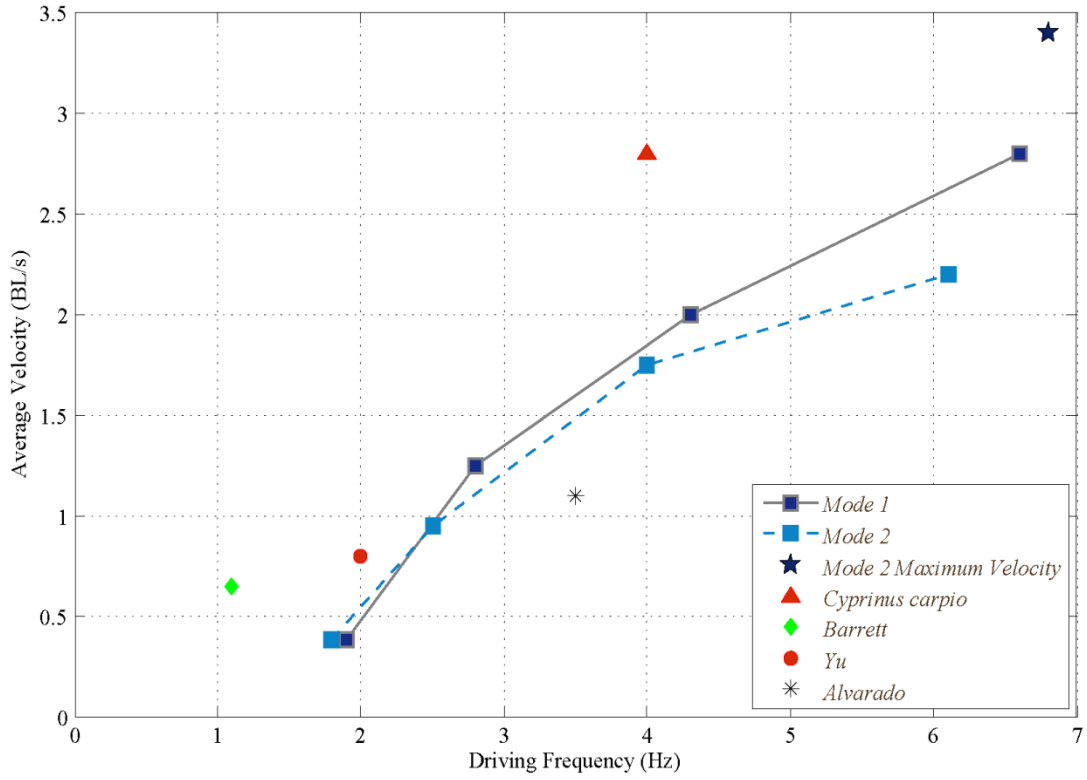

Figure 4.18: Comparison of average velocities achieved by both Modes, contrasted against current robotic fish and the common carp.

4.5.5. Average Thrust (N)

In Figure 4.19 we can notice that Mode 2 had an 85% increase of thrust and a 27% increase in velocity over Mode 1 whilst consuming only 7.68W of power at 2.8BL/s. As the power supply contributes to a significant portion of the total mass, high energy efficiency is important. The low energy consumption measured indicates that the next generation could carry its own power supply within a comparable geometric frame with good endurance.

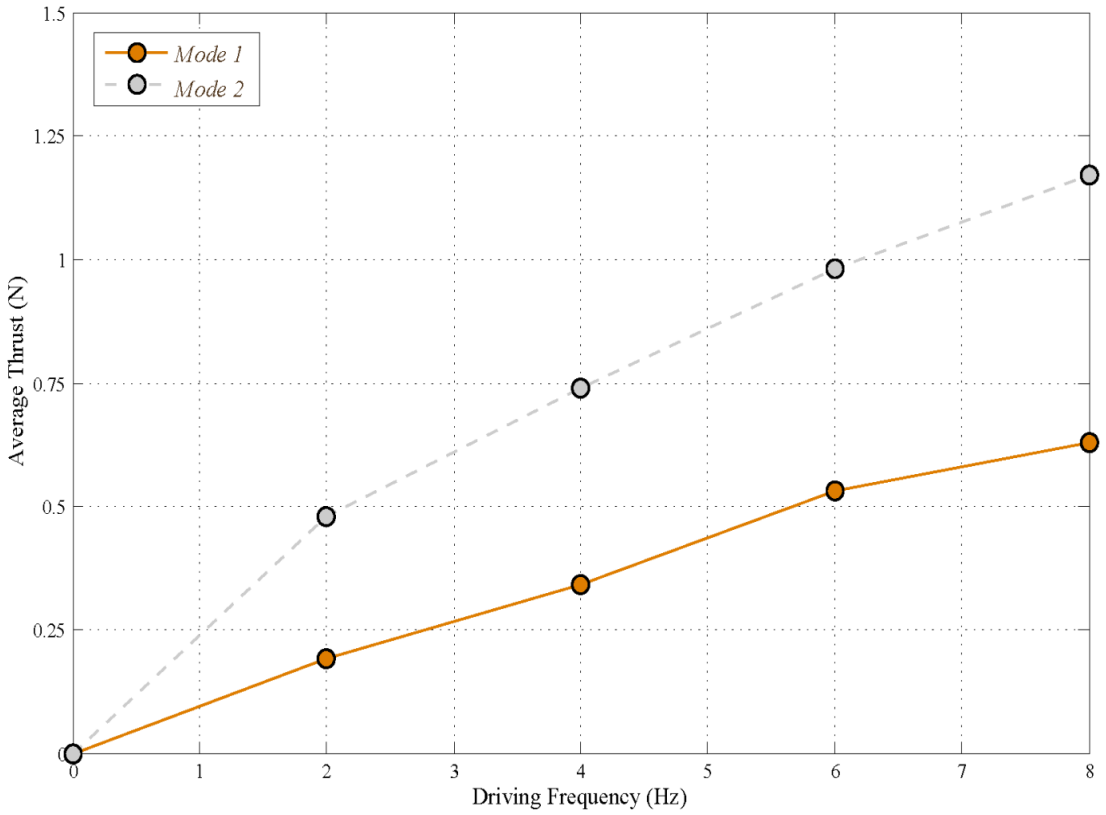

Figure 4.19: Comparison of average thrust in relationship to driven frequency achieved by both Modes.

4.5.6. Comparison of Non-dimensional Parameters and Key Metrics

A prominent parameter for analyzing BCF locomotive performance is the Strouhal number (*St*). *St* is considered optimal within the range of $0.25 < St < 0.40$. Mode 1 has a peak *St* of 0.48 under the condition of $Re = 1.3 \times 10^5$ and Mode 2 consistently measured a $St = 0.41$ and peaked at a $St = 0.34$ under a condition of $Re = 2.1 \times 10^5$. A comparable live fish was measured in [1] to have a $St = 0.34$, $Re = 2\sim8 \times 10^5$. This results show a high performance increase by applying Mode 2 within the *St* optimum range and achieving the higher cruising speeds of swimming fish.

As higher frequencies were applied velocity increased in both Modes, this has previously not always been measured in robotic fish [117]. From this it can be assumed that a further increase of frequency applied to this prototype would continue to increase its performance, as reported in the findings of live fish [51].

Analysis –

- Future experimental analysis will greatly benefit from visualization techniques, accurately measuring fluid flow. However, a few assumptions can be deduced to account for the increase in speed: 1) The magnitude of propulsive force was increased by initiating the starting moment of added mass upstream; 2) The developed structural arrangement allowed for smooth transition of flow along the length of body; 3) Anterior and/or mid-body vortices where formed, coordinated and propagated downstream; 4) Lateral and thrust forces were optimized around the center of mass; 5) A reduction in drag resistance was due to the reduced anterior amplitude errors.

4.6. Further Experimental Analysis of *iSplash*-I

In Section 4.5 it has been shown conclusively that a significant increase in performance, in terms of linear swimming speed, is gained over the traditional posterior confined wave form, by coordinating the full-body length of the Carangiform swimming motion. The proposed swimming motion coordinated anterior, mid-body and posterior displacements and was found to also reduce the large kinematic errors seen in free swimming robotic fish.

The experimental testing shown in Section 4.5 raised many questions that could not be answered without further analysis. Therefore it was proposed to continue conducting experimental tests on this platform by developing modifications to the mechanical structure to further analyses and improve performance.

4.6.1. Research Objectives

This experimental research project considered the factors contributing to the current hydrodynamic performance within linear locomotion. Three main objectives were proposed:

(i) Experimentally test untried lateral displacement parameters by measuring each segment's contribution to the performance in terms of swimming speed measured in BL/s and kinematic parameters accuracy (Section 4.6.2).

(ii) Experimentally test the developed skin which allowed for a smooth transition of flow along the body length, validating its improvement in terms of speed and mechanical resistance (Section 4.6.5).

(iii) Optimize the caudal fins aspect ratio, shape and magnitude by experimentally testing numerous variations in design to improve the prototypes swimming performance (Section 4.6.7).

4.6.2. Modes 3-5: Restricted Swimming Patterns

To provide a further investigation into the kinematic parameters of the Carangiform swimming motion Mode 2, each portion of the swimming pattern will be measured in terms of its contribution to the maximum velocity measured in BL/s. Three new operational Modes were proposed: Mode 3, as illustrated in Figure 4.20 will measure the contribution of the mid-body, actuating only the anterior and posterior holding the mid-body rigid; Mode 4, as illustrated in Figure 4.21 will measure the contribution of the posterior motion, applying actuation to only the anterior and mid-body; Mode 5, as illustrated in Figure 4.22 will measure the contribution of the posterior and mid-body combined, applying actuation to only the anterior segment. These swimming modes were compared against the results of Mode 2 and Mode 1, where Mode 1 provides the measurement of the anterior and mid-bodies combined contribution to the swimming performance.

4.6.3. Modifying the Mechanical Structure

Figure 4.5 shows the discrete link structure of *iSplash*-I, which distributes five links across the body length. This structure was found to provide the desired kinematics for the Mode 2 full body length wave motion (anterior, mid-body and posterior) and a smooth curvature for the outer body surface.

To achieve the required kinematic parameters of Modes 3-5 a modification of the mechanical structure was required. The structural changes adjusted the individual offset cams so that activation of its associate linkage would be disregarded or held along the midline during the actuators rotation, therefore allowing passive or rigid links at the potion of body length required by each mode for analysis. This was engineered by removing the baffle plates or offsetting the drive cams along the cam shaft far enough to miss the baffle plates coupled to the linkages. The components described above are identified in Figures 4.1 and 4.2. Mode 3 holds mid-body links II and III along the centreline, actuating only anterior link I and posterior links IV and V. Mode 4 holds posterior links IV and V rigid, actuating links I-III. Mode 5 holds mid-body and posterior links rigid, actuating only link I. The addition operational Modes allow every section along the length of the build to be individually

measured for its contribution to the prototypes maximum velocity. After the modification these described mechanical operation modes were easily accessible as the novel developed prototype allowed for all Modes 1-5 to be applied to the same prototype by adjusting the configuration.

4.6.4. Experimental Testing of the Restricted Swimming Patterns

Swimming Pattern Observation –

Figures 4.20 – 4.22 show an approximation of the midline curvature of Modes 3-5 in eight instances with time intervals of 0.02s throughout one body cycle. The midline was tracked at 50 frames per second to provide the amplitude envelopes of the anterior and posterior and the central pivot point for comparison of Modes 3, 4 and 5. Mode 3, which restricts the mid-body movement, was found to have no change in head or tail amplitude or midline line pivot point when compared to Mode 2. Mode 4, which restricts the posterior, had equal head amplitude to Modes 2 and 3 and an approximately identical pivot point to Mode 1. We can see that the tail amplitude was very small measured at 0.02 (0.005m) of the body length. Mode 5 confining movement to the anterior had equal head amplitude to Modes 2, 3 and 4, approximately equal pivot point to Mode 2 and tail amplitudes equal to Mode 4.

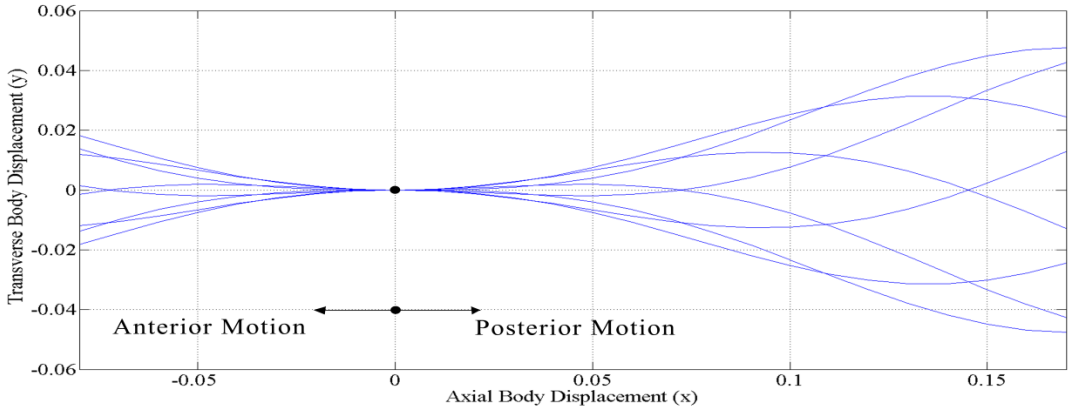

Figure 4.20: Mode 3: Transverse displacement of the mid-body is confined to the centreline with only displacement of the anterior 1/5 and posterior 2/5.

We can see from the observational results, that the kinematic parameters of Modes 4 and 5 are greatly altered, whereas Mode 3 had little effect on amplitude and pivot point in comparison to Mode 2. However, due to the removed mid-body links the entire build

generated a large sideways destabilization motion within the horizontal plane whilst operation in Mode 3 greater than Mode 2.

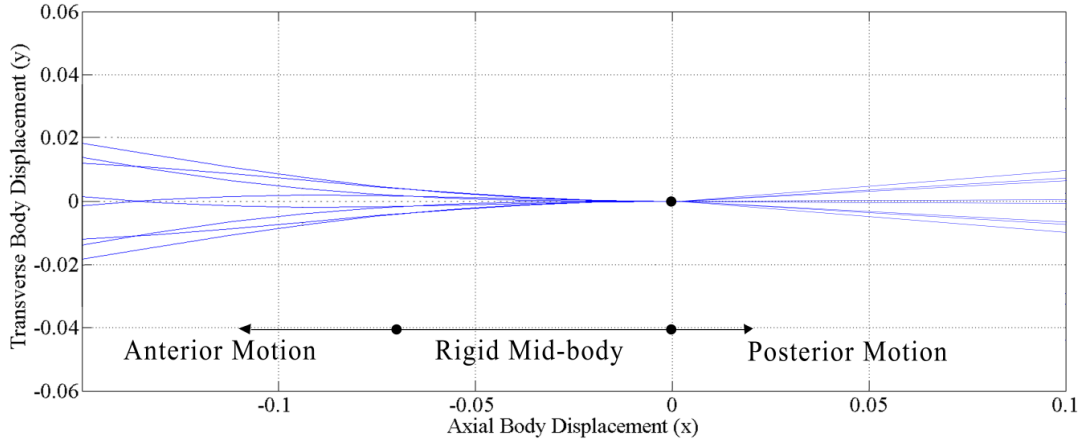

Figure 4.21: Mode 4: Transverse displacement is confined to the anterior and mid-body with a rigid posterior 2/5.

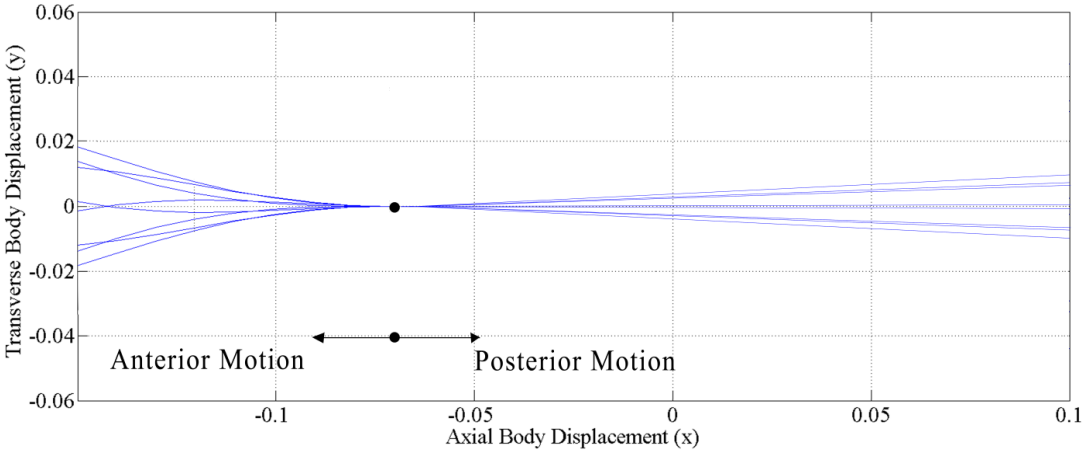

Figure 4.22: Mode 5: Transverse displacement is reduced to the anterior 1/5 with a rigid a mid-body and posterior (The generated midline approximations in Figures 4.20-4.22 were determined from experimental tests).

Experimental Results- BL/s, Watts and Hz –

- By removing the actuation of the mid-body for Mode 3, the prototype had a large reduction of 28.6% in average maximum velocity measuring 2.0BL/s (0.51m/s) indicating the significance of this segment to the full-body swimming pattern of Mode2, despite any change in kinematic amplitudes or pivot point. Removing the actuation of the posterior 2/5's (peduncle and caudal fin) for the Mode 4 swimming pattern, had a great impact on performance reducing maximum velocity to 0.2Bl/s (0.05m/s) showing the tail is required

for 92% of the prototype's speed (Figure 4.23). This result approximately agrees with Bainbridge's study [134] in which the tail was removed from a dace, also measuring a large reduction in performance of 80%. Lastly, Mode 5 removed actuation of the posterior and mid-body actuation. The prototype during operation in this swimming pattern measured no noticeable positive or negative movement.

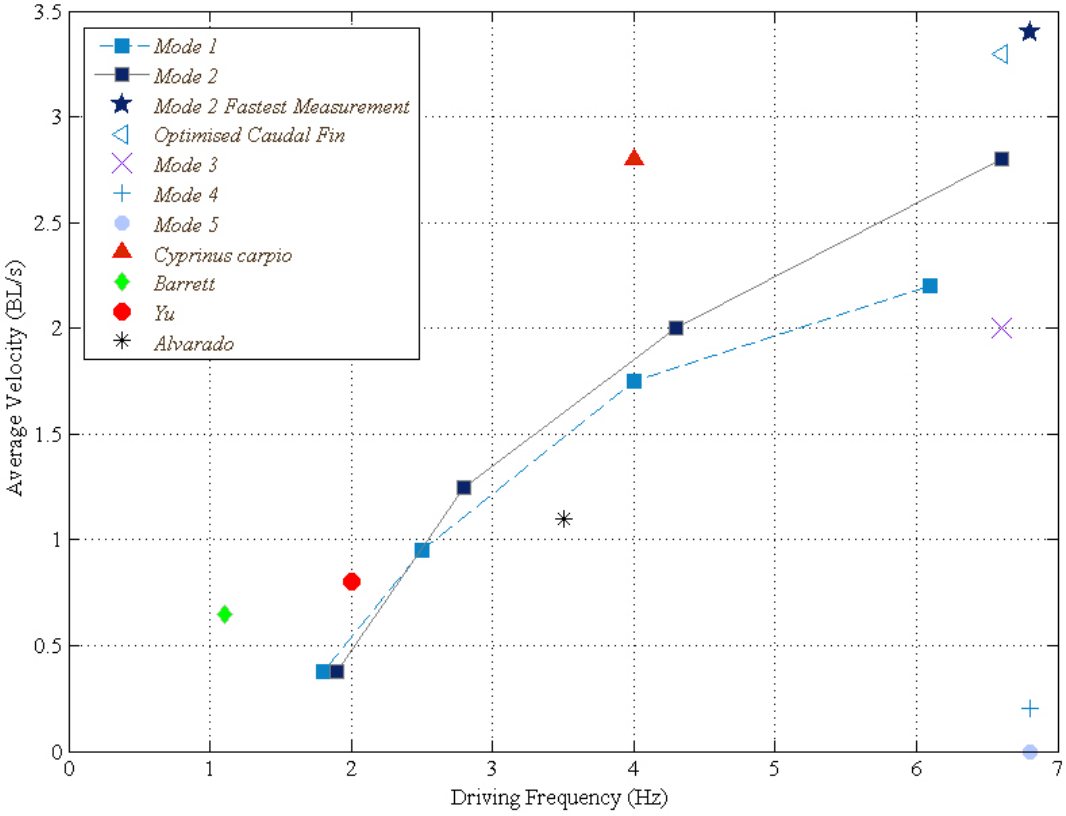

Figure 4.23: (Updated Figure 4.18) Comparison of average velocities achieved by *iSplash-I* Modes 1-5 and operation with the optimized caudal fin Tail 9, compared against current robotic fish and the common carp.

Table 4.3: Comparison of Test Results between Modes 3-5.

Parameters	Mode 3	Mode 4	Mode 5
Reynold Number: *Re* (10^5)	1.2	0.12	0.
Shrouhal Number: *St*	0.51	0.68	N/A
Consistant Maxium Velocity: BL/s (without skin)	2.0	0.2	0
Consistant Maxium Velocity: m/s (without skin)	0.51	0.05	0
Frequency: Hz	6.6	6.8	6.8
Swimming Number: *Sw*	0.31	0.02	0
Head Swing Amplitude: m	0.044±0.002	0.018±0.002	0.018±0.002
Tail Swing Amplitude: m	0.044±0.002	0.005±0.002	0.005 ±0.002
Test Run Distance: m	0.5	0.5	0.5

4.6.5. Developing a Skin

A significant development of the prototype was a watertight skin which was devised to allow for unrestricted flexing of the external surface and provided the volume needed to maintain neutral buoyancy. The skin was constructed of 0.2mm polypropylene sheet. This was heat sealed on to the prototype so that the exact geometries of the body could be attained, by tightly fitting around the space frames attached to the driven links. The skin was devised to aid the aerofoil section's (NACA (12)520) smooth shape and therefore aimed to provide a smooth transition of flow from nose tip to tail.

The prototype structure was modified to allow for external hardware cables to exit the sealed body through the top pivot point of joint III. This provided a more robust material of stainless steel for the cables to exit from as the developed skin fabricated from thin polypropylene was fragile. During the developmental stages of the process thicker materials such as latex, cotton and various plastic sheets were tested. These were found to require large forces to stretch or loose fabricated skins produced large salient edges, estimated to stall fluid flow or increase energy consumption.

4.6.6. Experimental Testing of the Developed Skin

Swimming speed tests were conducted to measure the velocity during swimming with and without the outer skin. The prototype whilst deployed with the developed skin was found to provide a performance increase of 24% in maximum velocity increasing from 2.12BL/s to 2.8BL/s. In addition no increase in energy consumption was measured during actuation in air

or test runs in water. Hence we can estimate the skins surface allows for a smooth transition of flow from nose tip to tail reducing stall in the fluid flow and the developed skin requires no additional energy during actuation.

4.6.7. Caudal Fin Optimization

Fish have evolved with thousands of diverse fin designs [3; 52; 136; 137; 138; 139; 140; 141; 142; 143; 144; 145; 146; 147] (Figure 4.24), analysis of the muscle structure has measured approximately fifty discrete muscles within the caudal fin. The large surface of the caudal fin is a key element in generating propulsion. Bainbridge studied the importance of the caudal fin to the propulsive thrust, measuring a value of 45% for a beam to 84% for a dace [23]. The caudal fin was also observed to be controlled during transverse movement where bending, stretching and un-stretching affected the swimming motion. Additional studies on the gestures of the caudal fin identify five motions: cupping, undulations, flat movement of the entire fin, w-shaped motion and rolling. Experimental research has found that variations in peduncle and caudal fin stiffness greatly affect propulsive thrust [52; 136; 138; 140; 143; 146]. Hence, optimizing the caudal fin for performance increase in terms of swimming speed may require a mechanism of great dexterity.

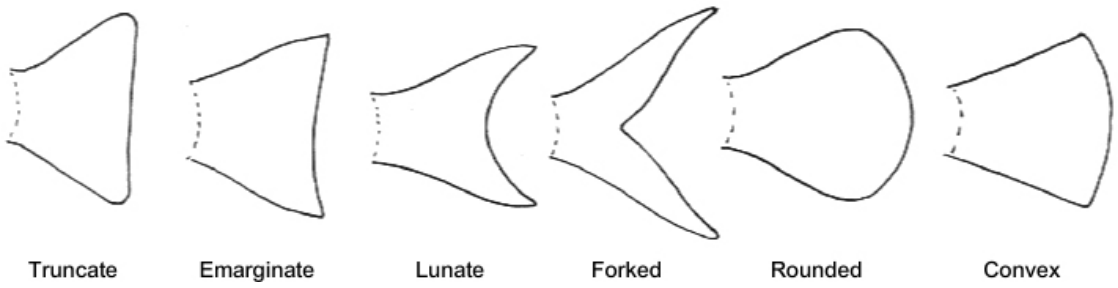

Figure 4.24: Side profiles of the prominent evolved caudal fins [144].

The first generation prototype is free swimming allowing for accurate unaffected measurements to be taken, as previous research has been measured on robotic fish supported by beams or isolated caudal fins without a complete body which effects the upstream flow. As caudal fins have not been experimentally tested on free swimming robotic fish at high speeds above 1BL/s, the conducted tests may provide improved data for optimizing caudal fins for Carangiform fish.

To tune the caudal fin shape on the free swimming prototype numerous profile designs were developed and experimentally tested at the prototypes maximum frequency to measure

their performance in terms of maximum velocity. The physical specifications of the developed Tails are given in Table 4.2 and illustrated in Figure 4.25. The numerous Tail designs are based on real fish or have been adapted in shape or scale to experiment previously untried caudal fins. The following adaptions of real fish fins are considered: Truncated, Forked, Emarginate and Forked (Figure 4.24) [148]. The adaption of high *AR* caudal fins are designed to minimise drag in fast cruising fishes, with the adaption of lower *AR* fins suitable for rapid acceleration and the caudal fin of the Carangiform considered a generalist with a middle range *AR* caudal fin.

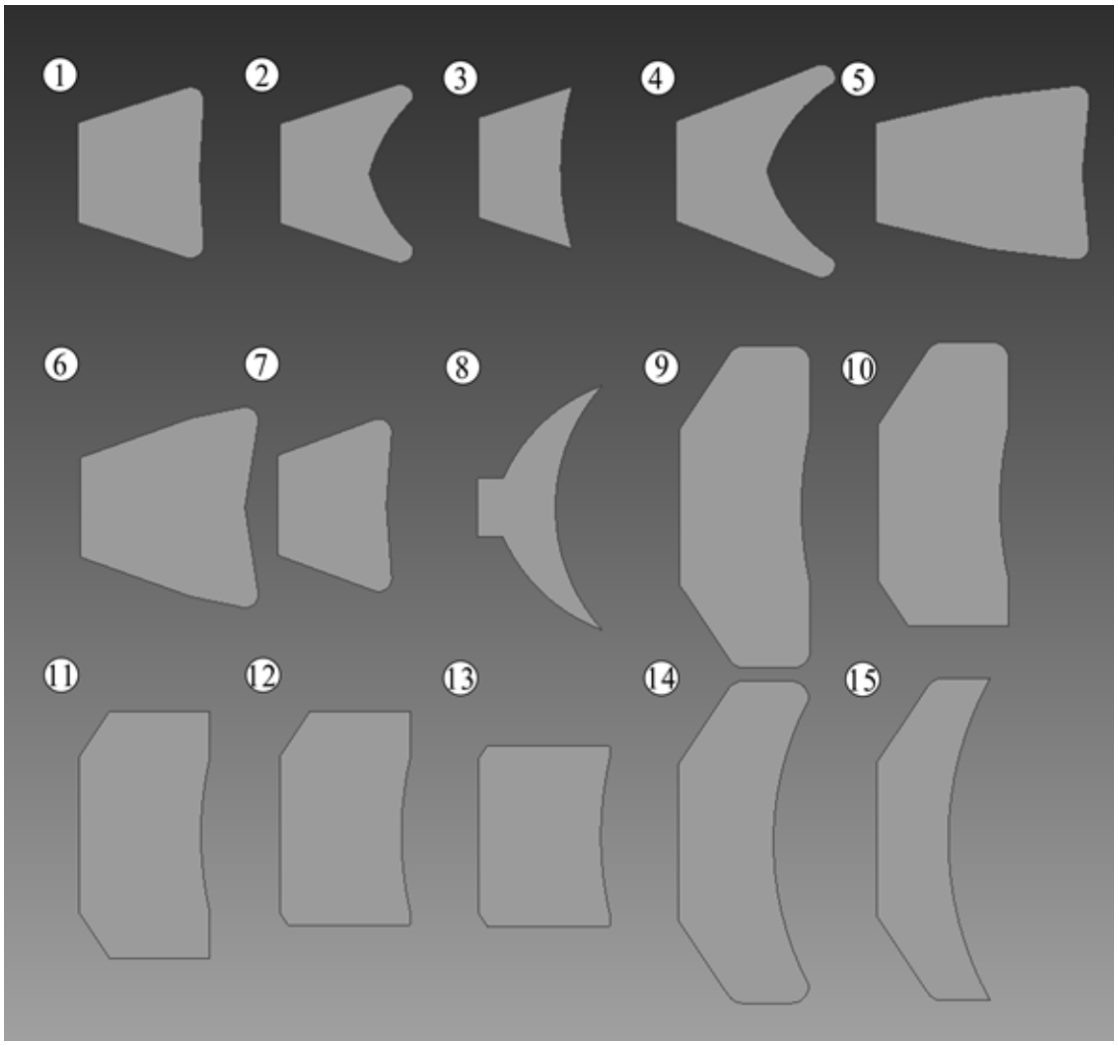

Figure 4.25: Side profiles of the caudal fins experimentally tested, Tails 1-15. The numerous Tail designs are morphological approximations of real fish caudal fins or have been adapted in profile to experimentally test previously untried fins.

The original tail design of *iSplash*-I was a morphological approximation of the common carp. This tail design i.e. Tail 1 had a variation in thickness of 1mm at the peduncle and

reduced to 0.5mm at the furthest tail tip. To increase the accuracy of the experimental testing of numerous tail designs each Tail 1-15 has a uniform thickness of 1mm. Tails 1-4 and 6-7 are approximations of the common carp or trout with slight adaptions in either height or length. Tail 5 is an approximation of a pike, extended in length. Tail 8 is an approximation of the lunate shaped tail of a tuna. Lastly Tails 9-15 are variations in height and length based on the highest performing caudal fin design from Tails 1-8.

4.6.8. Caudal Fin Observation and Results

All runs during the testing of the fifthteen caudal fins were conducted with attached stilts to the bottom of the prototype so that tail shapes with increased depth would not be affected by contact with the tanks bottom surface. In initial testing Tail 1 with a low aspect ratio (AR) =1.73, based on a real common carp provided a consistent swimming speed of 2.8BL/s (0.55m/s). The original tail with thickness variation and the newly tested Tail 1 with uniform thickness of 1mm recorded no change in swimming speed. AR is calculated using: AR=$b2/Sc$ where b squared is the fin span and Sc is the projected fin area. Although high aspect ratio (AR) caudal fins such as the lunate shaped tail of a tuna (Tail 8 with an AR=5.3) have been found to produce greater swimming performance for real fish [4; 7], Tails 9 and 10 with middle to low AR, 2.8 and 2.4 respectively were found to produce the greatest increase in speed, increasing the maximum velocity by a further 20% to 3.4BL/s (0.87m/s). The profile shape of Tail 9 and 10 have a significantly large surface area in comparison to a real common carp increasing from 3501mm^2 to 6739mm^2 in Tail 10 and 7397mm^2 in Tail 9. It was also found that the prototype showed no signs of failure from the increased pressure and the head amplitude of Mode 2 was unaffected, maintaining an amplitude of 0.0018m.

It can be noted that the new shape is comparable to lunate tail profile of the tuna modified by increasing the size of the Sc length. In addition the optimized tail also achieved a slight performance increase by reducing the frequency from 6.8Hz (measured from a one off run with an oil filled structure) to 6.6Hz equivalent to operational Mode 1 with deployed Tail 1 but with an increased BL/s of 20%.

It was observed due to the heterogeneous build, the posterior 2/5 of the body length deforms due to stiffness distribution providing a smooth transition phase between body and tail tip as shown in Figures 4.15 and 4.16. Although camera shots of the side and front views of the prototype were unable to be taken during swimming within the test tank it could be

seen from the above images that the tallest fins Tail 9,10,14 and 15 suffered from large deformation at the front, top and bottom edges due to the surrounding fluid pressure. We can estimate that developing a structure that is able to maintain rigidity along the front edge may significantly improve performance further. Variations in thickness, increased height, three-dimensional deformation and increased scale of Tail 9 or 10 may still increase performance further.

Table 4.4: Comparison of Tails 1-15.

Caudal Fin No and Description	Aspect Ratio	BL/s
Tail 1: Orginal Block Carp 55mm	1.7	2.8
Tail 2: Carp 49mm L	2.0	2.5
Tail 3: Short Carp 45mm L	2.3	2.1
Tail 4: Mackerel 72mm L	2.5	2.6
Tail 5: Longest Carp 93mm L	1.1	2
Tail 6: Long Carp 74mm L	1.4	2
Tail 7: Short Carp 49mm L	1.9	2.6
Tail 8: Tuna- Lunate Tail 110mm b	5.3	2.1
Tail 9: Tallest 145mm b	2.8	3.4
Tail 10: Tall Top 128mm b	2.4	3.4
Tail 11: Tall 111mm b	2.0	3.2
Tail 12: Tall Top 96mm b	1.7	3
Tail 13: Tall Front 80mm b	1.4	3
Tail 14: Tall Thin 43mm L	3.3	2.7
Tail 15: Tall Tail 31mm L	4.5	2.4

4.7. Summary

In this chapter, we show conclusively that a significant increase in performance, in terms of linear swimming speed (Section 4.5.4), is gained over the traditional posterior confined wave form, by coordinating the full-body length of the Carangiform swimming motion. The innovative mechanical drive system (Section 4.4.1) increased maximum velocity over current

published robotic fish. In fact, the robotic prototype continued to increase its velocity as increased frequencies were applied, indicating, that the high swimming speeds will continue to increase with an increase of frequency. The proposed swimming motion coordinated anterior, mid-body and posterior displacements and was found to reduce the large kinematic errors seen in free swimming robotic fish (Section 4.5.2). In the first experimental tests *iSplash*-I achieved a maximum velocity of 3.4BL/s and consistently achieved a velocity of 2.8BL/s at 6.6Hz with a low energy consumption of 7.68W (Section 4.5).

Further experimental analysis of the first generation was undertaken (Section 4.6). Firstly we showed, that applying a small change to the full-body length swimming pattern at the mid-body stage a significant reduction in performance of 28.6% is seen, indicating the importance of anterior, mid-body and posterior coordination. The results of testing Mode 5 identified the importance of the accurate posterior undulations to the swimming motion as the swimming speed was reduced by 92% to 0.2BL/s (Section 4.6.4). Secondly, the contribution of the developed skin, constructed with a sealed smooth surface from nose tip to tail was measured and found to greatly improve swimming speed performance by 24% from 2.12BL/s to 2.8BL/s without increasing mechanical resistance and therefore the energy consumption (Section 4.6.6). Lastly, a new caudal fin design was developed (Section 4.6.7). The profile shape was optimized on the free swimming robotic fish and found to improve the consistent swimming speed by a further 20% to 3.4BL/s. In addition, a slight reduction of driven frequency from 6.8Hz from 6.6Hz was measured. This design of caudal fin has a surface area approximately three times greater than a real common carp. It was also found that the prototype showed no signs of failure from the increased pressure and the head amplitude of Mode 2 was unaffected maintaining the amplitude of 0.0018m (Section 4.6.8).

The experimental analysis of the first generation has shown potential to improve the high performance swimming. The following points are of significant interest for the next stage of research:

1) The prototype showed no signs of peak, decline in velocity or failure as higher frequencies were applied. A prospective future investigation could be to apply a further increase of frequency where we estimate that the prototype would continue to increase its performance.
2) By improving the tail shape swimming performance was increased. We can further develop the tail by testing variations in materials, thickness and length of peduncle and therefore altering the deformation of the caudal fin. Previous research has been

recorded whilst either restricted by support beams at low swimming speeds or not attached to a body, hence affecting measurements. By conducting the test upon a free swimming fish the variations in caudal fin design will directly affect swimming speed. Other variations may include angle of attack and increasing rigidity of the top and bottom edges to reduce their deformation.

3) Further optimizing the kinematic parameters along the full length of the body may provide an improved performance, requiring a precision adjustment mechanical drive system, able to offset the discrete links of the body wave at varying amplitudes.

4) The low energy consumed indicates that the development of a prototype carrying its own power supply within a comparable sized frame is possible. We can estimate that a duration of swimming for long periods of time is feasible.

Chapter 5

iSplash-OPTIMIZE: Full-Body Wave Optimization

This chapter presents a new robotic fish, *iSplash*-OPTIMIZE [129], which is 0.6m in body length and deploys a single actuator to drive discrete links across the full-body length. The main focus is on optimizing the kinematic parameters of its linear Carangiform swimming motion in order to improve the distance travelled per beat. The experimental results show that the drive system can be actuated at high frequencies up to 20Hz due to deploying a continuous rotary power source. Each discrete link is able to be precisely tuned during non-productive actuation, providing accurate kinematics with little mechanical loss. Further experimental tests validating the swimming performance found the forward resistance to greatly overshadow the forward productive force and swimming speed was found to be lower than estimated in comparison to the first generation. This chapter details the design, construction, measurements and analysis of the second generation prototype.

The remainder of the chapter is organized as follows: After Section 5.1 Introduction, the research objectives are detailed in Section 5.2. Section 5.3 presents the linear carangiform swimming patterns to be investigated. Section 5.4 describes the mechanical design and construction method of the new build *iSplash*-OPTIMIZE with the deployed embedded system is given in Section 5.5. Section 5.6 describes the experimental procedure and results obtained. Concluding remarks and future work are given in Section 5.7.

5.1 Introduction

To measure the efficiency of the swimming motion a prominent parameter is the distance traveled per body length during one caudal fin oscillation. This can be calculated using the Swimming number (*Sw*) [118] (Section 3.1). The distance travelled per tail beat of the Cyprinus carpio (common carp) is highly efficient measuring a *Sw* of 0.7, with the highest recorded example of the Tursiops (Bottlenose dolphin) with a *Sw* of 0.82. Currently the *Sw* of existing robotic fish far lower than the measured common carp, with the highest examples being: Valdivia y Alvarado's compliant structure assembly recording a *Sw* of 0.3 at 1.1BL/s [117], Liu's and Hu's G9 Carangiform swimmer recording a *Sw* of 0.78 at 1.02BL/s [20] (The Swimming number of G9 is very large due to the effects of drifting) and Yu's discrete assembly recording a *Sw* of 0.4 at 0.8BL/s [116].

The second generation platform has been developed with the aim of improving the efficiency of the body wave and therefore the swimming performance. This is where fish surpass current man-made drive systems. As detailed the fish locomotive mechanics is able to coordinate with the surrounding flow, if precision kinematics are obtained, a passive body resonating within the *Karman Vortex Street* can generate forward locomotion with the highest locomotive efficiency [11; 30] (Section 2.6).

Previous research [113] has developed kinematic parameter optimization by utilizing a discrete link structure of connecting servo motors [116; 117]. This approach enables easy optimization by adjusting the variables of the actuators within the spatial and time vary body wave. Although this method has significant advantages such as simplicity of construction and tuning the kinematic parameters, the mechanical drive systems is greatly limited by force, frequency and morphological accuracy.

Motivation -

The first prototype *iSplash*-I (Chapter 3; 4) [114], (0.25m in body length, weighs 0.345kg, fabricated from aluminium and stainless steel and with a tethered power supply) achieved a high performance Carangiform swimming motion improving the accuracy of the kinematic displacements and greatly outperformed the posterior confined approach in terms of speed by 27% with a low energy consumption.

Based on intensive observation, the predetermined offsets of the discrete link assembly were set to generate the kinematic parameters of a common carp. Optimizing the discrete structure was limited as only the final link of over the full-body length was able to be

adjusted. Experimental testing found that its *Sw* of 0.42 was lower than a common carp's. The coordinated full-body length swimming motion provided accurate kinematics directly related to increased swimming performance, we estimate that further tuning of the kinematic parameters may provide a greater increase in maximum velocity and reduce the cost of transport. In consideration of this *iSplash*-OPTIMIZE was proposed, shown in Figures 5.1 and 5.12.

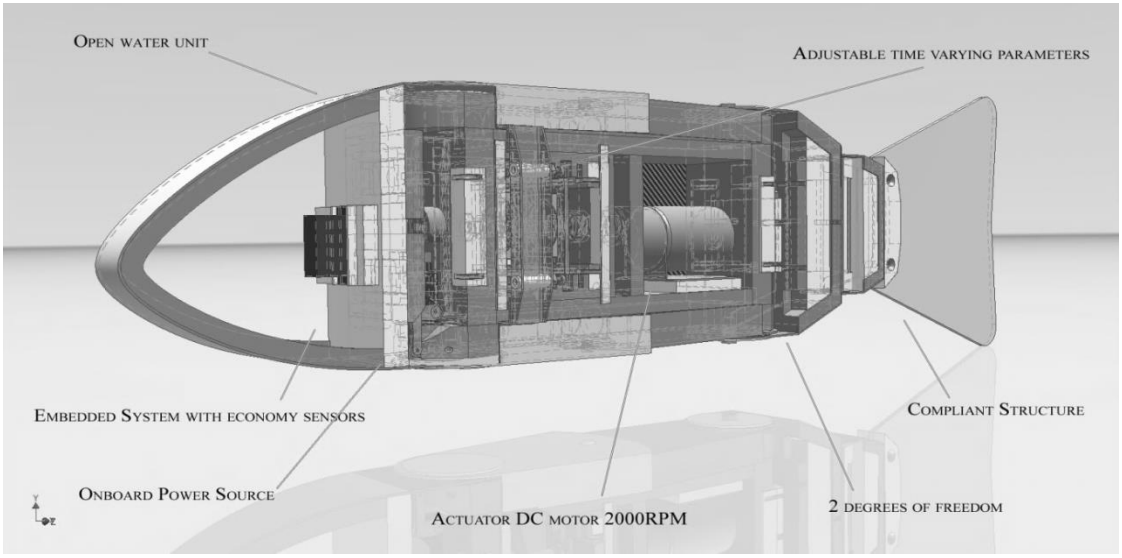

Figure 5.1: *iSplash*-OPTIMIZE.

5.2. Research Objectives

This research aims to improve the efficiency of the linear swimming motion with eight main objectives:

(i) to develop a new build mechanical drive system, capable of distributing power from a single actuator to discrete links across the full-body length;

(ii) to allow each discrete link of the assembly to be precisely tuned by devising a powertrain with innumerable adjustments;

(iii) to attain a structurally robust mechanical drive system capable of intensively high frequencies of 20Hz;

(iv) to devise a prototype able to carry a high capacity power supply to obtain consistent high force free swimming;

(v) to gain high speeds by developing a compact design taking into consideration geometric and kinematic parameters throughout the full tail beat cycle;

(vi) to obtain a low cost of transport by developing a mechanical drive system considering methods that may cause internal mechanical losses;

(vii) to deploy an electrical system accurately measuring energy consumption, destabilization, with perception sensing, wireless communication and ability to produce control signals for multiple actuators for future autonomy;

(viii) to validate the study by conducting a series of experiments measuring the prototype's achievements in terms of energy consumption and kinematic parameters.

5.3. Investigated Linear Swimming Patterns

This study aims to improve the accuracy of replicating the wave form of the Carangiform swimming mode, specifically the common carp, due to its high locomotive performance [118]. Identified by the portion of the body length actively displaced, the selected Carangiform applies the swimming method of body and/or caudal fin propulsion, associated with the method of added mass. A full description can be found in [119]. Fish have an improved cost of transport over man-made systems by generating the method of added mass efficiently [1].

Free swimming robotic fish applying posterior confined displacements have shown significant kinematic parameter errors [20; 117]. Hence, the linear locomotive swimming motion over the full length of body has large matching errors in comparison to real fish leading to reduced propulsive force and a higher cost of transport. In addition the *Sw* may be improved by applying large reaction forces (F_R) at the cost of energy consumption without certain gains in maximum velocity.

The full-body swimming pattern *o*f the *iSplash* platforms proposed in [12] coordinates the anterior, mid-body and posterior body motions. Our primary aim of this study is to further optimize this swimming motion by adjusting parameters, estimated to enhance performance. In particular the displacements of full-body swimming pattern drive the anterior into the direction of recoil, reducing amplitude errors by optimizing the F_R of the propulsive elements. $y_{\text{body}}(x,t) = (c_1 x + c_2 x^2)\sin(\mathrm{k}x + \omega t) - c_1 x \sin(\omega t)$ Furthermore the developed body motion enhances performance by producing a smooth transition of flow along the length of the body, effectively coordinating and propagating the anterior formed fluid flow interaction downstream. We can adjust the form in [9], an adaptation of (3.1) to generate the midline kinematic parameters of the full body displacements:

(5.1)

where the values c_1, c_2, k, ω can be adjusted to achieve the desired posterior swimming pattern for an engineering reference suitable for the geometric parameters of the second generation.

The mechanical drive system was devised to generate innumerable variations of the wave form, allowing a thorough investigation to identify the most efficient swimming motion within the limits of the structure. Some key deployed kinematic patterns are:

- The Traditional Carangiform swimming mode [1], applying a rigid mid-body and anterior, concentrating the undulatory motion to the posterior end of the lateral length, typically limited to <1/2 of the body length. The posterior confined kinematics of the Carangiform is of the form of (3.1) (Chapter 3) [7].
- The Thunniform swimming mode [1], confining the kinematic displacements to the caudal fin.
- The Anguilliform swimming mode [120]. Notably the fraction of the body length displaced of the full-body swimming motion of the *iSplash* platforms is equal to the anguilliform swimming mode (eel) but reflects changes in its kinematic form, as the full-body pattern applies an oscillatory motion to the anterior and mid-body segments and pivots the entire body around a single pivot point associated with the Carangiform swimming mode [118].
- Continued analysis of the full-body swimming motion by disregarding displacements of individual segments, to identify the contribution of each portion of the body length to the propulsion method.
- Advancing and retarding the timing of individual segments within the sequences of the spatial and time dependent full-body wave motion.
- Lastly, a series of tests investigating the effect of allowing individual segments to be passively moved by the surrounding fluid.

5.4. Construction Method for Full Body Optimization

5.4.1. Mechanical Design

The engineered platform 0.6m in body length is directly scaled from the structural link assembly of the first generation, as shown in Figure 5-2, Figure 5-3 and Figure 5-4. This method provides an arrangement that has previously achieved high performance, in which we aim to improve further by precisely optimizing the kinematic parameters. Previously the accuracy of replicating the wave form parameters has been limited by hardware and material constraints. The structural approach of the multi-link servo assembly has typically been applied to optimize the kinematic displacements. This method is limited by force, frequencies, volume and mass distribution which are also typically confined to the posterior, reducing accuracy of the wave form [116; 20; 78]. Alternative methods deploying single continuous rotary actuators have measured large internal mechanical losses due to the complexity of the mechanism [113].

The presented prototype deploys an assembly with structural compliance combined with rigid discrete links. The arrangement distributes three joints and one passive joint along the axial length to provide anterior, mid-body and posterior displacements and accurate midline curve alignment. The final posterior link V is coupled to a compliant scaled caudal fin, and is passively driven by four expandable tendons attached to the main chassis rear bulkhead, which can be adjusted experimentally to provide the targeted curves during free swimming at various frequencies, as achieved in [114]. Each of the discrete links across the body length can be configured to be actively displaced or held aligned with the centerline of the build. This development will allow analysis of each segments' contribution to the overall propulsion of the full-body wave form. In addition a significant aspect of drive system is the ability to attain free movement of individual links, allowing them to be passively moved by the surrounding fluid, as our subsequent work will investigate if the prototype is capable of extracting energy from the surrounding flow.

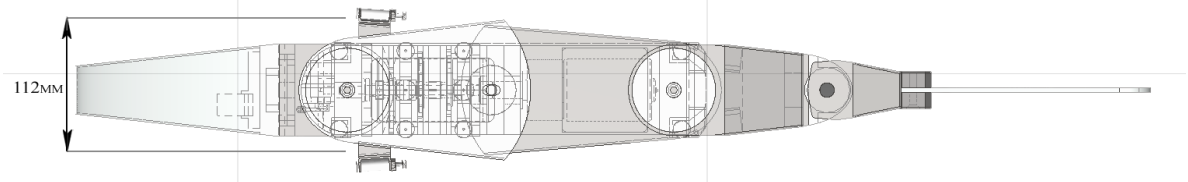

Figure 5.2: Plan view.

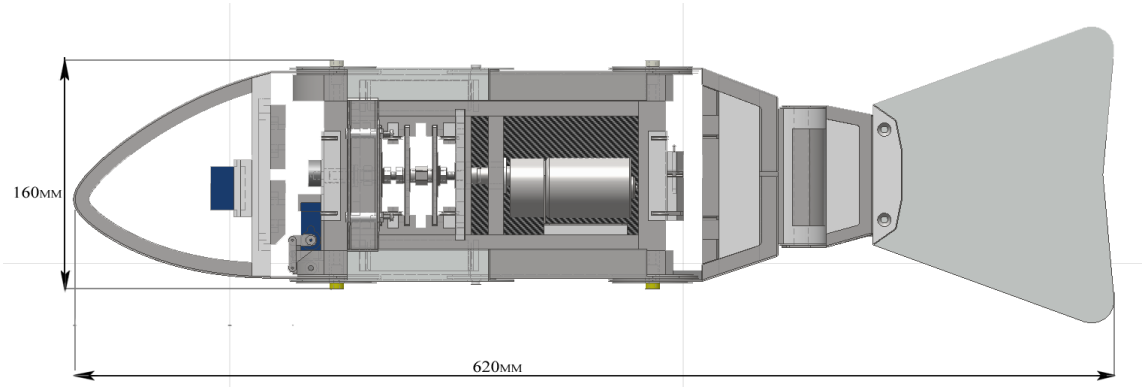

Figure 5.3: Side view.

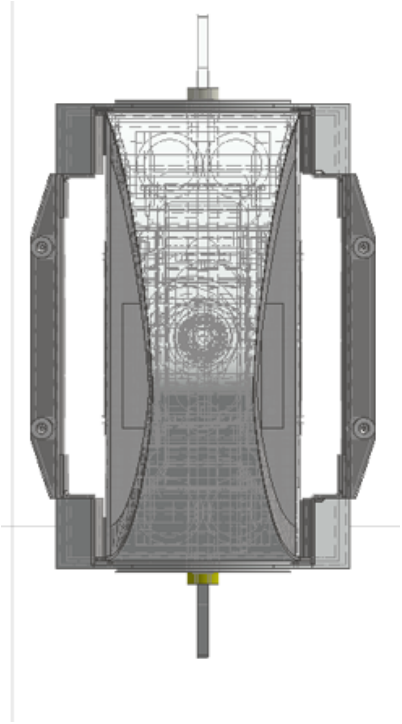

Figure 5.4: Front view.

5.4.2. Adjustable Offset Linkage Power Transmission System

The power transmission system was developed to transfer power to and provide precise adjustments of the discrete links (with innumerable sequences) with the smallest mechanical loss as possible, whilst actuating at intensively high frequencies due to deploying a single continuous high torque actuator. The developed powertrain transmitting rotary power to linear oscillating sliders (with 13mm displacements) is illustrated in Figures 5.5 - 5.8. The three key sliders are directly driven by the three adjustable offset discs (which are secured to

the drive shaft after adjustment), achieving equal power distribution, capable of transmitting power to discrete links across the full-body length from the lightweight tendons.

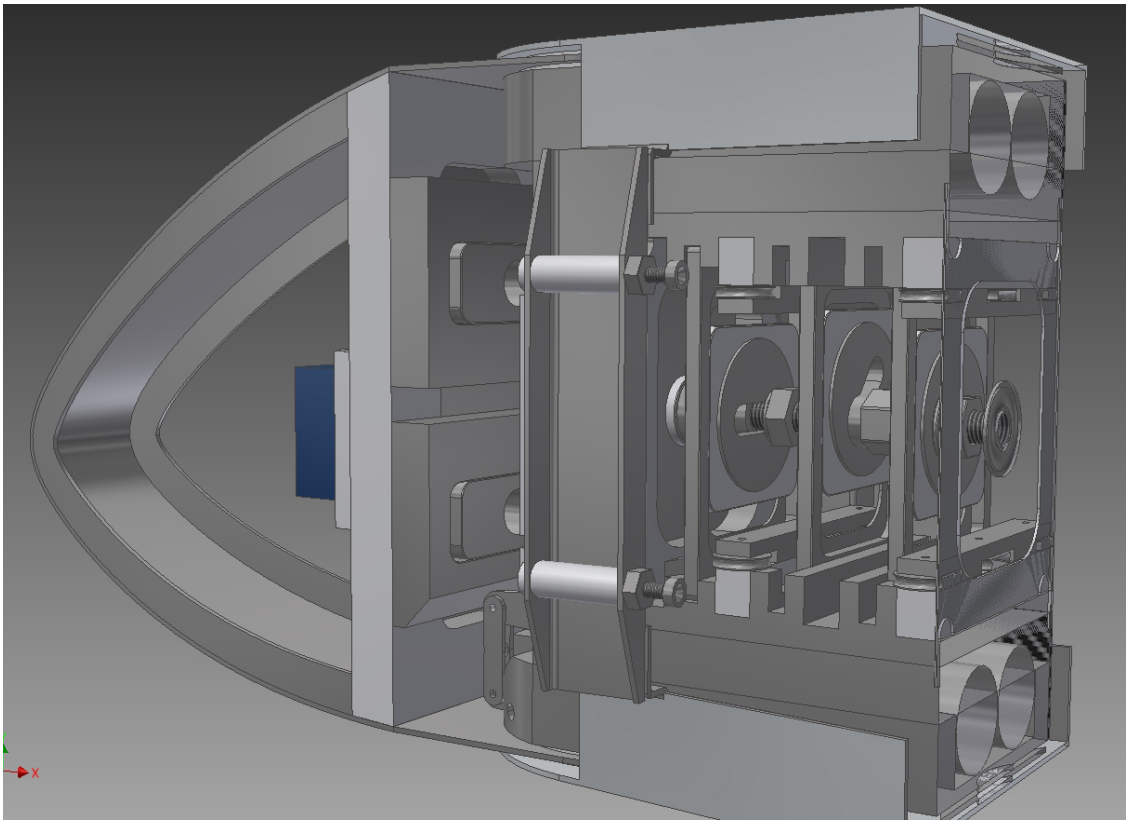

Figure 5.5: Adjustable power transmission system offset drive crank and linkage, cut through sectional image of front of platform.

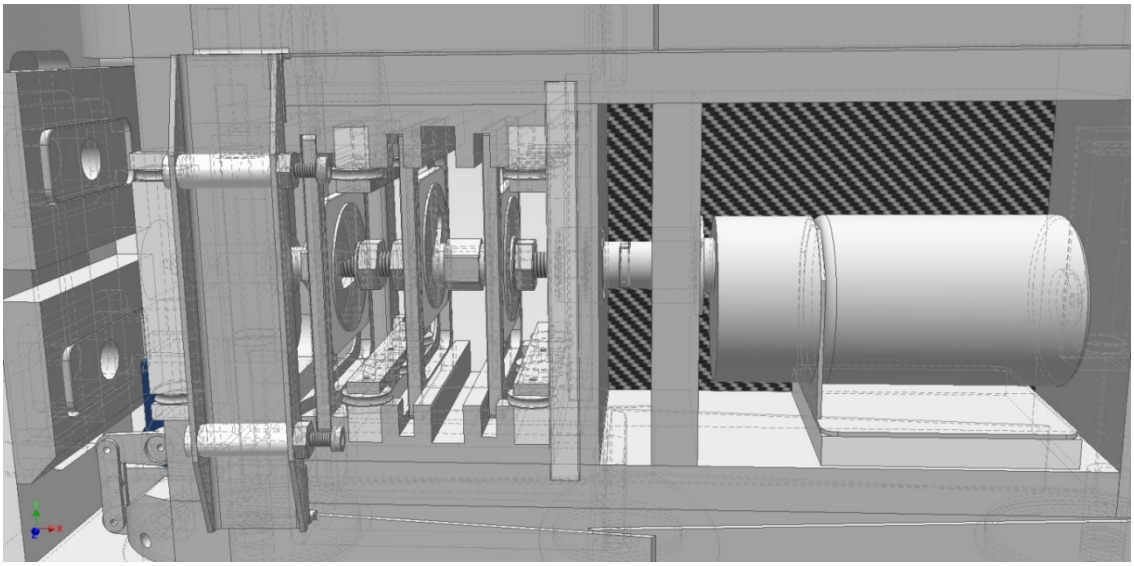

Figure 5.6: Adjustable power transmission system offset drive crank and linkage, side view includes actuator assembly.

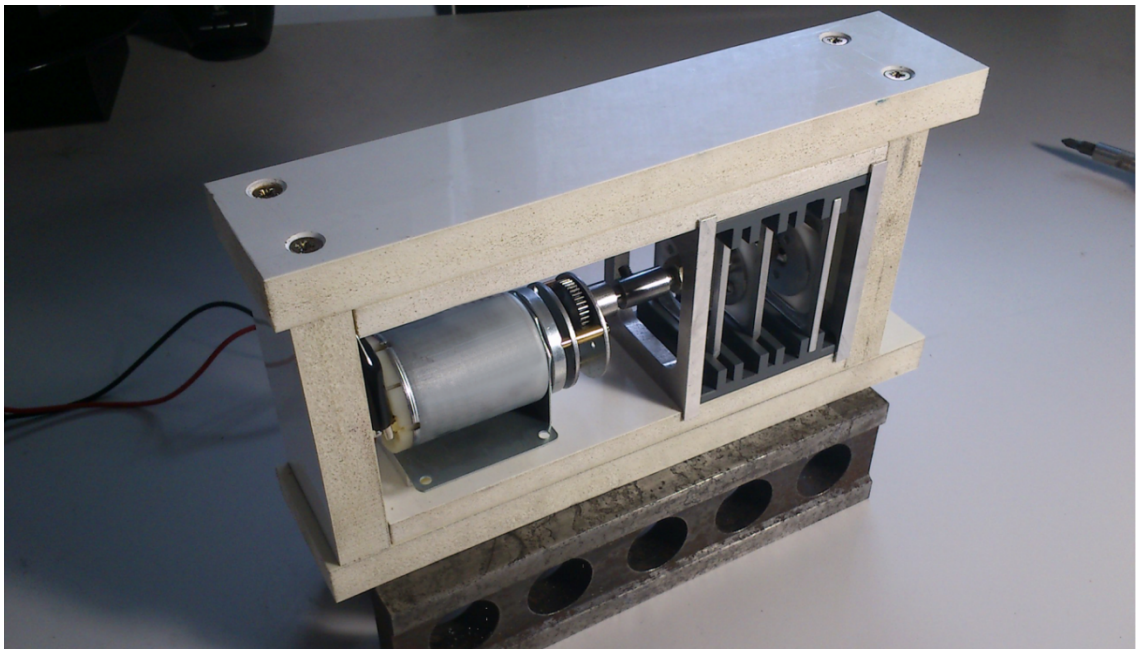

Figure 5.7: Inner structure of the central drive system.

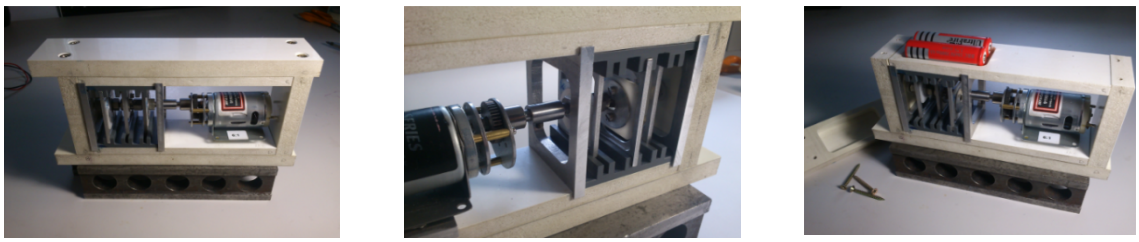

Figure 5.8: Inner structure of the central drive system.

Each of the discrete links was constructed with four adjusters increasing accuracy of the swimming patterns alignment by tuning the tendons (Figure 5.9). The developed mechanical drive system has high accuracy with unrestricted offset combinations, high structural strength and is small in size. This development is key to attaining an optimized swimming motion. The devised power transmission system required precision fitment of the chassis, crankshaft, cantilevers and linkages to avoid deadlock and reduce slide friction.

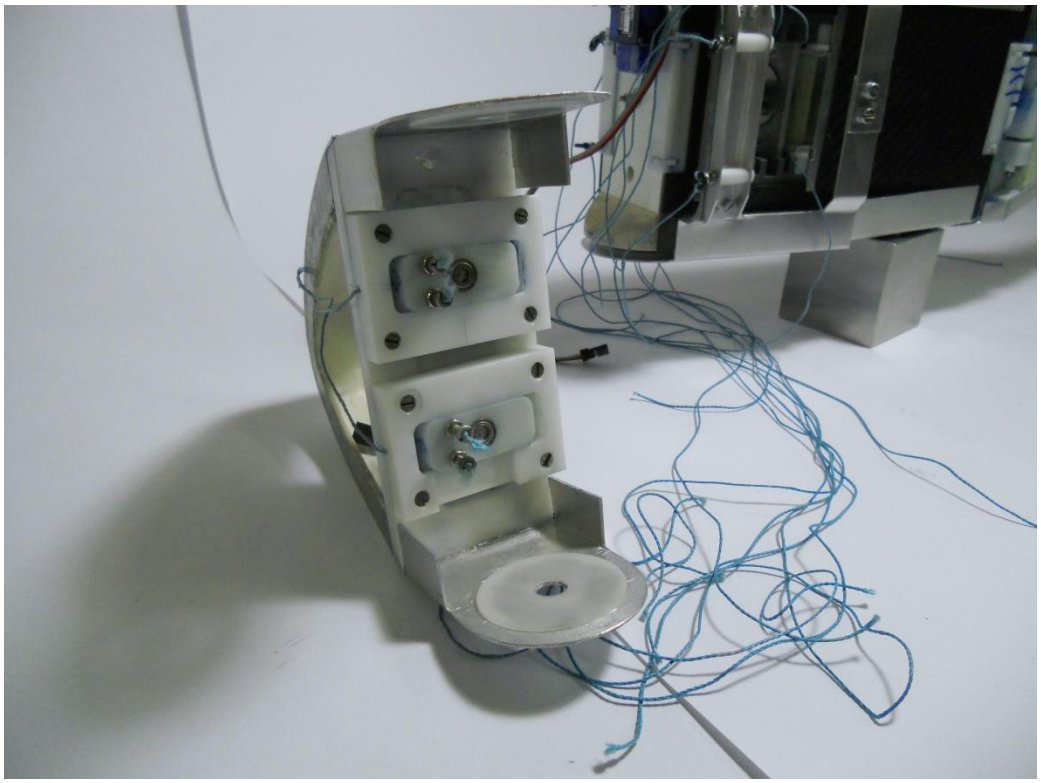

Figure 5.9: Adjusters for link I curve alignment.

5.4.3. Fabrication of the Modular Build

The modular prototype *iSplash*-OPTIMIZE, shown in Figure 5.10-5.12 was engineered as a morphological approximation of the common carp, fabricated using precision manufacturing techniques. The physical specifications are given in Table 1. A primary consideration of the development took into account the additional weight of the adjustable drive system, power supply and large electric motor (with dimensions of 85mm in length and 40mm in diameter), therefore no errors and excrescences in the geometry were required or kinematic parameters affected to compensate for the additional complexity of mechanical drive system. The geometric frame (the maximum cross section measured to be optimal at 0.2 of the body length) and midline camber was required to be accurate, as the outer profile of the coordinated full-body swimming pattern proposed in [114], represented by a deep camber aerofoil section (e.g. NACA (12)520) is estimated to aid the fluid flow interaction, producing greater locomotive speeds.

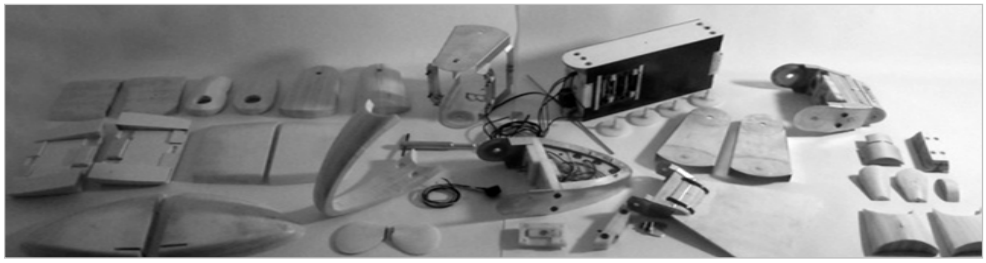

Figure 5.10: *iSplash*-OPTIMIZE: Disassembled view showing interchangeable parts of the modular build.

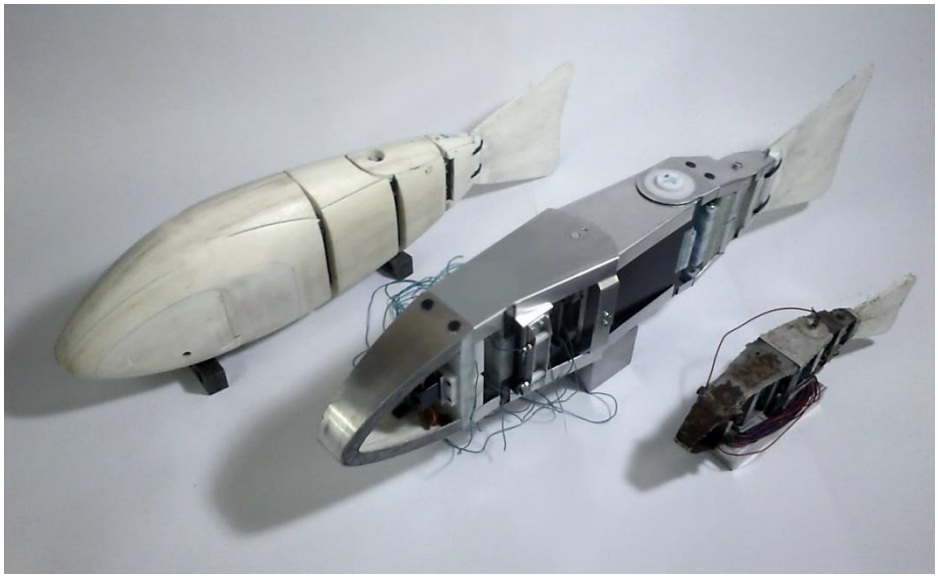

Figure 5.11: *iSplash*-OPTIMIZE final prototype alongside *iSplash*-I [114]. The image provides an indication of scale between the generations.

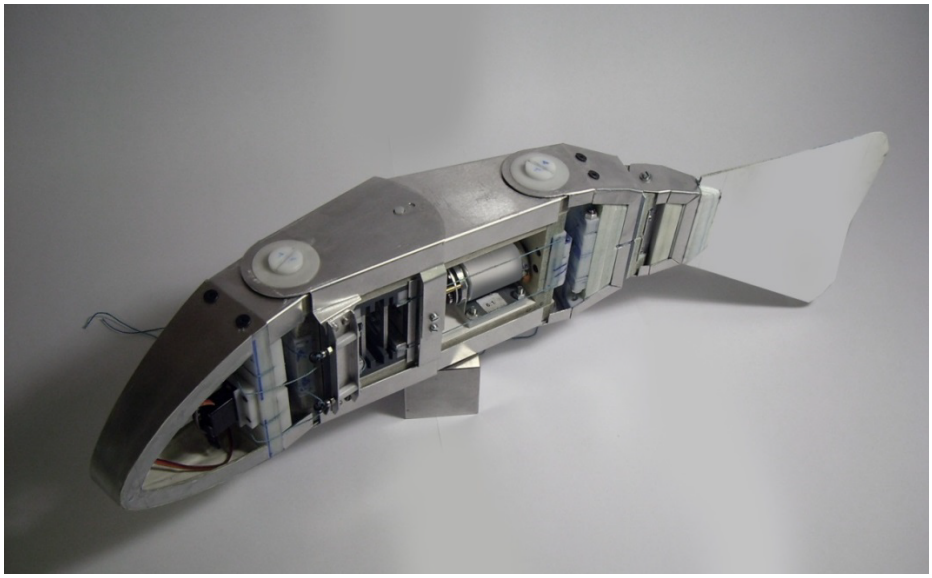

Figure 5.12: *iSplash*-OPTIMIZE: Final build with inner cover removable.

Table 5.1: Physical parameters of *iSpalsh*-OPTIMIZE

Parameters	**Specific Value**
Body size: m (L x W x H)	0.62 x 0.11 x 0.16
Body mass : Kg	0.9
Primary actuator:	Brushed DC motor
Power supply:	11.1v onboard LiPo battery
Manufacturing technique:	Precision engineering, machining
Primary swimming mode:	Linear locomotion
Additional maneuverability:	Yaw, pitch.
Additional control surfaces:	Pectoral fins
Tail Material:	Polypropylene
Thickness of caudal fin : mm	2.3
Caudal Fin Aspect Ratio: AR	1.6
Communication: (Additional)	2 x Zigbee 802.15.4, (27MHZ RF)
Tested signal distance: m	7.5
Microcontroller:	Arm Cortex M3 96Mhz
Data Storage:	SD card
Sensors:	Current, voltage, encoder, infrared, compass, accelerometer, gyroscope.
Materials:	Carbon Fiber, aluminum, stainless steel, acetal, low density foam.

The additional mass affected buoyancy. This was counteracted by improving the structures weight-to-strength ratio, deploying a combination of low density foam with carbon fiber layers, aluminum space frames and acetal inserts to strengthen sliding surfaces. This fabrication method achieved a structurally robust prototype, required for consistency of operation at high frequencies. In addition, natural buoyancy and open loop stability was achieved by positioning the large mass low and distributed across the main chassis (i.e. from DOF 2-3), therefore providing accurate density distribution properties to the first generation,

as it is optimal for the principal pivot point of the carangiform swimming motion to be positioned within the range of 0.15-25 of the body length.

Additional mobility mechanisms were devised for autonomous locomotion: (i) to turn within the vertical plane. Two rigid morphological approximations of pectoral fins were developed and positioned at the leading bulk head of the main chassis, actuated by a single servo motor (with 180° actuation); (ii) to turn within the horizontal plane. A mechanism was developed to adjust the swimming pattern to generate the form of a C-sharp turn [120], by offsetting the posterior tendons using adjustable cross sliders actuated by a single servo motor.

5.5. Embedded System

A modular electrical system was built, employed to measure and control the robotic fish motion, positioned within link I shown in Figure 5.14. The first study aims to measure various kinematic sequences in an attempt to reduce the cost of transport during linear locomotion. The central processor is a 32bit 96MHZ ARM Cortex-M3, which samples and filters data from multiple deployed sensors (i.e. incremental encoder, current, voltage sensors and an inertial measurement unit (IMU)), is employed to measure the energy economy and the extent of destabilization at various frequencies and swimming patterns. The energy consumption of *iSplash*-I was sampled by external electronics. The new onboard electronic system and free swimming robotic fish allows for measurements unaffected by a tethered power supplies or support beams. The data can be logged onboard by the SD module or sent instantaneously (tested up to a distance of approximately 7.5m) to an external PC for analysis by two onboard 802.15.4 wireless radios.

The planned future work was to achieve autonomy at high locomotive speeds. The system has been installed with four infrared sensors (tested to produce accurate data up to approximately 1m) and two control surface actuators so that the central processor will process data of the state of orientation, surrounding environment, energy economy and frequencies rate, and therefore perform decision making and produce the required control signals. The structure is shown in Figure 5.13. Autonomy will be a great challenge as locomotive speeds increase due to the deployed limited sensors.

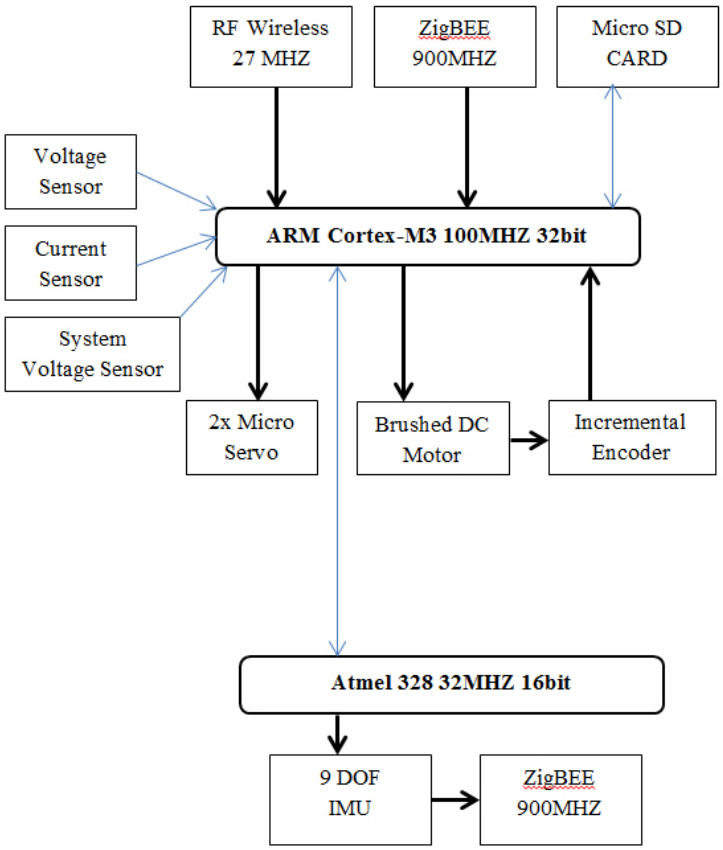

Figure 5.13: The structure of the energy and stability measurement and actuator control system.

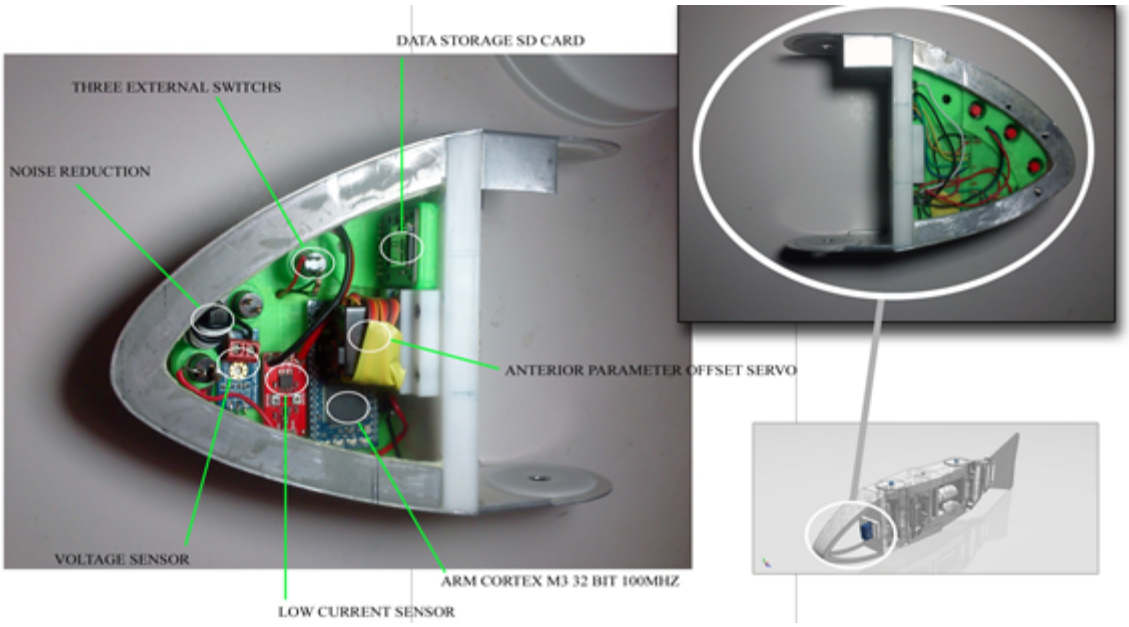

Figure 5.14: Inner Structure of link I showing the installed electrical system.

5.5.1. Deployed Sensors and Physical Constraints

The state of orientation and sensory feedback system plays a vital part in navigation as unstable structures must constantly re-correct destabilization due to disturbances in the environment and energy loss due to inefficiencies. A limited embedded system must be implemented within the platform due to profile and hardware constraints. The anterior section of the biological inspired robotic system has been waterproofed and constructed to counteract water pressure and house the embedded system. The following developed modular embedded system was deployed: The central computation is executed by a 32bit 100MHZ ARM processor. The Arm processor is employed to control 4 actuators and sample and filter data from multiple sensors:

- As the platform must be aware of its state within three dimensions a 9DOF IMU an IMU consisting of the following sensors has been built and employed: 1) *Accelerometer* 2) *Gyroscope* 3) *Compass*) to provide orientation data to calculate incorrect trajectory in the desired linear locomotion. Filters have been applied to the data provide reliable information.
- The following energy consumption sensors have been employed: *1) Rotary Encoder 2) Voltage 3) Current.* Positional feedback and power consumption information of the individual joints can be acquired to calculate a sensitive measurement of the overall energy economy including placement of a threshold as an indication of low level battery power.

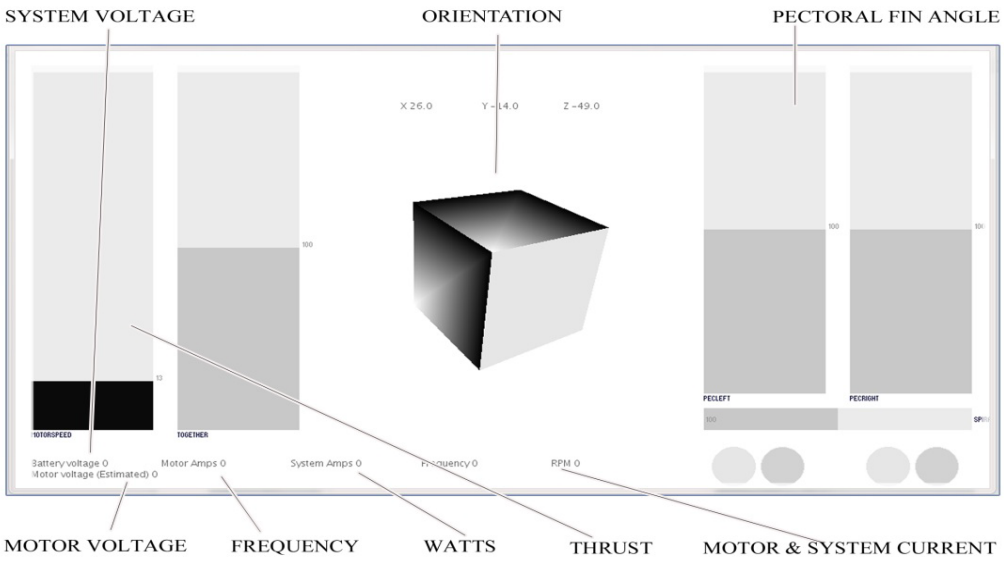

Figure 5.15: JAVA GUI -Instant feedback of data orientation and energy consumption.

A Graphic User Interface -

A Graphic User Interface has been developed in Java (Figure 5.15). This approach provides instant feedback of necessary information when the robotic platform is within a 25 foot range. For data acquisition outside of this range a SD card has been embedded within the system. The acquired data can later be analysed and inefficacies in orientation at varying frequencies could be removed to produce higher linear velocities.

5.5.2. Wireless Underwater Communication

The propagation of the wireless underwater communication has been tested and two wireless RF receivers have been implemented into the embedded system running at 27MHZ and 2.4GHZ. Excessive electronic noise due to increase torque of motors has been removed improving range of wireless communication underwater. Wireless underwater communication has been extended; the implemented RF transmitter into the embedded system running at 27MHZ has been modified to allow for greater control from a GUI or Simulation producing autonomous values.

5.5.3. Perceptual Sensor Testing

For real-time autonomous navigation to be achieved, bio-inspired asymmetric behaviours and sensory feedback systems must be deployed onto a system. Observational information of the surrounding geometry is gathered by individual or arrays of signal data. Infra-red sensors were tested which allow for detection of visible changes in the environment, due to the surrounding fluid noise is created which decreases range resolution. The usable range was found to be < 80cm. Limitations such as the undetectable objects can be resolved by applying a threshold to the received data from the accelerometer so that sharp increases in velocity are associated with collisions. It may be possible to make further improvements by the use of sonar.

5.6. Experimental Procedure and Results

5.6.1. Mechanical Energy Transfer

A series of experiments were undertaken in order to show the feasibility of the new prototype, evaluating performance in terms of kinematic parameters, robustness, open loop stability and energy consumption at frequencies within the range of 5-20Hz. The test results

are given in Table 2. The embedded system was employed to sample data reaffirmed by external electronics. The measurements were required to be averaged over many cycles to increase the accuracy of data once consistency of operation was achieved. The initial experimental testing highlighted areas of required development. During actuation at high frequencies it was found that the chosen materials and configuration enduring high forces failed as the build design was not suitable for the large increase in scale, which produced a significant increase in pressure in comparison to the first build. Rebuilds were undertaken and the appropriate materials suitable for intensively high frequencies within an aquatic environment were found. The rebuilds took into consideration mass and volume distribution and material properties, so that open loop stability was realized, which is a requirement for precise optimization of the swimming motion during linear locomotive. For the development of autonomy with mobility in yaw and pitch it is required that the weight is greatly concentrated at the center mass [3].

Once consistency of operation was achieved the devised mechanical drive system was found to be very robust, showing no signs of structural failure throughout experimental testing, whilst actuating at intensively high frequencies for long periods in air at 10Hz and short test periods of actuation at 20Hz in water. The power supply will contribute to a significant portion of the total mass therefore an efficient energy transfer is required for high performance. In Table 2 the average energy economy in relationship to driven frequency is shown, during non-productive power consumption (i.e. while operating in air). This comparison was used to measure the value of the increased resistance during actuation of each discrete link and during various link sequences. We measured the energy economy over many cycles, as the inertia of the oscillatory motion produces fluctuating readings within a cycle.

Operation whilst actuating all links at 10Hz at their maximum lateral excursion resulted in a small increase in energy consumption to 9.7W compared to the unloaded motor at 6.1W and the mechanical drive adjusters at 6.4W. Actuation of link I measured an energy consumption of 7.2W, links II and III measured 6.4W, link IV and V measured 6.8W. We can see that the developed mechanical drive system transfers continuous rotary motion to discrete oscillatory links across the platform with little internal mechanical loss. Therefore it was calculated that the prototype may be capable of carrying an onboard power supply within the current geometric frame.

Table 5.2: Experimental Test Results of *iSpalsh*-OPTIMIZE.

Parameters	Specific Value
Max Frequency tested in air: Hz	10
Max Power Consumption Motor No Load: W	6.1
Max Power Consumption Mechanical Drive Adjusters: W	6.4
Max Power Consumption only link I: W	7.2
Max Power Consumption only link II and III: W	6.4
Max Power Consumption only link IV and V: W	6.8
Max Power Consumption all links: W	9.7
Link I – Max Head displacement: m (Joint angle°)	0.060 (22)
Link II – Max Mid-body displacement: m (Joint angle°)	0.020 (14)
Link III – Max posterior link displacement: m (Joint angle°)	0.020 (11)
Link IV – Max Tail displacement: m (Joint angle°)	0.048 (28)
Link V – Max Tail displacement: m (Joint angle°)	0.040 (41)
Total anterior amplitude: m (of the body length°)	0.060 (0.1)
Total posterior amplitude: m (of the body length°)	0.167 (0.3)

5.6.2. Kinematic Parameters during Non-Productive Actuation

The midline kinematics of the full-body swimming pattern were tracked at 50 frames per second during actuation in air to provide the amplitude values of the anterior, mid-body and posterior, for comparison with real fish and *iSplash*-I. Good agreement with live fish kinematic data is a difficult task and current free swimming robotic fish have shown excessive head and tail amplitude errors during locomotion. All links were tested at half the maximum frequency (i.e. 10Hz) so that the build was not damaged due inertia forces. Link I was able to attain a maximum amplitude of 0.1 (0.06m) of the body length, measured from the midline to the maximum lateral excursion at a turning angle of 8°. Link II and III attained a maximum amplitude of 0.03 (0.02m) with 14° and 11° respectively. Link IV attained a maximum amplitude of 0.08 (0.048m) with 28° and Link V attained a maximum amplitude of 0.07 (0.040m) with 41°.

The maximum lateral head (i.e. 0.1) and tail (i.e. 0.27) excursions generated are significantly greater than the observed common carp and *iSplash*-I (Notably the tail amplitude of *iSplash*-I was measured to increase performance with larger values than the

common carp at 0.1 of the body length able to attain values of 0.17 (0.044m) due to achieving anterior stabilization). We can assume that applying the maximum attained amplitudes of *iSplash*-OPTIMIZE during locomotion will generate negative propulsive forces, therefore providing adequate displacements to find the optimized swimming pattern. Significantly, the build was able to adjust the mechanical drive system to generate numerous link sequences (with innumerable combinations of the cross sliders), therefore producing accurate swimming patterns during non-productive actuation.

5.6.3. Swimming Experimental Results

Experimental tests were conducted to validate the swimming performance of the second generation. The trial runs measuring swimming speed found the forward resistance to greatly overshadow the forward productive force and swimming speed was found to be lower than estimated in comparison to the first generation at 3.4BL/s, as the prototype measured a maximum velocity of 1.5BL/s. This result is in the region of the typical maximum velocity of existing robotic fish, with 1.1BL/s being the previously fastest recorded (Section 3.1).

The maximum tail beat frequency generated by the build during nonproductive actuation in air was measured at 10Hz. Test periods of actuation at 1-20Hz in water were conducted, which indicated that the prototype was only able to actuate at its maximum tail beats whilst in operation with a reduced scale caudal fin. If the prototype was deployed with a caudal fin morphologically accurate in scale and profile to the first generation, a tail beat frequency of approximately 2Hz was generated, far lower than required and had been estimated based on the in air testing and the first generations results. The pressure to displace the surrounding fluid was measured to be greater than the productive forces of the prototype. A caudal fin approximately half the scale was deployed which enabled the build to actuate at its maximum ability of 20Hz.

It was measured that no change in swimming speed was gained or lost by this modification, indicating that the required forces to generate higher velocities where greater than the maximum productive thrust of the drive system. In addition, modifications were made to streamline the prototype by reducing the scale of the body and adjusting the weight of the build so that the outer buoyancy layer fabricated of low density foam could be decreased in size. This adaption was not enough to greatly improve swimming speed as the scale could only be slightly reduced.

Therefore we were unable to test the *Sw*, finding that a significantly smaller drive system is required. In consideration of the limited actuators available the prototype was analyzed in terms of the forces acting upon the propulsive drive system. The drag acting upon the robotic fish is combination of two forces:

(i) Pressure drag, resulting from the pressure at the nose of the fish being higher than at the tail.

(ii) Skin friction drag, resulting from the viscosity of the water, as a boundary layer sticks to the fish's outer surface.

Hence the total drag retarding the forward motion of the prototype or any object is the combination of pressure drag and skin friction drag. Any drag reduction will be greatly advantageous as it will mean a fish can travel faster or further on its productive power output. Therefore, a reduction in the wetted area or applying a boundary layer control mechanism is required for future development.

5.7. Summary

This chapter details the design (Section 5.3), fabrication (Section 5.4) and mechanical efficiency tests (Section 5.6) for a bio-robotic marine vehicle, showing its feasibility as a platform to accurately optimize the Carangiform straight line swimming motion over previous methods. Devised to reduce the kinematic errors by precisely tuning the reaction forces of the propulsion elements during locomotion, the developed mechanical drive system has shown the capability to generate accurate spatial and time dependent discrete link sequences during non-productive actuation at 10Hz with a small energy consumption of 9.7W over a non-loaded motor at 6.1W (Section 5.6.1). The swimming patterns at high frequencies were attained by realizing a powertrain with high accuracy, unrestricted disc offset combinations, with high structural strength, able to transfer power to and provide precise adjustments of the oscillatory discrete links across the full assembly from a single continuous rotary actuator. The details of the onboard electrical system were given (Section 5.5) showing its practicality for measuring and controlling the energy consumption, stability and mobility by deploying control mechanisms for the actuation of pectoral fins and adjustment of the linear swimming motion to generate the form of a C-sharp turn.

Further experimental tests validating the swimming performance found drag to greatly overshadow the forward productive force and swimming speed was found to be lower than

estimated in comparison to the first generation. Modifications were undertaken to reduce the magnitude of the body shape. These structural changes recorded no change in performance as the required force to increase velocity could not be provided (Section 5.6.3).

The experimental analysis of the second generation has highlighted important factors in improving the swimming agility of the next generation. The following points are of significant interest for the next stage of research:

(i) *Reduction in scale* - The devised adjustable mechanical drive system requires a reduction in scale, relating to reduce forward resistance. This development is the principle factor to consider for future research taking the limited hardware into consideration.

(ii) *Link Parameter Offset Optimization* – If the next generation could achieve higher productive forces by implementing a high torque actuator (or the swimming speeds of 1BL/s are found adequate for the required kinematic optimization test) it may be greatly advantageous for an autonomous parameter adjustment system to be deployed, utilizing a series of servo motors coupled to the discrete link adjusters, to attain swimming motion adjustment across the range of frequencies during locomotion. In addition the compact drive mechanism may be suitable to distribute power to additional links, increasing redundancy without greatly increasing mechanical complexity.

(iii) *Reverse Karman Street Vortex* - A series of tests investigating the effect of allowing individual segments to be passively moved by the surrounding fluid may provide the ability to extract energy from the surrounding environment. Although the swimming ability of the second generation was lower than the first, its ability to allow passive body segments may provide an opportunity to measure interaction with a Reverse Karman Street Vortex. As described in [6; 11; 133], a fish may produce positive locomotion without active body motion. This experimental test could be advanced by adjusting the individual segments through different stages of rigidity, hence measuring the segments contribution to the fluid body interaction.

Chapter 6

iSplash-II: Outperforming the Swimming Speeds of Real Fish

This chapter introduces a novel robotic fish, *iSplash*-II [130; 132], capable of outperforming real carangiform fish in terms of average maximum velocity (measured in body lengths/second) and endurance, the duration that top speed is maintained. A completely new fabrication technique and mechanical drive system were devised, effectively transmitting large forces at intensively high frequencies to obtain high-speed propulsion. The lateral and thrust forces were improved around the center of mass, generating accurate kinematic displacements and greatly increasing the magnitude of added mass. Significantly improving the performance of previous man-made systems, the presented prototype with a body length of 32cm has achieved consistent unrestricted stabilized swimming at speeds of 11.6BL/s (i.e. 3.7m/s), with a frequency of 20Hz.

The remainder of the chapter is organized as follows: Section 6.1 presents the Introduction and Section 6.2 the research objectives. Section 6.3 presents the investigated Carangiform swimming patterns. Section 6.4 describes the new construction method. Section 6.6 discusses the field trials undertaken and the experimental results obtained. Concluding remarks are given in Section 6.7.

6.1 Introduction

To navigate through a marine environment, a robotic vehicle requires mobility to effectively contend with the physical forces exerted by the surrounding fluid. Live fish can coordinate their body motions to generate large transient forces efficiently, as opposed to rigid hull underwater vehicles (UV) powered by rotary propellers [66; 112; 1; 118]. For a man-made vehicle to achieve greater locomotive capability there is potential to engineer a structure that can accurately replicate the wave form and therefore ability of swimming fish.

Detailed in Section 3.1 we aim to achieve the swimming speeds of real fish, measured to attain an average maximum velocity of 10 body lenghts/ second [112; 116]. A single high performance of a Cyprinus carpio was noted, achieving the swimming speed of 12.6BL/s (1.7m/s) with a stride rate of 0.66 (Section 2.1.1). Though the swimming speeds of fish are high, endurance at the highest velocities is limited and burst speeds can only be maintained for short durations of approximately one second. Velocities were measured to decrease to 7BL/s in 2.5s of swimming, to 5BL/s in 10s and to 4BL/s in 20s [172].

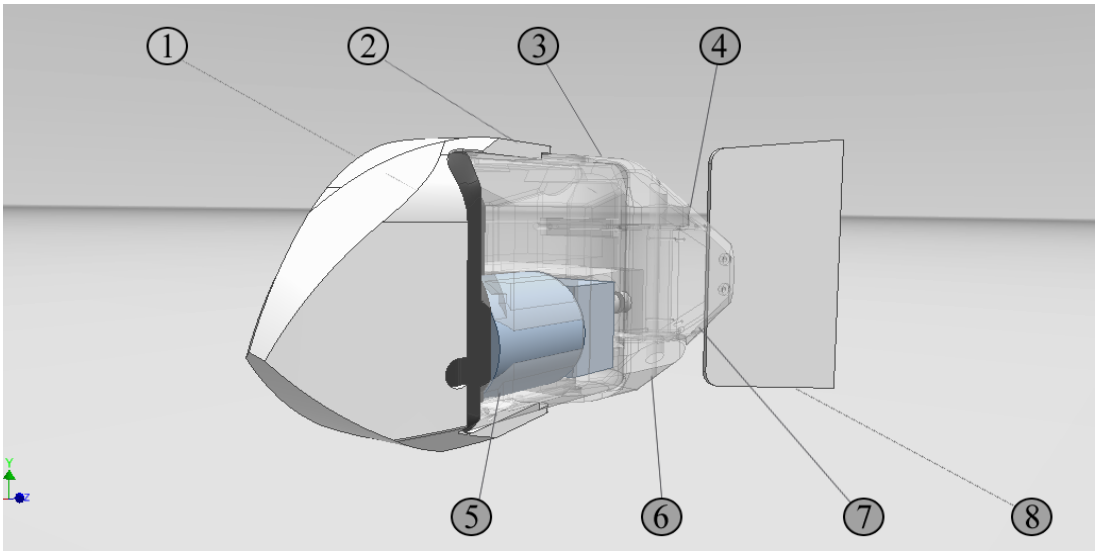

Figure 6.1: *iSplash*-II: 1-Anterior link; 2-Midbody transition links; 3- First posterior link; 4-Final posterior pivot; 5-Primary actuator; 6- Direct drive offset crank; 7- Tendon driven peduncle; 8-Compliant caudal fin.

The development of the new generation's mechanical drive system refers to the analysis of Chapter 3, where current robotic fish are unable to gain the locomotive efficiencies of live fish, proving a complex challenge, with two limitations in particular (Section 3.3 and 3.5):

(i) Robotic fish are unable to achieve accurate replication of the linear swimming motion as they generate significant kinematic parameter errors and therefore reduced propulsion.

(ii) Robotic fish-like swimming mechanisms have low force transfer due to the complexity of developing the powertrain, limited by mass, volume, force, frequencies and internal mechanical losses.

Motivation –

This research is based on the experimental findings of the first and second generation prototypes:

- The First Generation: *iSplash*-I (Chapter 4) [114], (25cm, 0.35Kg, with an external power supply and formed of aluminum and steel) achieved a high-performance swimming motion. The developed novel mechanical drive system operated in two swimming patterns, (i) The traditional posterior confined undulatory swimming pattern (ii) The introduced full body length swimming pattern. The proposed swimming motion significantly improved the accuracy of the kinematic displacements by coordinating the anterior, mid-body and posterior displacements optimizing forces around the center of mass and initiating the starting moment of added mass upstream, in particular it significantly reduced the anterior recoil seen in previous robotic fish. Hence outperforming the posterior confined approach in terms of speed, achieving a consistent maximum velocity of 3.4BL/s (equivalent to the top cruising speeds of real fish) at 6.6Hz with a low energy consumption of 7.68W and distance travelled per tail beat of 0.42.
- The Second Generation: *iSplash*-OPTIMIZE (Chapter 5), (0.6m, 0.9Kg, cross sectional dimensions: 23cm H x 28cm W), was unable to improve upon the maximum velocity of the first generation, achieving 1.5BL/s (Approximately equivalent to the maximum velocity of the previously fastest published robotic fish with a maximum velocity 1.1Bl/s at MIT [117] (Section 3.5.2). The analysis found the magnitude of the geometric frame generated significant forward resistance. Hence this generation takes in consideration the importance of a high force production contained within the smallest dimensions possible.

It was noticed that throughout the field trials *iSplash*-I was able to replicate the key swimming properties of real fish. As frequencies were raised the prototype continued to increase velocity in both swimming modes. This matches Bainbridge's study of swimming fish, measuring no noticeable change in kinematics after tail oscillations are raised beyond

5Hz, indicating that only an altered frequency is required to increase swimming speed. Hence it is expected, that combining the critical aspects of the *iSplash*-I mechanical drive system with frequencies higher than 6.6Hz could significantly increase maximum velocity. In consideration of this, *iSplash*-II was proposed as shown in Figures 6.1 and 6.9.

6.2 Research Objectives

The project aimed to achieve the fastest swimming speeds of live fish with seven main objectives:

(i) to devise a prototype which operates in two swimming patterns, for further investigation of the carangiform swimming motion to be conducted;

(ii) to significantly increase force transfer by achieving a high power density ratio in combination with an efficient mechanical energy transfer;

(iii) to achieve unrestricted high force swimming by realizing a prototype capable of carrying a high powered energy supply;

(iv) to develop a structurally robust mechanical drive system based on the critical properties proposed in [114], capable of intensively high frequencies of 20Hz;

(v) to greatly reduce forward resistance by engineering a streamlined body considering individual parts' geometries and alignment throughout the kinematic cycle;

(vi) to stabilize the free swimming prototype's unsteady oscillatory motion during intensively high frequencies to achieve a greater efficiency force transfer;

(vii) to conduct a series of experiments measuring the prototype's achievements in terms of kinematic data, speed, thrust, and energy consumption in relation to driven frequency.

6.3 Design Methodology for Increasing Straight-line Speed

The kinematic swimming motion of the traditional approach during linear locomotion of the first generation was measured with a lower Swimming number than the proposed coordinated body wave. The distance travelled per tail beat (*Sw*) of the full body swimming pattern was 0.42, increasing the Swimming Number by 16.6% in comparison to the traditional approach with a *Sw* of 0.36. It was calculated that the prototype can significantly increases it maximum velocity over the traditional approach as frequencies are further raised. Therefore, to further investigate we deploy the new generation build with both swimming patterns:

The Traditional Approach –

The form of this propulsive segment, within the horizontal plane can be represented by a travelling wave, identified by the portion of the body length actively displaced. The body motion applies a rigid mid-body and anterior, concentrating the undulatory motion to the posterior end of the lateral length. The deployed traditional approach limits the displacements to <1/2 of the body length, with the posterior propagating wave smoothly increasing in amplitude from approximately the mid-body towards the tail [112] (Chapter 3). Described as Mode 1 and illustrated in Figure 6.11, the deployed posterior confined kinematics of the Carangiform is of the form [112; 113]:

$$y_{\text{body}}(x,t) = \left(c_1 x + c_2 x^2\right)\sin\left(\mathrm{k}x + \omega t\right) \qquad (6\text{-}1)$$

where y_{body} is the transverse displacement of the body; x is the displacement along the main axis beginning at the nose; $\mathrm{k} = 2\pi/\lambda$ is the wave number; λ is the body wave length; $\omega = 2\pi f$ is the body wave frequency; c_1 is the linear wave amplitude envelope and c_2 is the quadratic wave. The parameters $P = \{c_1, c_2, \mathrm{k}, \omega\}$ can be adjusted to achieve a the desired posterior swimming pattern for an engineering reference.

Detailed thoroughly in Section 3.1, accurately matching the kinematic data of real fish is complex and free swimming robotic fish applying posterior confined displacements have shown significant kinematic parameter errors [20; 117]. In particular, the lateral (F_L) and thrust (F_T) forces are not optimized. As a result, large anterior destabilization in the yaw plane is generated due to the concentration of posterior thrust, recoiling around the center of mass. Consequently the inaccurate anterior kinematics create significant posterior midline displacement errors. Hence, the linear locomotive swimming motion over the full length of body has large matching errors in comparison to real fish leading to reduced propulsive force and a higher cost of transport.

The Full-Body Swimming Pattern -

Mode 2, illustrated in Figure 6.12 is the full body Carangiform swimming pattern of the *iSplash* platforms described in [114] and Chapter 3.4, which coordinates the anterior, mid-body and posterior body motions. This was based on intensive observation [114] and fluid flow theory [23; 6] (Chapters 3 and 4) which lead to a greater understanding of the carangiform swimming motion.

The Mode 2 displacements on the first generation drive the anterior into the direction of recoil, reducing amplitude errors by optimizing the reaction force (F_R) of the propulsive

elements. This enhances performance, increasing the magnitude of added mass by initiating the starting moment upstream, generating optimized F_L and F_T forces around the center of mass, increasing the overall magnitude of thrust contributing to increased forward velocity. A full description of the method of added mass can be found in [119] and Section 3.1. Furthermore the developed body motion increases performance by allowing a smooth transition of flow along the length of the body, effectively coordinating and propagating the anterior formed fluid flow interaction downstream. Deployed is the extended form of [20], an adaptation of (1) to generate the midline kinematic parameters of the full body displacements:

$$y_{\text{body}}(x,t) = \left(c_1 x + c_2 x^2\right)\sin\left(\mathrm{k}x + \omega t\right) - c_1 x \sin\left(\omega t\right) \qquad (6\text{-}2)$$

By evaluating the x location at the center of mass, measured optimal at 0.15-0.25 of the body length and tail amplitude at 0.1 [118], the relationships between the defined parameters P ={0.63,0,21.6,8}, shown in Figure 6.12, can be calculated taking in consideration the geometric parameters of the third generation build.

The full-body swimming motion of *iSplash*-I significantly reduced kinematic matching errors over the full body length (Section 4.5.2). Mode 2 was found to reduce the head amplitude by over half, from 0.17 (0.044m) in Mode 1 to 0.07 (0.018m). The tail amplitude was measured to increase performance with larger values than the common carp at 0.1. Both Modes were able to attain values of 0.17 (0.044m) due to achieving anterior stabilization. The location of the center of mass was improved and close to the optimum range (Observed in [118]) , Mode 2 with a reduced error location of 0.33 in comparison to Mode 1 of 0.5. Reviewing the kinematic data we can see, that the prototype achieved high kinematic accuracy with a low cost of transport. In consideration of this, we aimed to precisely replicate its swimming motion parameters.

6.4 New Construction Method for High Performance

6.4.1 Mechanical Design

In order to generate a high performance swimming speed a new mechanical drive system was required, able to effectively transmit large forces at intensively high tail oscillation frequencies. In consideration of this, a feasible design structure to fit the linear swimming patterns of both modes was developed. Although more complex to devise without internal mechanical loss [113], a powertrain utilizing a single motor with continuous rotation was

developed, advantageous in comparison to multilink servos or smart materials, which are limited by force, frequency, volume and mass distribution [116; 20; 75].

As the build required a high power density ratio, the structural arrangement was governed by the dimensions of the large electrical motor 83mm long x 50mm diameter. This required a slight increase in body length from 250mm to 320mm and a significant adjustment to the link structure to take the mass of the actuator into consideration, removing the passive mid-body degrees of freedom (DOF) and the associated discrete linkages. The discrete construction method, defined as a series of links or N links, aims to achieve accurate midline kinematic parameters whilst minimizing complexity of the mechanical drive and linkages. The sequence of links can generate the required swimming motion by locating the joints to the spatial and time dependent body wave. The fully discretized body wave fitting method is given in [116; 20].

The assembly of *iSplash*-II is illustrated in Figures 6.2-6.8, showing the three links distributed along the axial length. Three rigid links coupled to a passive fourth link and caudal fin with stiffness distribution, devised to generate a smooth body to tail transition phase of the posterior undulations. The developed modular build allowed for both Modes of operation to be applied to the same prototype by adjusting the configuration. Links III and IV are actuated to generate the posterior kinematics of operational Mode 1, Mode 2 actuates all links along the axial length to provide anterior, mid and posterior body displacements.

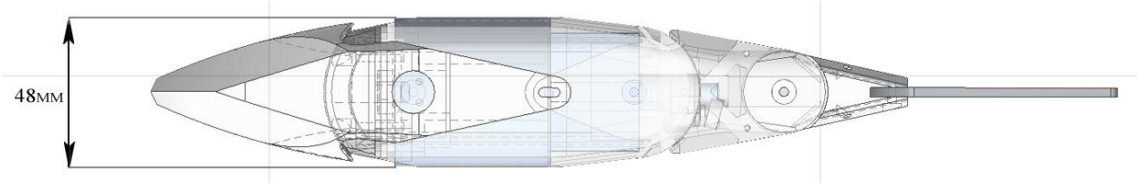

Figure 6.2: Plan view.

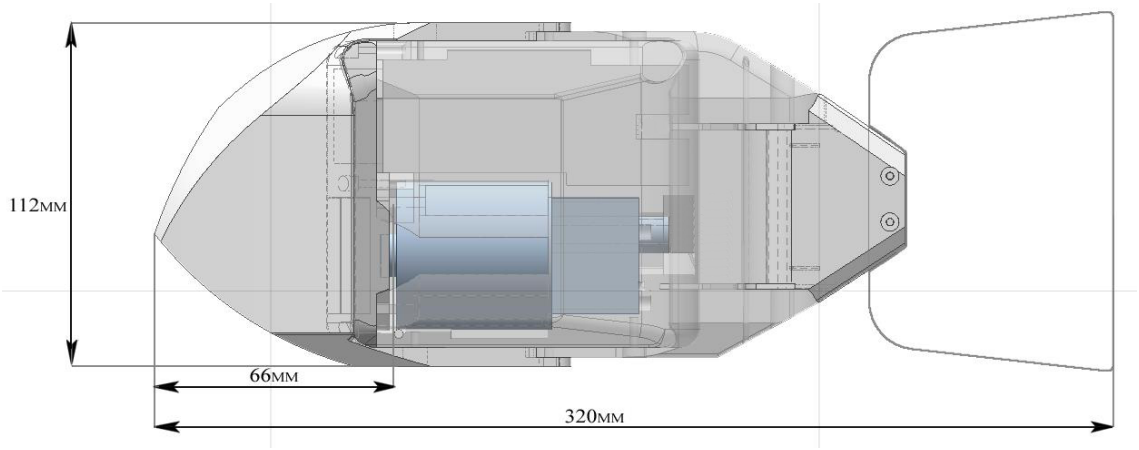

Figure 6.3: Side view.

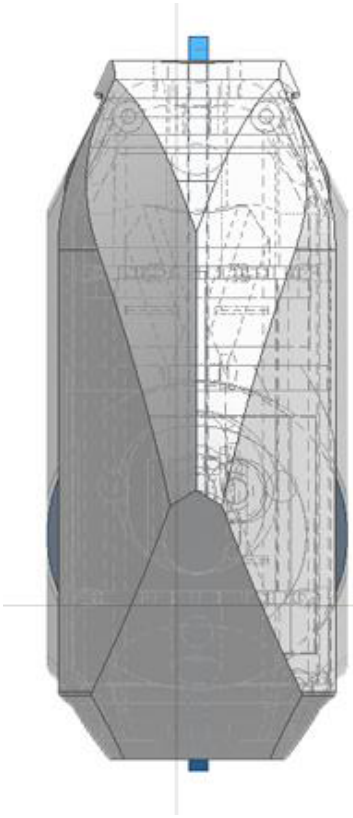

Figure 6.4: Front view

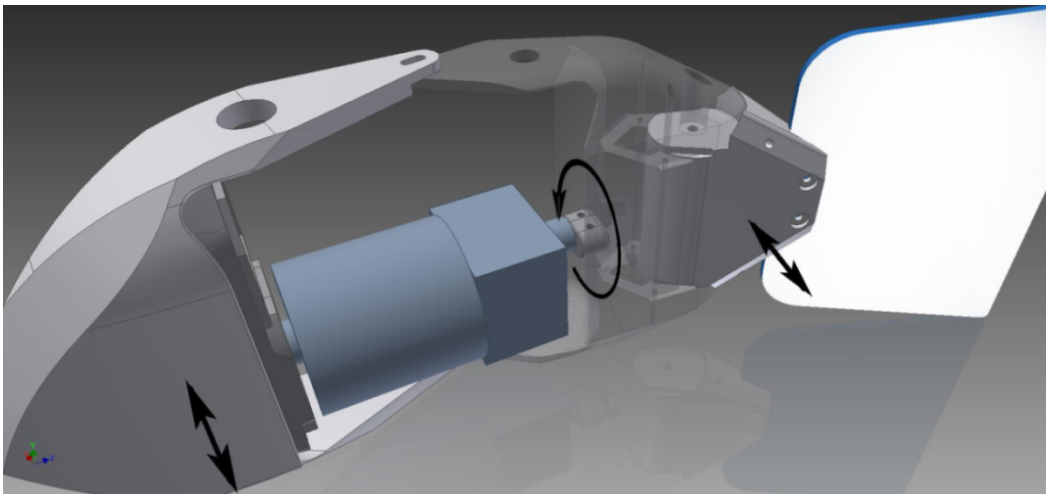

Figure 6.5: Power transmission system: Arrow diagram indicating direction of motion.

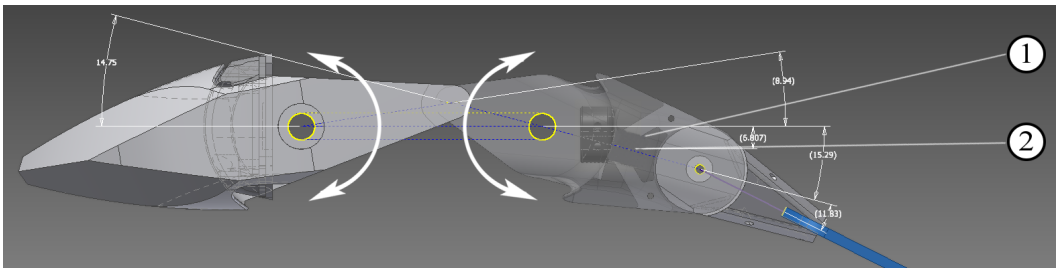

Figure 6.6: Power transmission system: 1-Offset crank; 2-Posterior link.

It was proposed in [114] (Section3.4), that the outer profile of the coordinated full-body swimming pattern, represented by the aerofoil section NACA (12)520 aids the fluid flow interaction, producing greater locomotive speeds. In consideration of the simplified link assembly and estimated center of mass, the head and tail amplitudes were increased. We can see in Figure 6.7 that the approximation of a traveling wave using link end points I-IV and turning angles of joints 1-3 of the reduced link arrangement provides an accurate curve alignment agreeable with the form of (2), therefore reducing errors and excrescences in the outer profile and achieving accuracy with the required aerofoil section.

6.4.2 Powertrain & Link Amplitude Offsets

The leading tail discrete link III is directly driven by the single bearing crank shaft attached to the output shaft of the primary actuator, increasing power distribution to the posterior. As link III is actuated, link IV is passively displaced. This final posterior linkage IV, coupled to the compliant caudal fin is anchored by 4 expandable tendons attached to the main chassis rear

bulkhead, crossing through linkage III. The anterior link I is transmitted motion by paired linkages fixed at points P_5 and P_6, located at the top and bottom of the main chassis. The developed mechanical design required precision fitment of the chassis, crankshaft, cantilevers and linkages to reduce internal mechanical losses, avoid deadlock and reduce friction.

Illustrated in Figures 6.5, 6.6 and 6.8 is the developed powertrain transmitting rotary power to linear oscillating links. All driven link amplitudes are determined by the single offset crank. L_3 represents the leading tail discrete link of the structure. `The maximum amplitude of the link length L_3 and L_1 at point P_2 and P_4 respectively are determined by the predetermined maximum crank offset P_1. The coordinates of P_1 (P_{1x}, P_{1y}), P_2 (P_{2x}, P_{2y}), P_3 (P_{3x}, P_{3y}) and P_4 (P_{4x}, P_{4y}) can be derived by:

$$\begin{cases} P_{1x} = A + B \\ P_{1y} = (A + B)\tan\theta_1 \end{cases} \quad \begin{cases} P_{2x} = P_{1x} + C\cos\theta_1 \\ P_{2y} = P_{1y} + C\sin\theta_1 \end{cases} \tag{6.3}$$

$$\begin{cases} P_{3x} = -F\cos\theta_1 \\ P_{3y} = -F\sin\theta_1 \end{cases} \quad \begin{cases} P_{4x} = -(L_2 + D) \\ P_{4y} = -P_{3y} D / E \end{cases} \tag{6.4}$$

The length of L_1 can be derived by $L_1^2 = P_{4x}^2 + P_{4y}^2$. Assume that ω_1 is the angular velocity of the link L_1, and the velocity vector V_{P4} is perpendicular to L_1. We have:

$$\begin{cases} V_{p4x} = -\omega L_1 \sin\theta_3 \\ V_{p4y} = \omega L_1 \cos\theta_3 \end{cases} \tag{6.5}$$

where V_{p4x} and V_{p4y} are the decomposed vectors of the velocity vector $V_{P4} = \omega_1 L_1$.

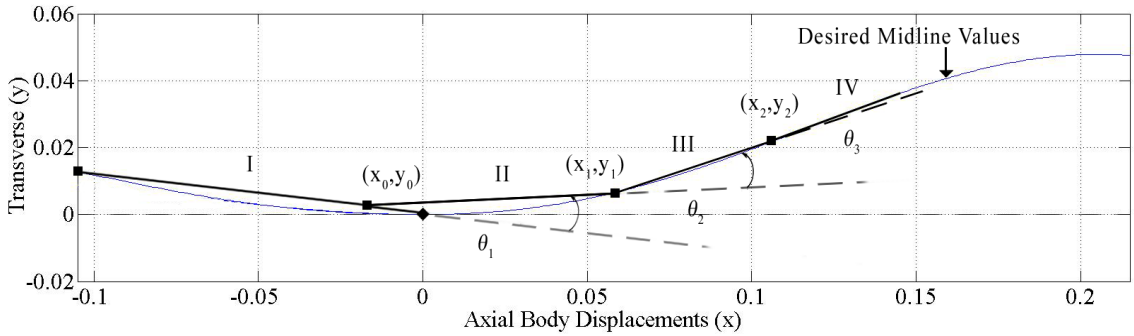

Figure 6.7: Link approximation, illustrating accurate kinematic matching.

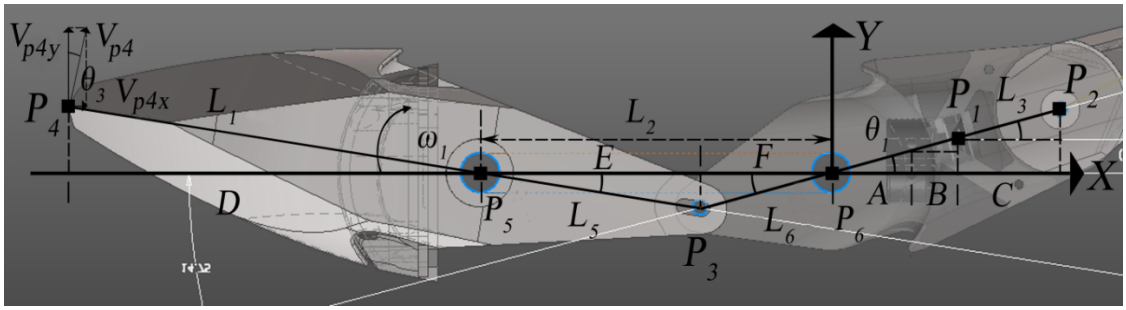

Figure 6.8: Schematic drawing of the offset drive crank and linkages;

6.5 Fabrication Method for High Speeds

The prototype *iSplash*-II is shown in Figure 6.9 with the physical specifications given in Table I. The entire body was digital modeled and formed using 3D printing techniques, at layers of 0.09mm in PLA filament. This method produced precise 3D structural geometries of the individual segments and pre-determining alignment tolerances throughout the complete kinematic cycle. It was a complex challenge to develop a high power density build, small in size with high structural strength. The individual printed parts were optimized for robustness through physical strength tests and computational stress analysis, highlighting initial areas of weakness. These parts were re-printed many times in order to realize high frequency actuation. As PLA filament has a low melting point softening at approximately 60°C, material wear at the pivots and actuated surfaces was reduced by acetal bushes and inserts, at the cost of additional weight.

Figure 6.9: Physical model of third generation platform *iSplash*-II.

It was necessary for the body size to be compact, as increasing the build geometric magnitude will increase the resistance during forward motion and therefore the power consumption required [113; 114]. An accurate approximation of the streamlined body shape of the common carp was achieved within the horizontal plane illustrated in Figure 6.2. The maximum thickness of the cross section is measured optimal at 0.2 of the body length [118] and was favorably positioned therefore reducing pressure drag.

The static stability in the horizontal and vertical planes is affected by material density distribution. For linear locomotive research open loop stability is beneficial, this was achieved by the relative position of buoyancy being higher than the center of mass, as the surrounding fluid counterbalances the gravitational weight [3]. The short body length significantly increased the difficulty in achieving stability as the finest weight change in structure of individual pieces distributed across the assembly dramatically affected stability and buoyancy. This was solved by collaborating the individual parts of the modular build by adjusting the geometries and the inner structure's weight to strength configuration.

Table 6.1: Physical parameters of *iSplash*-II.

Parameter	Specific Value
Body Size: m (LxWxH)	0.32 x 0.048 x 0.112
Body Mass: Kg	0.835
Actuator:	Single electric motor
Actuator Mass: Kg	0.63
Power Supply:	11.1V onboard LiPo battery
Manufacturing Technique:	3D Printing
Materials:	PLA Filament, Acetal, Stainless
Primary Swimming Mode:	Linear Locomotion
Additional Manueverbilty:	Vertical plane
Additional Control Surfaces:	Pectoral fins
Caudal Fin Material:	Polypropylene
Thickness of Caudal Fin: mm	1
Caudal Fin Aspect Ratio: AR	2.3

The prototype was designed with increased stability in roll and pitch as the large mass of the electric motor, 0.6kg, 75% of the total mass, was positioned low within the structure. To achieve a short body length, contain the embedded system and power supply and counteract the large mass of the primary actuator, the prototype volume was increased vertically. This aided stability, as the lightweight PLA material and increased height positioned the center of buoyancy at the top of the prototype.

Mobility within the vertical plane was achieved to maintain a stable mid tank trajectory during free swimming. Two rigid morphological approximations of pectoral fins were developed and positioned at the leading bulk head of the main chassis, actuated by a single servo motor. A cross beam anchored on both sides of the centralized motor was formed to link, support and actuate the control surfaces. The addition of pectoral fins required a compact mechanism to be devised due to the very restrictive space available.

6.6 Experimental Procedure and Results

A series of experiments were conducted in order to verify the prototype by evaluating the locomotive performance of Modes 1 and 2 in terms of kinematic parameters, speed, force and energy consumption at frequencies of 5-20Hz. The measurements were averaged over many cycles to increase the data accuracy. Once consistency of operation was achieved and stabilized free swimming was obtained. The results are summarized in Table II. Experiments were conducted within a test tank, 5m long x 2m wide x 1.5m deep. Free swimming between two fixed points at a distance of 4m was used to evaluate maximum speed. The prototype had sufficient space to move without disturbances from side boundaries and the free surface, capable of consistent untethered swimming at mid height of the tank aided by adjusting the angle of pectoral fins during swimming.

Locomotion at high speeds was unachievable without extensive stability optimization. This was configured by modifying the structures surface area and weight distribution around the center of mass, this process was greatly simplified by fabricating the prototype on a three dimensional printer, as parts could be quickly altered and reprinted. Once achieved, an accurate straight line trajectory was possible. In addition, the devised mechanical drive system was found to be very robust, showing no signs of structural failure throughout the field trials whilst actuating at intensively high frequencies over long periods and accidentally hitting the walls of the test tank.

6.6.1 Swimming Pattern Observation

The frame sequence of Mode 2 in eight instances, at time intervals of 0.006s throughout one complete body cycle at 19Hz is illustrated in Figure 6.10. The obtained midline was tracked at 50 frames per second and is plotted against the desired amplitude envelopes of the anterior and posterior from Figure 6.12 for comparison. The desired midline (—) (Based on the observational studies undertaken in [118]) (Illustrated in Figure 6.12) and the generated kinematics (- -) (Illustrated in Figure 6.11) from locomotion at 20Hz are shown for comparison. We can see the prototype achieved an anterior amplitude value of 0.04L (0.013m) and a tail amplitude value of 0.20L (0.063m).

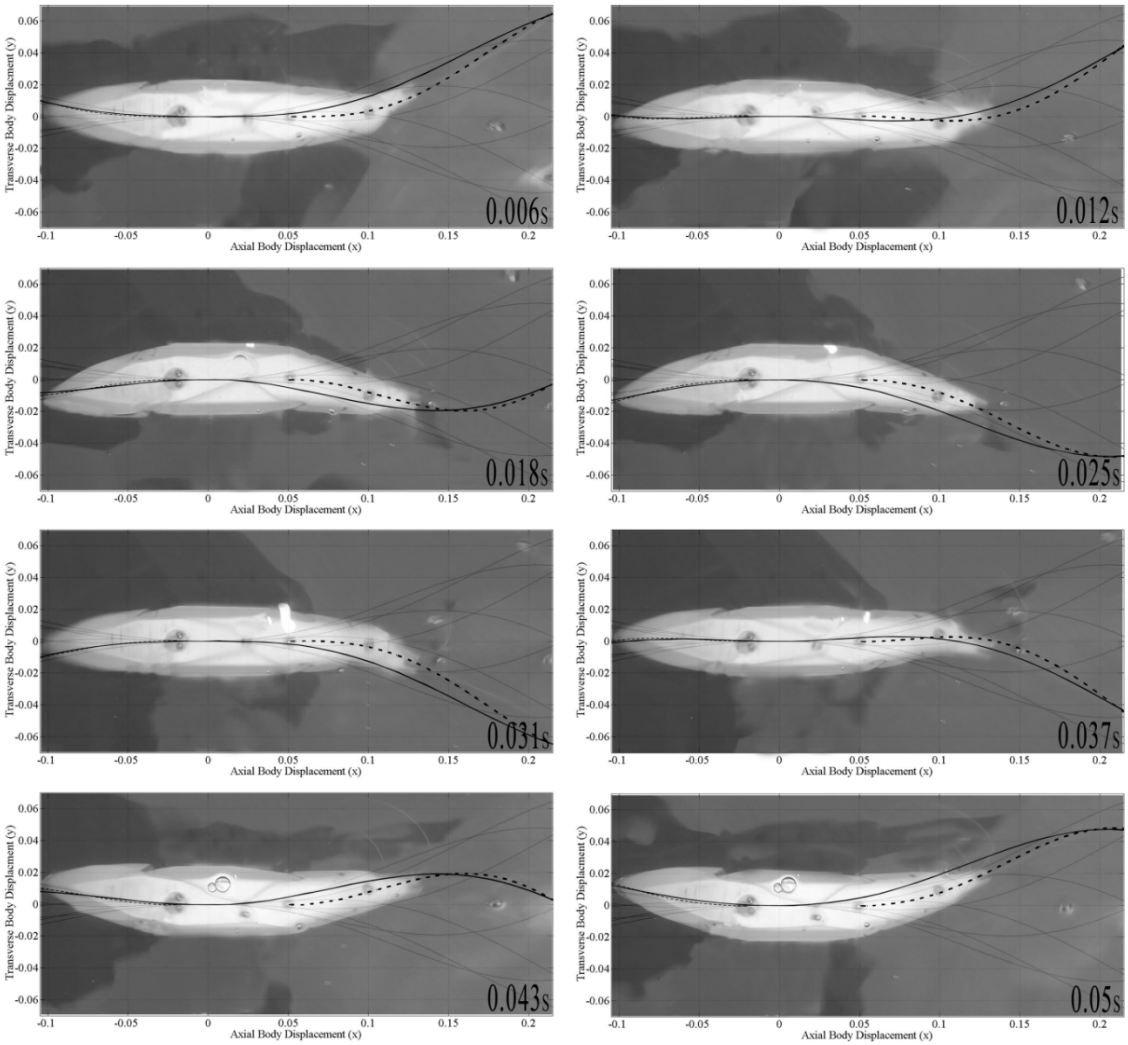

Figure 6.10: Frame sequence of Mode 2 during one full body cycle, eight instances every 0.006s.

When observing the midline of Mode 2 it can be seen, that the desired full body coordination presented in [114], was not achieved. As previously described in Section III-A the build required a simplified link structure due to power density constraints. Although the estimated midline curve alignment tested during stationary actuation was accurate, the excessive mass of the primary actuator held the main chassis (the entire length of link II) fixed in line with the forward heading and no single pivot point was obtained. Consequently, the swimming motion during locomotion was found to produce matching errors over the full-body in comparison to the desired swimming pattern of *iSplash*-I.

We compare both Modes taking into consideration that the mid-body was held rigid. The anterior amplitude of Mode 2 was measured to be 0.04 (0.013m) of the body length, equivalent to the common carp, whereas Mode 1 was found to generate <0.01 (0.003m) head amplitude. In addition, the large centralized mass arrangement and increased depth of body effectively minimized recoil forces and aided the stability of the posterior, allowing for accurate posterior amplitude and large thrust forces to be generated.

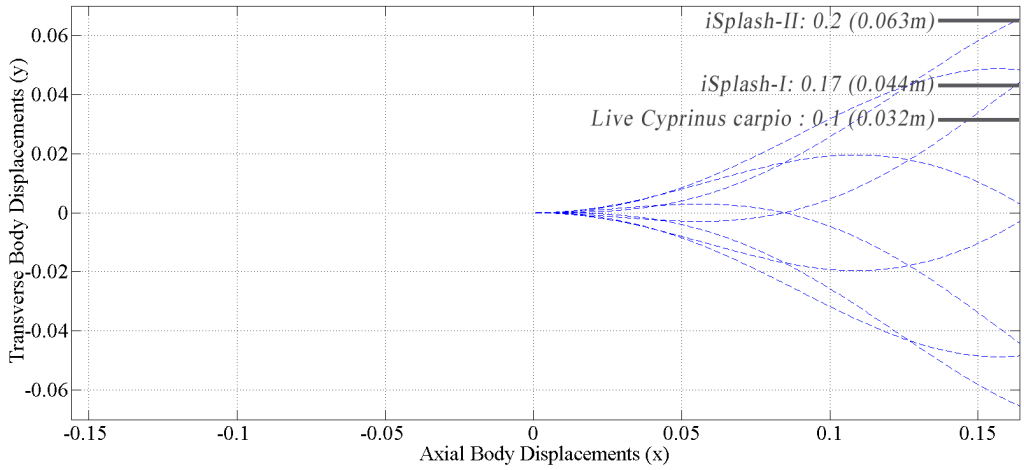

Figure 6.11: Mode 1: The wave form is confined to the posterior 1/2. (Parameters have been measured from experimental tests).

It can be seen, that the developed posterior structure can accurately mimic the undulatory parameters of real fish, as the components of link IV can be adjusted experimentally to provide the targeted midline during free swimming at various frequencies. Both Modes were able to generate accurate amplitudes of 0.1 of the body length and attain large tail amplitudes of 0.2 (0.063m) which was found to significantly increase performance. This value is twice the size of the observed value of the common carp at 0.1 and is increased over the first

generation at 0.17 (Section 4.5.2). This generated amplitude is greater than the highly efficient swimming motion of a dolphin measured at 0.175 [118].

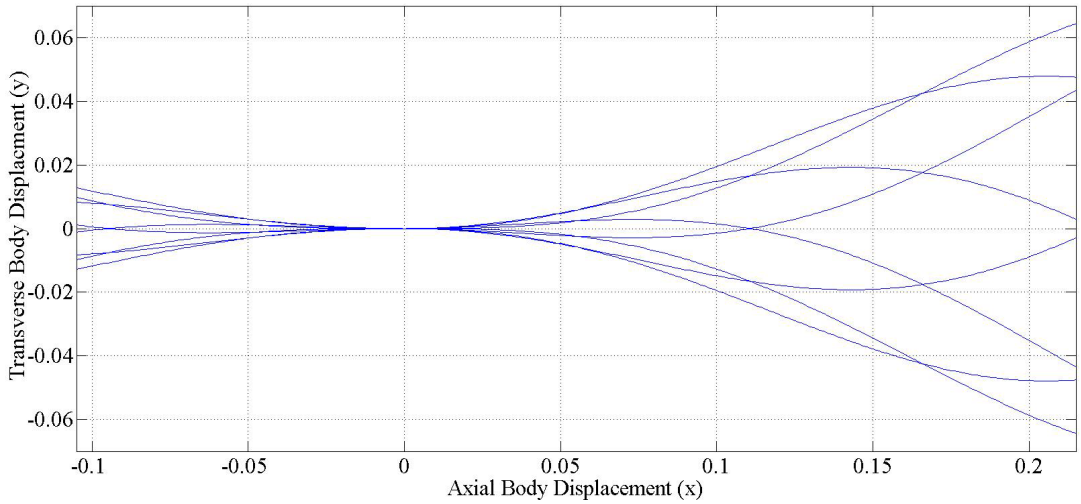

Figure 6.12: Mode 2: Showing the desired coordinated full-body kinematic parameters, generated based on the swimming motion of *iSplash*-I and the developed structural assembly parameters of *iSplash*-II.

Table 6.2: Comparison of Test Results between Modes 1 & 2.

Parameters	**Mode 1**	**Mode 2**
Maximum Velocity: BL/s (m/s)	11.6 (3.7)	11.6 (3.7)
Acceleration time to Max Velocity: s	0.6s	0.6s
Frequency: Hz	20	20
Reynold Number: Re (10^6)	1.2	1.2
Shrouhal Number: *St*	0.34	0.34
Maxium Thrust: N	9	9
Max Power Comsumption Air: W	120	120
Max Power Comsumption Water: W	120	120
Swimming Number: *Sw*	0.58	0.58
Head Swing Amplitude: m	0.003	0.013
Tail Swing Amplitude: m	0.063	0.063
Body length displaced: %	51	76

The caudal fin was formed with a low aspect ratio (AR). Although not yet thoroughly investigated, this tail was measured to achieve the highest maximum velocity and

acceleration during the initial field trails. AR is defined as: AR=*b*2/*Sc* where *b* squared is the fin span and *Sc* is the projected fin area. In this case the AR was 1.6.

6.6.2 Experimental Results: W, N, BL/s *vs.* Hz

Energy Consumption - In Figure 6.13 the average energy economy in relationship to driven frequency is shown, comparing both operational Modes in air and water. It can be seen that both Modes actuating in water consumed a maximum 120W at 20Hz. This measurement was obtained by a connecting tethered power supply and no noticeable increase in energy consumption was measured due to a resistance of the surrounding liquid. The result of high energy consumption can be significantly improved as the tests indicated large mechanical gains when actuating the mechanical drive system without link IV, improving from a 120W to 70W consumption.

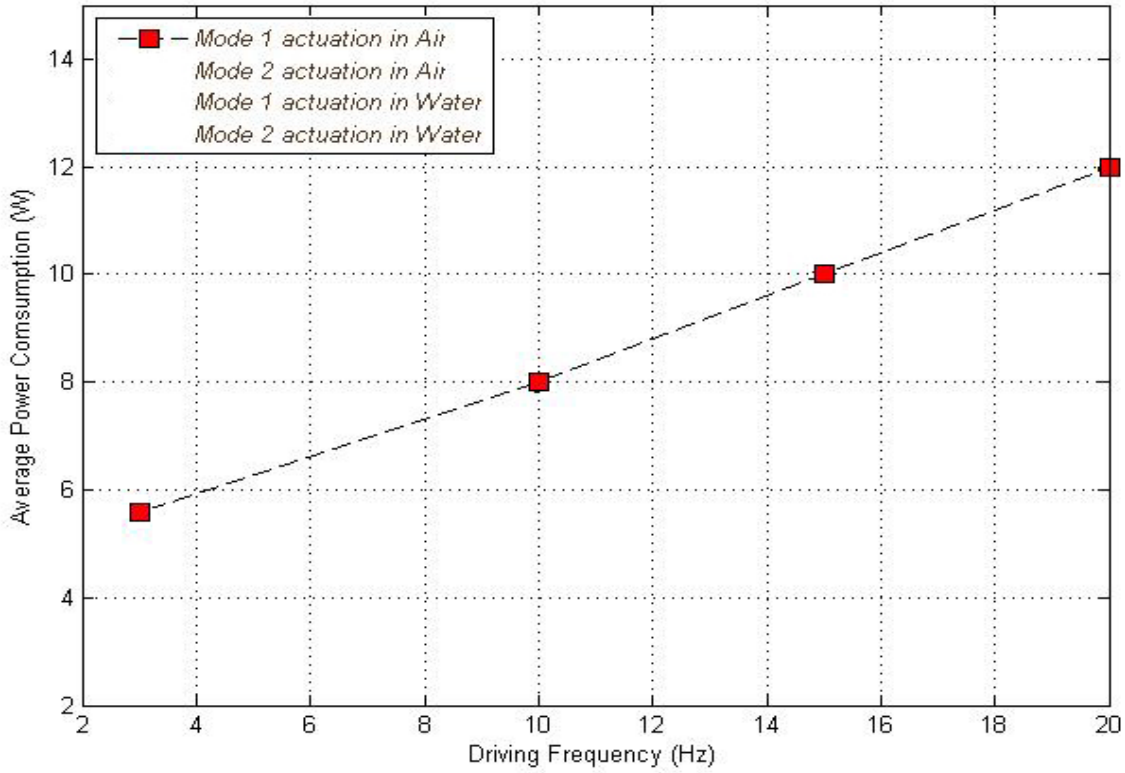

Figure 6.13: Comparison of average electrical power consumption over driven frequency of both Modes, actuating in air and water. No noticeable change was measured during testing.

This was a result of pressure increase at higher velocities, as link IV was actuated, the tendons were required to be tighter to provide the desired posterior kinematics, putting

increased strain on the mechanism. Despite the high energy consumption, the prototype can maintain an operational time of approximately ten minutes at maximum velocity, far surpassing the endurance of live fish, as equivalent burst speeds can only be maintained for short times of around one second [172]. We can assume that engineering a greater mechanically efficient drive of link IV in the next generation may significantly improve endurance, relating to an estimated reduced energy consumption of approximately 50%.

- *Thrust Production* – Shown in Figure 6.14, the developed build with a high power density ratio can generate a great amount of force of up to 9N. This can be effectively transferred in the water, accelerating both Modes to maximum velocity in approximately 0.6s.

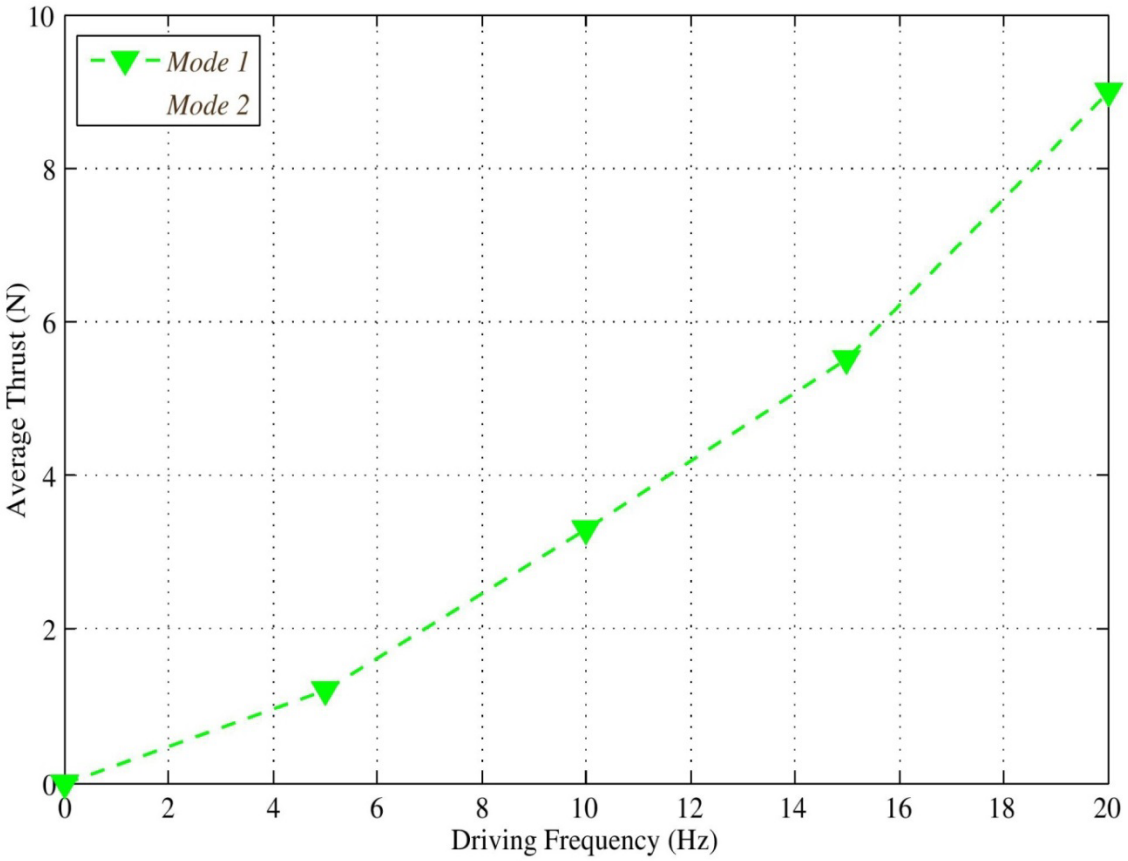

Figure 6.14: Comparison of average thrust in relationship to driven frequency. Modes 1 and 2 have equivalent measurements.

- *Maximum Velocity* - The relationship between velocity (speed divided by body length) and driven frequency is shown in Figure 6.15. The corresponding values of Modes 1 and 2 during consistent swimming are shown and compared to current robotic fish. Both operational Modes can achieve an average maximum velocity of 11.6BL/s, (i.e. 3.7m/s) at 20Hz, significantly increasing performance in comparison with *iSplash*-I and current

published robotic fish which typically peak around 1BL/s. This result also outperforms the average maximum velocity of real fish measured at 10BL/s. The values illustrated in Figure 6.15 show that applying the operational Mode 2 swimming pattern had no effect on performance due to kinematic alignment errors, discussed in Section 6.6.1, therefore it is predicted that the magnitude of added mass in both modes is equal. Hence, we can estimate that accurately applying the coordinated full-body swimming pattern of *iSplash*-I may increase speed by a further 27%.

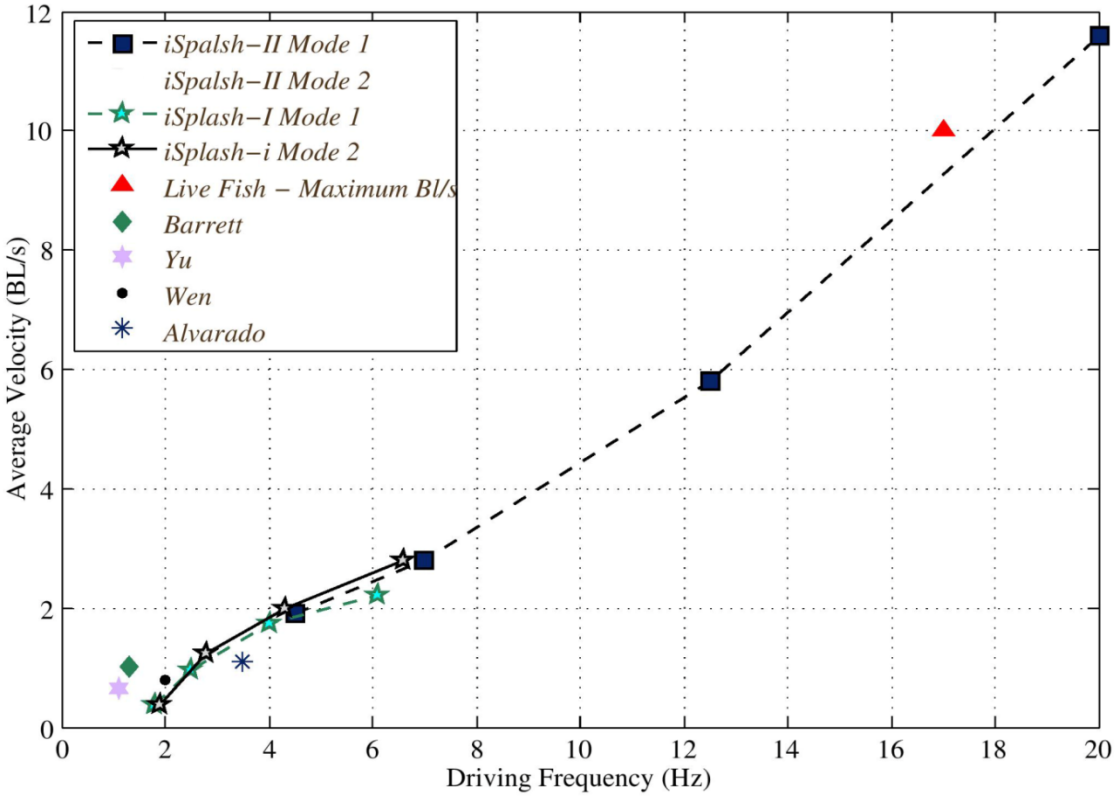

Figure 6.15: Comparison of average velocities achieved by both Modes, against robotic and live fish. Modes 1 and 2 measured equal velocities.

A prominent parameter for analyzing BCF locomotive performance is the Strouhal number (*St*), defined as $St=fA/U$, where f denotes the frequency, A denotes the tail amplitude and U is the average forward velocity. *St* is considered optimal within the range of $0.25 < St < 0.40$ [6]. The measured $St = 0.34$ under the condition of $Re = 1.2 \times 10^6$, in both Modes is within the desired range. The prototypes Swimming number (*Sw*) (distance travelled per tail beat) is highly efficient, measuring a *Sw* of 0.58 in comparison to the previous build with a *Sw* of 0.42 and close to the particular efficient common carp with a *Sw* of 0.70 [51; 118].

We have undertaken experiments to gain knowledge if raising driven frequencies greater than the previous build of 6.6Hz would continue to increase speed without peak or decline. This was achieved measuring a continued increase in velocity up to intensively high frequencies of 20Hz. Mimicking the swimming properties of real fish, frequency has become the key variable to enhance the linear locomotive performance of the *iSplash* platforms.

6.7 Summary

This chapter describes the development and experimental analysis of *iSplash*-II. At this stage of research the objective was to achieve the fastest speeds of live fish. This required a high-performance prototype, robust, compact, naturally buoyant, carrying its own power supply, with a high power density and able to effectively transmit large forces at intensively high tail oscillation frequencies for untethered high-speed propulsion.

Although the desired kinematics over the full body could not be attained due to the power density requirements (with the primary actuator 75% of the total mass) (Section 6.4), the devised assembly was able to significantly reduce the recoil around the center of mass (Section 6.6.1), therefore generating an effective propulsive mechanism. As a result, large posterior forces and tail amplitudes 0.2 of the body length (with smooth generated undulations from mid-body to tail tip) were attained. The prototype was able to accelerate to steady state swimming in an approximate time of 0.6s, maintain an endurance at maximum speed for approximately ten minutes (far greater than the measurement of real fish of approximately one second), realize a highly efficient stride rate (*Sw*) and attain intensively high tail oscillatory frequencies without early peak, decline or mechanical failure (Section 6.6.2).

In this chapter we presented a biomimetic mechanism which is capable of outperforming the recorded average maximum velocity of real fish measured in BL/s, attaining speeds adequate for real world applications. *iSplash*-II, a 32cm untethered carangiform swimmer, 0.835kg, formed in PLA filament, consistently achieved a maximum velocity of 11.6BL/s (i.e. 3.7m/s) at 20Hz with a stride rate of 0.58 and a force production of 9N.

The experimental analysis of the third generation has shown potential to improve upon the high performance swimming further. The following points are of significant interest for the next stage of research:

(i) Raise driven frequency to increase swimming speeds, with potential to achieve greater performance than the fastest measurement of live fish. As the build showed no signs of failure an initial aim of 40Hz can be estimated.

(ii) Accurately emulate the kinematic parameters of the full-body swimming motion [114], indicating that maximum velocity may increase a further 27% (Section 4.5.2).

(iii) Replace the drive mechanism of link IV, to significantly improve the energy consumption (Section 6.6.2).

(iv) Optimize the tail amplitude, shape, 3D deformation and magnitude (Section 4.6.7).

(v) Apply the behavioral technique of burst and coast, as live fish generating 10BL/s at the burst stage have been measured to reduce the cost of transport by approximately 50% [48].

(vi) Decrease the scale of the geometric frame, as the developed structure complexity was greatly reduced in comparison to the first generation, we can estimate that a reduced body size may be realized with less forward resistance and greater locomotive ability.

Chapter 7

iSplash- MICRO: Swimming at the Speed Similar to Real Fish

This chapter presents a new millimeter scale robotic fish, namely *iSplash*-MICRO (Figure 7.1) [131], able to accurately generate the posterior undulatory pattern of the Carangiform swimming mode at intensively high frequencies. Anterior stabilization is investigated to reduce the large kinematic errors and optimize forces around the center of mass. Applying large scale dorsal and pelvic fins relative to body size enables predictable optimization of the anterior and posterior displacements. During the field trials, the small fish with a length of 50mm has generated an average maximum velocity to real fish, measured in body lengths/second (BL/s), greatly improving upon previous robotic fish, achieving a consistent free swimming speed of 10.4BL/s (0.52m/s) at 19Hz with a low energy consumption of 0.8 Watts. The remainder of the chapter is organized as follows: Section 7.1 Introduces the chapter and Section 7.2 details the research objectives. Section 7.2 details the applied swimming pattern and introduces a novel destabilization solution. Section 7.3 describes a new construction method for micro builds. Section 7.4 describes the field trials undertaken and the experimental results obtained. Concluding remarks and future work are given in Section 7.5.

7.1 Introduction

During marine exploration a miniaturized underwater vehicle can benefit operations by allowing greater mobility as the turning diameter and body geometry is small. Current rotary propeller driven vehicles operating during low speed locomotion have particularly high cost of transport [66] requiring large a power supply, increasing body size. In addition the drive method of rigid hull UVs create large propulsive wakes causing increased environmental noise. In contrast, this is where fish excel, generating large transient forces efficiently and smoothly by coordinating their body motion in harmony with the surrounding fluid [112; 1]. Hence, the miniaturization of bio-robotic propulsion can provide greater mobility, unobtrusive navigation, reduced noise to the environment and a lower cost of transport.

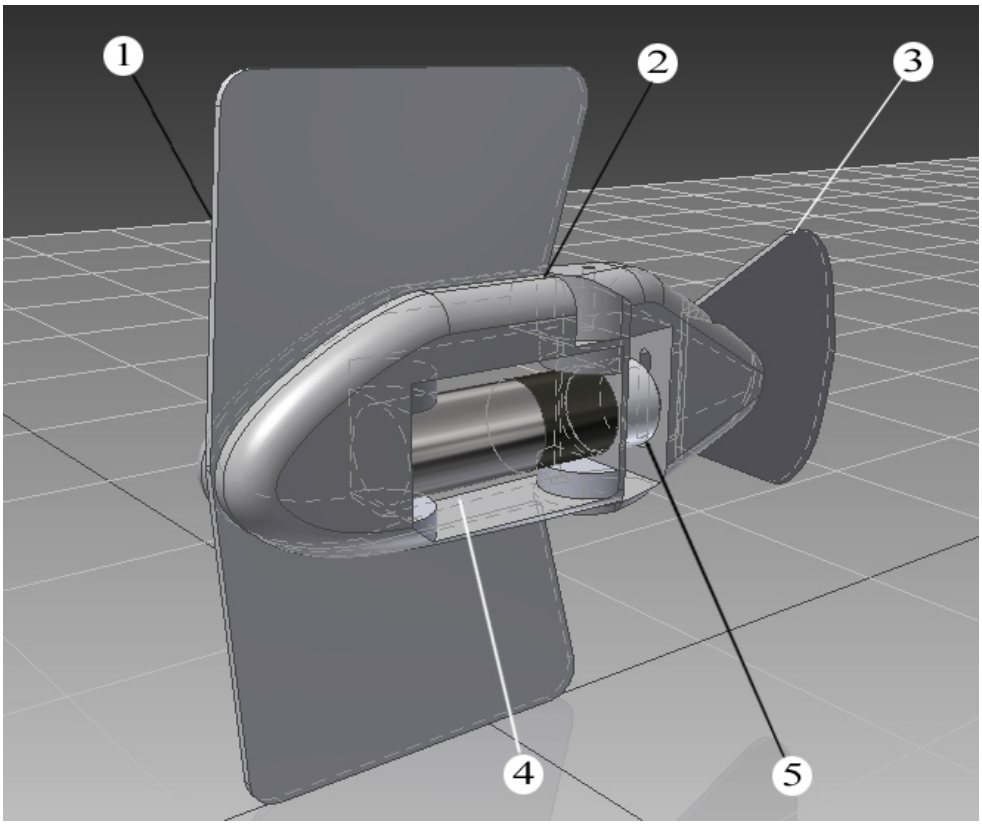

Figure 7.1: *iSplash*-MICRO, 50mm in body length: 1-Large scale anterior fins; 2-Modular mid-body chassis; 3-Compliant caudal fin and peduncle; 4-Power transmission system; 5-Driven tail plate.

Although smaller fish are measured with an overall slower speed in relation to size, they are able to generate higher tail oscillatory frequencies and therefore greater speed, measured in body lengths/ second (BL/s), a great benefit to overcome position destabilization flows.

Detailed through previous chapters the project aimed to achieve the measured average maximum velocity of real fish at 10BL/s, an exceptional example of a small fish (Cyprinus carpio), 135mm in body length, achieved a maximum velocity of 12.6BL/s (i.e. 1.7m/s) and a stride rate of 0.66 [51; 122].

Micro scale design requires developing the propulsive motion in relation to the developed body size and desired surrounding environment. The required propulsion method can be calculated using the Reynolds number (*Re*). *Re* relates to the ratio of inertia to viscous forces (Figure 7.2). If the *Re* is large, the viscous forces are negligible (*Re* 10^3-10^7) [122]. Viscous force is dominant when the body length is approximately <1mm. The two methods of propulsion are categorized as:

(i) Inertia Force Propulsion, generating locomotion by creating a reaction force (F_R) against the mass of the water.

(ii) Resistance Force Propulsion, adopting a kinematic motion to generate locomotion from the viscosity of the water.

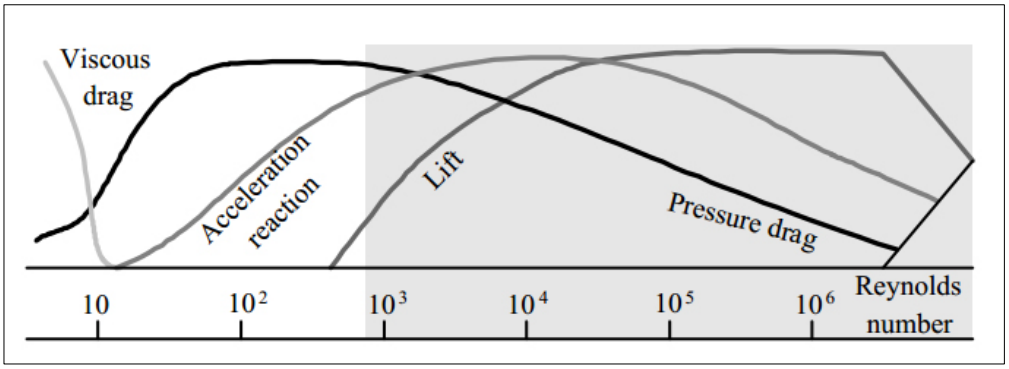

Figure 7.2: The required propulsion method can be calculated using the Reynolds number. The figure shows the relationship of the Reynolds number to the ratio of inertia to viscous forces [122].

Although millimetre scale builds apply an identical swimming motion to larger fish, the complexity of developing a mechanical structure at the micro scale is increased due to material and hardware constraints. Some examples of novel micro builds and their maximum speeds are Ye's IPMC actuated fish, 98mm's in body length which achieved a maximum velocity of 0.24BL/s (24mm/s) [123], Guo's ICPF actuated prototype, 45mm's, achieving a velocity of 0.11BL/s (5.21mm/s) [124] and Wang's SMA manta ray, 243mm's, achieving a velocity of 0.23BL/s (57mm/s) [125]. We can see that the millimetre scale robotic fish generate speeds far lower than the previously highest performing prototype devised by Valdivia y Alvarado, which achieved a velocity of 1.1BL/s (0.32m/s) [117].

7.2. Research Motivation and Objectives

This research is based on the experimental findings of the first, second and third generation prototypes:

- The First Generation: *iSplash*-I (Chapter 4) [114], 250mm in length, 0.367kg and fabricated from stainless steel and aluminum (Section 4.4.4). In particular it achieved anterior stabilization by significantly reducing recoil and optimizing the lateral (F_L) and thrust forces (F_T) around the center of mass (Section 4.5.2), assumed to initiate the starting moment of added mass upstream, by applying a full body length coordinated swimming motion introduced in Chapter 3. Notably, the mechanical drive system of *iSplash*-I operating in the simplified body motion of posterior confined undulations also measured a high performance of 2.2BL/s (0.55m/s) at 6.1Hz (Section 4.5.4). Hence this generation takes into consideration that the millimeter scale builds require simplistic construction techniques whilst retain high performance.
- The Second Generation: *iSplash*-OPTIMIZE (Chapter 5) (600mm in length, 0.9kg (Section 5.4)) [129]. The analysis found the magnitude of the geometric frame significant affects forward resistance (Section 5.6.3). Hence this generation takes in consideration the importance of a high force production contained within the smallest dimensions possible and continues this development.
- The Third Generation: *iSplash*-II (Chapter 6) [130], achieved high-speed swimming. The prototype was developed to be robust, compact (320mm in length, 0.835kg (Section 6.5)), naturally buoyant, carrying its own power supply and able to effectively transmit large forces of 9N at intensively high tail oscillation frequencies of 20Hz for untethered high-speed propulsion (Section 6.6.2). The high power density with the primary actuator 75% of the total mass was critical in improving the performance over the previous generations (Section 6.5).

  Hence the fourth generation took into consideration the previous findings that require the lateral and thrust forces to be optimized around the center of mass, to generate accurate posterior kinematic displacements and greatly increase the magnitude of added mass, as the devised assembly of *iSplash*-II was able to significantly reduce the anterior recoil (Section 6.6.1), therefore generating an effective propulsive mechanism.

Throughout the field trails the prototypes *iSplash*-I and II showed no peak or decline in velocity as frequency was raised in both swimming modes. Mimicking the swimming

variables of real fish, as measured in the observational studies of Bainbridge, indicating swimming above 5Hz has no variation in kinematics and only frequency is changed to increase swimming speed, providing a key swimming parameter. Therefore applying higher frequencies to either swimming motion of *iSplash*-I and II may continue to increase velocity, and in consideration that fish employ an identical swimming motion of inertia force propulsion at the millimeter scale, we proposed *iSplash*-MICRO.

The research project for the fourth generation aimed to achieve the fastest speeds of live fish and proposed five main objectives:

(i) Develop a structural build only 50mm in length, able of accurately replicating the kinematic parameters of the posterior confined undulatory swimming pattern of *iSplash*-I;

(ii) Significantly raise driven frequency in comparison to the first generation, to be capable of intensive tail oscillations of up to 19Hz by fabricating a robust naturally buoyant structure, a complex challenge at such a small scale;

(iii) Allow for a high efficiency mechanical energy transfer by engineering a drive system that takes hardware and material parameters into account;

(iv) Devise a novel solution to improve the predicted excessive destabilization in yaw, by optimizing the F_L and F_T around the center of mass;

(v) Realize a mechanism capable of consistent steady state swimming, measuring its achievements in terms of speed, kinematic accuracy and energy consumption over a range of frequencies from 5-19Hz.

7.3. Millimeter Scale Design Methodology

7.3.1. Posterior Undulatory Swimming Motion

The prototype is deployed with the selected Carangiform swimming motion, which applies the method of body and/or caudal fin (BCF) propulsion and has been chosen for replication due to its exceptionally high locomotive performance [118; 5]. If the propulsive method is accurately replicated, a robotic fish is able to achieve the high performance in straight line swimming required for real world environments as shown in Chapters 4 and 6.

Inertia Force Propulsion of the Carangiform swimming mode is associated with the method of added mass [119]. Added mass is initiated as each individual segment of the undulatory wave passes backwards during the body wave cycle creating a force F_R against the surrounding fluid and an opposing force against the body, generating forward motion of

the entire body. The F_R is decomposed in to F_T and F_L, which must be optimized for efficient propulsion. The added mass is the product of the water accelerated and the momentum of water accelerated by the propulsive segments. Fish can achieve low cost of transport by generating the method of added mass efficiently. Hence, there is great potential accurately mimicking this propulsive method. Replicating this method at the millimeter scale is a greater challenge, as the small build cannot be deployed with the full body motion seen in real fish.

The deployed posterior kinematic pattern of the Carangiform inertia force propulsion method is represented in the form of a traveling wave and can be identified by its propulsive wave length. The adopted body wave parameters will concentrate the wave motion to approximately 1/2 of the body length, initiated at the center of mass, smoothly increasing in amplitude along the body length towards the tail tip [112]. The observed posterior amplitude of live fish is 0.1 of the body length, measured from the midline to the furthest lateral tail excursion. The location of the pivot point is optimum at 0.15-0.25 [118]. The commonly adopted swimming kinematics were proposed in [113] adapted in [20] (Chapter 3). The posterior undulatory swimming motion applied to iSplash-MICRO is of the form:

$$y_{\text{body}}(x,t) = \left(c_1 x + c_2 x^2\right)\sin\left(\text{k}x + \omega t\right) - c_1 x \sin\left(\omega t\right) \qquad (7\text{-}1)$$

where y_{body} is the transverse displacement of the body; x is the displacement along the main axis starting from the nose of the robotic fish; k =2π/λ is the wave number; λ is the body wave length; $\omega = 2\pi f$ is the body wave frequency; c_1 is the linear wave amplitude envelope and c_2 is the quadratic wave.

The desired wave form motion consists of one positive phase and one negative phase throughout the complete cycle [118]. The parameters $P = \{c_1, c_2, k, \omega\}$ can be adjusted to achieve the required posterior swimming pattern, providing an engineering reference. This operational mode will be described as Mode 1 and is illustrated in Figure 7.9.

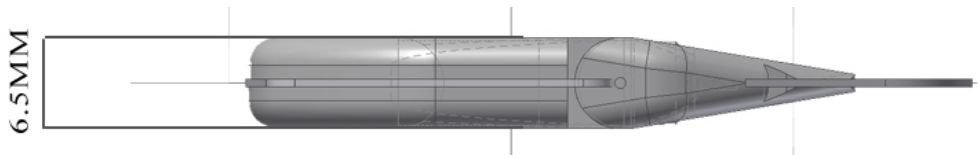

Figure 7.3: Plan view.

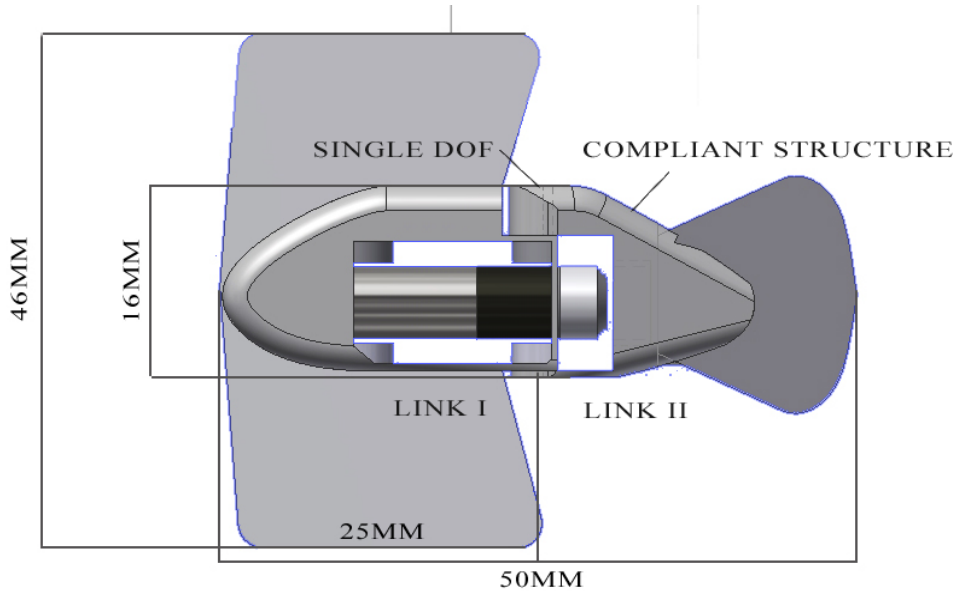

Figure 7.4: Profile view.

Figure 7.5: Front view.

7.3.2. Anterior Stabilization Approach

It was detailed by Lighthill [112], that several morphological adaptations of Carangiform fish reduce the severe yaw destabilization that is seen in free swimming robotic fish, without affecting propulsive efficiency by increasing drag:

(i) Vertical compression along the full body length. The measured maximum thickness is 0.2 of the body length and reduces in size towards either extremity [118]. This form must be applied to reduce roll and yaw destabilization and also forward resistance. This structure is realized when engineering a morphological approximation of a Carangiform swimmer;

(ii) Reduced depth of body at the peduncle, most defined by the Thunniform swimming mode [10]. This structural adaptation is complex to fabricate at any scale due to material limitations, particularly at the micro scale as the posterior mechanism must be narrow, structurally robust and mimic the smooth curves of the kinematic undulations;

(iii) Accurate weight distribution. Imprecise configurations generate large destabilization within the horizontal plane, as a consequence of the F_R not being optimized, typically seen on multi-link servo assemblies [116; 20];

(iv) Increased depth of body towards the anterior, a distinctive adaptation of the Carangiform morphological parameters. As previously described, anterior destabilization is challenging to control [114]. Passive rigid anterior mechanisms recoil around the center of mass. Current free swimming robotic fish can be seen with excessive head swing, similar in magnitude to the posterior, greatly increasing drag [117]. As a micro scale structure limits the ability to apply the coordinated full-body motion [119] due to the complexity of the mechanical linkage, we propose a novel approach to significantly increase the anterior depth of body by applying large scale dorsal and pelvic fins, relative to body size.

The anterior destabilization solution of anterior and mid-body fins provides the required surface area without creating excessive resistance to forward motion as the fins are vertically compressed. Flow visualization techniques from published biological studies [23; 6] and mechanisms such as “undulating pump” and “vortex peg” have measured a fluid-body interaction that may contribute to propulsion, is generated upstream to the posterior section. Therefore, it is predicted that reducing the anterior amplitude to the observed optimal value of a common carp at approximately 0.04 of the body length (Section 3.4) will initiate the starting moment of added mass upstream and optimize the F_L and F_T forces around the center of mass, increasing the overall magnitude of thrust contributing to increased forward velocity. This operational mode will be referred to as Mode 2, illustrated in Figure 7.10.

7.3.3. Posterior Amplitude Variations

To provide a further investigation into the kinematics parameters of the Carangiform swimming motion, and the proposed stabilization solution of operating Mode 2, a variation in tail amplitude was applied. This operational mode will be referred to as Mode 3 and illustrated in Figure 7.11. A larger kinematic parameter than the value of real Carangiform swimmers will first be applied to Modes 1 and 2, as a large tail amplitude value of 0.17 applied to *iSplash*-I was previously found to significantly increase performance. Due to the predicted destabilization whilst operating in Mode 1 [114], the body and tail kinematic data during locomotion will be inaccurate. If the anterior destabilization solution of Mode 2 and 3 is operationally correct the posterior kinematic parameters will also align with the desired amplitude value. Mode 3 will further investigate the Carangiform swimming motion of Mode 2, by applying structural changes to the mechanical drive offset, to test a tail amplitude which is closer to the observed measurement of a common carp.

7.4. Construction Method for Micro Scale Builds

A mechanical drive system able to accurately mimic the displacements of the travelling wave sets a great challenge. This is significantly increased at the millimeter scale. The drive system must be simple, compact, lightweight and robust to provide high frequencies under large forces for high-speed performance. Various novel approaches using the advances in hardware to achieve micro scale actuation have been attempted [126; 127; 92]. Smart materials have mainly been adopted to reduce body size but have shown limited frequencies, response time, actuation and force, therefore measuring low linear velocities [123; 124; 125; 128].

We set an aim for the prototypes build length of 50mm. Live Carangiform fish of this body size employ identical swimming motions to larger fish of 250mm to generate linear locomotion, by employing the inertia force propulsion method of added mass. Therefore, we aimed to devise a simplified powertrain, capable of replicating the posterior confined undulatory swimming motion of *iSplash*-I without loss of accuracy.

The developed arrangement illustrated in Figures 7.6 and 7.7 employs a single electric motor and a single DOF along the axial length. The two rigid discrete links are coupled with a stiffness varying posterior, beginning at link II and continuing to the tail tip. The discrete assembly method can be defined as a series of links or N links. Applying more links reduces midline curve alignment errors and increases mechanical complexity. Details of the fully

discretized body wave fitting method are given in [116; 20]. To provide the undulatory motion, a compliant caudal fin is coupled to link II which can be removed. This method allowed the material stiffness of the caudal fin to be adjusted experimentally, to provide the targeted curves during free swimming. The presented design approach achieved complexity of motion with a significant reduction in structural parts, allowing a build only 50mm in length to be realized.

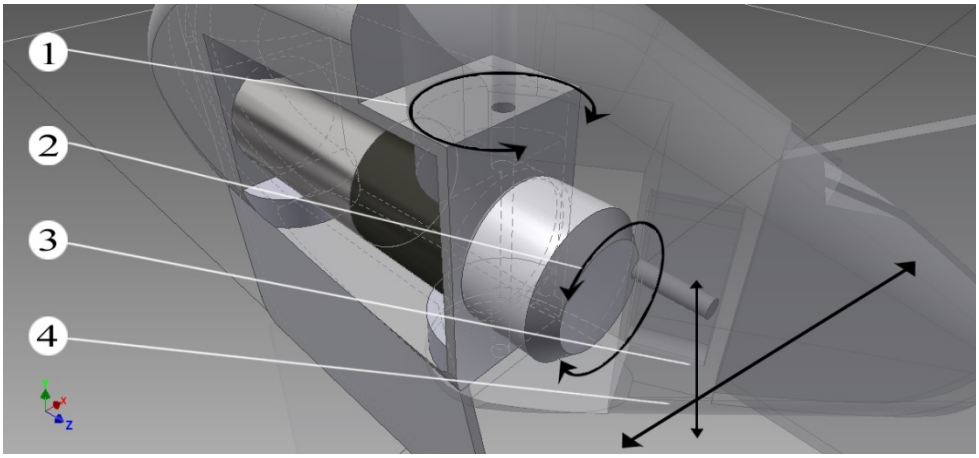

Figure 7.6: Power transmission system: 1-Tail connecting pivot; 2-Crankshaft; 3-Transistion plate; 4-Link II coupled to caudal fin.

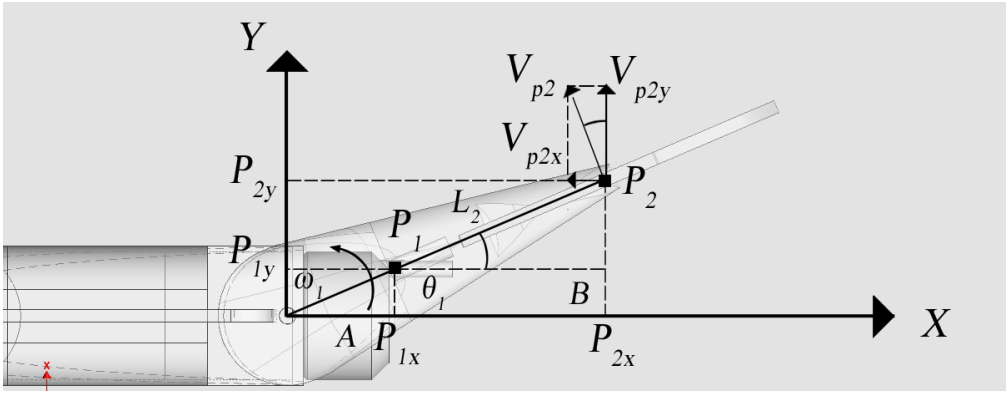

Figure 7.7: Schematic drawing of the tail offset drive crank and linkage.

In addition, a modular build was devised allowing each part to be easily changed and modified during fabrication, and for all Modes of operation to be applied to the same prototype by adjusting the configuration. Mode 3 can be put in operation by adjusting the single offset crank, driving link II shown in Figure 7.7. Mode 2 can be applied by removing the outer structure of link I and replacing with the required form.

7.4.1. Micro Scale Power Transmission System with High Frequency

A single crankshaft attached to the output shaft of the primary actuator directly drives link II, by transmitting continuous rotary power to linear oscillations, illustrated in Figures 7.6 and 7.7. The devised powertrain increases power distribution to the posterior and required high-precision of the chassis, link structures and crankshaft to avoid deadlock, reduce friction and significantly improve energy transfer, which can be lost in many stages of the mechanical drive.

The driven link amplitude is determined by the offset crank, L_2 represents posterior link of the discrete structure. The maximum amplitude of the link length L_2 at point P_2 is determined by the predetermined maximum crank offset P_1. The coordinates of P_1 (P_{1x}, P_{1y}) and P_2 (P_{2x}, P_{2y}) can be derived by:

$$\begin{cases} P_{1x} = A\cos\theta_1 \\ P_{1y} = A\sin\theta_1 \end{cases} \begin{cases} P_{2x} = P_{1x} + B\sin\theta_1 \\ P_{2y} = P_{1y} + B\sin\theta_1 \end{cases} \tag{7-2}$$

The length of L_2 can be derived by $L_2^2 = P_{2x}^2 + P_{2y}^2$. Assume that ω_1 is the angular velocity of the link L_2, and the velocity vector V_{P2} is perpendicular to L_2. We have:

$$\begin{cases} V_{p2x} = -\omega_1 L_2 \sin\theta_1 \\ V_{p2y} = \omega_1 L_2 \cos\theta_1 \end{cases} \tag{7-3}$$

where V_{p2x} and V_{p2y} are the decomposed vectors of the velocity vector $V_{P2} = \omega_1 L_2$.

7.4.2. Fabricating a Micro Scale Prototype

iSplash-MICRO in operational Mode 2 with a total mass of 3.35g (2.45g in Mode 1) is illustrated in Figure 7.8, with the physical specifications given in Table 7.1. The build was first digital modeled taking hardware constraints and material properties into account, so that the kinematic and geometric parameters were not affected, reducing the resistance during forward locomotion. The inner structural frames and bulkhead were formed from the material polypropylene, chosen to provide the required density (lower than water) and the structural strength for high frequency actuation. All structural parts were hand cut, fitted and assembled. This devised method produced a structurally robust prototype allowing for consistency of operation at intensively high frequencies, generating large forces relative to body size, which are applied to the water and reactively, the opposing force exerted on to the vehicle [119].

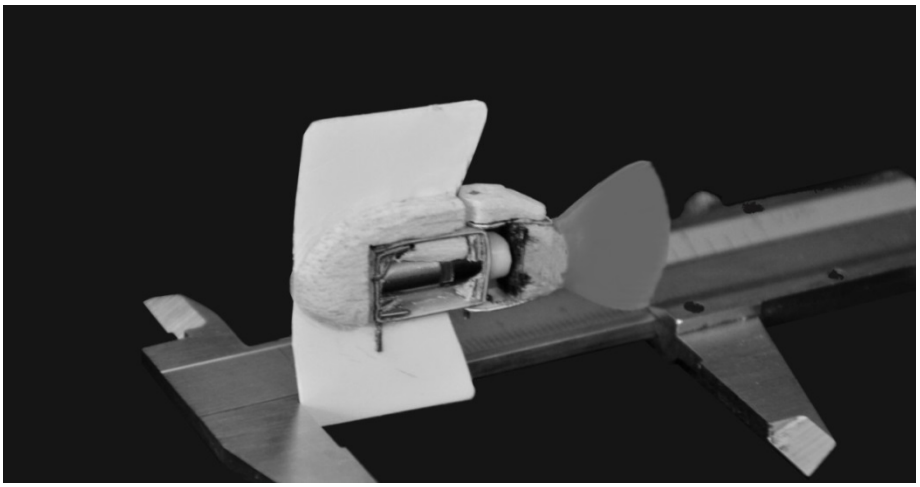

Figure 7.8: *iSplash*-MICRO with large dorsal and pelvic fins.

For fast locomotive performance, a high power density is required to attain high frequency actuation. Although complexity of developing the mechanical drive system is increased, a single electrical motor with continuous actuation was deployed and positioned in the optimum location [112; 118], in contrast to other construction methods which limit accuracy of weight and volume arrangement and force production [116; 20; 117]. The power-to-weight ratio was greatly increased by achieving a configuration in which the electric motor is 50% of the total mass in operational Mode 1 and 37% in Modes 2 and 3. To counteract the large weight of the primary actuator relative to body size, the build volume was increased vertically, to realize natural buoyancy.

For operational Mode 2, large fins, 48mm in height with vertical compression were devised, a similar morphological trait as real fish fins. By forming large dorsal and pelvic fins made of polypropylene the buoyancy was greatly increased, this was counteracted by applying weight to the lower chassis of link I. During free swimming stability could not be maintained as frequencies were raised. Although the anterior fins were devised as an initial solution to reduce destabilization within the horizontal plane, the configuration of material properties significantly increased stabilization in roll. This development enabled the prototype to achieve open loop stability, as the relative position of buoyancy is higher than the center of mass. Therefore the surrounding fluid counterbalances the gravitational weight [3].

Table 7.1: Physical parameters of *iSplash*-MICRO.

Parameter	Specific Value
Maxium Velocity: BL/s (m/s)	10.4 (0.52)
Body Size: mm (LxWxH)	50 x 7 x 16 (Without Fins)
Body Mass: g	2.45 (Without Fins)
Anterior Fin Size: mm (LxWxH)	26 x 0.8 x 48
Anterior Fin Mass: g	0.9
Maximum Frequency: Hz	19
Actuator:	Single electric motor
Actuator Mass: g	1.23
Power Supply:	4V LiPo external battery supply
Materials:	Balsa wood, polypropylene, acetal
Swimming Modes:	Linear locomotion
Tail Material:	Polypropylene
Thickness of Caudal Fin : mm	0.8
Caudal Fin Aspect Ratio: AR	1.5

7.5. Experimental Procedure and Results

Experimental Setup - Experiments were conducted within a 1000mm long x 500mm wide x 250mm deep test tank. The prototype had sufficient space to move without disturbances from side boundaries and the free surface, able to maintain swimming at mid-height of the test tank. A series of experiments were undertaken in order to verify the locomotive performance of all Modes in terms of speed, energy consumption and kinematic observation at frequencies between 5-19Hz. The test results of all Modes are summarized in Table 7.2. Steady free swimming over a fixed distance of 450mm was used to measure speed (shown in Figure 7.12), once the prototype had reached its maximum velocity at each tail oscillation frequency. Measurements were averaged over many cycles once the prototype was able to achieve consistent operation.

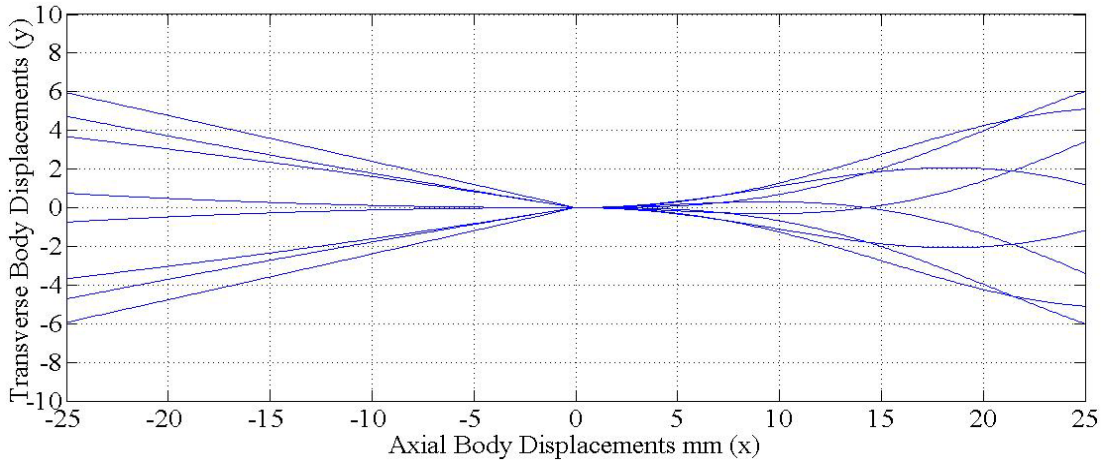

Figure 7.9: Mode 1: Kinematic data of midline during free swimming. 6mm tail amplitude and 6mm head amplitude (0.12 of the body length).

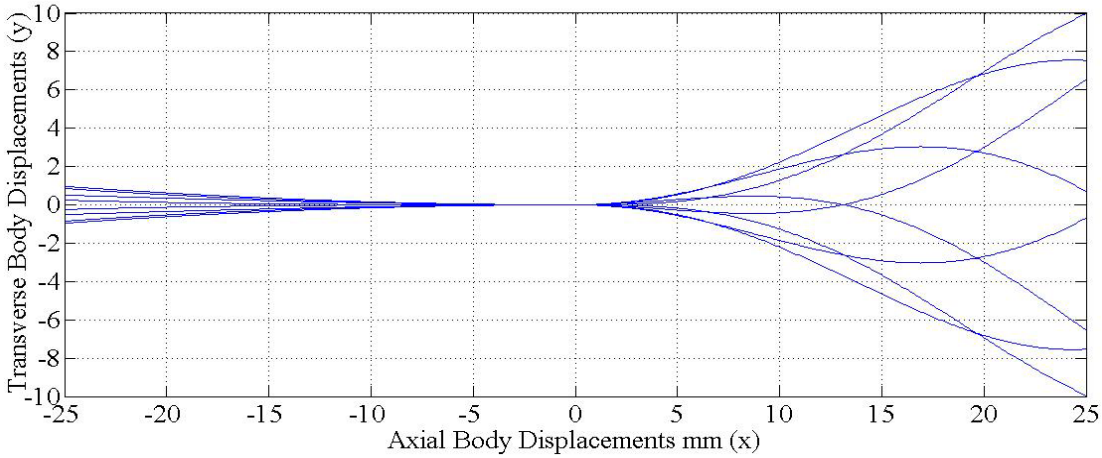

Figure 7.10: Mode 2: Appling large scale dorsal and pelvic fins relative to body size to reduce yaw destabilization, generating 1mm head amplitude and 10mm tail amplitude (0.20 of the body length).

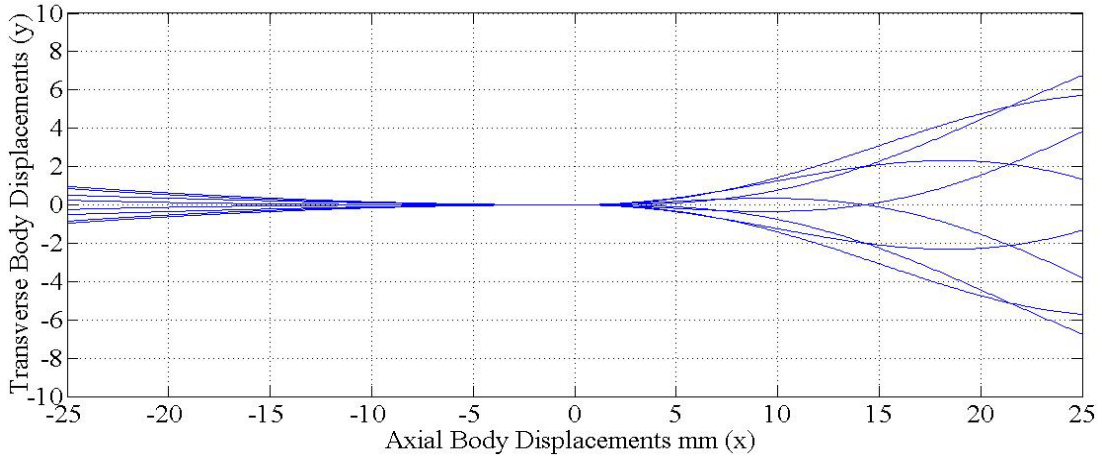

Figure 7.11: Mode 3: Operating with a reduced tail amplitude of 7mm (0.14 of the body length).

7.5.1. Swimming Pattern Observation

Illustrated in Figures 7.9, 7.10 and 7.11 are the midline kinematic parameters, tracked at 50 frames per second to provide the anterior and posterior wave forms of Modes 1-3 for comparison. We aimed to achieve and analyze the kinematic parameters of live fish and *iSplash*-I. Good matching with live fish kinematic data is a complex task, as the wave forms of free swimming robotic fish have shown extensive head amplitude errors and inaccurate displacement parameters over the full body length.

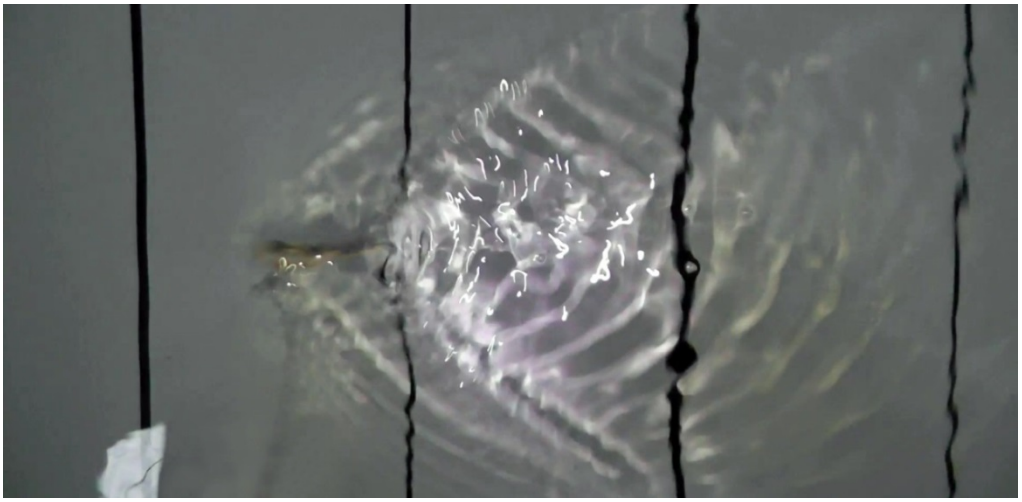

Figure 7.12: *iSplash*-MICRO during experimental testing of maximum velocity at 19Hz. Measured over a fixed distance of 450mm.

When comparing Modes 1 and 2, Mode 2 reduced the head amplitude from 0.12 (6mm) of the body length in Mode 1 to 0.02 (1mm), generating a smaller value than the common carp at 0.04 [118]. The observed tail amplitude of the common carp is 0.1 and *iSplash*-I is 0.17. Mode 1 with anterior destabilizing, lost posterior amplitude displacements and measured 0.12 (6mm), in comparison Mode 2 was able to generate a large value of 0.20 (10mm). Analyzing the midline sequence of the Mode 1 illustrated in Figure 7.9, we can notice the excessive head swing amplitude equivalent to the posterior value as predicted, based on previous work in [119] and current robotic fish [20; 117]. The stabilizing solution of Mode 2 has significantly improved matching errors, greatly reducing the recoil from the concentrated posterior thrust and in turn creating accurate posterior displacements. Figure 7.11 shows that Mode 3 has a reduced posterior amplitude of 0.14 (7mm), closer to the observed measurement of live fish and an equivalent anterior displacement to Mode 2. The tail

amplitude of Mode 3 was able to be calculated prior to the experimental testing using (7-3), as the devised anterior fins of the free swimming robotic fish have enabled a predictable kinematic optimization. In addition, it was found that Mode 1 had an erratic forward heading during test runs, affected by the tethered cables. In contrast, Mode 2 provides a very directional forward heading, not deterring once in motion.

A principal aim of the research was achieving accurate posterior kinematic matching to *iSplash*-I, with a significantly simplified assembly. The tracked midline shows that the developed prototype generates a precise travelling wave ½ the body length and has achieved a smooth transition phase from body to tail tip, due to the compliant structure. The formed caudal fin provided higher speeds in initial testing with a low aspect ratio, future optimization is planned. AR is calculated using: AR=$b2/Sc$ where b squared is the fin span and Sc is the projected fin area. AR in this case was 1.6.

Table 7.2: Comparison of test results between modes 1, 2 & 3.

Parameters	Mode 1	Mode 2	Mode 3
Reynold Number: *Re* (10^4)	2.6	2.6	1.6
Shrouhal Number: *St*	0.22	0.36	0.41
Swimming Number: *Sw*	0.54	0.54	0.33
Maxium Velocity: BL/s	10.4	10.4	6.4
Maxium Velocity: m/s	0.52	0.52	0.32
Frequency: Hz	19	19	19
Max Power Comsumption Air: W	0.68	0.68	0.68
Max Power Comsumption Water: W	0.8	0.8	0.8
Head Swing Amplitude: mm	6	1	1
Tail Swing Amplitude: mm	6	10	7
Test Run Distance: mm	450	450	450

7.5.2. Energy Consumption at 19Hz

The average energy economy in relationship to driven frequency is shown in Figure 7.13. A comparison measuring the cost of transport in water and actuation in air was made. We can notice that all Modes actuating in water resulted in a slight increase in energy consumption,

from 0.6W in air to 0.8W, at the maximum frequency of 19Hz. The very low cost of transport measured indicates the replicated swimming motion of [119] and the novel mechanical drive system is energy efficient. We can calculate that the next generation will be capable of carrying an onboard power supply.

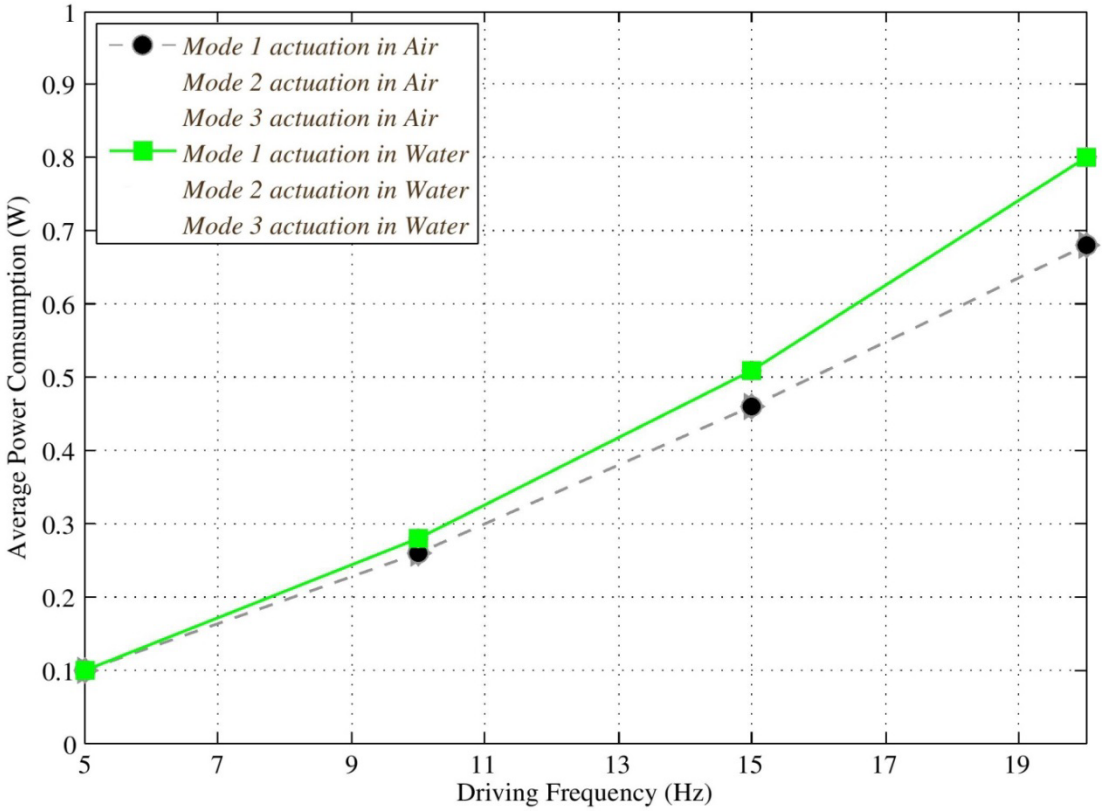

Figure 7.13: Comparison of average electrical power consumption over driven frequency of all Modes actuating in air and water.

7.5.3. Maximum Velocity – BL/s Equal to Real Carangiform Fish

The relationship between velocity (speed divided by body length) and driven frequency is shown in Figure 7.14. The corresponding values of all Modes during consistent swimming were measured and compared to current robotic fish. Modes 1 and 2 consistently achieved a maximum velocity of 10.4Bl/s (0.52m/s) at 19Hz. Mode 3 had a decreased maximum velocity of 6.4BL/s (0.32m/s) at 19Hz. Although the tail amplitude of Mode 3 was closer to the value of the common carp, performance was lower, reaffirming data from the first generation [119]. In addition, no energy consumption was saved from the tail amplitude reduction. Hence, we estimate the next generation may have enough power to further increase of tail amplitude beyond the value of Mode 2 (the furthest lateral excursion that could be applied to this structure). *iSplash*-MICRO has significantly increased performance in

comparison with current robotic fish which typically peak at approximately 1BL/s and has equivalent speeds of the fastest real fish, measured with an average maximum velocity of 10BL/s [51; 112].

Identical to the previous generation as frequencies were raised, velocity increased in all Modes. From this we can assume that raising this key swimming parameter of the developed mechanical drive system beyond 19Hz will continue to increase performance further.

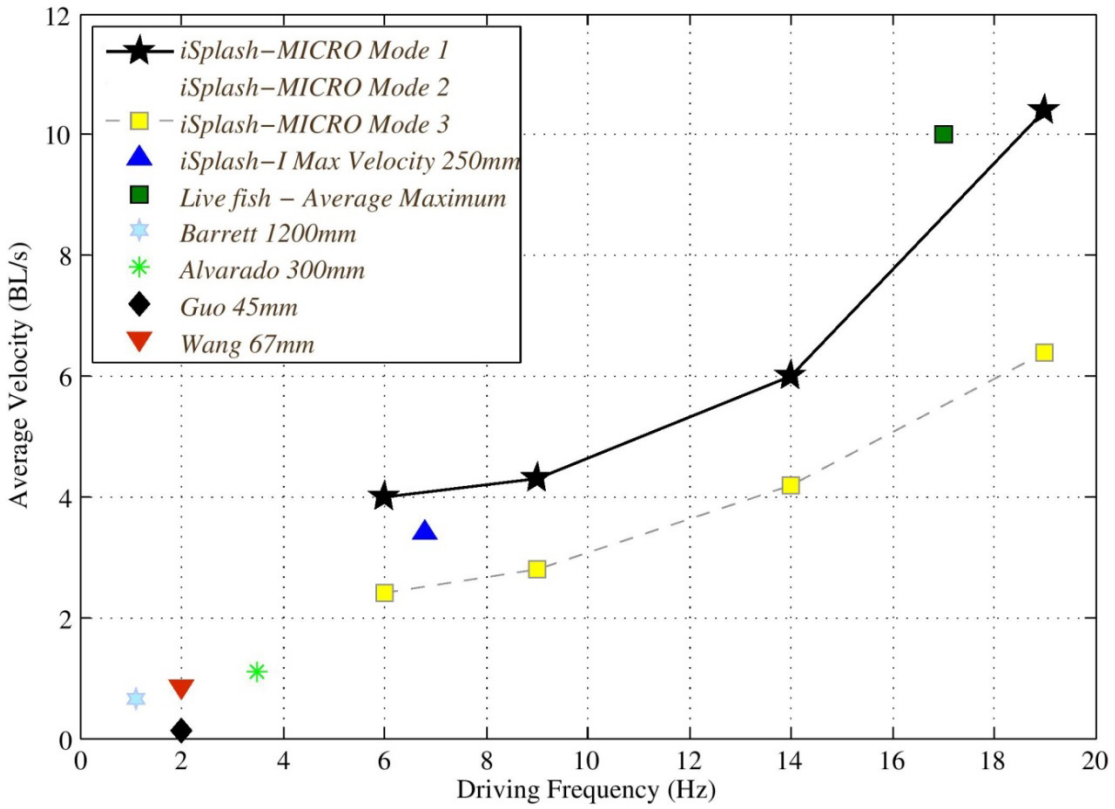

Figure 7.14: Comparison of average velocities achieved by all Modes, contrasted against current robotic fish and real fish.

Despite Mode 2 significantly improving displacement parameters along the full body length, no noticeable increase or decrease in velocity was found. This result was not expected as the coordinated full-body swimming motion of the first generation increased velocity by 27%. Differences in structure can be noted as previously mentioned in Section 7.3, as a consequence the midline kinematics do not generate a smooth curve from head to tail. This may have stalled the fluid flow interaction at a point located around the center of mass. The

location of the pivot point is inaccurate, due to structural constraints, the optimum range being 0.15-0.25 of the body length. All Modes were measured at 0.5.

The prominent parameter for analyzing BCF locomotive performance is the Strouhal number (*St*). Mode 1 has a *St* of 0.22 under the condition of $Re = 2.6 \times 10^4$, Mode 2 has a *St* of 0.36 under the condition of $Re = 2.6 \times 10^4$ and Mode 3 measured a $St = 0.41$ under a condition of $Re = 1.6 \times 10^4$. The *St* of Mode 2 is within the desired range with both Modes 1 and 3 approximately optimal. The prototypes Swimming number (*Sw*) (distance travelled per tail beat) of Modes 1 and 2 is highly efficient, measuring a *Sw* of 0.54, increasing performance over the previous build with a *Sw* of 0.42 and close to the particular efficient common carp with a *Sw* of 0.70 [118].

In addition, the prototype was actuated at high frequencies for long periods during construction and test runs, without need of rebuild or showing wear, indicating the robustness of the developed micro prototypes mechanical drive system.

7.6. Summary

This chapter described the development of a small robotic fish prototype *iSplash*-MICRO, a man-made system able to generate the average maximum velocity of real fish. A greatly simplified structural built at the millimeter scale is able to accurately replicate the kinematic parameters of the posterior confined undulatory swimming pattern of *iSplash*-I and II [114] (Section 7.5.1). Considering that the kinematic model over the full body length has large matching errors, a novel stabilization technique was deployed. The large scale dorsal and pelvic fins relative to body size optimize the F_L and F_T around the center of mass, generating accurate anterior amplitude and effectively stabilizing the platform in the horizontal and vertical planes. This enabled a predictable adjustment of the anterior and posterior kinematic amplitude parameters so that large posterior propulsive forces and amplitudes could be generated and accurate straight-line trajectories attained.

The developed prototype is compact, naturally buoyant and robust, with a high power density and the ability to actuate at intensively high frequencies (Section 7.4). Notably, the applied high frequencies increased velocity in all Modes without peak, decline or failure (Section 7.5.2). We can therefore estimate that a further increase of frequency applied to this developed mechanical drive system may continue to increase its maximum velocity beyond the fastest live fish. *iSplash*-MICRO 50mm in body length achieved a consistent free

swimming speed of 10.4BL/s (i.e. 0.52m/s) at a frequency of 19Hz with a stride rate (*Sw*) of 0.54 and a low energy consumption of 0.8W.

The experimental analysis of the fourth generation has shown potential to improve its high performance swimming further. The following points are of significant interest for the future research:

(i) The low energy consumed during propulsion indicates the next generation is capable of carrying a power supply. The challenge will be in developing a platform with accurate weight distribution on a micro scale.

(ii) Posterior amplitudes of a magnitude greater than 0.2 of the body length may improve propulsion.

(iii) The robust structure may generate higher tail oscillation frequencies than 19Hz. An initial aim of a 50% increase can be made based on commercial hardware available, predicting an approximately equivalent increase in performance.

(iv) Optimize the tail shape and aspect ratio as describe in Section 4.6.7.

(v) The devised mechanical system is suitable for further reduction in scale as appropriate hardware becomes available.

Chapter 8

Conclusions

8.1. Research Summary

After the background research was studied in Chapter 2, this thesis conducted an intensive research investigation in order to study the linear Carangiform swimming motion due to the current low swimming speeds of robotic fish in comparison to real fish. Chapter 3 presented the observational studies undertaken on real fish and details the proposed swimming pattern to overcome previous kinematic errors within the wave form.

An investigation of the kinematics, morphology and swimming mechanics of existing robotic fish were carried out, identifying the large errors in applying the traditional swimming motion approach (Section 3.3). A full-body length Carangiform swimming motion was introduced (Section 3.4), in which the anterior, mid-body and posterior displacements are coordinated to reduce the large kinematic errors in the existing free swimming robotic fish, by optimizing the forces around the centre of mass and initiate the starting moment of added mass upstream for better performance, in terms of linear swimming speed. The state of the art mechanical engineering developments were analysed in Section 3.5 along with possible solutions for increasing the performance of the mechanical drive system.

Then, the four generations of new robotic fish were developed and detailed in Chapters 4-7, which are summarised below.

- The First Generation robotic fish (*Novel Carangiform Kinematic Pattern*) detailed in Chapter 4 was developed to provide a platform for investigating the Carangiform body motion. The devised novel mechanical drive system was built operating in two swimming patterns (Section 4.3). By coordinating the full-body length of the Carangiform swimming motion, a significant increase in performance, in terms of linear swimming speed, is gained over the traditional posterior confined wave form. The large kinematic errors seen in existing free swimming robotic fish are reduced (Section 4.5.2), generating the required propulsion to achieve equivalent cruising speeds to real fish (Section 4.5.4). This paved the way for three further generations of robotic fish development.
- The Second Generation (*Precision Link Optimization Platform*) presented in Chapter 5 was based on the theory that further tuning of the kinematic parameters may provide a greater performance increase in the distance travelled per tail beat (Section 4.5.2). Hence a platform was devised with precise adjustable links distributed along the full body length, transmitted power from a single actuator (Section 5.4.1).
- The Third Generation (*Free Swimming, High Force and Hz Platform*) was introduced in Chapter 6 it was proposed that by combining the critical aspects of the first generation's mechanical drive system (Section 4.4) with higher frequencies and higher productive forces may significantly increase maximum velocity. It is able to outperform real Carangiform fish in terms of average maximum velocity (measured in body lengths/ second) and endurance, the duration that top speed is maintained (Section 6.6.2).
- The Fourth Generation (*Micro Platform*) presented in Chapter 7 is a small robotic fish able to generate an equivalent maximum velocity to real Carangiform fish. It can improve navigational exploration capability whilst retaining high-speed swimming performance (Section 7.6).

8.2. Discoveries, Contributions and Overall Remarks

Through systematic development and analyses, many scientific contributions have been successfully achieved during this thesis research. The findings can be applied to disciplines within underwater robotics such as kinematics, morphology, mechanics, energy transfer, mechanical engineering, micro builds, but more precisely the scientific contributions provide extended knowledge to the research area of linear swimming for underwater robotics:

Hypothesis –

- **H**$_1$: The hypothesis tested whether the observational analysis of a full-body length swimming motion seen in real Carangiform fish could be applied to the swimming motion of robotic fish to improve performance, proposing to coordinate the anterior, mid-body and posterior displacements in an attempt to reduce the large kinematic errors in the existing free swimming robotic fish, whereby the swimming pattern would optimize the forces around the centre of mass and initiating the starting moment of added mass upstream therefore increasing performance, in terms of (i) kinematic parameter accuracy (ii) maximum velocity (iii) distance travelled per tail beat.

Findings –

- The novel mechanical drive system (*iSplash*-I: Chapter 4) was devised to operate in two swimming patterns. A thorough comparison between the traditional posterior confined undulatory swimming pattern (Mode 1) and an introduced full body length swimming pattern (Mode 2) was made. The proposed pattern was found to coordinate the anterior, mid-body and posterior displacements, reducing the kinematic errors over the full body length seen in free swimming robotic fish over the full lateral length. In particular it achieved anterior stabilization by significantly reducing recoil and optimizing the lateral (F_L) and thrust forces (F_T) around the center of mass, assumed to initiate the starting moment of added mass upstream.

  Accurate kinematics along the full-body length of the first generation prototype was measured: Mode 2 was found to reduce the head amplitude by over half from 0.17 (0.044m) of the body length in Mode 1 to 0.07 (0.018m). The tail amplitude of the common carp is 0.1 [9] [10], larger values were found to increase performance. Both Modes 1 and 2 were able to attain amplitudes of 0.17 (0.044m). The location of the midline pivot point should be in the range of 0.15-0.25 of the body length [10]. Mode 2 has a reduced error location of 0.33 in comparison to 0.5 in Mode 1, indicating that Mode 2 significantly reduces the kinematic errors within the swimming motion (Section 4.5.2).

  From the comparison, the proposed swimming motion of Mode 2 significantly outperformed the traditional approach by 27%, in terms of swimming speed consistently achieving a velocity of 2.8BL/s (0.70m/s) at 6.6Hz. This prototype greatly surpassed previous robotic fish in terms of maximum velocity and achieved speeds of 3.4BL/s (0.88m/s) equivalent to the cruising speeds of real fish (Section 4.5.4) [112]. The distance

travelled per tail beat (*Sw*) of the full body swimming pattern was measured to increase the Swimming Number by 16.6%, with a *Sw* of 0.42 in comparison to the traditional approach with a *Sw* of 0.36. Hence we can calculate that the prototype can significantly increase its maximum velocity over the traditional approach as frequencies are further raised.

Hypothesis –

- **H**$_2$: The hypothesis tested whether the rotary motion of deploying a single actuator could be transferred into oscillatory motion and distributed to multiple links across the full-body length without high internal mechanical loss, typically produced from multiple link structures (This approach had not been attempted for a robotic fish actuating additional links from the mid-body to anterior).

Findings –

- We found that the deployed five link structure (*iSplash*-I: Chapter 4) could achieve precise curve alignment with the proposed swimming motion. The average energy economy in relationship to driven frequency was measured. Both Modes actuating in water at 8Hz recorded low energy consumptions, Mode 2 measuring 7.68W and Mode 1 5.76W (Section 4.5.3). Hence it was estimated based on commercially available batteries that future generations may be capable of providing power from an onboard source.

Hypothesis –

- **H**$_3$: The hypothesis tested whether: (i) a mechanical drive system deploying a single actuator could be devised to allow each discrete link of the assembly to be precisely tuned. Therefore providing a vehicle with the ability to optimize the reaction forces of the propulsion elements during locomotion; (ii) a further tuning of the proposed full-body length kinematic parameters may provide a greater performance increase in the distance travelled per tail beat (*Sw*).

Findings –

- The developed mechanical drive system (*iSplash*-OPTIMIZE: Chapter 5) has shown the capability to generate accurate spatial and time dependent discrete link sequences during non-productive actuation at 10Hz with an energy consumption of 9.7W over a non-loaded motor at 6.1W (Section 5.6.1). A series of kinematic patterns at high frequencies were attained by realizing a powertrain with high accuracy, unrestricted disc offset

combinations, high structural strength, able to transfer power to and provide precise adjustments of the oscillatory discrete links across the full assembly from a single continuous rotary actuator. In addition, the maximum lateral head (i.e. 0.1) and tail (i.e. 0.27) excursions generated during non-productive actuation are significantly greater than the observed common carp, and *iSplash*-I (Section 5.6.2).

Test periods of actuation at 1-20Hz in water were conducted, which indicated that the prototype was only able to actuate at its maximum tail beats whilst in operation with a reduced scale caudal fin. The experimental trials showed that the build was unable to swim at greater speeds than 1.5BL/s equivalent to the typical speeds of existing robotic fish and far slower than the first generation. Experimental testing found that the large geometric scale required a higher force production than the generated force of the limited actuator (Section 5.6.3). Therefore we were unable to test the *Sw* finding that a significantly smaller drive system is required.

Hypothesis –

- **H**$_4$: The hypothesis tested whether combining the critical aspects of the first generation's mechanical drive system with frequencies higher than previously tested may continue to increase maximum velocity. The observational analysis found that the first generation was able to replicate the key swimming properties of real fish. As frequencies were raised the build continued to increase velocity in both swimming modes. This matches Bainbridge's [51] and Lighthill's [112] study of swimming fish, measuring no noticeable change in kinematics after tail oscillations are raised beyond 5Hz, indicating that only an altered frequency may be required to greatly increase swimming speed.

Findings –

- We undertook experiments to gain knowledge if raising driven frequencies greater than the previous build (*iSplash*-I: Chapter 4) of 6.6Hz would continue to increase speed without peak or decline. A continued increase in velocity up to intensively high frequencies of 20Hz was measured (*iSplash*-II: Section 6.6.2), enabling the prototype to consistently achieve a maximum velocity of 11.6BL/s (i.e. 3.7m/s) with a stride rate of 0.58, capable of outperforming the recorded average maximum velocity of real Carangiform fish measured at 10BL/s. The swimming mechanics of *iSplash*-II mimic the swimming properties of real fish with frequency becoming the key variable to enhance the linear locomotive performance of the presented research platforms. In addition: (i) By

applying high frequencies and productively transmitting high forces, the prototype was found to accelerate to steady state swimming (11.6BL/s) in an approximate time of 0.6s. (ii) The high forces allowed for a large caudal fin in relation to the scale of the body hence the prototypes distance travelled per tail beat is highly efficient, measuring a *Sw* of 0.58 in comparison to the previous build with a *Sw* of 0.42 and close to the particular efficient common carp with a *Sw* of 0.7.

Hypothesis –

- $\mathbf{H}_5$: The hypothesis tested whether a high frequency, high force output mechanical drive system could replicate the required full-body wave form.

Findings –

- To make a thorough investigation the prototype *iSplash*-II was devised to operate in two swimming patterns the traditional posterior confined approach (Mode 1) and the newly introduced full-body swimming pattern (Mode 2) (Section 6.4) replicating the first generations investigative approach. The experimental tests found the developed platform could not achieve the desired full-body length kinematic parameters over the full lateral length of the body (Section 6.6.1). This was not attained due to the power density requirements, as the prototype was developed with the primary actuator 75% of the total mass (Section 6.5). Although the full-body swimming motion could not be realized, the devised assembly was able to stabilize in the horizontal plane hence reducing the anterior recoil around the centre of mass and therefore generating an effective propulsive mechanism. Generating an accurate posterior kinematic pattern of smooth undulations from mid-body to tail tip (Section 6.6.1).

  In addition, both operational swimming Modes were able to attain large tail amplitudes of 0.2 (0.063m) of the body length which was found to significantly increase performance (Section 6.6.1). This value is twice the size of the observed value of the common carp at 0.1 and is increased over the first generation at 0.17. The generated amplitude is also greater than the highly efficient swimming motion of a dolphin measuring 0.175 [13].

Hypothesis –

- $\mathbf{H}_6$: The hypothesis tested whether a free swimming platform with an on board power source actuating at high frequencies and high forces could attain high endurance at

maximum velocity, due to the estimated high energy consumption required for high-speed swimming.

Findings –

- The third generation prototype (*iSplash*-II: Chapter 6) was measured to far surpass the endurance of real fish, in terms of the duration that top speed is maintained, as equivalent burst speeds of real fish can only be maintained for short times of around one second [51]. In comparison the prototype can maintain an operational time of approximately ten minutes at maximum velocity. It can be seen that both swimming Modes of the third generation build actuating in water had an energy consumption of 120W at 20Hz and swimming at an average maximum velocity of 11.6BL/s (i.e. 3.7m/s) (Section 6.6.2).

Hypothesis –

- $\mathbf{H}_7$: The hypothesis tested whether the mechanical drive system could be reduced in magnitude, to improve navigational exploration, whilst retaining (i) high-speed swimming performance. The hypothesis tested whether applying higher frequencies to the Mode 1 swimming motion of the first generation may continue to increase velocity, in consideration that fish employ an identical swimming motion of inertia force propulsion at the millimetre scale as the previous generations of robotic fish. (ii) Accurate kinematic pattern and amplitude parameters.

Findings –

- We found that the prototype (*iSplash*-MICRO: Chapter 7) recorded an average maximum velocity equivalent to real Carangiform fish. The small robotic fish prototype, 50mm in body length, achieved a consistent free swimming speed of 10.4BL/s (i.e. 0.52m/s) at a frequency of 19Hz with a stride rate (*Sw*) of 0.54 and a low energy consumption of 0.8W (Section 7.6). The kinematic model over the full body length had large matching errors therefore a novel stabilization technique was deployed as detailed in $\mathbf{H_8}$.

Hypothesis –

- $\mathbf{H}_8$: The hypothesis tested whether applying large scale dorsal and pelvic fins relative to body size would reduce the kinematic errors in the millimetre scale build swimming motion. The deployed anterior destabilization solution of anterior and mid-body fins provides the required anterior surface area without creating excessive resistance to forward motion as the fins are vertically compressed. This solution was deployed as a

micro scale structure limits the ability to apply the coordinated full-body motion due to the complexity of the mechanical linkage.

Findings –

- The large scale dorsal and pelvic fins relative to body size (*iSplash*-MICRO: Chapter 7), were found to optimize the F_L and F_T around the center of mass, generating accurate anterior amplitude and effectively stabilizing the platform in the horizontal and vertical planes. This enabled a predictable adjustment of the anterior and posterior kinematic amplitude parameters so that large posterior propulsive forces and amplitudes could be generated and accurate straight-line trajectories attained (Section 7.5.1).

  A principal aim of the research platform was achieving accurate posterior kinematic matching to *iSplash*-I, with a significantly simplified assembly. The tracked midline (Section 7.5.1) shows that the developed fifty millimeter prototype generates a precise travelling wave half the body length and has achieved a smooth transition phase from body to tail tip. Hence the greatly simplified structure, built at the millimeter scale is able to accurately replicate and improve upon the kinematic parameters of the posterior undulatory swimming pattern of real fish, by applying large tail amplitudes than found on real Carangiform fish and minimizing the anterior recoil.

8.3. Publication List

Over the duration of this PhD research, four scientific papers and one book chapter have been published in the proceedings of various highly reputable international conferences after passing the peer-review process. They are listed here in chronological order:

[1] R.J. Clapham and H. Hu, *iSplash*-I: High Performance Swimming Motion of a Carangiform Robotic Fish with Full-Body Coordination, IEEE International Conference on Robotics and Automation, May 31 - June 7, 2014, pp. 322 – 327, Hong Kong, China.

[2] R.J. Clapham and H. Hu, *iSplash*-OPTIMIZE: Optimized Linear Carangiform Swimming Motion, Springer International Publishing, Proceedings of the 13th International Conference IAS-13, Padua, Italy, 15-19/07/2014, pp. 567-579.

[3] R.J. Clapham and H. Hu, *iSplash*-II: Realizing Fast Carangiform Swimming to Outperform a Real Fish, IEEE/RSJ International Conference on Intelligent Robots and Systems (IROS 2014), Sept. 14-18, 2014, pp. 1080-1086, Chicago, IL, USA.

[4] R.J. Clapham and H. Hu, *iSplash*-MICRO: A 50mm robotic fish generating the maximum velocity of real fish, IEEE/RSJ International Conference on Intelligent Robots and Systems, 14-18 Sept. 2014, pp. 287-293, Chicago, IL, USA.

[5] R.J. Clapham and H. Hu, *iSplash*: Realizing Fast Carangiform Swimming to Outperform a Real Fish, Springer Berlin Heidelberg, A book chapter, Springer Tracts in Mechanical Engineering (Book: Bio-inspired Fishlike Underwater Robots 2015), May. 07, 2015, pp 193-218.

8.4. Future Research

The experimental analysis of the developed four generations of robotic fish has shown potential to improve the high performance swimming further. The following points are of significant interest for the future research:

- ***Full-body Kinematic Parameters During High-Speed Swimming***

  The first generation build showed conclusively that by coordinating the full-body length of the Carangiform swimming motion a significant increase in performance of 27% in terms of linear swimming speed is gained over the traditional posterior confined wave form (Section 4.5). To accurately emulate the kinematic parameters of the full-body swimming motion, a structural rebuild of the third generation is required to actuate the mid-body linkages so that a smooth transition of flow along the body length is achieved.

- ***Mechanically Efficient Drive Mechanism***

  The endurance of an underwater robotic vehicle is a core aspect of the operation, whereby efficient swimming techniques and mechanical efficiency significantly affect locomotive duration. The endurance of *iSplash*-II can be significantly improved by developing a replacement drive mechanism of link IV, improving the consumption from 120W to approximately 70W (Section 6.6.2). This was a result of a pressure increase at higher velocities. As link IV was actuated, the tendons were required to be tightened to provide the desired posterior kinematics, putting increased strain on the mechanism. A replacement drive mechanism was developed using rigid levers, indicating the feasibility of the mechanism for frictionless actuation. We can assume that engineering a greater mechanically efficient drive of link IV in the next generation may significantly improve endurance, relating to an estimated reduced energy consumption of ~50%. *Reduction in*

scale - The devised mechanical system is suitable for further reduction in magnitude as appropriate hardware becomes available, therefore reducing forward resistance and improving the cost-of-transport.

- ***Optimized Caudal Fin***

  The swimming speed of *iSplash*-II may further be increased by optimizing the caudal fin:

  (1) *Amplitude*: shown in the tests of Section 6.6 an amplitude value of 0.2 of the body length improved performance over the observed measurement of the common carp's at 0.1 and the first generation build at 0.17. This generated amplitude was also greater than the highly efficient swimming motion of a dolphin measured at 0.175. An investigation of optimizing the body wave further by increasing the amplitude parameters of the posterior may generate increased performance. This can be continued until a decline in velocity.

  (2) *Profile*: we can make the assumption that an approximate 20% improvement in swimming speed may be generated by optimizing the shape of caudal fin based on the research test runs detailed in Section 4.6.7. In addition, by increasing the magnitude of the tail the swimming number may also be improved as discovered in Section 6.6.1. This may be disproportionally increased in scale due to the large force production measured by the third generation. This investigation will provide caudal fin research on a free swimming robot not restricted by tethers or low speeds, where improvements will directly affect maximum velocity.

  (3) *3D Deformation*: as observed in real fish during linear locomotive swimming the caudal fin deforms in the middle of the surface, defined as cupping. This is assumed to increase the thrust force F_T [3; 52; 138]. In addition, applying increased rigidity to the top and/ or bottom edges may be investigated, whereby the top or bottom edge leads the other within the body wave cycle.

- ***Three Dimensional Manoeuvrability***

  Perhaps the most important next stage in reaching real world applications is the development of mobility within the horizontal plane. By utilizing the developed pectoral fin mechanism (Section 5.4.2) for pitch and developing a horizontal mechanism for yaw and combining these actuators, precision 3D locomotive manoeuvring during high-speed swimming may be possible. For lower speeds weight distribution, buoyancy and C-sharp Turn mechanisms may be preferable.

In addition, throughout experimental testing it was observed during moments of loss in stability, the free swimming robotic fish (*iSplash*-II: Chapter 6) actuating at frequencies of 20Hz generated a tuning radius within the horizontal and vertical planes within an approximate turning diameter of < 1L. If controllable, this measurement during high-speeds would provide a very agile platform for navigation.

- ***Burst-and-Coast***

  The first prospective investigation in intelligence could be to deploy the behavioural technique of burst-and-coast which has been measured to reduce the cost of transport by approximately 50% [18]. This was previously impossible to be implemented accurately as live fish have been measured to apply this technique whilst generating 10BL/s at the burst stage. This is now possible to experimentally test and may be achieved by deploying a simple algorithm applied to an on-board system to adjust the frequency of the solitary actuator to replicate the observed acceleration and deceleration parameters illustrated in Figure 8.1. Ideally a buoyance pump would adjust the depth of the vehicle but this may be equally efficient to employ the pectoral fins as the main source of depth control.

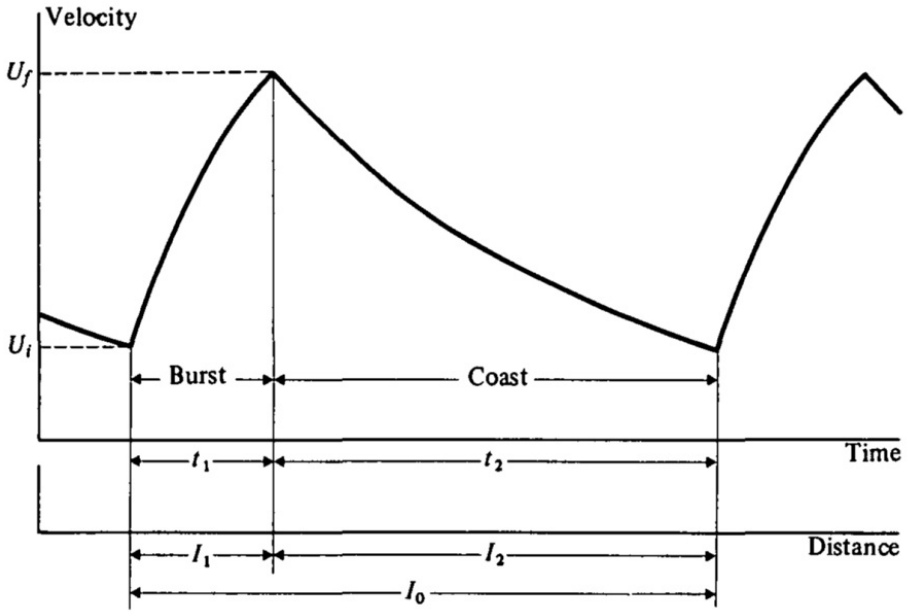

Figure 8.1: Velocity against time and distance during a burst-and-coast swimming cycle, measured by Bainbridge [18].

- ***Raising Driven Frequency***

  A prospective future investigation would be to continue raising the driven frequency to generating even greater speeds over the fastest real fish. The robust structure (*iSplash*-II

Section 6.6.2) attained high tail oscillatory frequencies without early peak, decline or mechanical failure. Therefore, an aim of a 100% increase in Hz would be an initial realistic target, whereby we can predict an increase in maximum velocity to 23.2BL/s, calculated by using the distance per tail beat of *iSplash*-II (*Sw*) at 0.58*Sw*. To evade capture or view the surrounding environment an action of jumping may prove beneficial. Throughout testing the prototype was found to greatly clear the water surface indicating the possibility of future implementation.

In summary, it is clear that a performance increase to 35.5BL/s may be realized by increasing the tail beat frequency to 40Hz, optimizing the caudal fin scale and shape and developing mid-body linkages to gain the full-body swimming pattern accurately. This value, if achieved, is significantly higher than the swimming speeds of real fish. By applying the behavioural technique of burst-and-coast and developing the posterior link IV mechanism, a significantly increases in energy consumption may also be gained. Based on the findings presented it is exciting to think of the next stages possible. In a few years, a biological inspired robotic underwater vehicle may completely outperform real fish in every aspect of locomotion. Utilizing the efficient swimming performance found in the studies of fish we may further explore the oceans with ease and precision.

References

[1] J. J. Videler, *Fish swimming*, 1st ed. New York: Chapman and Hall, 1993.

[2] C. M. Breder, 'The locomotion of fishes,' *Zoologica*, (New York Zoological Society) Vol. 4, no. 5, pp. 159–256, 1926.

[3] G. V. Lauder and E. G. Drucker, 'Morphology and Experimental Hydrodynamics of Fish Fin Control Surfaces', *IEEE Journal of Oceanic Engineering*, vol. 29, no. 3, pp. 556–571, Jul. 2004.

[4] G. V. Lauder, 'Function of the Caudal Fin During Locomotion in Fishes: Kinematics, Flow Visualization, and Evolutionary Patterns', *American Zoologist*, vol. 40, no. 1, pp. 101–122, Feb. 2000.

[5] S. M. Triantafyllou, H. A. Techet and S. F. Hover, 'Review Of Experimental Work In Biomimetic Foils', *Oceanic Engineering, IEEE Journal of* (Vol: 29, Issue: 3), pp. 585-594, July, 2004.

[6] M.J. Wolfgang, J.M. Anderson, M.A. Grosenbaugh, D.K. Yue and M.S. Triantafyllou, 'Near-body flow dynamics in swimming fish,' *J Exp Biol 202* (Pt 17), pp. 2303-2327, Sept 1, 1999,

[7] J. E. Colgate and K. M. Lynch, 'Mechanics and Control of Swimming: A Review', *IEEE Journal of Oceanic Engineering*, vol. 29, no. 3, pp. 660–673, Jul. 2004.

[8] P. Kodati And X. Deng, 'Bio-inspired Robotic Fish with Multiple Fins', *Underwater Vehicles*, Chapter 6, (Ed.), ISBN: 978-953-7619-49-7, InTech, DOI: 10.5772/6698, Jan, 2009.

[9] J. Tangorra, C. Phelan, C. Esposito, and G. Lauder, 'Use of Biorobotic Models of Highly Deformable Fins for Studying the Mechanics and Control of Fin Forces in Fishes',*Integrative and Comparative Biology*, Vol. 51, no. 1, pp. 176–189, Jun. 2011.

[10] O. M. Curet, N. A. Patankar, G. V. Lauder And M. A Maciver, 'Mechanical Properties Of A Bio-Inspired Robotic Knifefish With An Undulatory Propulsor" *Bioinspiration & Biomimetics*, Vol 6, Num 2, IOP Publishing, 7 April, 2011.

[11] G.S. Triantafyllou, M.S. Triantafyllou, M.A. Grosenbaugh,'Optimal thrust development in oscillating foils with applications to fish propulsion,' *J. Fluid Struct*. 7, issue 2, pp. 205-224, Feb. 1993.

[12] D. Richard Blidberg, 'The Development Of Autonomous Underwater Vehicles (AUV); A Brief Summary,' *IEEE International Conference on Robotics and Automation* – (ICRA), May 21-26, 2001.

[13] P P. R. Bandyopadhyay, 'Trends in Biorobotic Autonomous Undersea Vehicles', *IEEE Journal of Oceanic Engineering*, vol. 30, no. 1, pp. 109–139, Jan. 2005.

[14] D. Barrett, A. Grosenbaugh and M. Triantafyllou, 'The Optimal Control of a Flexible Hull Robotic Undersea Vehicle Propelled by an Oscillating Foil'. IEEE Symposium on Autonomous Underwater Vehicle Technology, pp. 1 – 9, 2-6 Jun, 1996.

[15] T. Kambe, 'The dynamics of carangiform swimming motions', *Journal of Fluid Mechanics*, Cambridge University Press, Vol. 87, Issue. 03, pp. 533-560, Aug. 1978.

[16] J. Lighthill, 'Aquatic animal locomotion', *Proceedings of the 13th International Congress of Theoretical and Applied Mechanics, Moskow University*, IUTAM Symposia, pp. 29–46, Jan. 1973.

[17] M. J. Lighthill, 'Large-Amplitude Elongated-Body Theory of Fish Locomotion,' *In Proc. The Royal Society. London. B*, Vol. 179, Issue: 1055, pp. 125-138, 1971.

[18] M. J. Lighthill, 'Hydrodynamics of aquatic animal propulsion,' *Annual Review of Fluid Mechanics*, Vol 1: pp. 413-46, Jan, 1969.

[19] M. J. Lighthill, 'Aquatic animal propulsion of high hydromechanical efficiency,' *Journal of Fluid Mechanics*. Vol 44, Issue 02, pp.265-301, 1970.

[20] J. Liu and H. Hu, 'Biological Inspiration: From Carangiform Fish To Multi-Joint Robotic Fish', *Journal of Bionic Engineering* 7, pp. 35–48, 2010.

[21] X. Lu, X. Yin, J. Yang, B. Tong, 'Studies Of Hydrodynamics In Fishlike Swimming Propulsion,' *Bio-mechanisms of Swimming and Flying*, Part 2, pp. 143-154, Oct 11-15, 2010.

[22] R. Blickhan, C. Krick, D. Zehren, W. Nachtigall, T. Breithaupt, R. Blickhan, C. Krick, D. Zehren, W. Nachtigall, and T. Breithaupt, 'Generation of a vortex chain in the wake of a Suhundulatory swimmer', *Naturwissenschaften*, vol. 79, no. 5, pp. 220–221, May, 1992.

[23] M. J. V. Rosen, 'Water flow about a swimming fish,' *U.S Naval Ordnance Test Station Technical Publication 2298*, University of California in Los Angeles, pp. 1-96, 1959.

[24] G. Taylor, 'Analysis of the Swimming of Long and Narrow Animals', *Proceedings of the Royal Society A: Mathematical, Physical and Engineering Sciences*, vol. 214, no. 1117, pp. 158–183, Aug. 1952.

[25] T. Y.-T. Wu, 'Swimming of a waving plate', *Journal of Fluid Mechanics*, vol. 10, no. 03, p. 321, May 1961.

[26] M. S. Triantafyllou, 'Vorticity Control in Fish-like Propulsion and Maneuvering', *Integrative and Comparative Biology*, vol. 42, no. 5, pp. 1026–1031, Nov. 2002.

[27] J.-Y. Cheng, L.-X. Zhuang, and B.-G. Tong, 'Analysis of swimming three-dimensional waving plates', *Journal of Fluid Mechanics*, vol. 232, no. -1, p. 341, Nov. 1991.

[28] C. Tapia S. and R. Chellali, 'Simple Karman Street model', *OCEANS'10 IEEE SYDNEY*, May 2010.

[29] A. Belmonte, H. Eisenberg, and E. Moses, 'From Flutter to Tumble: Inertial Drag and Froude Similarity in Falling Paper', *Physical Review Letters*, vol. 81, no. 2, pp. 345–348, Jul. 1998.

[30] D. N. BEAL, F. S. HOVER, M. S. TRIANTAFYLLOU, J. C. LIAO, and G. V. LAUDER, 'Passive propulsion in vortex wakes', *Journal of Fluid Mechanics*, vol. 549, no. -1, p. 385, Feb. 2006.

[31] P. R. Bandyopadhyay, D. N. Beal, and A. Menozzi, 'Biorobotic insights into how animals swim', *Journal of Experimental Biology*, vol. 211, no. 3, pp. 466–466, Feb. 2008.

[32] R. W. Blake, 'The swimming of the mandarin fish Synchropus picturatus (Callionyiidae: Teleostei)', *Journal of the Marine Biological Association of the United Kingdom*, vol. 59, no. 02, p. 421, May 1979.

[33] J. Brown, L. Chambers, K. M. Collins, O. Akanyeti, F. Visentin, R. Ladd, P. Fiorini, and W. Megill, 'The Interaction between Vortices and a Biomimetic Flexible Fin', *Towards Autonomous Robotic Systems*, pp. 418–419, Jan. 2011.

[34] W. J. Usab, J. Hardin, and A. J. Bilanin, 'Bioinspired Delayed Stall Propulsor', *IEEE Journal of Oceanic Engineering*, vol. 29, no. 3, pp. 756–765, Jul. 2004.

[35] I. L. Y. Spierts, And J. L. Van Leeuwen, 'Kinematics and Muscle Dynamics of C- and S-Starts of CARP (*CYPRINUS CARPIO* L.),' *The Journal of Experimental Biology,* 202, pp. 393–406, 1999.

[36] P. Domenici, 'Escape trajectory, ecological,' *Encyclopaedia of Environments*, Vol 2, pp 708-711, Sept, 2002.

[37] F. W. H. Beamish, 'Swimming capacity,' *Fish Physiology*, Vol. VII Locomotion (ed. W. S. Hoar and D. J. Randall), pp. 101–187, 1978.

[38] J. Conte, Y. Modarres-Sadeghi, M. N. Watts, F. S. Hover, and M. S. Triantafyllou, 'A fast-starting mechanical fish that accelerates at 40 m s −2', *Bioinspiration & Biomimetics*, vol. 5, no. 3, p. 035004, Aug. 2010.

[39] D. Weihs, 'The mechanism of rapid starting of slender fish,' *Biorheology*, Vol 10, pp. 343-350, 1973.

[40] J. M. Wakeling, 'Fast-start Mechanics', *Fish Biomechanics*, Elsevier, Inc. pp. 333–368, 2006.

[41] P. Domenici And R. W. Blake, 'The Kinematics and Performance of Fish Fast-Start Swiming,' The Journal of Experimental Biology 200, pp. 1165–1178, 1997.

[42] T. E. Higham, 'Constraints on starting and stopping: behavior compensates for reduced pectoral fin area during braking of the bluegill sunfish Lepomis macrochirus', *Journal of Experimental Biology*, vol. 208, no. 24, pp. 4735–4746, Dec. 2005.

[43] E. J. Anderson, W. R. Mcgillis and M. A. Grosenbaugh, 'THE BOUNDARY LAYER OF SWIMMING FISH,' *The Journal Of Experimental Biology,* vol. 204, pp. 81–102, 2001.

[44] E. F. Fish, 'Imaginative Solutions By Marine Organisms For Drag Reduction', *In Proceedings Of The International Symposium On Seawater Drag Reduction,* J. C. S. Meng, Ed. Newport, Rhode Island, pp. 443-450, 1998.

[45] M. Nagai, 'A review of Gray's paradox,' *Ryukyu Daigaku Kogakubu Kiyo (Bulletin of the Faculty of Engineering, University of the Ryukyus)* 62: pp.1-6, 2001.

[46] E. A. van Nierop, S. Alben, and M. P. Brenner, 'How Bumps on Whale Flippers Delay Stall: An Aerodynamic Model', *Physical Review Letters*, vol. 100, no. 5, Feb. 2008.

[47] S. R. Noren, G. Biedenbach, J. V. Redfern, and E. F. Edwards, 'Hitching a ride: the formation locomotion strategy of dolphin calves', *Functional Ecology*, vol. 22, no. 2, pp. 278–283, Nov. 2007.

[48] J. Videler and D. Weihs, 'Energetic Advantages of Burst-And-Coast Swimming of Fish at High Speeds', *Journal of Experimental Biology.* Vol 97, pp. 169-178, 1981.

[49] G. Wu, Y Yang and L Zeng, 'Kinematics, Hydrodynamics and Energetic Advantages of Burst-And-Coast Swimming of Koi Carps (Cyprinus Carpio Koi)', *The Journal Of Experimental Biology 211, 2007.*

[50] F. E. Fish, J. F. Fegely, and C. J. Xanthopoulos, 'Burst-and-coast swimming in schooling fish (Notemigonus crysoleucas) with implications for energy economy', *Comparative Biochemistry and Physiology Part A: Physiology*, vol. 100, no. 3, pp. 633–637, Jan. 1991.

[51] Bainbridge R, 'The Speed Of Swimming Of Fish As Related To Size And To The Frequency And Amplitude Of The Tail Beat', *Journal of Experimental Biology,* Vol 35, pp.109-133, 1957.

[52] J. H. Long, N. M. Krenitsky, S. F. Roberts, J. Hirokawa, J. de Leeuw, and M. E. Porter, 'Testing Biomimetic Structures in Bioinspired Robots: How Vertebrae Control the Stiffness of the Body and the Behavior of Fish-Like Swimmers', *Integrative and Comparative Biology*, vol. 51, no. 1, pp. 158–175, May 2011.

[53] J. R. Hunter, J. Zweifel 'Swimming Speed, Tail Beat Frequency 7 Tail Beat Amplitude, and Size in Jack Mackerel, *Trucharzcs Symmetricas,* and Other Fishes,' *FISHERY BULLETIN*: VOL. 69, NO. 2. 1971.

[54] D. Weihs, 'Stability Versus Maneuverability in Aquatic Locomotion', *Integrative and Comparative Biology*, vol. 42, no. 1, pp. 127–134, Feb. 2002.

[55] M. J. Lighthill, 'Note on the swimming of slender fish', *Journal of Fluid Mechanics*, vol. 9, no. 02, p. 305, Oct. 1960.

[56] F. Jing and E. Kanso, 'Effects of body elasticity on stability of underwater locomotion', *Journal of Fluid Mechanics*, vol. 690, pp. 461–473, Nov. 2011.

[57] W. Weibing , Y. Junzhi, W. Ming, D. Rui, 'Mechanical Design And Preliminary Realization Of Robotic Fish with multiple Control Surfaces', *Proceedings Of The 29th Chinese Control Conference* July 29-31, 2010, Beijing, China.

[58] P. W. Webb, 'Control of Posture, Depth, and Swimming Trajectories of Fishes', *Integrative and Comparative Biology*, vol. 42, no. 1, pp. 94–101, Feb. 2002.

[59] P. J. Flanagan, 'Unsteady Navier-Stokes Simulation of Rainbow Trout Swimming Hydrodynamics', Washington State University, Department of Civil and Environmental Engineering, May 2004.

[60] D. T. Swain, I. D. Couzin and N. E. Leonard, 'Real-time feedback-controlled robotic fish for behavioral experiments with fish schools,' P*roceedings of the IEEE* (Volume:100 , Issue: 1), pp. 150-163, Jan, 2012.

[61] D. Shin1, S. Y. Na, J. Y. Kim, S. J. Baek, I. Jeong, 'Mapping System of Water Pollution by Autonomous Fish Robots,' *Proceedings of the 7th WSEAS International Conference on Robotics*, Control & Manufacturing Technology, Hangzhou, China, April 15-17, 2007.

[62] Z. Wang, G. Hang, J. Li, Y. Wang, and K. Xiao, 'A micro-robot fish with embedded SMA wire actuated flexible biomimetic fin', *Sensors and Actuators A: Physical*, vol. 144, no. 2, pp. 354–360, Jun. 2008.

[63] J. Liang, H. Wei, T. Wang, L. Wen, S. Wang And M. Liu, 'Experimental Research On Biorobotic Autonomous Undersea Vehicle,' *Underwater Vehicles,* 49-7, pp. 582, Dec. 2008.

[64] D. Zhang, H. Xie, L. Shen and K. H. Low, 'Advances And Trends Of Bionic Underwater Propulsors,' GCIS '09. Vol:1, *Global Congress On Intelligent Systems*, pp. 13-19, May. 2009.

[65] F. Fish, G. Lauder, R. Mittal, A. Techet, M. S. Triantafyllou, J. Walker, and P. Webb, 'Conceptual Design For The Construction Of A Biorobotics AUV Based On Biological Hydrodynamics,' In *Proc. Int. Symp. Unmanned Untethered Submersible Technology*, pp.1-8, 2003.

[66] P. R. Bandyopadhyay, 'Manoeuvring Hydrodynamics of Fish and Small Underwater Vehicles', *INTEG. AND COMP. BIOL*, Vol 42. pp. 102–117, 2002.

[67] J. Yuh, 'Design and Control of Autonomous Underwater Robots: A Survey,' *Autonomous Robots 8*, Vol 8, Issue 1, Kluwer Academic Publishers, pp. 7–24, 2000.

[68] F. E. Fish, 'Limits of nature and advances of technology: What does biomimetics have to offer to aquatic robots?', *Applied Bionics and Biomechanics*, Vol. 3, No. 1, pp. 49–60, Jan. 2006.

[69] Y. Valdivia and k. Youcef-Toumi, 2005, 'Design Of Machines With Compliant Bodies For Biomimetic Locomotion In Liquid Environments,' *Proc. Of ASME Journal Of Dynamic Systems, Measurement, And Control,* Vol. 128 Issue 1, pp. 3-13, March 2006.

[70] C. Fiazza, T. Salumae, M. Listak, G. Kulikovskis, R. Templeton, O. Akanyeti, W. Megill, P. Fiorini, and M. Kruusmaa, 'Biomimetic mechanical design for soft-bodied underwater vehicles', *OCEANS'10 IEEE SYDNEY*, May 2010.

[71] H. El Daou, T. Salumae, A. Ristolainen, G. Toming, M. Listak, and M. Kruusmaa, 'A bio-mimetic design and control of a fish-like robot using compliant structures', *2011 15th International Conference on Advanced Robotics (ICAR)*, Jun. 2011.

[72] J. M. Anderson and N. K. Chhabra, 'Manoeuvring And Stability Performance Of A Robotic Tuna,' *Integr. Comp. Biol., 42(5),* pp. 1026–1031, 2002.

[73] P. Liu, K. He1, X. O, R. Du, 'Mechanical Design, Kinematic Modeling And Simulation Of A Robotic Dolphin,' *Proceeding Of The IEEE International Conference On Information And Automation*, pp. 738-743, June 2011

[74] J. Yu, Y Hu, J. Huo, L. Wang, 'Dolphin-Like Propulsive Mechanism Based On An Adjustable Scotch Yoke,' *Mechanism And Machine Theory 44*, pp. 603–614, 2009.

[75] L. Wen, J. Liang, G. Wu, J. Li, 'Hydrodynamic Experimental Investigation On Efficient Swimming Of Robotic Fish Using Self-Propelled Method,' *International Journal Of Offshore And Polar Engineering*, Vol. 20, No. 3, pp. 167–174, Sep 2010.

[76] J.Yu, M. Wang, W. Wang, M. Tan and J. Zhang, " Design And Control Of A Fish- Inspired Multimodal Swimming Robot," *IEEE International Conference on Robotics and Automation* (ICRA), pp 3664-3669, May 2011.

[77] J. Yu, L. Wang, and M. Tan, 'Geometric Optimization of Relative Link Lengths for Biomimetic Robotic Fish', *IEEE Transactions on Robotics*, vol. 23, no. 2, pp. 382–386, Apr. 2007.

[78] P. Nilas, N. Suwanchit, and R. Lumpuprakarn, 'Prototypical Robotic Fish with Swimming Locomotive Configuration in Fluid Environment,' *Multiconfrence of Engineers and computer Scientists* Vol II Hong Kong, pp 850-855, 2011.

[79] Z. Su, J. Yu, M. Tan, and J. Zhang, 'A closed-loop method to generate fast C-start for a robotic fish', *IEEE International Conference on Mechatronics and Automation*, pp. 365-370, Aug. 2011.

[80] J. Tangorra, C. Phelan, C. Esposito, and G. Lauder, 'Use of Biorobotic Models of Highly Deformable Fins for Studying the Mechanics and Control of Fin Forces in Fishes',*Integrative and Comparative Biology*, vol. 51, no. 1, pp. 176–189, Jun. 2011.

[81] G. V. Lauder, 'How fish swim: flexible fin thrusters as an EAP platform',*Electroactive Polymer Actuators and Devices (EAPAD) 2007*, Apr. 2007.

[82] P. R. Bandyopadhyay, D. N. Beal, and A. Menozzi, 'Biorobotic insights into how animals swim', *Journal of Experimental Biology*, vol. 211, no. 3, pp. 466–466, Feb. 2008.

[83] P R. Bandyopadhyay, 'Biology-Inspired Science And Technology For Autonomous Underwater Vehicles,' *IEEE JOURNAL OF OCEANIC ENGINEERING*, vol. 29, no. 3, pp. 542-546, July 2004.

[84] J. Palmisano, R. Ramamurti, K.-J. Lu, J. Cohen, W. Sandberg, and B. Ratna, 'Design of a Biomimetic Controlled-Curvature Robotic Pectoral Fin', *Proceedings 2007 IEEE International Conference on Robotics and Automation*, pp. 966-973, Apr. 2007.

[85] S. Licht, V. Polidoro, M. Flores, F. S. Hover, and M. S. Triantafyllou, 'Design and Projected Performance of a Flapping Foil AUV', *IEEE Journal of Oceanic Engineering*, vol. 29, no. 3, pp. 786–794, Jul. 2004.

[86] P. A. Dewey and A. J. Smits, 'Bioinspired propulsion mechanisms based on manta ray locomotion, *Marine Technology Society Journal* 45 (4), pp. 110-118, 2011.

[87] J. Gao, S. Bi, J. Li, and C. Liu, 'Design And Experiments Of Robot Fish Propelled By Pectoral Fins,' *ROBIO'09 Proceedings Of The 2009 International Conference On Robotics And Biomimetics*, pp. 445-450 Dec 19-23, 2009.

[88] C. W. Chong, Y. Zhong, C. L. Zhou, K. H. Low, G. L. G. Seet, and H. B. Lim, 'Can the swimming thrust of BCF biomimetics fish be enhanced?', *IEEE International Conference on Robotics and Biomimetics*, pp. 437-442, Feb. 2009.

[89] K. Mohseni, 'Zero-mass Pulsatile Jets for Unmanned Underwater Vehicle Maneuvering', *AIAA 3rd 'Unmanned Unlimited' Technical Conference, Workshop and Exhibit*, Sep. 2004.

[90] K. Suzumori, S. Endo, T. Kanda,N. Kato, H. Suzuki, 'A Bending Pneumatic Rubber Actuator Realizing Soft-Bodied Manta Swimming Robot,' *IEEE International Conference On Robotics And Automation*, Roma, Italy, pp. 4975-4980, April 2007.

[91] D. K. Sutantyo and S. Kernbach, 'Minimalistic Approach Towards Underwater Swarm Robotic Development,' *International Workshop on Bio-inspired Robots*, Stuttgurt, Germany, 2011.

[92] E. Lee, 'Design of a soft and autonomous biomimetic micro-robotic fish' *In Proceedings of IEEE Industrial Electronics and Applications (ICIEA)*, pp. 240 – 247, June 2010.

[93] T. D. Jorgensen, C. C. F. Norlund, 'The Use Of Mechanical Accumulators In Robot Herrings,' University Of Portsmouth, 2013. Ref: 10.1.1.128.4408.

[94] S. Heo, T. Wiguna, H. C. Park, N. S. Goo, 'Effect of an Artificial Caudal Fin on the Performance of a Biomimetic Fish Robot Propelled by Piezoelectric Actuators,' *Journal of Bionic Engineering 4*, Vol 4, Issue 3, pp. 151−158, 2007.

[95] A. C. H. Tan and F. S. Hover, 'Thrust and wake characterization in small, robust ultrasonic thrusters', *OCEANS 2010 MTS/IEEE SEATTLE*, pp. 1-9 Sep. 2010.

[96] W. Zhang, S.-X. Guo, and K. Asaka, 'A new type of hybrid fish-like microrobot',*International Journal of Automation and Computing*, vol. 3, no. 4, pp. 358–365, Oct. 2006.

[97] J. J. Abbott, K. E. Peyer, L. X. Dong, and B. J. Nelson, 'How Should Microrobots Swim?', *Springer Tracts in Advanced Robotics*, pp. 157–167, Jan. 2011.

[98] X. Ye, Y. Su, S. Guo, and L. Wang, 'Design and realization of a remote control centimeter-scale robotic fish', *2008 IEEE/ASME International Conference on Advanced Intelligent Mechatronics*, Jul. 2008.

[99] H. Wang, S. S. Tjahyono, B. Macdonald, P. A. Kilmartin, J. Travas-Sejdic, And R. Kiefer, 'Robotic Fish Based On A Polymer Actuator,' *Proceedings of the 2007 Australasian Conference on Robotics and Automation*, Pages 9, 2007

[100] J. Liu, 'Modelling And Online Optimisation Of Robotic Fish Behaviours,' *LAP LAMBERT Academic Publishing*, Pages 256, May. 2013.

[101] J. Yu, M. Wang, M. Tan, and Y. F. Li, 'Step function based turning maneuvers in biomimetic robotic fish', *2009 IEEE International Conference on Robotics and Automation*, May 2009.

[102] A. Qualtieri, F. Rizzi, M.T. Todaro, A. Passaseo, R. Cingolani, M. De Vittorio, "Stress-Driven Aln Cantilever-Based Flow Sensor For Fish Lateral Line System," Microelectronic Engineering, Vol. 88, Issue. 8, pp 2376-2378, Aug 2011.

[103] M. S. Triantafyllou and G. S. Triantafyllou, 'An Efficient Swimming Machine', *Scientific American*, vol. 272, no. 3, pp. 64–70, Mar. 1995.

[104] T. Salumae, I. Rano, O. Akanyeti, and M. Kruusmaa, 'Against the flow: A Braitenberg controller for a fish robot', *2012 IEEE International Conference on Robotics and Automation*, pp. 4210-4215, May 2012.

[105] M. S. Triantafyllou, G. S. Triantafyllou, and D. K. P. Yue, 'Hydrodynamics of Fishlike Swimming', *Annual Review of Fluid Mechanics*, vol. 32, no. 1, pp. 33–53, Jan. 2000.

[106] S. Wood, "Autonomous Underwater Gliders," *Florida Institute of Technology,* USA, 26 Pages, Sep. 2008.

[107] J. Liu and H. Hu, 'A 3D Simulator for Autonomous Robotic Fish,' *International Journal Of Automation And Computing 1*, pp. 42-50, 2004.

[108] R. W. Blake, 'On Balistiform Locomotion,' *Journal of the Marine Biological Association of the United Kingdom*, Volume 58, Issue 01, pp 73-80, February 1978.

[109] H. Loofbourrow, 'Hydrodynamics of Balistiform Swimming in the Picasso Triggerfish, Rhinecanthus Aculeatus,' MSc Thesis, *University of British Columbia*, 2006.

[110] E. A. Jones, K. S. Lucey, and D. J. Ellerby, 'Efficiency of labriform swimming in the bluegill sunfish (Lepomis macrochirus)', *Journal of Experimental Biology*, vol. 210, no. 19, pp. 3422–3429, Oct. 2007.

[111] B. Dean and B. Bhushan, 'Shark-skin surfaces for fluid-drag reduction in turbulent flow: a review', *Philosophical Transactions of the Royal Society A: Mathematical, Physical and Engineering Sciences*, vol. 368, no. 1929, pp. 4775–4806, Sep. 2010.

[112] S. J. Lighthill, 'Mathematical Biofluiddynamics', *-Infinity*, Jan. 1975.

[113] D. S. BARRETT, M. S. TRIANTAFYLLOU, D. K. P. YUE, M. A. GROSENBAUGH, and M. J. WOLFGANG, 'Drag reduction in fish-like locomotion', *Journal of Fluid Mechanics*, vol. 392, pp. 183–212, Aug. 1999.

[114] R. J. Clapham and H. Hu, 'iSplash-I: High performance swimming motion of a carangiform robotic fish with full-body coordination', *2014 IEEE International Conference on Robotics and Automation (ICRA)*, May 2014.

[115] B. Dean and B. Bhushan, 'Shark-skin surfaces for fluid-drag reduction in turbulent flow: a review', *Philosophical Transactions of the Royal Society A: Mathematical, Physical and Engineering Sciences*, vol. 368, no. 1929, pp. 4775–4806, Sep. 2010.

[116] J. Yu, M. Tan, S. Wang, and E. Chen, 'Development of a Biomimetic Robotic Fish and Its Control Algorithm', *IEEE Transactions on Systems, Man and Cybernetics, Part B (Cybernetics)*, vol. 34, no. 4, pp. 1798–1810, Aug. 2004.

[117] P. Valdivia y Alvarado, and K. Youcef-Toumi, 'Modeling and design methodology for an efficient underwater propulsion system,' *Proc. IASTED International conference on Robotics and Applications*, Salzburg, June. pp. 161-166, 2003.

[118] M. Nagai. 'Thinking Fluid Dynamics with Dolphins,' *IOS Press*, Ohmsha, LTD, Japan, p. 119, 1999.

[119] P. W. Webb, 'Form and function in fish swimming,' *Sci. Amer*., vol. 251, pp.58–68, 1984.

[120] J. Gray, 'Studies in Animal Locomotion,' *J Exp Biol* Vol: 10, pp. 88-104, Jan 1933.

[121] J. M. Anderson, 'Maneuvering and Stability Performance of a Robotic Tuna',*Integrative and Comparative Biology*, vol. 42, no. 1, pp. 118–126, Feb. 2002.

[122] P. W. WEBB, 'Simple Physical Principles and Vertebrate Aquatic Locomotion',*American Zoologist*, vol. 28, no. 2, pp. 709–725, May 1988.

[123] X. Ye, Y. Su, S. Guo and L. Wang, 'Design and Realization of a Remote Control Centimeter-Scale Robotic Fish', *Proceedings of the IEEE/ASME International Conference on Advanced Intelligent Mechatronics*, pp. 25-30, 2008.

[124] S. Guo, T. Fukuda and K. Asaka. 'Fish-like Underwater Microrobot with 3 DOF', *In Proceedings of IEEE International Conference on Robotics and Automation*, Washington, USA, pp. 738−743, May 2002.

[125] Z. Wang, Y. Wang, L Jian and G. Hang, 'A micro biomimetic manta ray robot fish actuated by SMA', *Proc. IEEE Int. Conf. on Robotics and Biomimetics* (Guilin, February) pp 1809–13, 2009.

[126] X. Deng and S. Avadhanula, 'Biomimetic micro underwater vehicle with oscillating fin propulsion: System design and force measurements,' *Proc. of IEEE International Conference on Robotics and Automation*, pp.3312-3317, April, 2005.

[127] T. Fukuda, A. Kawamoto, F. Arai and H. Matsuura, 'Mechanism and Swimming Experiment of Micro Mobile Robot in Water', *Proc. IEEE Con. on Robotics and Automation*, Vol.1, pp.814-819, San Diego, California, May 1994.

[128] C. Rossi, W. Coral, J. Colorado and Barrientos, 'A motor-less and gear-less bio-mimetic robotic fish design', *Proc. IEEE Int. Conf. on Robotics and Automation*, pp 3646–51, Shanghai, May 2011.

[129] R.J. Clapham and H. Hu, '*iSplash*-OPTIMIZE: Optimized Linear Carangiform Swimming Motion', Springer International Publishing, *Proceedings of the 13th International Conference IAS-13* (IAS 2014), July. 15-19, 2014, pp. 567-579, Padua, Italy.

[130] R.J. Clapham and H. Hu, '*iSplash*-II: Realizing Fast Carangiform Swimming to Outperform a Real Fish', *IEEE/RSJ International Conference on Intelligent Robots and Systems* (IROS 2014), Sept. 14-18, 2014, pp. 1080-1086, Chicago, IL, USA.

[131] R.J. Clapham and H. Hu, '*iSplash*-MICRO: A 50mm robotic fish generating the maximum velocity of real fish', *IEEE/RSJ International Conference on Intelligent Robots and Systems* (IROS 2014), Sept. 14-18, 2014, pp. 287-293, Chicago, IL, USA.

[132] R.J. Clapham and H. Hu, '*iSplash*: Realizing Fast Carangiform Swimming to Outperform a Real Fish', *Springer Berlin Heidelberg, Springer Tracts in Mechanical Engineering* (Bio-inspired Fishlike Underwater Robots 2015), May. 07, 2015, pp 193-218.

[133] T. Schnipper, A. Andersen And T. Bohr, 'Vortex wakes of a flapping foil,' *J. Fluid Mech*. (2009), Cambridge University , vol. 633, pp. 411–423, 2009.

[134] R. Bainbridge, 'Caudal Fin and Body Movement in The Propulsion of Some Fish', *J. Exp. Biol*, pp. 23-56, 1963.

[135] A. D. Marchese, C. D. Onal, and D. Rus, 'Autonomous Soft Robotic Fish Capable of Escape Maneuvers Using Fluidic Elastomer Actuators', *Soft Robotics*, vol. 1, no. 1, pp. 75–87, Mar. 2014.

[136] C J. Esposito, J L. Tangorra, B E. Flammang and G V. Lauder, 'A robotic fish caudal fin: effects of stiffness and motor program on locomotor performance,' *J Exp Biol*. 215, 56-67. Jan, 2012.

[137] J Liao and G V. Lauder, 'Function Of The Heterocercal Tail In White Sturgeon: Flow Visualization During Steady Swimming And Vertical Manoeuvring,' *The Journal of Experimental Biology* 203, pp. 3585–3594, 2000.

[138] J. H. Long, T. J. Koob, K. Irving, K. Combie, V. Engel, N. Livingston, A. Lammert, and J. Schumacher, 'Biomimetic evolutionary analysis: testing the adaptive value of vertebrate tail stiffness in autonomous swimming robots', *Journal of Experimental Biology*, vol. 209, no. 23, pp. 4732–4746, Dec. 2006.

[139] J. H. Long, M. E. Porter, R. G. Root, and C. W. Liew, 'Go Reconfigure: How Fish Change Shape as They Swim and Evolve', *Integrative and Comparative Biology*, vol. 50, no. 6, pp. 1120–1139, Jun. 2010.

[140] B. Shushengi, C. Yueri, 'Effect of spanwise flexibility on propulsion performance of a flapping hydrofoil at low Reynolds number,' *Chinese Journal of Mechanical Engineering*, CJME, Vol. 25, Issue 1, pp. 12-19, 2012.

[141] S. Kusuda, S. Takeuchi, and T. Kajishima, 'Genetic Algorithm Optimisation of Fish Shape and Swim Mode in Fully-Resolved Flow Field', *Parallel Computational Fluid Dynamics 2006*, pp. 301–308, 2007.

[142] J C. Nauen, G V Lauder, 'Hydrodynamics of caudal fin locomotion by chub mackerel, Scomber japonicus (Scombridae),' *J Exp Biol*, pp 1709-24, 2002.

[143] P L. Nguyena, V P. Doa, B R. Lee, 'Dynamic Modeling and Experiment of a Fish Robot with a Flexible Tail Fin,' Journal of Bionic Engineering, pp 39–45, Volume 10, Issue 1, January 2013.

[144] G. V. LAUDER, 'Caudal Fin Locomotion in Ray-finned Fishes: Historical and Functional Analyses', *American Zoologist*, vol. 29, no. 1, pp. 85–102, Feb. 1989.

[145] B E. Flemmang, G V. Lauder, 'Caudal fin shape modulation and control during acceleration, braking and backing maneuvers in bluegill sunfish, Lepomis Macrochirus', *J Exp Biol*, pp. 277-86, 2009.

[146] A J. Clark, J M. Moore, J. Wang, X. Tan, P K. McKinley, 'Evolutionary Design and Experimental Validation of a Flexible Caudal Fin for Robotic Fish', *Thirteenth International Conference on the Synthesis and Simulation of Living Systems* (ALIFE-13) pp 325-332, July, 2012.

[147] B E. Flammang, G V Lauder, 'Speed-dependent intrinsic caudal fin muscle recruitment during steady swimming in bluegill sunfish, Lepomis Macrochirus', *J Exp Biol*, pp. 587-98, 2008.

[148] T P. Simon, R Wallus, 'Reproductive Biology and Early Life History of Fishes in the Ohio River Drainage: Ictaluridae - Catfish and Madtoms, Volume 3', *CRC Press*, 232 Pages, Dec. 2003.

[149] L. Wen, J C. Weaver and G V. Lauder, 'Biomimetic shark skin: design, fabrication and hydrodynamic function', *J Exp Biol* 217, pp. 1656-1666, May 15, 2014.

[150] Peter Reuell, Harvard Staff Writer, 'A swimsuit like shark skin? Not so fast.' [Online]. Available: http://news.harvard.edu/gazette/story/2012/02/a-swimsuit-like-shark-skin-not-so-fast/

[151] Hydroid, 'A whale of a wind turbine.' [Online]. Available: http://www.geotimes.org/webcasts/article.html?id=windturbine.html

[152] Frank E. Fish, 'FLIPPERS PROVIDE LIFT, REDUCE DRAG: HUMPBACK WHALE.' [Online].Available: http://www.asknature.org/strategy/3f2fb504a0cd000eae85d5dcc4915dd4#.VXdVXPlVhBc

[153] Hydroid, 'REMUS 6000.' [Online]. Available: http://www.geo-matching.com/products/id1964-remus-6000.html

[154] MIT Mechatronics, 'Robot fish from MIT Mechatronics Appears on Discovery Channel.' [Online]. Available: https://www.youtube.com/watch?v=e3KAi5Xf7LE

[155] Frances Reed, 'How Servo Motors Work.' [Online]. Available:http://www.jameco.com/jameco/workshop/howitworks/how-servo-motors-work.html

[156] J M. Kumph, 'Maneuvering of a robotic pike,' Thesis (S.M.), *Massachusetts Institute of Technology*, Dept. of Ocean Engineering, p. 75-76, 2000.

[157] H E L Daou, T Salumäe, A Ristolainen, G Toming, M Listak, and M Kruusmaa, 'A Bio-mimetic Design and Control of a Fish-like Robot using Compliant Structures', *Advanced Robotics (ICAR), 2011 15th International Conference* on, pp. 563 – 568, 20-23 June 2011.

[158] FILOSE, 'Rainbow Trout Swimming.' [Online]. Available:https://www.youtube.com/watch?v=gfNKJO5pfnE

[159] R. W. Blake, *Fish locomotion*. Cambridge: Cambridge University Press, 1983.

[160] J J. Videler, 'Swimming Movements, Body Structure and Propulsion in Cod *Gadus morhua*', Symp. Zool. Soc. Lond. No 48, pp. 1-27, 1981.

[161] Q. Bone and N. B. Marshall, '*Biology of fishes'*. New York: Distributed in the USA by Chapman and Hall, 1982.

[162] The NACA Airfoil Series, 'NACA 4 digit airfoil generator (NACA 2412 AIRFOIL).' [Online]. Available: http://airfoiltools.com/airfoil/naca4digit

[163] K Mulleners, A L Pape, B Heine, M Raffel, 'The Dynamics of Static Stall', *16th Int Symp on Applications of Laser Techniques to Fluid Mechanics*, Lisbon, Portugal, pp. 9-12, July, 2012.

[164] G McCullough, D Gault, 'Examples of three representative types of airfoil-section stall at low speed'. *Tech. rep, NASA TN 2502*, Sept, 1951.

[165] Maritime Safety Information, 'Tides and Tidal Currents. Orgins of Tides', NAV Publications, Chapter 9. [Online].
Available: http://msi.nga.mil/MSISiteContent/StaticFiles/NAV_PUBS/APN/Chapt-09.pdf

[166] Maritime Safety Information, 'Ocean Currents. Types and Causes of Currents.' NAV Publications, Chapter 31. [Online].
Available: http://msi.nga.mil/MSISiteContent/StaticFiles/NAV_PUBS/APN/Chapt-32.pdf

[167] R. Du, Z. Li, K Youcef-Toumi, P Valdivia y Alvarado, 'Robot Fish. Bio-inspired Fishlike Underwater Robots', Robot Fish, Bio-inspired Fishlike Underwater Robots, *Springer Tracts in Mechanical Engineering*, pp 1-24, Jan 2015.

[168] Z. Li and R. Du, 'Wire-Driven Robot Fish', Robot Fish, Bio-inspired Fishlike Underwater Robots, *Springer Tracts in Mechanical Engineering*, pp. 51–92, Jan. 2015.

[169] H. Dewar and J B. Graham, 'Studies of Tropical Tuna Swimming Performance in a Large Water Tunnel', *Journal of Experimental Biology*. 192, pp. 13-31, 1994.

[170] M. Sfakiotakis, D M. Lane, and J. Bruce C. Davies 'Review of Fish Swimming Modes for Aquatic Locomotion', Dept. of Comput. & Electr. Eng., Heriot-Watt Univ., Edinburgh IEEE Journal of Oceanic Engineering, pp. 237 – 252, 1999.

[171] A R. Chowdhury, B. Prasad, V. Vishwanathan, R. Kumar, S K. Panda, 'Kinematics study and implementation of a biomimetic robotic-fish underwater vehicle based on Lighthill slender body model', Autonomous Underwater Vehicles (AUV), IEEE/OES, pp. 1 – 6, 24-27 Sept. 2012.

[172] R. Bainbridge, 'Speed and stamina in three fish', J. Exp. Biol, pp 129—153, 1960,

Appendix A

Bio-Inspired Carangiform Engineering Concepts

During the initial stages of my PhD I developed many concept designs and tried many paths before the completion of the first robotic fish build *iSplash*-I. This included concept sketches, digital models, prototype construction and experimental testing. This Appendix A presents several of these ideas (within the field of robotic fish). These designs are presented in chronological order:

A.1 Hydraulic Pressure Feed Pocket System

The mechanical drive system shown in Figures A.1-A.6 is proposed as a novel structure to generate kinematic displacements within three dimensions along the full body length of a robotic fish with high precision and smooth curvature. An aim of the concept was to produce a design that would be capable of high frequencies and forces so that high speed swimming could be achieved with the advantage of three-dimensional locomotion.

The structure of the proposed concept design consists of eighty-four individual pockets able to expand and contract, whereby twenty-one vertical segments are distributed along the lateral body length, providing dexterity within the horizontal and vertical plane for precision control of a hyper-redundant body wave. The moment varying actuation and the ability to place multiple hydraulic feed pockets may allow for advanced replication of the three dimensional deformations, progressing towards a fully continuous structure.

More specifically, Figure A.3 shows inner structure of hydraulic pockets. The cross section shows the body in a state of maximum curvature, whereby all pockets along the lateral length of the structure are expanded fully and the opposed pocket fully contracted. Each segment in Figure A.4 contains four pockets which may be expanded and contracted in volume independently. Miniaturization of a hydraulic pressure rail and valve system would be required due to the size constraints and large quantity of components.

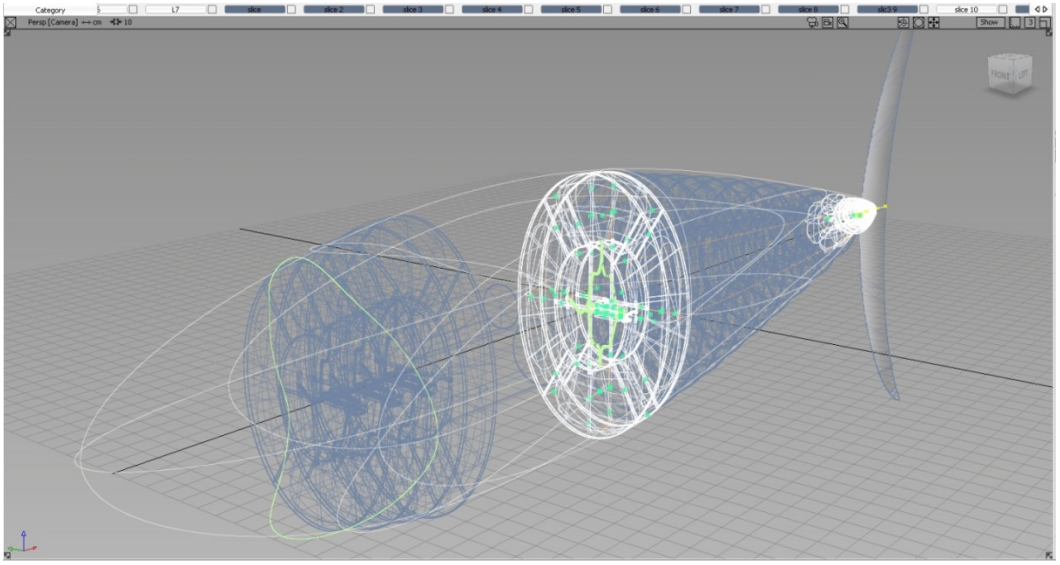

Figure A.1: Hydraulic Pressure Feed Pocket Drive System - Front profile view.

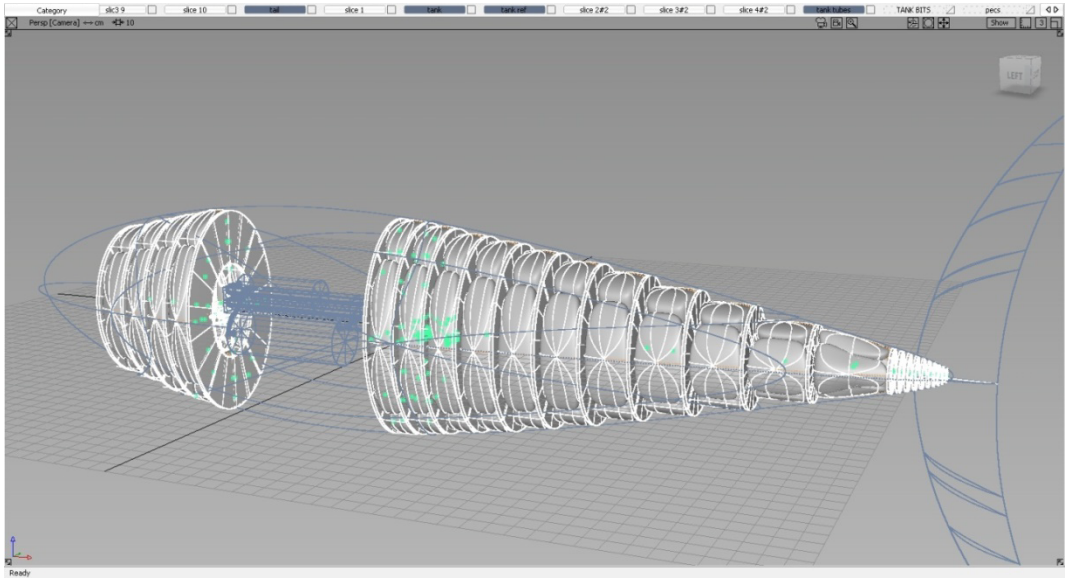

Figure A.2: Hydraulic Pressure Feed Pocket Drive System- Rear profile view.

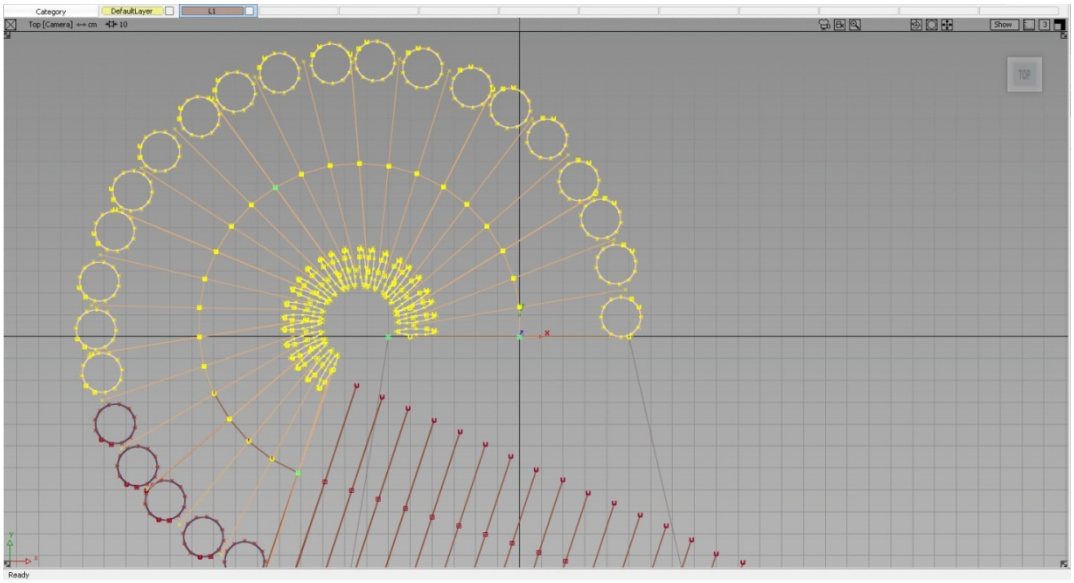

Figure A.3: Cross section view from above.

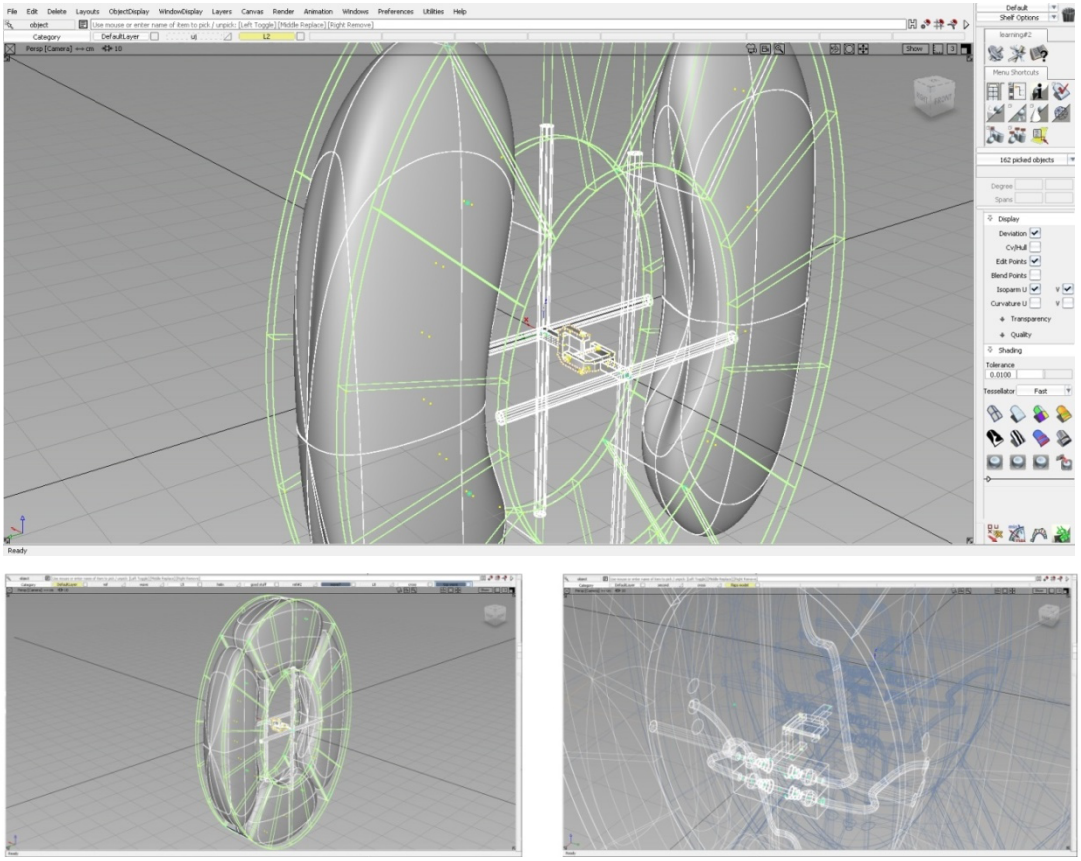

Figure A.4: Showing one of the individual segments of the design.

Figure A.5 shows a miniaturized hydraulic pressure rail and valves positioned within the centre of the main build so that the midline curvature is not resisted by a rigid structure in

comparison to the required kinematics of the Carangiform swimming motion. Figure A.6 shows the novel designs of the hydraulic valves inlets and exhausts along the pressure rail.

Deploying an intelligent algorithm may be the most appropriate way to accurately mimic the kinematics of the travelling wave and may lead to surrounding fluid flow maintenance and the ability to produce forward locomotion from a passive system by resonating and extracting energy from external flows. A disadvantage of the proposed concept is the large number of linkages and components which increase complexity of construction and energy consumptions due to internal mechanical losses [113; 121].

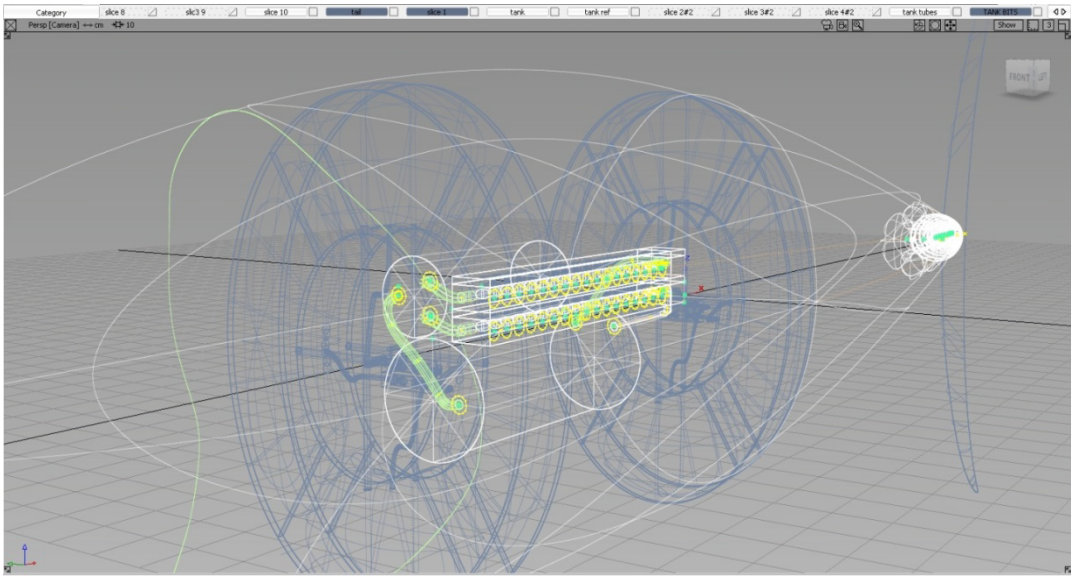

Figure A.5: Miniaturized hydraulic pressure rail and valves.

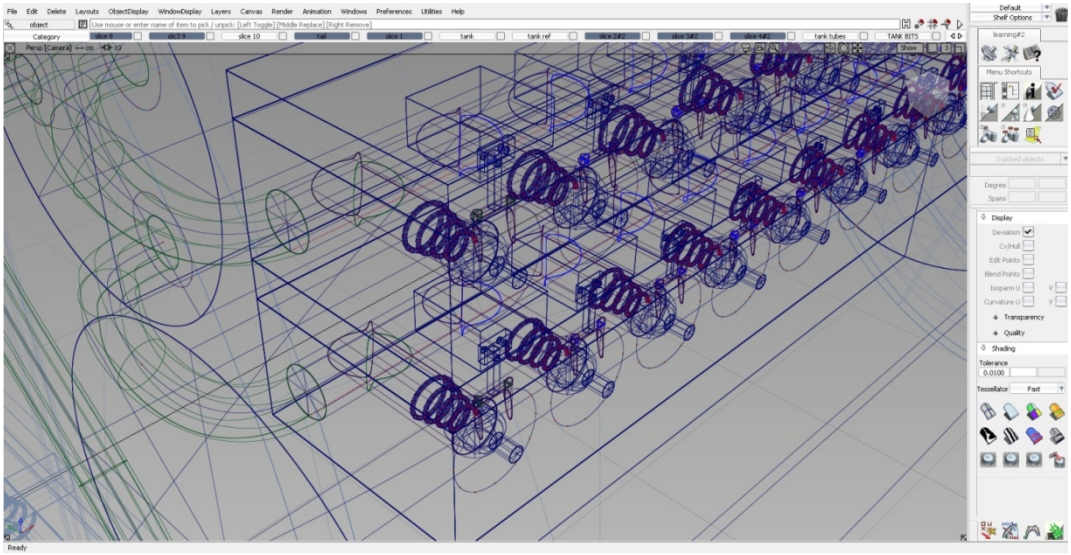

Figure A.6: Miniaturized hydraulic pressure rail and valves.

A.2 Two DOF Pectoral Fin

The necessity to apply additional forces due to inefficient body shapes increases forward resistance and therefore energy consumption. To reduce inefficient energy transfer a proposed solution is the facility to retract control surfaces from drag resistant positions. Due to the constraints of body size restricting the use of multiple actuators within the geometric frame, conventional pectoral fin mechanisms have control surfaces which protrude permanently from the body, therefore increasing drag.

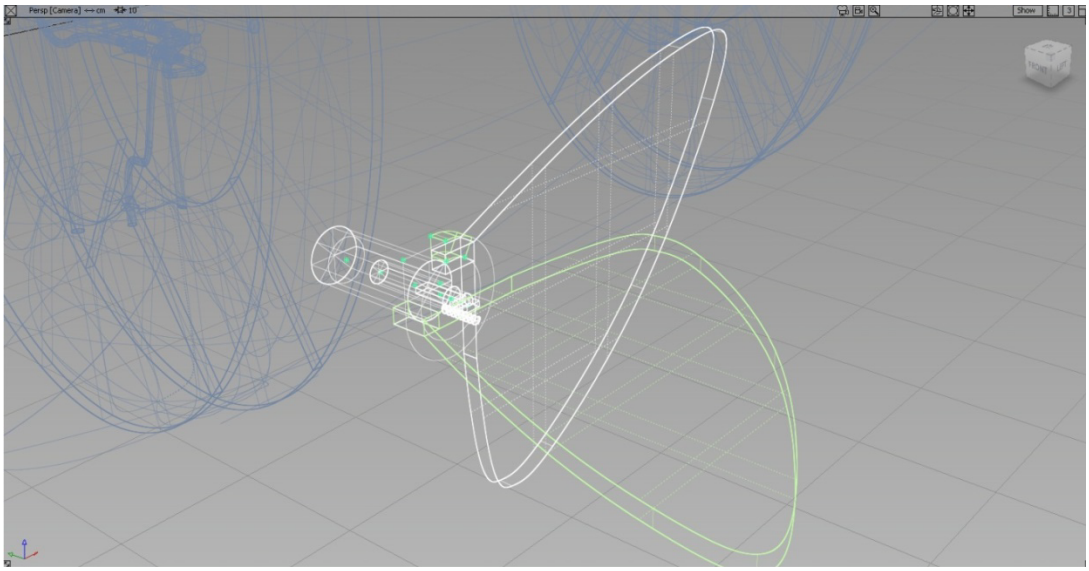

Figure A.7: Showing the proposed pectoral fin mechanism.

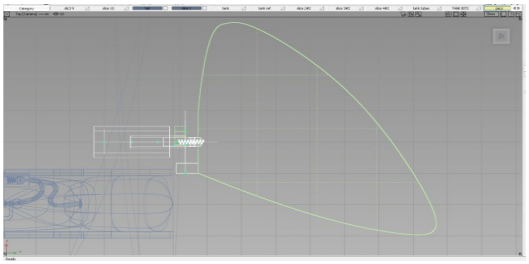

Figure A-8: Top View.

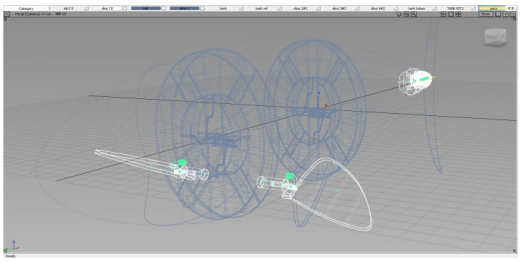

Figure: A.9: Location of mechansims.

The proposed design shown in Figures A.7-A.10 introduces a pectoral fin mechanical design with two degrees of freedom from a single actuated shaft. More specifically, Figure A.7 presents the proposed pectoral fin mechanism, with two DOF from single axis actuation. Figure A.8 shows the two DOF pectoral fin mechanisms from an above view. Figure A.9 illustrates the proposed mechanism with a robotic fish structure, highlighting the small dimensions of the mechanism within the build. Figure A.10 shows the two DOF pectoral fin mechanisms from the front of the prototype.

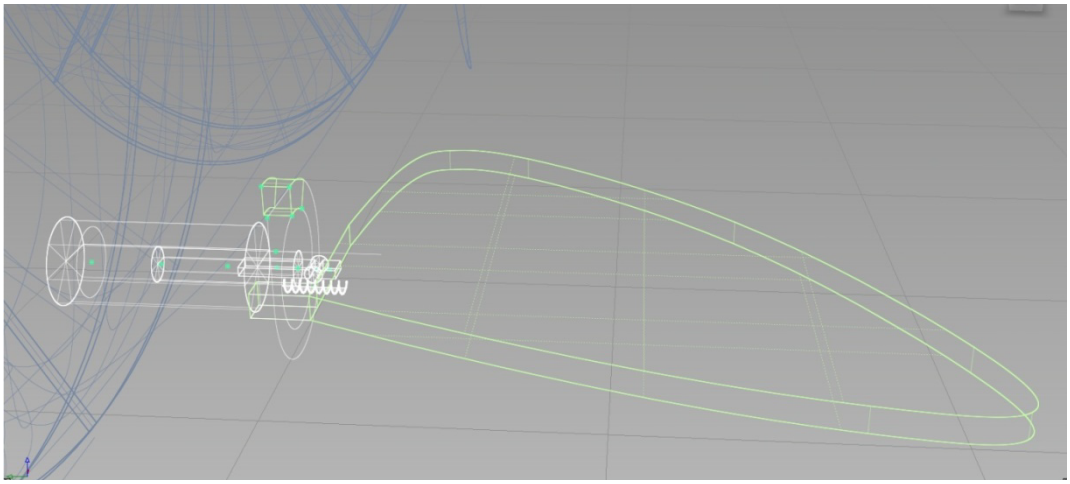

Figure A-10: Front view of 2-DOF pectoral fin mechanism.

Once rotated above 358 degrees in the vertical plane axis the control surface will be forced to pivot in the horizontal plane, if the actuator is rotated to its full 360 degrees the control surface will be fully retracted and lie alongside the body allowing for a streamlined shape to be formed such as the morphological approximation of a real fish, hence reducing inefficient energy conversion and simplifying the mechanical components and required intelligence.

A.3 Angle Accumulator: Concept and First Prototype

Micro scale propulsion is an attractive area due to the opportunities in simplification of construction and advances in navigation by reducing wake size, turning radius and the increased potential to explore the environment in areas with small geometries. Current bio-robotic fish such as Valdivia's compliant structure [117] (Section 3.6) make use of a simplified construction to produce linear locomotion by deploying a single actuator to generate the kinematic pattern of the Carangiform swimming motion and utilizing the compliant composition of silicone for use as a body and tail, deforming to shape by the pressure of the surrounding fluid. Although the method simplifies construction, large errors across the body length were produced.

Figure A.11 shows a proposed mechanical angle accumulator mechanism. The prototype is developed to generate the kinematic patterns of the straight line swimming motion and CST for horizontal mobility from deploying a single micro servo-motor. As the servo-motor actuates in either direction past centre the combination of gearing generates an accumulated curved along the midline of the body. By rotating the actuator to its maximum valve the kinematics pattern of C Sharp Turn can be generated, which is required for

increased horizontal mobility. The design has also utilized pectoral fins that generate movement at the latter stage of the CST turn phase, which may create greater thrust during the contraction.

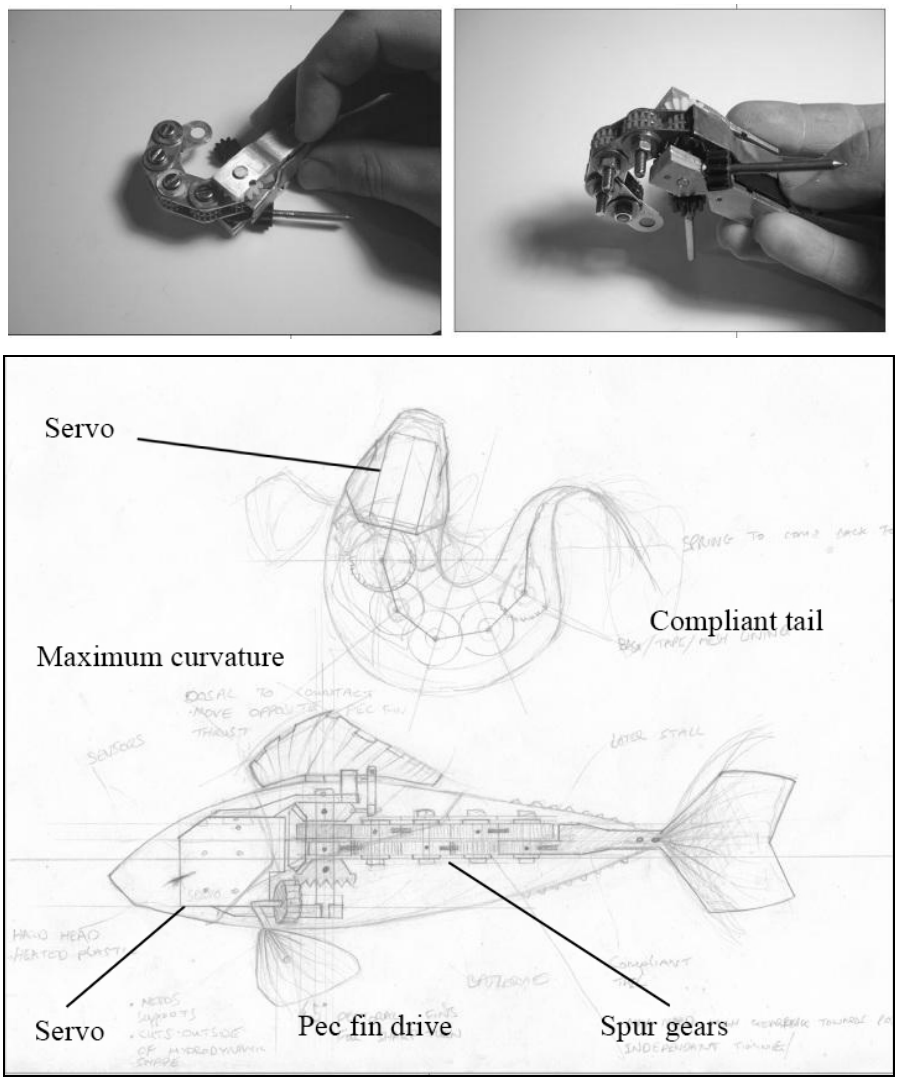

Figure A.11: Showing the angle accumulator prototype whilst in a state of maximum midline curvature, required for the swimming technique of CST and the original concept design for the robotic fish build.

Although it was measured during the development of the build that the actuation of the full travelling wave was energy inefficient due to the number of components and measured a reduced power at the tail tip, this approach may advance the development of single actuator propulsion by integrating CST within the linear locomotive mechanism.

A.4 Integrated Acceleration Mechanism

Mechanical accumulators were proposed as an appropriate mechanism to store the required energy to overcome large perturbations from the surrounding environment, which create destabilizing forces during station holding and navigation. An intelligent platform could be implemented with an accumulative and regenerative power source that may equal the force of a fast starting fish. The proposed mechanical accumulators shown in Figure A.12 and A.13 may be integrated alongside a conventional rotary actuated mechanical drive system and are required to be intelligently enabled when required.

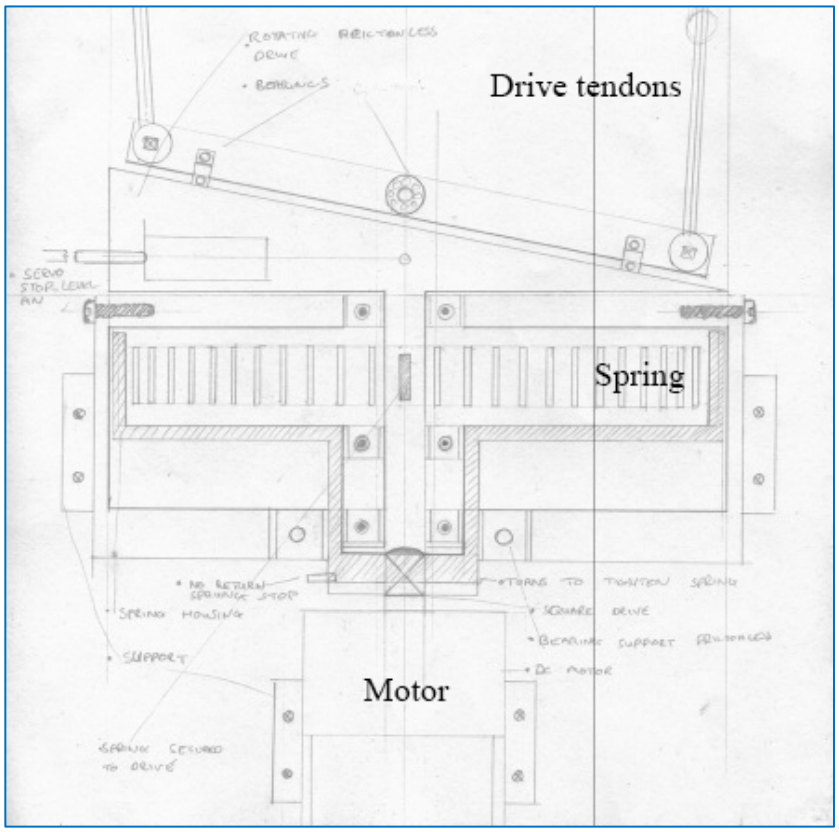

Figure A.12: Mechanical accumulator design with single actuator.

Both Figures A.12 and A.13 show the mechanical accumulator mechanisms implemented into a conventional rotary actuator system. The acceleration mechanical design proposed acuminates power by tightening a high torque spring on a ratchet mechanism until the power required is generated. The power can then be transferred into the installed system for straight-line swimming when necessary.

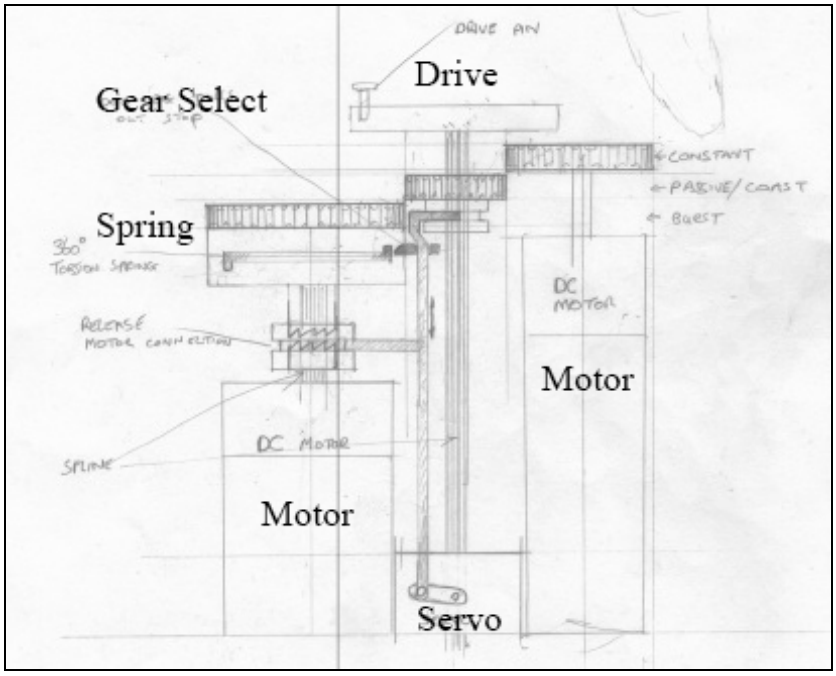

Figure A.13: Mechanical accumulator design with gear selection.

A.5 Vertical Plane Mobility Mechanism

Shown in Figures A.14-16 is the concept design for the construction of a centimetre-scale robotic fish with horizontal and vertical plane mobility mechanisms. The biomimetic concept consists of a three link structure to mimic the Carangiform swimming mode with advanced manoeuvrability within the vertical plane over previous builds.

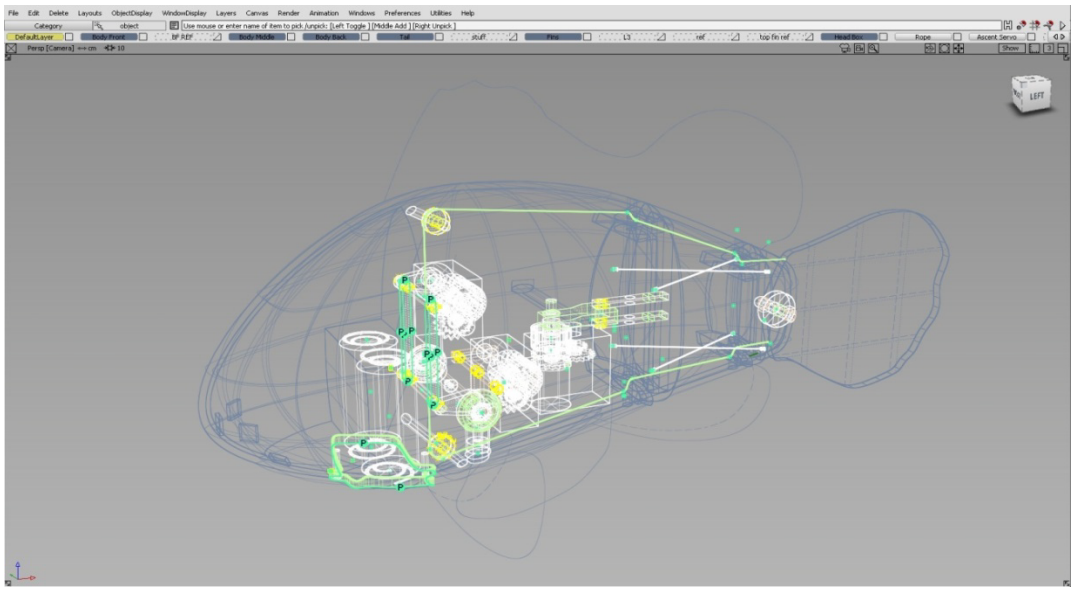

Figure A.14: The centimetre-scale bio-robotic fish with highlighted inner mechanical drive system including the proposed caudal fin mechanism.

- *Vertical Plane Mobility* –Figures A.14-16 show the proposed mechanism to increase the turning radius within the vertical plane. The actuation is provided by a single actuator, the tendons located across the top and bottom surfaces of the body are linked to an actuator and to the caudal fin structure at two fixing points located around the centre point. The tail has a single pivot point in the vertical plane and therefore able to be adjusted to be offset above or below the midline providing a directional force as required.
- Figure A-17 shows the tendons deployed for transferring the servo motors actuation to the caudal fin to generate the force and kinematics required for linear locomotion and pitch mobility. The path of the deployed tendons utilized the vertical plane mechanism have also been highlighted, the location points of the path shown allow for unrestricted movement of the tail in either direction.

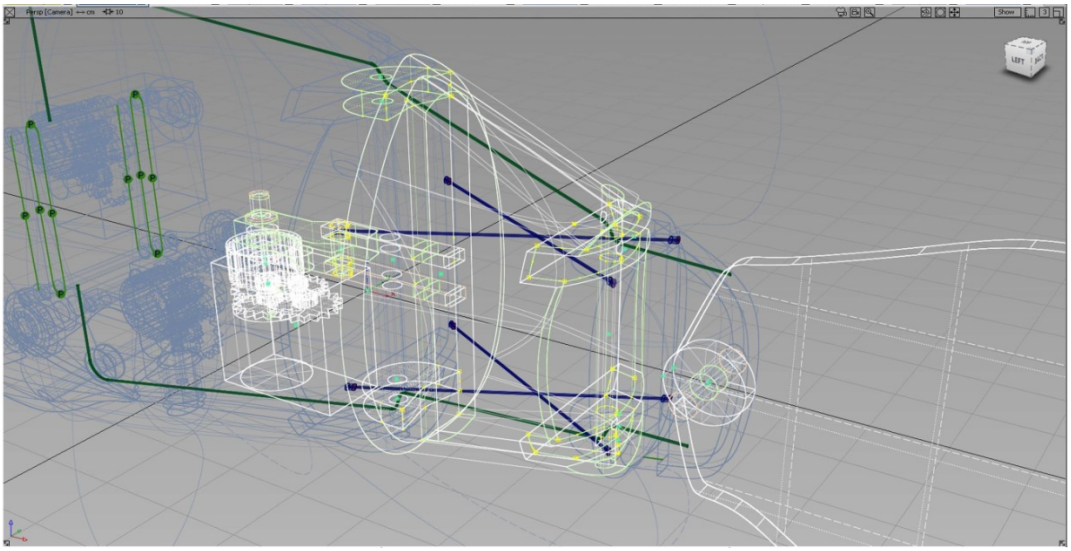

Figure A.15: Showing the tendons deployed for transferring the servo motors actuation to the caudal fin.

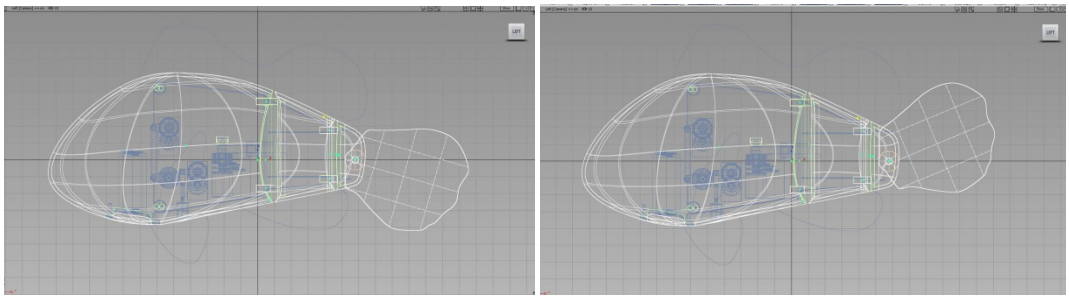

Figure A.16: Illustrating the vertical plane mechanism with the amplitude offset shown the both upward and downward position.